TUNING METAL-ORGANIC FRAMEWORKS AND POROUS POLYMERS FOR GAS STORAGE AND SEPARATIONS

A Dissertation

by

MATHIEU R BOSCH

Submitted to the Office of Graduate and Professional Studies of
Texas A&M University
in partial fulfillment of the requirements for the degree of
DOCTOR OF PHILOSOPHY

Chair of Committee, Hong-Cai Joe Zhou
Committee Members, Marcetta Y. Darensbourg
David P. Barondeau
Xiaofeng Qian
Head of Department, Simon North

August 2017

Major Subject: Chemistry

ABSTRACT

The focus of this research is to investigate how the exact shape, functionalization, and pore structure, specifically the distribution and filling of meso- and micropores, affects the chemical environment within the pores, especially when it comes to the adsorption and condensation of gas molecules. This is accomplished through pore engineering, tuning the nanostructures of the material for a particular application. However, the true rational design of MOFs and other porous materials is still a goal we have taken only a few small steps towards. Thus, considerable effort has also been devoted to the development of synthetic techniques necessary to grow new kinds of MOFs and PPNs in a planned manner.

The development of an extensive library of synthetic and post-synthetic modification techniques for MOFs and porous polymers is how researchers will be able to eventually achieve 'total synthesis' of desired porous materials, rather than relying on trial and error and serendipitously discovered existing materials. Organic chemists were able to achieve the total synthesis of complex natural products only after centuries of synthetic and theoretical study. Porous materials chemists will eventually be able to design or mimic complex pore environments such as enzyme active sites or catalysts for complex tandem and multistep reactions. However, this will only occur if we can develop a

similarly massive library of complicated synthetic techniques and improved theoretical understanding of crystallization processes.

Our work towards this goal begins with a comprehensive review of recent developments in MOF synthesis, especially the development of new synthetic methods to impart intricate functionality into ultrastable MOFs. Our group's development of Kinetically Tuned Dimensional Augmentation, Post-synthetic Metathesis and Oxidation, and Sequential Linker Installation and Cluster Metalation have contributed to the grand challenge of the rational design and total synthesis of MOF structures and greater control of pore environments. As a related subject, we also cover recent development in the design of various types of porous carbons for hydrogen storage.

We then cover the development of pre-synthetic modulation methods to alter MOF properties and produce new MOFs. Using lithium salts as a modulator, the porosity and hydrogen uptake of anionic MOFs can be improved. We can also use Mn sources in different oxidation states to produce Mn(II) MOFs with different structures and porosities with the same linker.

Post-synthetic modification techniques are explored through the loading of sorbents for CO_2 and methane uptake with liquid alkylamines and alkanes, respectively, in order to combine adsorption and absorption in a single material and efficiently use an available volume. Both techniques demonstrate improvements in uptake over the unmodified materials, with a focus on their exceptional stability, cyclability, and cost-effectiveness, as they are targeted for widespread application.

DEDICATION

To Laura and Rosie,

You are my reason for living.

ACKNOWLEDGEMENTS

I would like to take this opportunity to express my deepest gratitude to my research advisor, Prof. Hong-Cai Zhou, for his guidance, patience and encouragement throughout the past four years. He has been a great mentor not only for my research, but also for my life. I believe the knowledge, skills, and insights, that I have developed under his guidance will greatly benefit me over my future career and entire life. I am exceptionally grateful for his guidance and support. I would like to thank my committee members, Prof. Darensbourg, Prof. Barondeau and Prof. Qian, for their guidance and patience throughout my research. I would also like to thank my group members, who with Prof. Zhou have made a positive and engaging environment for research and learning. Finally, I would like to thank my family, especially my wife Laura, without whose support and encouragement this would not have been possible.

CONTRIBUTORS AND FUNDING SOURCES

Contributors

I would like to acknowledge the help, guidance, and supervision of my committee, consisting of my advisor, professor Hong-Cai Zhou, and my committee members, professors Marcetta Y. Darensbourg, David P. Barondeau, and Xiaofeng Qian.

All work for this dissertation was completed by the student, in collaboration with Muwei Zhang for Chapters 2 and 6, Shuai Yuan for Chapters 3 and 5-8, William Rutledge for Chapter 5, Xuan Wang and Ying-Pin Chen for Chapters 6 and 7, Dawei Feng for Chapter 6, Yu Fang for Chapters 8 and 9, Xing Sun for Chapter 6, Qi Wang for Chapter 6, Elizabeth Joseph for Chapters 8 and 9, Koray Ozdimir for Chapter 9, Jeremy Willman for Chapter 8, Sayan Banerjee for Chapter 9, and Professor Hong-Cai Zhou for all Chapters, all of the Department of Chemistry.

Funding Sources

This work was supported as part of the Center for Gas Separations Relevant to Clean Energy Technologies, an Energy Frontier Research Center funded by the U.S. Department of Energy (DOE), Office of Science, Office of Basic Energy Sciences under Award Number DE-SC0001015, part of the Hydrogen and Fuel Cell Program under Award Number DE-FC36-07G017033, part of the Methane Opportunities for Vehicular Energy (MOVE) Program, an ARPA-e project under Award Number DE-AR0000249. I

also acknowledge the Texas A&M graduate merit fellowship, and the U.S. Department of Energy award number DE-EE0007049. Work was also supported by the Welch Foundation through a Robert A. Welch chair in Chemistry (A-0030), and the Dr. William D. James and the Texas A&M University Center for Chemical Characterization and Analysis for their contributions to this project.

Use of the Advanced Photon Source was supported by the U. S. Department of Energy, Office of Science, Office of Basic Energy Sciences, under Contract No. DE-AC02-06CH11357. The X-ray diffractometers in the X-ray Diffraction Laboratory at the Department of Chemistry, Texas A&M University, were purchased with funds provided by the National Science Foundation (CHE-9807975, CHE-0079822, and CHE-0215838).

NOMENCLATURE

AC	Activated Carbon
ANG	Adsorbed Natural Gas
BDC	1,4-benzene dicarboxylic acid, or Terephthalic Acid
BET	Brunauer-Emmett-Teller
BTC	1,3,5-benzenetricarboxylate
CDC	Carbide-Derived Carbon5
CNG	Compressed Natural Gas
CNT	Carbon Nanotubes
COD	bis(1,5-cycloocatdiene)
COP	Covalent Organic Polymer
CVD	Chemical Vapor Deposition
DBA	Benzene-1,3-diboronic acid
DMA	*N*,*N*-Dimethyl Acetamide
DMF	*N*,*N*-Dimethyl Formamide
DMSO	Dimethyl Sulfoxide
DOE	United States Department of Energy
FESEM	Field-emission Scanning Electron Microscopy

GO	Graphene Oxide
GOF	Graphene Oxide Framework
HCPM	Hierarchically Porous Carbon Monolith
HMS	Hexagonal Mesoporous Silica
IRMOF	Isoreticular Metal-Organic Framework
K	Degrees Kelvin
LNG	Liquefied Natural Gas
LC	Liquid Crystalline, Liquid Crystal, or Liquid Chromatography
MDC	MOF-derived Carbon
MeOH	Methanol
MOF	Metal-Organic Framework
MOP(s)	Metal-Organic Polyhedron(Polyhedra)
MS	Mesoporous Silica
MWCNT	Multi-walled Carbon Nanotubes
NPC	Nanoporous Carbon
NMR	Nuclear Magnetic Resonance
PAF	Porous Aromatic Framework
PCN	Porous Coordination Network

PIM	Polymer of Intrinsic Microporosity
PPN	Porous Polymer Network
PXRD	Powder X-Ray Diffraction
SBB	Supramolecular Building Block
SBU	Secondary Building Unit
SCXRD	Single-Crystal X-ray Diffraction
SSA	Specific Surface Area
SWCNT	Single-Walled Carbon Nanotubes
TEM	Transmission Electron Microscopy
TGA	Thermogravimetric Analysis
Wt. %	Weight Percent
XRD	X-Ray Diffraction
ZIF	Zeolitic Imidazolate Framework
ZTC	Zeolite Templated Carbon

TABLE OF CONTENTS

Page

LIST OF FIGURES

Page

LIST OF REACTION SCHEMES

Page

.

LIST OF TABLES

Page

CHAPTER I

INTRODUCTION

Metal-Organic Frameworks(MOFs) are materials generated by the linkage of rigid or semi-rigid organic polytopic ligands with metal ions or clusters to form an ordered, repeating crystalline pattern that contains potential pores, or voids.[1] These pores can often be evacuated or "activated" with vacuum and temperature, allowing the measurement of permanent porosity and the adsorption of other molecules within the material.[2] A wide variety of other molecules can interact with the framework within its pores. Furthermore, the shape, arrangement, size, and content of these pores can be manipulated through continually advancing synthetic techniques.[3,4] Because of this, MOFs can be used for gas storage or separations, catalysis, chemical sensing, drug delivery, photosensitive materials, or any of a wide variety of other applications that can take advantage of the ability to precisely influence the arrangement of atoms and functional groups in a well-defined porous material.[3-22]

Of particular importance for the field of gas storage is that a MOF possesses a Brunauer–Emmett–Teller (BET) surface area exceeding that of any other known material, and MOFs in general can be synthesized with very high surface area and porosity.[23] Gas molecules undergo adsorption, or binding to the surface of a material, and materials with more internal surface area often have higher uptake, depending on the size of the pores, temperature, pressure, molecule adsorbed, and affinity of that molecule for the adsorbent surface.[24] Appropriately combined metals and linkers can produce MOFs with both high

surface area, and pores with size and arrangement optimized for sorption of a particular molecule.

In the last several years, the Zhou group has helped develop several new crystallization methods in order to increase the stability, porosity, and ability to tune the pore environment of MOF materials. Previously, only copper, zinc, and other low-valence metals could be used to grow MOF crystals suitable for single crystal X-ray diffraction(SCXRD) measurements necessary to find the structure of a MOF, a prerequisite to being able to rationally alter that structure for different applications. These metals, due to their low charge and overall lability when bound to commonly used carboxylate ligands, produced MOFs that were vulnerable to degradation by water or humidity. This drastically reduced their practical application potential, as merely being left open to the air overnight could result in their complete framework collapse and loss of porosity. [25]

For some applications, precise control over the pore size, shape, and functionality is not required. For example, to enable the widespread application of CO_2 flue gas capture, the most important criteria by far is the overall cost of capture per kilogram of CO_2. This cost includes material synthesis cost, cyclability, and the energy cost for sorbent regeneration and CO_2 sequestration. When designing porous materials for this application, porous polymer networks(PPNs) are appropriate. They are organic polymers of intrinsic porosity, typically branched copolymers grown under carefully controlled conditions from two monomers where at least one is rigid and tri- or tetratopic. Unlike MOFs, PPNs are disordered in structure and pore size, and are thus much less ‘designable’, but can still

reach very high surface areas and pore volumes.

The overall goal of this research is to produce gas adsorbents with optimized performance by tuning the size and contents of pores to be appropriate for hydrogen, methane, or CO_2 sorption in temperature and pressure ranges needed for practical application. This will be accomplished both by changing the pore size and contents of existing MOFs, and through synthesis of new MOFs with lighter metals that still retain high porosity and the appropriate pore size.

This is accomplished via several methods: First, lithium doping will be investigated as a method to increase hydrogen uptake. Lithium carboxylate ligands will be used to allow synthesis of ionic MOFs which are better suited for hydrogen storage. Second, Metal-Ligand-Fragment coassembly, a method developed by the Zhou group, will be explored to easily tune the pore size and functionalization in a way that can increase pore size and change pore shapes, unlike standard isoreticular ligand exchange. Third, Kinetically Tuned Dimensional Augmentation(KTDA) will be used to synthesize MOFs with targeted metal clusters and topology suitable for maximizing gas uptake.3 In this way, the current highest performance hydrogen, methane, and carbon dioxide sorbents will be tuned to achieve even higher uptake.

The KTDA method combines the “dimensional augmentation” of linking pre-synthesized or known metal clusters, complexes, or Secondary Building Units (SBUs) with the “kinetic tuning” of modulated synthesis, where added monocarboxylic acids lower the pH hindering ligand deprotonation, act as a surface capping agent, and compete with the linking ligand, slowing nucleation and growth. Different choices of starting metal

sources can also alter the nucleation rate.[26] By tuning the amount and type of starting metal complex or salt and the modulating monocarboxylic acid, large single crystals can be grown of MOFs that were either only found as powder or not reported at all. Furthermore, the increased crystallinity as well as defect modulation introduced by tuning the temperature and amount and strength of competing acid can alter the porosity of the MOF, for example by introducing mesoporous defects or extra open metal sites.[27,28]

Another method our group has developed to increase the stability of MOFs is the Post-Synthetic Metathesis and Oxidation(PSMO) method, or the related reductive labilization or metal metathesis methods.[29-31] First, a MOF is synthesized and characterized with a more labile metal such as Mg(II) or Fe(II). This MOF is preferably not chemically stable, as it is then either oxidized to Fe(III) or immersed in a solution containing a less labile metal such as Fe(III) or Cr(III). As long as the ligand field of the MOF is compatible with the higher-valence metal, the higher valence metal will replace the lower-valence, more labile metal within the framework. After this exchange, the framework will exhibit drastically increased chemical stability.[30]

Perhaps more importantly, these ranges of parameters can be reported for a wide variety of MOF systems, which should facilitate the prediction and rationalization of MOF crystal engineering. Previously, the main method of produced predesigned MOF structures has been through isoreticular expansion of a framework by substituting lengthened or functionalized linkers with the same metal nodes. However, if more parameters were known, MOF synthesis could be better rationalized and predicted. MOFs can be synthesized in a range of conditions, which can produce a range of crystallinity and crystal

sizes in the products. By varying these conditions, most notably the amount and type of modulating reagent, the crystal sizes of the products can be controlled by a certain extent. As mentioned in section 1.2, storage gain is dependent on the bulk density of the material, as inter-granular pore space is "wasted." To some extent, densification or other techniques can minimize this with minimal loss of crystallinity or porosity, as long as compaction is stopped at the ideal single crystal density.[32] It has been shown that the specific surface area and pore volume of MOF crystals can vary widely based on their size and morphology, which can be altered by minor changes in solvent polarity and concentration ratios.[33] Thus, high-throughput synthesis of a range of MOF samples with different crystal sizes has allowed synthesis of MOFs with optimized gas uptakes.

Though precise control of the pore size and functionalization of polymers is less developed than for MOFs, porous polymers are still a promising sorbent material, due to their low cost and weight, high chemical stability, and their high porosity and functionalizability. One promising application for porous polymers is in acid gas capture, such as flue gas CO_2 capture from fossil fuel power plants. Flue gas CO_2 capture is most efficient through the reaction of amines and CO_2 to form carbamate salts. The first reason for this is the temperature range needed – adsorption must be around 40°C, a temperature that is too high for good uptake with most CO_2 physisorbents. The second is the presence of water and possible presence of SO_2 or other molecules that could quickly collapse chemically fragile MOFs. Water assists amine-CO_2 capture, as it can act as a proton acceptor after amine attacks the CO_2, eventually resulting in bicarbonate formation that requires only one amine per CO_2 molecule captured instead of two. The most relevant

parameters for amine-based CO_2 sorbents are the density of accessible amine moieties, the cost, the cyclability, and the energy cost for regeneration.

CHAPTER II

INCREASING THE STABILITY OF METAL-ORGANIC FRAMEWORKS[1]

2.1 OVERVIEW

Metal-Organic Frameworks (MOFs) are a new category of advanced porous materials undergoing study by many researchers for their vast variety of both novel structures and potentially useful properties arising from them. Their high porosities, tunable structures and convenient process of introducing both customizable functional groups and unsaturated metal centers have afforded excellent gas sorption and separation ability, catalytic activity, luminescent properties, and more. However, the robustness and reactivity of a given framework is largely dependent on its metal-ligand interactions, where the metal-containing clusters are often vulnerable to ligand substitution by water or other nucleophiles, meaning that the frameworks may collapse upon exposure even to moist air. Other frameworks may collapse upon thermal or vacuum treatment, or simply over time. This instability limits the practical uses of many MOFs. In order to further enhance the stability of the framework, many different approaches, such as the utilization of high-valence metal ions or nitrogen-donor ligands, were recently investigated. This

[1] Reproduced with permission from "Increasing the Stability of Metal-Organic Frameworks," Mathieu Bosch, Muwei Zhang, and Hong-Cai Zhou, Advances in Chemistry, vol. 2014, Article ID 182327, 8 pages, 2014. doi:10.1155/2014/182327 Copyright 2014 by the authors.

review details the efforts of both our research group and others to synthesize MOFs possessing drastically increased chemical and thermal stability, in addition to exemplary performance for catalysis, gas sorption, and separation.

2.2 INTRODUCTION

Metal-Organic Frameworks are composed of metal-containing secondary building units (SBUs) connected by rigid or semi-rigid polytopic organic linkers. Depending on the geometry and connectivity of the SBUs, this can often create a structure with inherent porosity, with the void volume in the framework initially filled by solvent molecules.[2] These frameworks are often robust enough to survive a desolvation process termed activation by heating and/or vacuum, resulting in materials with extremely high surface areas. Some representative MOFs include MOF-5, MIL-101, HKUST-1, PCN-14, and UiO-66.[34-38] MOF development has experienced a rapid expansion after the discovery of MOF-2 in 1998.[39] Even though MOF-2 only possesses a modest porosity, it is one of the earliest MOFs that were demonstrated to have permanent porosity, as it was stable enough to survive solvent exchange with chloroform followed by vacuum desolvation, or activation.

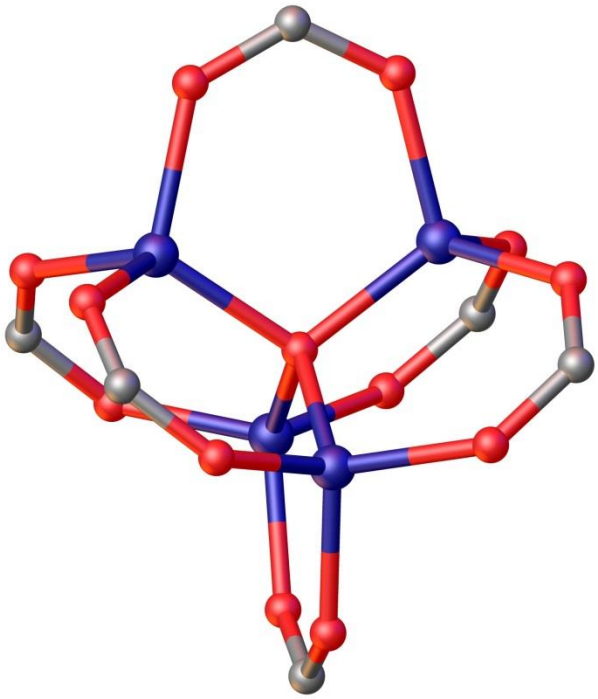

Figure II-1. The $Zn_4(\mu_4\text{-}O)$ unit of MOF-5 shown coordinated by 6 carboxylates.[40]

Soon after, MOF-5 was published, which is composed of $Zn_4(\mu_4\text{-}O)$ SBUs (Figure II-1) and benzene-1,4-dicarboxylate (BDC) linkers in a pcu topology. Subsequent sorption measurements showed an exceptional surface area, breaking all porosity records at the time. However, while MOF-5 is thermally stable to approximately 300°C, it is not water stable, and thus cannot survive long after exposure to humid air.[41] The thermal and chemical stability of MOFs are both of great interest to researchers for multiple reasons. First, a MOF must be stable enough to undergo characterization. For example, a MOF that decomposes quickly is difficult to characterize by X-ray diffraction (XRD), and thus its crystal structure is difficult to determine. A MOF that collapses upon solvent removal

cannot be said to be practically “porous”, because its experimental surface area and gas sorption cannot be determined. Furthermore, many applications of MOFs, such as gas storage and separation, hinge on their chemical stability, as materials that are not air-stable are often much less cost-effective than materials that may have inferior absolute performance but that are more robust. Some applications may also rely on thermal stability, such as catalysis.[42]

The vulnerability of MOFs typically lies in the lability of ligand-metal bonds. According to ligand field theory, because Zn^{2+} is a transition metal ion with d^{10} electron configuration, it experiences no ligand field stabilization energy overall. Thus, its ligand environment will be controlled primarily by steric factors. This favors a tetrahedral environment, but is not heavily destabilized when this environment is disturbed during ligand exchange. Facile ligand exchange allows the formation of a crystalline framework with high surface area, and favors the formation of larger single crystals, allowing more precise structural characterization through single-crystal XRD.[43] However, it also lowers the chemical stability of the resulting MOF, as easily exchanged carboxylates will be displaced by water or other nucleophiles, and if too many of the linking carboxylates are displaced, the framework will collapse. Even if the bond strength is high, if the energy barrier for ligand substitution is low, the MOF will not be chemically stable.

In general, MOFs with SBUs consisting of tetrahedral Zn^{2+} are not chemically stable. However, MOFs containing Zn^{2+} in a different coordination environment, such as MOF-69, have been shown to be more stable than those with purely tetrahedral Zn^{2+} ions.

MOF-69 contains both tetrahedral and octahedral Zn centers which share oxygens to form infinite columns, and exhibited chemical stability to exchange with a variety of solvents.[44]

To increase the chemical stability of MOFs, early effort involved the employment of SBUs containing Cu^{2+} ions with d^9 configuration. Compared to a d^{10} transition metal like Zn, metal ions with d^9 configuration possess ligand field stabilization energy, regardless of what coordination environment it adopts. This increased ligand field stabilization energy should make the ligand substitution processes less favorable. HKUST-1, composed of copper paddlewheel SBUs (Figure II-2) capped by axial water ligands and 1,3,5-benzene-tricarboxylate (BTC) displays an increased chemical stability and shelf-life over MOF-5.[45,46] When this material is activated, the water ligand on its axial position will be removed, leaving a relatively stable square planar coordination geometry on cupric SBUs in the activated sample. However, this material was reported to be unstable to direct contact with water, indicating only a limited increase in stability.[47]

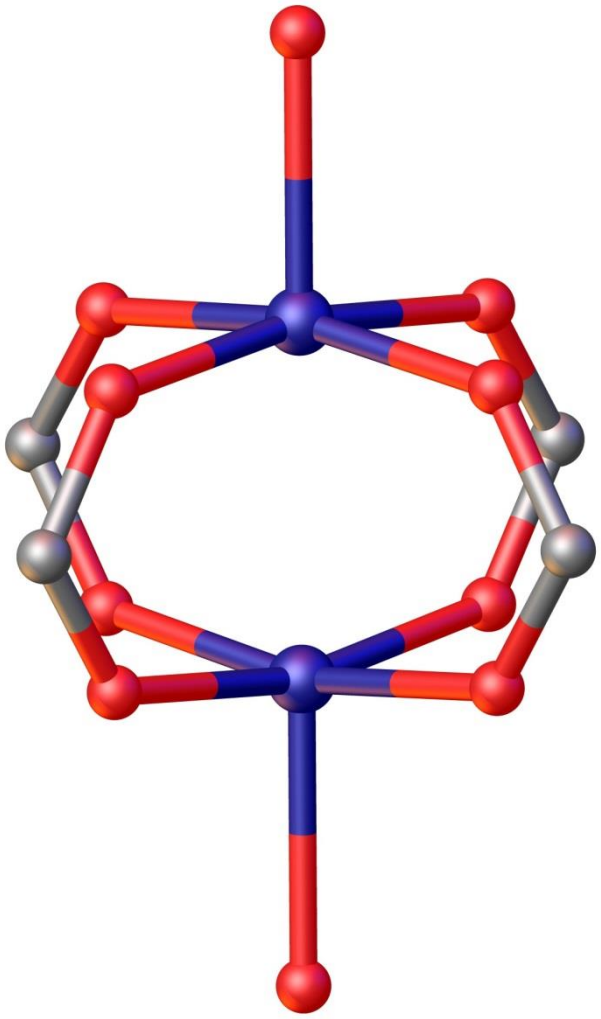

Figure II-2. The copper paddlewheel unit of the PCN-6X series, found in many MOFs. Typically, it is coordinated equatorially by 4 ligand carboxylates, while the axial ligands are solvent molecules that may be removed by activation. The zinc paddlewheel is almost identical, but unlike the copper paddlewheel, attempted activation usually causes framework collapse.

Our group has reported the PCN-6X series of (3,24)-connected isoreticular MOFs using copper paddlewheel SBUs and extended trigonal planar ligands with isophthalate groups as linkers on each arm, which exhibited both surface areas of up to 5109 m^2 g^{-1}

and moderately good stability.[48] The framework structure itself can also impact the stability, as in PCN-61 where the mesoporous structure is stabilized by areas of less open connectivity, i.e., the microwindows into the mesopores.[49] The control of framework topology and how it might impact framework stability was comprehensively reviewed elsewhere and will not be further covered here.[50] In general, the chemical stabilities of Cu-paddlewheel based MOFs were improved compared to $Zn_4(\mu_4\text{-}O)$ based MOFs, but are still insufficient for certain applications. For example, HKUST-1 was reported to undergo framework collapse under steaming conditions at temperatures above 343 K.[45]

2.3 FRAMEWORK TEMPLATING, METAL-ION METATHESIS, AND HIGH-VALENT MOFS

Our group has explored a technique called framework templating, in which single crystals of a MOF using a more labile metal (such as zinc) are synthesized, which are then metal exchanged with a less labile metal (such as copper) that is still stable in the coordination environment produced in the Zn MOF. The lability of the metal-ligand bond is decreased and the stability is enhanced by replacing, for example, the zinc in a paddlewheel SBU with copper. Many frameworks based on Zn paddlewheel SBUs also possess an isostructural MOF with Cu paddlewheels. [51] Consequently, a zinc based MOF, PCN-921, by metal exchange with copper, was transformed to an isostructural MOF named PCN-922 via a single-crystal-to-single-crystal transformation. Zinc-based PCN-921 collapsed upon activation, while copper-based PCN-922 exhibited a BET surface area of 2006 $m^2\ g^{-1}$ after activation, showing a permanent porosity.[52] Interestingly, it also

changed its color from green to blue, which is consistent with copper's change in coordination environment from a distorted square-pyramidal geometry with an axially coordinated solvent molecule to a square planar one stabilized by the Jahn-Teller effect due to its d^9 configuration.[53] On the other hand, Zn^{2+}, upon loss of the axial solvent ligand, presumably twists into a tetrahedral geometry which destroys the framework.[54] Metal exchange like this is also known as metal-ion metathesis, and has been used to synthesize many MOFs which were not able to be synthesized directly. [55]

To further increase the chemical stability of MOFs, researchers can go further along the path of using high-valence metal ions, such as Cr^{3+}, Fe^{3+}, Zr^{4+} and so on. [56] With all the coordination environments being equal, an increased charge will decrease lability simply by increasing the electrostatic interaction between the metal ions and the ligands. This trend can also be rationalized by the hard/soft acid-base principle, where soft acids like low-oxidation state metals form less stable coordination bonds with harder bases like the oxygen donors on carboxylate ligands. It is not just the charge of the metal ion that increases stability, but also the charge density. Small, hard ions with high charge density, such as Cr^{3+} or Zr^{4+}, are able to bond more strongly to carboxylates than larger, soft ions like Zn^{2+} could. [57] This was exploited in the synthesis of MIL-101, which has a complex structure consisting of large clusters of four smaller $Cr_3(\mu_3\text{-}O)$ SBUs (Figure II-3) joined by BDC linkers. This produces a framework with both a high BET surface area (4100 m^2 g^{-1}) and very high chemical stability, being stable for several months in air and also being stable to various solvents and conditions.[36]

Among metal units of a particular charge and coordination number, different metals can have ligand-metal exchange constants that are slower, which would result in a more chemically stable MOF. For example, $Ni(bdc)(ted)_{0.5}$ (BDC= 1,4-Benzenedicarboxylate, TED =triethylene diamine) was shown to undergo slower ligand substitution with water vapor than $Cu(bdc)(ted)_{0.5}$, $Zn(bdc)(ted)_{0.5}$, or $Co(bdc)(ted)_{0.5}$, even though these MOFs were isostructural. [46] This is analogous to the differences found in the water exchange rate constants among the metal ions, though carboxylate-water exchanges will have different values than the known water-water exchange rate constants. Al^{3+} has a lower water exchange constant than Fe^{3+}, and Cr^{3+} is lower still, and so MOFs based on Cr^{3+} and Al^{3+} should be more water stable, all other things being equal, than isostructural MOFs based on Fe^{3+} or Ti^{3+}.

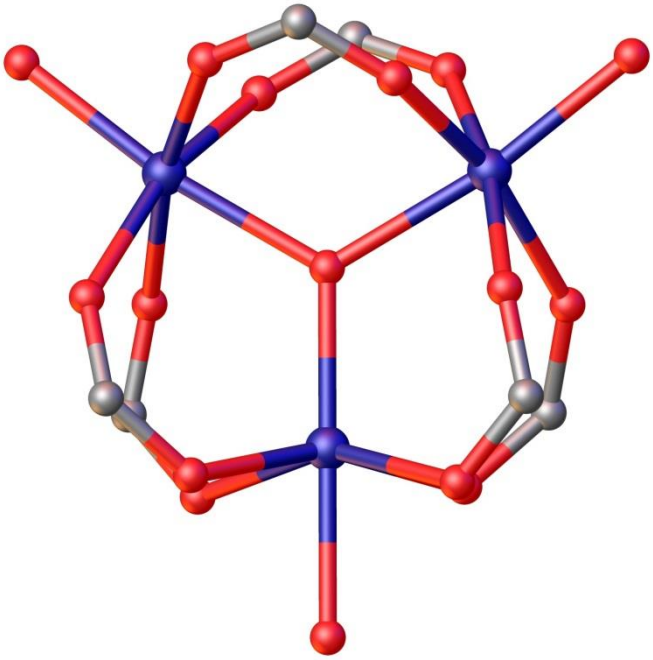

Figure II-3. The $Cr_3(\mu_3\text{-}O)$ SBU of MIL-101, shown bound by 6 carboxylates and 3 solvent oxygen atoms.

Increased chemical stability is also reported in UiO-66 and its isoreticular derivatives.[35] UiO-66 possesses 12-connected Zr_6O_8 SBUs in which the Zr^{4+} ions have stronger interactions with carboxylate ligands than copper or zinc, and thus these SBUs are less vulnerable to ligand substitution.[58] Additionally, the larger, more highly connected cluster means the framework suffers proportionally less disconnection if substitution were to occur. In general, higher nuclearity in the metal-containing unit of MOFs can increase stability in this manner. This is also shown by the increased stability of infinite chain SBUs. For example, as discussed earlier, MOF-69 is more chemically stable than Zn^{2+} MOFs containing tetrahedral Zn^{2+} paddlewheels and other discrete SBUs. [44] MIL-140,

with its infinite Zr-oxide chains, is more water stable than MOFs containing the same 1,4-BDC linker but a discrete Zr_6 SBU such as UiO-66. [59,60]

However, the increased chemical stability reported for Cr^{3+}, Zr^{4+}, and other MOFs comes at a cost: the decreased lability that causes the higher chemical stability also makes it more difficult for the researchers to obtain high-quality single crystals for single crystal XRD purposes, typically producing only microcrystalline powders. Even Cu^{2+} MOFs are more difficult to crystallize than labile but unstable Zn^{2+} ones.[52] Lability, and a relative equilibrium of ligand substitution, is essential to the formation of single crystals. If the ligands bind very strongly to the metals with slow exchange and the equilibrium shifted toward precipitation, any nucleation will resort in the formation of either microcrystalline powder, or of amorphous products of typically low porosity and little use. Both laboratory research and industrial application of MOFs rely on accurate characterization of the products, and single-crystal XRD requires relatively large single crystals. Scientifically, development of MOFs requires study and understanding of the relationships between the structure of the MOF and its particular properties, which can only happen when the structure is well understood. Undoubtedly, many MOF and other products that may have had great application potential have been shelved or thrown away because of an inability to adequately characterize them, so synthesis of single-crystalline products over microcrystalline powders is very often highly preferred in a research setting.

2.4 MODULATED SYNTHESIS TO INCREASE CRYSTAL SIZE AND CRYSTALLINITY OF HIGH-VALENCE MOFS

It is desirable to find suitable reaction conditions that give the MOF ligands high lability during synthesis, while producing a framework with extremely strong bonds and low ligand lability after synthesis is complete. In order to produce large single crystals with high chemical stability despite the fact that the metals producing this stability are correlated with decreased lability and lower crystal size and crystallinity, modulated synthesis, originally developed by Kitagawa[43] and very successfully used by Behrens[61], should be employed. In this approach, non-bridging ligands are used to influence crystal growth. The addition of modulating reagents, such as monocarboxylic acids, can allow the formation of large single crystals of a MOF that otherwise may have only been synthesized as a powder.[57,62]

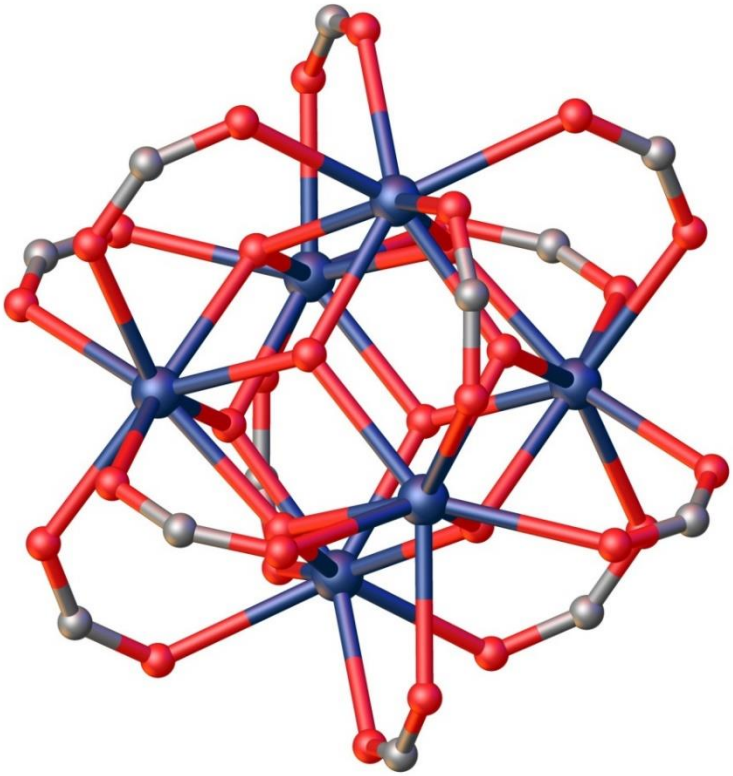

Figure II-4. The Zr_6O_8 "brick" of UiO-66 shown coordinated by 12 carboxylates.

MOFs containing high-valence Zr^{4+} cations such as UiO-66 (Figure II-4), PIZOF-1, and PCN-222 have been demonstrated to be stable towards air and water.[35,62,63] Additionally, zirconium is attractive as a MOF component due to its high abundance and low cost, [57] both important when designing novel catalysts or sorbents. Note that much said about zirconium-based MOFs can also be applied to isostructural hafnium based MOFs due to the two elements' high chemical similarity, but Hf-based MOFs are less studied due to that element's higher expense. As discussed above, there were previously few examples of Zr MOFs being isolated in a single-crystalline state, due to the fact that

using less labile metal-ligand bonds simultaneously increases chemical stability and hinders the crystallization process. Through the use of carefully tuned modulated synthesis, our group has recently synthesized and characterized single crystals of several Zr-MOFs for both gas sorption and catalysis study.[63-65] This is done by adding a varying amount of acetic, trifloroacetic, or other monocarboxylic acid that can both change the pH of the solution and bind competitively to the metal ions during crystal formation.[43,61] Equilibria in chemical reactions are governed not only by the energetic differences between the different atoms and molecules, but by the concentrations of the products and reactants. By simply introducing an excess amount of modulating ligand, we can drive the equilibria of crystal formation away from overly quick structure formation and towards the consecutive binding, release, and rebinding of ligands that allows ordered and large single crystal formation. However, since the mechanisms of crystal formation and solution equilibria under these conditions are difficult to predict, the exact amount and type of competing reagent must be tuned over many trials to produce large single crystals, as opposed to microcrystalline powders or no product at all. Catalysis is a possible application of MOFs that is especially demanding of chemical and thermal stability.[66] The MOF catalyst must not only possess appropriate sites, such as Lewis acidic or basic sites that are well exposed in accessible pores, but it must also be stable to the solvents, reagents, and temperatures that the reaction demands.[67] Based on synthesis conditions, the same catalytic cluster can exhibit different connectivity without compromising its stability. For instance, besides 12-connected Zr_6O_8 in UiO-66, 8-connected (in PCN-222 and PCN-521) and 6-connected (in PCN-225) Zr_6O_8 has also been found. Furthermore, by

varying reaction conditions, MOFs based on cubic Zr_8O_6 have also been isolated in our laboratory.

In PCN-222, our group synthesized single crystals of an extremely stable Zr-based MOF with porphyrin-containing ligands that can themselves bind different metal ions, enabling a variety of catalytic activities, which was enabled both by the actual catalytic sites and by the high pore size and water and temperature stability of this MOF.[63] PCN-222 is stable to not only to air and boiling water, but also to immersion in concentrated HCl for 24 hours. Similar Zr-porphyrin MOFs PCN-224 and PCN-225 exhibited different catalytic activity[64] or pH-dependent fluorescence[65]. Additionally, by using similar Zr SBUs along with tetrahedral ligands, stability was maintained alongside a higher surface area (BET 3411 $m^2 g^{-1}$) in PCN-521 (Figure II-5), which mimicked the topology of fluorite by exploiting the cubic nature of the 8-connected Zr_6O_8 clusters in combination with the 4-connected tetrahedral linkers.[57] All of these Zr-MOFs exhibited high chemical stability due to the strong Zr-O bonds, and all were synthesized as single crystals by carefully varying the type and amount of modulating reagent. However, while many Zr-MOFs have demonstrated stability to neutral or acidic aqueous solutions, their stability towards base was lower, with only NO_2-functionalized UiO-66 retaining its crystallinity in pH 14 aqueous NaOH among tagged UiO-66 derivatives, and PCN-225 being stable from pH 1-11. [65,68]

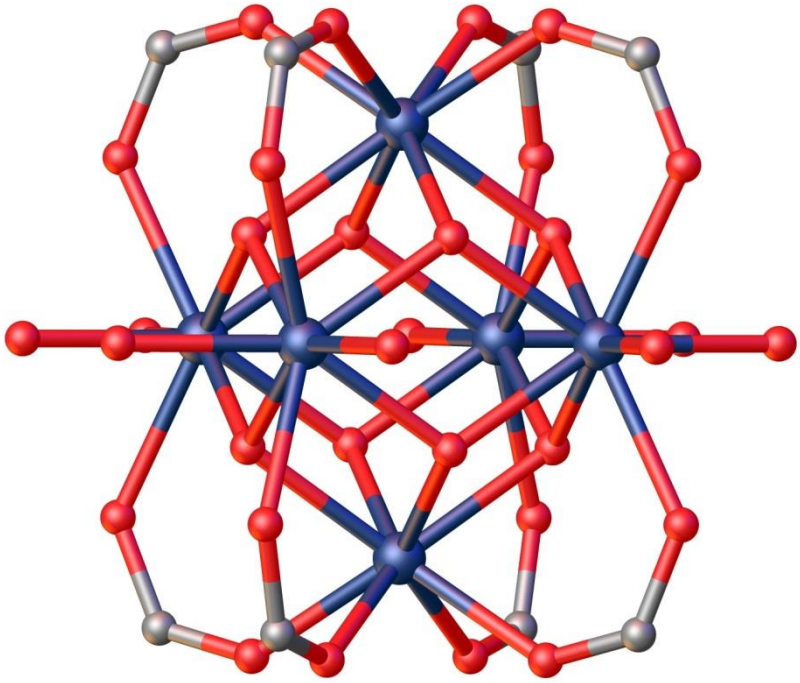

Figure II-5. The Zr_6O_8 unit of PCN-521, which is similar to that of UiO-66 except that it is 8-connected instead of 12 connected, having a "cubic" symmetry that is compatible with the tetrahedral ligands used. The equatorial Zr atoms are coordinated by hydroxyl groups on the periphery of the unit.[57]

Behrens et al. developed a series of porous interpenetrated zirconium-organic frameworks (PIZOFs,) using Zr^{4+} and $HO_2C[PE\text{-}P(R^1,R^2)\text{-}EP]CO_2H$ linkers. These MOFs demonstrated high porosity, tunability, and high stability against moisture and temperature. The very long organic linkers in these MOFs retain chemical stability, unlike UiO-67 and other UiO-66 derivatives with extended ligands. This is an example of modulated synthesis being used to prepare single crystals of a high valence metal containing MOF, with single-crystal X-ray diffraction studies produced for PIZOF-1, -2, and -8 after they were synthesized with benzoic acid as modulating reagent. [62] Other

examples of water-stable Zr^{4+}-based MOFs after the use of modulating reagents have also been published.[69]

2.5 N-DONOR LIGANDS

So far, carboxylates are the most commonly used ligands in MOF synthesis. Utilization of high valence metals as hard acids appears to be the most straightforward approach for the construction of stable MOFs by taking advantage of the existing ligand database. In addition to this approach, the interactions between softer ligands (such as imidazolates, triazolates, tetrazolates, and other nitrogen containing heterocycle-incorporated ligands) with softer metal ions (such as Zn^{2+} and Co^{2+}) can also be exploited in stable MOF synthesis. An early example of this by the Long group was the synthesis of a framework using Mn^{2+} and 1,3,5-benzenetristetrazolate.[70] Detailed stability measurements were not conducted, but a crystal remained single through activation at 150°C allowing single-crystal XRD structural determination of the desolvated framework, implying high stability. Chen et al. published Zn^{2+} MOFs with imidazolate ligands and zeolite topology that possessed high thermal stability, Eddaoudi et al. developed zeolite-like MOFs using indium and bis(bidentate) imidazoledicarboxylic acid ligands, and the Yaghi group also introduced Zeolitic Imidazolate Frameworks (ZIFs), using soft Zn^{2+} and Co^{2+} and imidizolate linkers to construct a wide variety of highly stable frameworks that mimic zeolite topology, due to the metal ions adopting a tetrahedral environment while the imidizolates link them at angles similar to the oxides in zeolite minerals.[71-73]

The Rosi group synthesized a mesoporous framework bio-MOF-100, which is, to our knowledge, the highest BET surface area material known using N-donor ligands with 4,300 $m^2 g^{-1}$.[18] However, this material uses soft nitrogen containing adeninate only to build Zn^{2+} SBUs with the SBUs linked by biphenyl dicarboxylate (BPDC) ligands. Thus, its overall stability would actually be expected to be much lower than that of Zn^{2+} MOFs linked exclusively by soft N-donor ligands, and this was confirmed by the fact that "gentle" supercritical CO_2 activation methods were required to achieve high porosity, with "harsh" conventional activation methods producing low N_2 adsorption consistent with collapse of the framework. This is in contrast with Bio-MOF-1 developed by the same group, which survived activation and demonstrated porosity at 125°C.[74] This is likely partially due simply to its relatively lower porosity compared to bio-MOF-100.

Similarly, our group reported another adenine-incorporated MOF, PCN-530, which consists of 2 distinct Zn-adeninate SBUs forming 1-D zinc-adeninate chains linked by 4,4′,4″-*s*-triazine-2,4,6-triyl-tribenzoate (TATB) ligands. [75] Even though the porosity of this framework is not impressive due to the utilization of low symmetry ligands, this framework has demonstrated a significantly improved stability over the traditional Zn MOFs.

Using 1,3,5-tris(1H-pyrazol-4-yl)benzene (H_3BTP) and Ni, Co, Zn, and Co salts, Long et al. synthesized several different frameworks that are very stable both thermally and chemically compared to most carboxylate-based MOFs, due to the less labile linkages between the pyrazolate-based ligand and metal,. $Ni_3(BTP)_2$ in particular was stable to both

430° C in air and immersion in boiling acid (pH=2) or base (pH=14), while retaining crystallinity and possessing a BET surface area of 1650 m^2g^{-1}. This framework is both extremely stable and can expose Ni metal sites, making it promising for catalysis, even for reactions in harsh conditions.[76] The same group later reported $Fe_2(BDP)_3$, which has a BET surface area of 1230 m^2 g^{-1} and is based on a benzene dipyrazolate ligand. This material was stable to 280° C in air and boiling in aqueous acid (pH=2) and base (pH=10) for two weeks, and was proven to be useful in separation of hexane isomers. Though the BET surface areas of these frameworks are not record-breaking, their extreme stability while retaining high porosity makes them extremely promising materials that showcase the capabilities of N-based MOFs. [77]

2.6 LIGANDS WITH SUPERHYDROPHOBICITY

Our group also attempted a method of synthesizing moisture-stable MOFs that did not involve altering the metal-containing units at all: synthesis of superhydrophobic MOFs by functionalizing the ligands with pendant hydrophobic groups. By partially filling the pores with $-O^nHex$ groups attached to [1,1':4',1"]terphenyl-3,3',5,5'-tetracarboxylic acid (TPTC) ligands, the water stability was drastically increased as compared to the non-functionalized copper paddlewheel containing NOTT-10X structure, or even compared to ligands functionalized with shorter hydrophobic groups. [78] Predictably, some porosity was sacrificed, but a moderate BET surface area of 1083 m^2 g^{-1} was retained. Most interesting was the superhydrophobic behavior of $Cu_2TPTC\text{-}O^nHex$, which completely resisted any absorption of water under standard conditions. However, this behavior was inversely

proportional to the thermal stability of the material, with a loss of crystallinity found in the –O^{n}hex variant at 292°C as compared to 315°C for the –O^{n}Et variant. (Figure II-6)

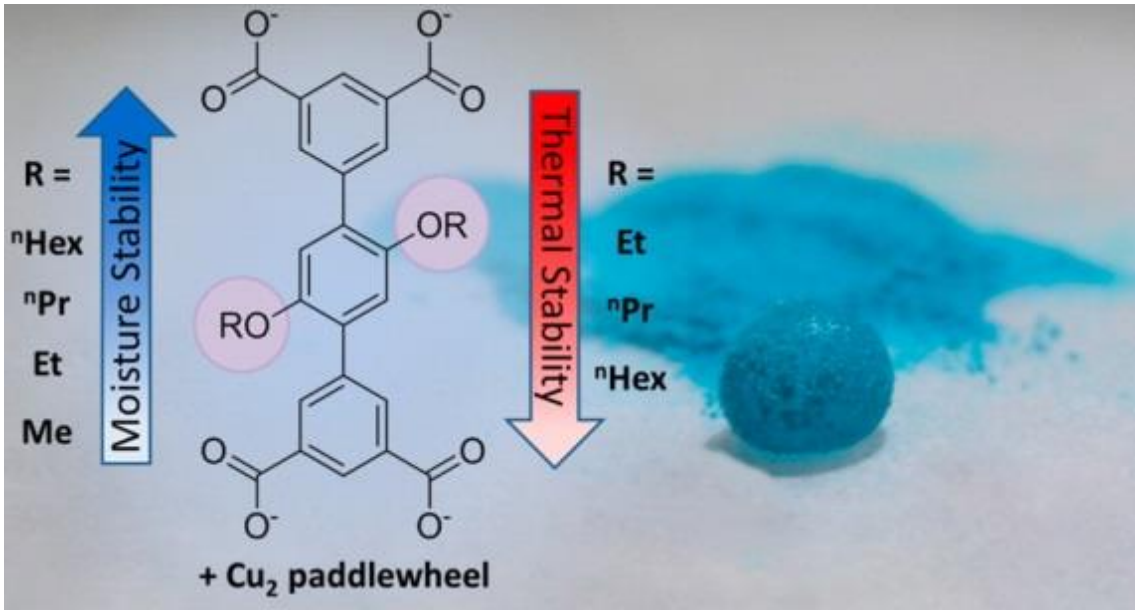

Figure II-6. Superhydrophobicity shown in Cu_2TPTC-O^{n}Hex. (Reprinted with permission from 78. Copyright 2013 American Chemical Society.)

The Omary group developed the fluorous MOFs FMOF-1 and FMOF-2, which showed no water adsorption found near 100% relative humidity and no solvent adsorption after being immersed in distilled water for extended periods, despite its large channels that show high and selective adsorption of C_6-C_8 hydrocarbons. [79] FMOF-1 is built from 3,5-bis(trifluoromethyl)-1,2,4-triazolate and Ag^{+}, and FMOF-2 is produced by annealing FMOF-1 followed by resynthesis from a toluene and acetonitrile solution, so these can also be counted as examples of stable N-based MOFs. Serre et al. studied a series of MIL-88 derivatives with many different functional groups attached to the terephthalate and

4,4'-biphenyl dicarboxylate ligands of the Fe^{3+} MOFs, including various fluorinated ligands. Permanent porosity was retained in the $2CF_3$ versions of MIL-88B, with a BET surface area of 330 m^2g^{-1}, while very little surface area was found in the 4F derivative, likely because the pore size in that version is too small to accommodate N_2 molecules. This study mainly covered how the functional groups changed the flexibility and swelling of the framework, but it also showed that most functional groups (except for the BDC-2OH linker) did not cause a large change in the thermal stability of the framework. [80]

Another example of superhydrophobic N-based MOFs stable to moisture were the Ni- bis-pyrazolate MOFs developed by Navarro et al.[81] These were designed to take advantage of the more stable bonds between azolates and softer "borderline" metal ions.[21] Their hydrophobicity was tuned by changing the ligand length to change pore size, and by using trifluoromethyl and methyl-functionalized ligands. $[Ni_8(L5\text{-}CF_3)_6]$, the most hydrophobic MOF presented, effectively captured a flow of diethylsulfide, a hydrophobic and volatile organic compound, under 80% relative humidity, unlike similar non-hydrophobic MOFs. High water stability was further demonstrated by water adsorption-desorption isotherms.

2.7 CONCLUSION AND PERSPECTIVE

MOF research, though based on decades of research on coordination polymers and traditional porous materials (such as zeolites or mesoporous silica), blossomed after the discovery of porous, functionalizable Zn^{2+} and Cu^{2+} frameworks that could be grown as single crystals and thus easily characterized.[34,37] Due to the limited stability of the early

frameworks, researchers tried various methods to create more robust frameworks. One of the most popular and successful methods, incorporation of high-valence metals, had the downside of decreasing crystal size and crystallinity.[35] This has caused difficulties in structural characterization that have been partially surmounted through the use of novel techniques[82] for deeper elucidation of MOF structures.[83] A modulated synthesis strategy for the growth of larger single crystals of stable high-valence MOFs can also be used to allow structural characterization through single crystal X-ray diffraction.[43,61]

As discussed in a recent review of our and other work on the rational design of MOFs [67], it should also be noted that modulated synthesis techniques have also been reported to increase the porosity and catalytic activity of UiO-66, due to the introduction of defects that leave coordinated modulator in place of some proportion of the linking ligands.[84,85] However, it is possible that this defect creation may reduce the stability of the resulting MOF as well. Our group has used these techniques to synthesize a variety of Zr-MOFs of lower cost and high stability and porosity, as well as exploring the use of soft N-donor and hydrophobic ligands to increase the stability of MOFs using bivalent metals. Many promising recently reported MOFs for gas storage and catalysis have used high-valence metals that have low ligand exchange rates, and so promising avenues of near future MOF research likely involve the use of modulating reagents, metal exchange, and other new techniques to synthesize highly porous and stable MOFs from other readily available high-valence metals, such as iron, chromium, or aluminum.

So far, most stability measurements on MOFs have been concentrated on their thermal and water stabilities, but further avenues of possible research are to determine their stabilities towards contaminants such as salts, body fluids, or corrosive molecules such as H_2S or NH_3. Some studies of this sort have been done, especially on MOFs designed for drug delivery, and have been reviewed elsewhere.[86] As future MOFs are developed for more widespread application, their stability towards more varied chemicals and contaminants should be determined, and application-built MOFs should be rationally designed to be stable towards conditions present in their targeted environment.

CHAPTER III

GROUP 4 METALS AS SECONDARY BUILDING UNITS: TI, ZR, & HF-BASED MOFS[2]

3.1 OVERVIEW

Many early Metal-Organic Frameworks (MOFs) made from copper or zinc showed exceptional porosity and other properties and promise for a wide variety of applications, but ultimately proved unsuitable for further development because of their lack of stability to ambient moisture. To overcome this problem, many researchers have in recent years been concentrating on the development of MOFs based on high-valence group 4 metals, which tend to possess much greater moisture and chemical stability due to the strength of the carboxylate M^{4+} bonds and, under some circumstances, connectivity of the M^{4+} clusters.

3.2 INTRODUCTION

Metal-Organic Frameworks, abbreviated as MOFs, are composed of metallic clusters, also known as Secondary Building Units(SBUs), or rarely single metal nodes, and organic ligands. The metal component plays an important role in determining the MOF's properties.[87] First, the metal-ligand bond is usually the most labile site of the MOF

[2] Reused with permission from "Group 4 Metals as Secondary Building Units: Ti, Zr, and Hf-based MOFs. In *The Chemistry of Metal–Organic Frameworks*", Bosch, M.; Yuan, S.; Zhou, H.-C.: Wiley-VCH Verlag GmbH & Co. KGaA, 2016; pp 137-170. Copyright 2016 Wiley-VCH Verlag GmbH & Co. KGaA.

structure, and determines the MOF stability. Second, certain metallic clusters imbue the structure with various functions. For example, the open metal sites produced after activation and the removal of solvent interact strongly with gas molecules, which enhances the gas uptake of the material. Some metal-oxo clusters exhibit catalytic properties, which combined with the inherent porosity of MOFs makes them a new platform for designing novel catalysts. [88]

The metallic clusters are mainly composed of monovalent (Na^{+}, Cu^{+}, K^{+}, Ag^{+}, etc.) divalent (Mg^{2+}, Mn^{2+}, Fe^{2+}, Co^{2+}, Ni^{2+}, Cu^{2+}, Zn^{2+}, Cd^{2+},etc.), trivalent (Al^{3+}, Sc^{3+},Cr^{3+}, Fe^{3+}, In^{3+}, lanthanides^{3+},etc.) or tetravalent (Ti^{4+}, Zr^{4+}, Hf^{4+}) metals.[89] The MOFs based on tetravalent metals have drawn particular attention due to their high stability which has made them feasible for use in wide-scale practical applications. There are two main reasons that the tetravalent metals have significantly enhanced chemical stability compared to MOFs produced from other metals. The first is that a higher charge and charge to radius ratio(Z/R) makes them hard acids, and a better match to the relatively hard carboxylate oxygens used in most MOF ligands, in addition to the higher positive charge itself producing a stronger ionic attraction.[90] This first reason is connected to why many zirconium MOFs have nearly identical halfnium analogues: in addition to Hf^{4+} having a d^{0} electronic configuration as Zr^{4+} has, it also has a nearly identical radius to Zr^{4+} despite being in a lower period, due to the lanthanide contraction. These factors contribute to the observed fact that hafnium is chemically almost identical to Zr, reacting to the same ligands in the same fashion, which allows it to form the same MOF structures.[91] Due to the fact that these MOFs behave in a nearly identical fashion to their zirconium analogues,

mainly distinguished only by their increased weight and cost, they will not be extensively covered here.

The increased valence of the group 4 metals also contributes to a challenge in MOF crystal growth, that partially explains why there was a gap of several years before Zr-based MOFs were discovered and widely studied: the higher strength of the oxygen-M^{4+} interaction lower ligand lability and a slower rate of ligand exchange, which makes the MOFs more chemically stable, but also makes the MOF structure slower and less likely to grow in the first place. Furthermore, a key part of MOF research is the crystallographic characterization of the MOF product. MOFs can only be rationally designed because of extensive study of their structure-property relationships, which requires that their structure is investigated. However, many Zr-based MOFs are grown, at least in initial studies, as polycrystalline powders that can not be characterized by single-crystal X-ray diffraction(XRD), likely due to their lower metal-ligand lability preventing an appropriate equilibrium between ligand association and dissociation required to form large single crystals. In these MOFs, the ligand association is faster and stronger than that in lower-valence MOFs, and the dissociation is less favored. This causes relatively fast crystal growth, and in addition to the presence of many nucleation sites, results in a polycrystalline product.

However, in recent months and years, synthesis techniques have been developed that can partially overcome this difficulty. In 2009, the Kitagawa group reported that acetic acid could be added to the solvothermal solution prepared for a copper MOF synthesis, resulting in different products than those obtained without the presence of the non-linking

carboxylic acid.[43] This „modulating reagent“ competes with the linker, but should not be so strong that it cannot be eventually displaced completely by the linker to make the MOF the thermodynamically favored product. In the case initially explored by Kitagawa and in several other places, this can result in a completely different product composition than is found without the modulator. However, in some cases, it serves to slow down crystal growth, reduce the number of sites of initial nucleation, and ultimately allow the growth of larger single-crystals. This phenomenon has been investigated and expanded upon extensively in the last several years, especially in zirconium systems which produce acid-stable product MOFs.

The second reason that most group 4-based MOFs have much higher chemical stability than many other MOFs is that the SBUs they form as the MOF structure grows have much higher nuclearity than the SBUs of other MOFs. For example, copper and zinc MOFs often form paddlewheels, which are 2-metal units surrounded by 4 carboxylate ligands and (before activation) a solvent or water ligand in the axial position such that each metal has a square pyramidal ligand field. Thus, each SBU is considered 4-connected. By contrast, MIL-125, the most studied titanium-based MOF, has a 12 connected SBU, as described below. Zirconium-based MOFs have a larger variety of SBUs and connectivity, but are commonly formed of, for example, Zr_6O_8 SBUs. These SBUs can have varying but high connectivity, such as being 12-connected, 8-connected, or 6-connected depending on the demands of the topology in which the MOF forms. In each of these cases, the higher connectivity of these clusters will make the MOF framework more resilient to ligand substitution by alternative nucleophiles such as water.

A MOF with 4-connected SBUs will be "disconnected" 3 times as much by a ligand substitution event than a MOF with 12 connected SBUs. This hypothesis is given support by the fact that even for notoriously unstable zinc-based MOFs, MOFs with infinite chain Zn-SBUs, like MOF-69, tend to have measureably higher chemical stability than those based on zinc paddlewheels or other SBUs of lower connectivity.[44] However, this field of study is still new, and further investigation of how MOF structures and their chemical stability are related is needed.

3.3 TITANIUM-BASED MOFS

Among them, the Ti-MOFs are especially interesting due to their high stability and photocatalytic activity. However, only a limited number of Ti-MOFs (MIL-125, MIL-125 derivates and NTU-9) have been reported. MIL-125 is constructed from Ti_8O_8 clusters and BDC (BDC= 1,4-benzenedicarboxylate) linkers. It demonstrates high stability, permanent porosity and photocatalytic activity towards alcohol oxidation.[92] Further work has been done to functionalize the BDC linker with amino groups to adjust its band-gap.[93] Recent work also demonstrates that MIL-125 and its NH_2-functionalized derivative (MIL-125-NH_2) can catalyze light-driven water splitting[94] and CO_2 reduction[95], which makes Ti-MOFs more attractive as photocatalysts.

Compared with Zr-MOFs, the Ti-MOF field is less developed because of difficulty in achieving high crystallinity. Unlike the Zr-MOFs, there is no comprehensive method yet developed to synthesize Ti-MOFs. Two reasons account for the difficulties in synthesis. First, in order to obtain single crystals, a reversible bond and an

association/dissociation process is required to allow sufficient structure reorganization and defect reparation. The strong Ti-O bond, however, makes the bond dissociation extremely difficult. The Z/R of titanium may simple be too much of a match to that of oxygen, preventing the ligation reversibility necessary for MOF growth.

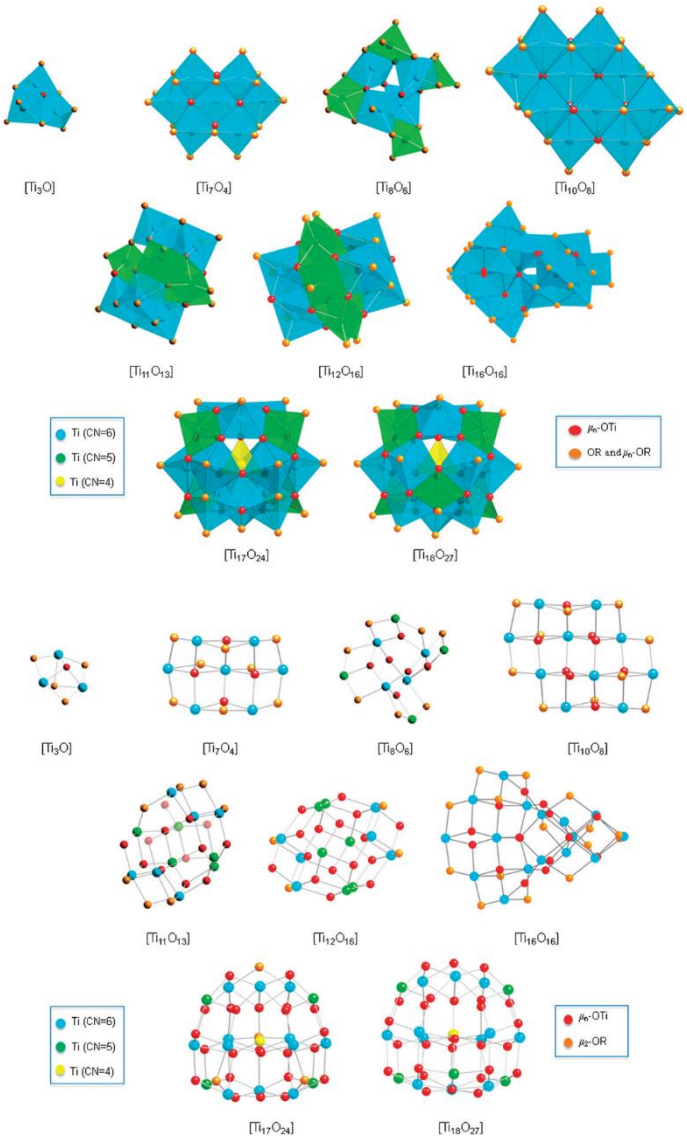

Figure III-1. Isolated Ti-O clusters. Reprinted with permission of The Royal Society of Chemistry from Reference 96.

Second, an overview of reported Ti-oxo clusters found that the symmetry, connectivity, or stability of the clusters is not suitable for MOF formation, as seen in Figure III-1.

Many of these clusters are synthesized by the controlled hydrolysis of titanium alkoxides, and their shape and size are controlled by the bulkiness of the ligands surrounding them. These conditions may not be compatible with common MOF synthesis conditions. Also, the low symmetry of many of these clusters is such that they could not connect with common linkers to form an energetically favored MOF topology, and so other products are favored overall. Finally, most of these clusters have low hydrolytic stability, due to the presence of residual monodentate alkoxy ligands left over from their synthesis.[96]

Interestingly, one of the titanium clusters with high hydrolytic stability, $Ti_8O_8(OOCR)_{16}$, is very similar to the SBU of one of the only reported titanium MOFs, MIL-125. This may be a clue to the conditions required for synthesis of titanium MOFs with new SBUs, especially considering the development of Kinetically Tuned Dimensional Augmentation as a strategy to synthesize new MOFs starting from pre-formed clusters.[97] Ti-MOFs, due to their applications, will be a promising field as a general synthetic methodology for them is developed.

3.3.1 MIL-125

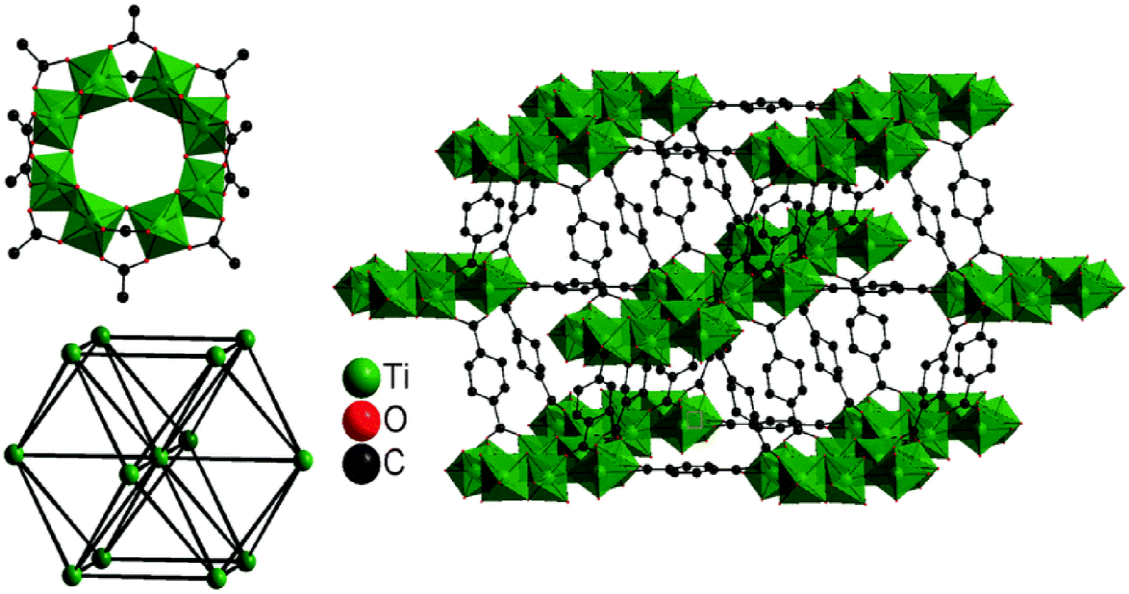

Figure III-2. Structure of MIL-125. Top left: $Ti_8O_8(OH)_4(CO_2)_{12}$ unit; right: crystal structure; bottom left: fcu topology. Reprinted with permission from reference 92.

To date, only a limited number of Ti-MOFs have been reported. The first crystalline Ti MOF based on carboxylate ligand are MIL-125 with a formula of $Ti_8O_8(OH)_4(O_2C\text{-}C_6H_4\text{-}CO_2)_6$.(Figure III-2) The structure of MIL-125 contains a Ti_8O_8 ring as inorganic building unit that is composed of eight TiO_6 octahedra connected by oxygen in a corner/edge sharing fashion. This SBU is almost identical in structure to that of the isolated cluster described above, with the exception of being linked by dicarboxylate ligands instead of being separated by monocarboxylate ligands. The wheel shaped Ti_8O_8 rings are further connected through twelve BDC linkers to form a 12-connected network. The arrangement of the 8-rings can be viewed as cubic centered packing and the overall

structure is simplified into a fcu topology. Two types of cages, distorted octahedral and tetrahedral cages respectively, are found in MIL-125.

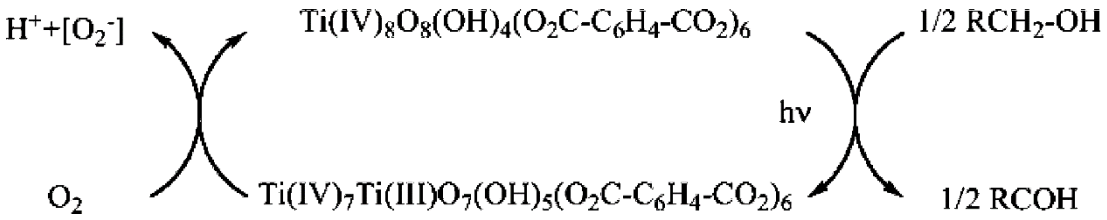

Figure III-3. Alcohol oxidation catalyzed by MIL-125 under UV radiation. Reprinted with permission from reference 92.

Interestingly, MIL-125 exhibits photocatalytic properties associated with Ti_8O_8 clusters.(Figure III-3) MIL-125 is able to oxidize adsorbed alcohols under UV irridation, giving rise to a photochromic behavior resulting from the generation of Ti^{3+}/Ti^{4+} mixed valence MOFs. The Ti^{3+} are back oxidized to Ti^{4+} in the presence of oxygen to close the catalytic cycle. The overall reaction is photocatalytic alcohol oxidation into aldehyde. This is indicative of the potential applications of MIL-125 as a MOF-based photocatalyst.[92]

3.3.2 MIL-125 Derivatives and Studies

Novel titanium MOF structures are rarely reported, but considerable efforts have been made to modify MIL-125 for photocatalysis.[93-95,98-100] The major disadvantage of MIL-125 for photocatalysis is its large band gap which limits its light absorption to the UV region. The visible light absorption of MIL-125 can be enhanced by replacing BDC with functionalized linker as photosensitizer. Walsh and coworkers reported the band-gap engineering of MIL-125 by ligand modification. Through a combination of synthesis and

computation, they demonstrate that the band gap of MIL-125 could be controlled by adopting linkers with different functional groups (-OH, -CH_3, -Cl). The band gap decrease was observed when the functionalized linker, NH_2-BDC(NH_2-BDC= 2-amino-1,4-benzenedicarboxylate), was used instead of BDC. The band gap change arises from donation of the N 2p electrons to the aromatic linking unit, resulting in a raised valence-band edge. The $(NH_2)_2$-BDC linker was predicted to further lower the band gap of MIL-125 to 1.28 eV, which was confirmed experimentally. This study illustrates the possibility of tuning the optical response of MOFs through rational design of the linker.[93]

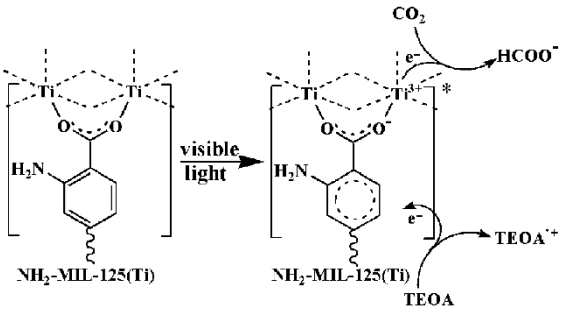

Figure III-4. Photocatalytic CO_2 reduction over NH_2-MIL-125 under visible light irradiation. Reprinted with permission from reference 95.

The NH_2-MIL-125 system behaves as an active photocatalyst under visible light irradiation. (Figure III-4) Li and co-workers demonstrate that the NH_2-MIL-125 can reduce CO_2 to formate anion under visible-light irradiation with TEOA (triethanolamine) as an electron donor. This work highlights the potential of MOFs as photocatalysts for the reduction of CO_2. Although the activity for the reduction of CO_2 over the NH_2-MIL-125

is still relatively low, highly efficient MOF-based photocatalysts for the reduction of CO_2 could be developed considering the variability of MOF structure and properties.[95]

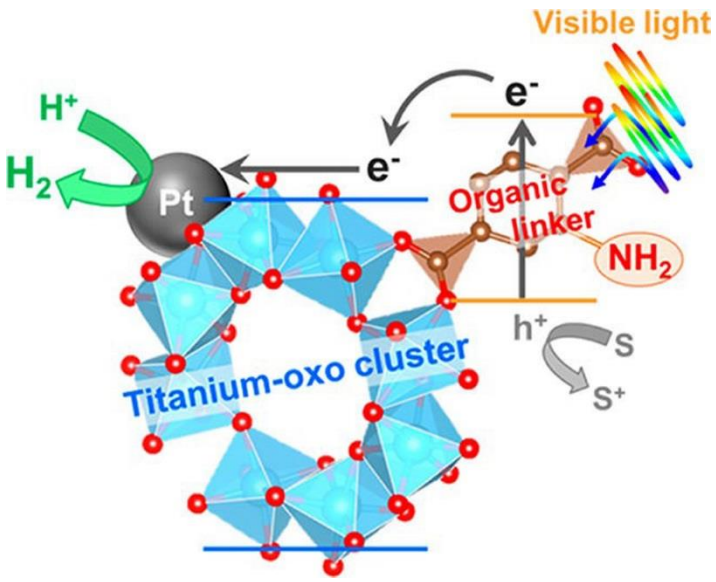

Figure III-5. Schematic illustration of photocatalytic hydrogen production reaction over Pt@ NH_2-MIL-125. Reprinted with permission from reference 94.

Subsequently, Matsuoka and co-workers demonstrate that NH_2-MIL-125 system behaves as an effective photocatalyst for visible light promoted hydrogen evolution reaction.(Figure III-5) Pt nanoparticles as cocatalysts are deposited onto NH_2-MIL-125 via a photodeposition process, giving rise to Pt@ NH_2-MIL-125. Pt@ NH_2-MIL-125 as a catalyst shows photocatalytic activity towards hydrogen production from an aqueous solution containing triethanolamine (TEA) as a sacrificial electron donor under visible-light irradiation. In this process, the organic linker is excited by visible light, and transfers electrons to the conduction band of the titanium-oxo cluster which generates hydrogen at

the presence of Pt hydrogen evolution catalyst. The longest wavelength available to drive the reaction is 500 nm.[94] In a following up work, the Pt@NH_2-MIL-125 demonstrated to be efficient photocatalyst towards nitrobenzene reduction. The photocatalytic activity was improved through the optimization of the deposition amount of Pt as a cocatalyst. In situ ESR measurements clearly indicate that the reaction proceeds through the electron transfer from the organic linker to deposited Pt through titanium-oxo clusters. This work offered new insight into the design of functional MOFs that have applications in the fields of photocatalysis.[98]

The selective oxidation of alkyl-substituted phenols, for example 2,3,6-trimethylphenol and 2,6-di-*tert*-butylphenol, with the clean oxidant H_2O_2 catalyzed by MIL-125 and NH_2-MIL-125 were also reported.[98] NH_2-MIL-125 can be further functionalized post-synthetically with dye-like molecular fragments. The new material (methyl red-MIL-125) exhibits improved light absorption over a wide range of the visible spectrum, and shows enhanced photocatalytic activity towards benzyl alcohol oxidation under visible light illumination.[99]

Besides photocatalytic applications, MIL-125 has also been investigated for its porosity and high-stability. The H_2S resistant NH_2-MIL-125 is studied for the concomitant elimination of CO_2 and H_2S from biogas and natural gas. The stability of MIL-125 can be enhanced by modification of its ligands. A methyl-modified MIL-125 using a tetramethyl benzene-1,4-dicarboxylate ligand (BDC-Me_4) shows significantly enhanced hydrolytic stability than unmodified MIL-125.[101]

The first Ti MOF based on carboxylate ligands (MIL-125) was published in 2009. The second Ti MOF was not reported until 2014 (NTU-9).[102] NTU-9 is based on single-atom Ti nodes and the DOBDC ligand (DOBDC = 1,4-dioxido-2, 5-benzenedicarboxylate). In this MOF, the Ti is chelated by an oxygen atom from the phenol group and another carbonyl oxygen on the adjacent carboxylic group, forming a 2D honeycomb-like layer. These layers are stacked along the c-axis, giving rise to 1D channels. NTU-9 displayed strong absorption in the visible region with a band-gap of 1.72 eV. Photoelectrochemical studies indicated that NTU-9 acts as a p-type semiconductor. Its catalytic properties were studied by the degradation of rhodamine B and methylene blue in aqueous solution under visible light irradiation.

3.4. ZIRCONIUM-BASED MOFS

The Zr based MOFs have attracted considerable attention in recent years. There are three advantages of Zr MOFs, which is the stability, predictability and diversity. The predominant advantage of Zr MOFs over other MOFs is their high stability. To date, lack of hydrolytic and chemical stability has hindered the performance of MOFs when subject to numerous adsorption/desorption cycles. However, some Zr MOFs are reported to be stable in water or even acidic conditions, while the stability under basic aqueous conditions is quite limited. Zr^{4+}, with high Z/r ratio, interacts strongly with the carboxylate ligands, which helps account for the excellent stability of Zr MOFs. Furthermore, the structure and topology of Zr MOFs can sometimes be predicted based on the expected SBU and the linker used.

The two difficulties that need to be overcome for this sort of rational design to be possible are as follows: First, the ligand conformation must be predicted, and second, the cluster structure must be controlled. The conformation of the ligand can be controlled by adopting rigid ligands. However, the cluster connectivity and symmetry can be hard to control as the structure of metal-oxo clusters can vary greatly. The Zr_6O_8 cluster is a unique building unit, as most of the reported Zr-MOFs are found to possess similar Zr_6O_8 clusters. This inorganic building unit is highly symmetric and robust, which facilitates the prediction of the resulting MOF structure.

In addition, the structure of Zr-MOFs can be varied based on adjusting connectivity between very similar Zr_6 clusters, with the unused coordination spots on the cluster being replaced with non-linking ligands like water or hydroxyl groups as necessary to balance charge, or even monocarboxylate ligands like acetic acid if any are used in the synthesis as modulating reagents. The connectivity of Zr_6O_8 clusters, unlike most of the metal-oxo clusters, can easily vary based on synthetic conditions. The connectivity of Zr clusters can be 12, 11, 10, 8, and 6, which adds to the diversity of Zr MOF structures.

3.4.1 UiO-66 and Derivatives

The first zirconium-based MOF to be discovered, and one of the most widely studied and used MOFs in the last several years, is the zirconium MOF UiO-66. [35] In the roughly 6 and half years between its publication in 2008 and the writing of this book, it has been cited over 180 times. A large proportion of those citations are either direct studies of various properties or adsorbed species or catalysts using UiO-66 or -67, or directly derivative MOFs consisting of the Zr_6O_8 SBU. A comprehensive evaluation of all the

research involving UiO-66 could easily fill its own book. It would be beyond the scope of this book to give a detailed description of each paper studying UiO-66 or its derivatives, but the most important and interesting results will be highlighted.

The high impact of the UiO-66 series is due to its porosity, ease of synthesis, low cost, and most importantly its extremely high thermal, chemical, and mechanical stability. As shown in Figure III-6, UiO-66 and its isoreticular derivatives are 12-connected frameworks with fcu topology, and can most simply be described as a cubic close packing(CCP) of linker-separated $Zr_6O_4(OH)_4(CO_2)_{12}$ SBUs, with tetrahedral and octahedral pores corresponding to the tetrahedral and octahedral holes of the CCP structure. This SBU consists of 8-coordinated zirconium atoms each coordinated by 4 carboxylate oxygens, 2 O^{2-} anions which are shared between 3 zirconium cations, and 2 OH^- anions also shared between 3 zirconium atoms. These SBUs are each surrounded by up to 12 linear dicarboxylate linkers. The $Zr_6O_4(OH)_4(CO_2)_{12}$ SBUs are hereafter referred to as Zr_6O_8 clusters, as 8 of the oxygens are incorporated in the cluster itself as opposed to being part of the carboxylate linkers.

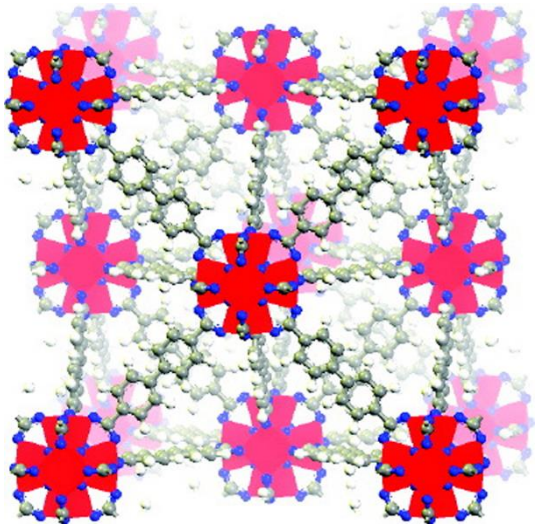

Figure III-6. The structure of UiO-67, an isoreticular derivative of UiO-66 distinguished by using a biphenyl dicarboxylate(BPDC) organic linker instead of UiO-66's benzene dicarboxylate(BDC) linker. Reprinted with permission from reference 61. Copyright 2008 American Chemical Society.

3.4.1.1 Stability of the UiO-66 Series

UiO-66 has a Langmuir surface area of 1167 m^2/g, while its extended-linker isoreticular derivative UiO-67 has 3000 m^2/g, and UiO-68 has 4170 m^2/g. It was initially reported that the higher surface area derivatives had the same stability as UiO-66, but it has been reported more recently that UiO-67 is less stable than UiO-66 to moisture or aqeuous media.[61,103] These more recent studies show that UiO-66 analogues can readily exchange ligands in dimethylformamide(DMF) or aqeuous solutions.[104] Post-synthetic exchange of BDC for hydroxyl-BDC or azido-BDC was observed, suggesting that thermodynamic, rather than kinetic, stability is responsible for the stability of UiO-66. Zirconium is water-soluble as $[Zr_4(OH)_8]^{8+}$ or other clusters and not monometallic aquo complexes, meaning that it is energetically unlikely to leave the cluster under aqueous

conditions. Facile Zr-carboxylate ligand exchange is plausible because d^0 metals like Zr^{4+} have no ligand field stabilization energy(LFSE). Ligand exchange rates depend on many factors including both charge density and on the electronic structure of the metal , so depending on the conditions Zr^{4+} may exchange a given ligand more quickly than, for example, Cr^{3+}, despite chromium's lower charge, due to d^3 chromium's LFSE increasing the activation energy for a ligand removal or displacement, which would disrupt the shape of the complex and the ligand field. [104,105] Due to its d^0 nature, Zr^{4+}'s square antiprismatic coordination in the Zr_6O_8 SBU can be changed to any other without loss of geometry-based stability.

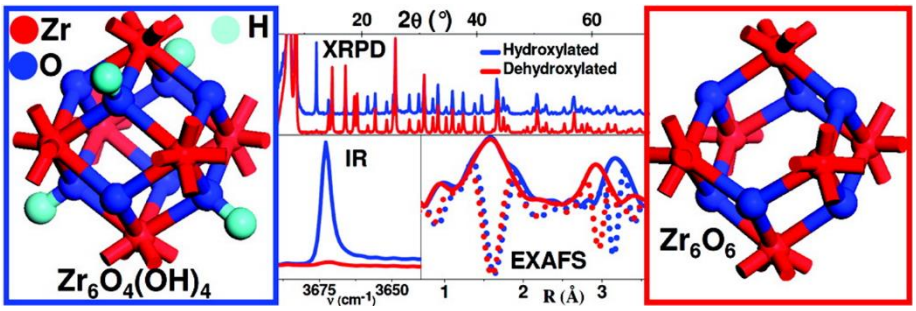

Figure III-7. The Zr_6O_8 can be dehydrated to form a Zr_6O_6 SBU of identical linker connectivity. Reproduced with permission from reference 58. Copyright 2011 American Chemical Society.

The Zr_6O_8 SBU is also interesting in that it can be dehydrated to form a similar Zr_6O_6 SBU in UiO-66 through the loss of two oxygens and four protons as shown in Figure III-7.[58] This does not change the overall charge of the cluster, but it does reduce the

zirconium coordination number to 7. This is an example of the mutability of this cluster that is explored in more detail in the porphyrinic zirconium MOF section below.

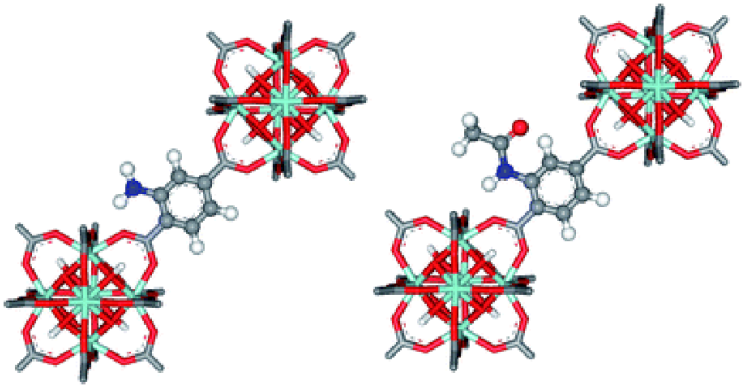

Figure III-8. Post-synthetic modification of UiO-66-NH_2 (left) with acid anhydrides leads to stoichiometric reaction with the amino functional group. The product formed with acetic anhydride is shown (right). Reprinted with permission from reference 106. Copyright 2010 The Royal Society of Chemistry.

Post-synthetic modification of UiO-66-NH_2 with acid anhydrides was demonstrated as shown in Figure III-8, but lower stability was observed in these modified frameworks.[106,107] Lowered thermal stability was also independently confirmed for UiO-66-NH_2 and UiO-66-NO_2, while UiO-66-Br had similar thermal stability to unfunctionalized UiO-66, with steric and electronic effects not rationally correlating with these changes in stability.[68] Chemical stability was tested by immersion in water, pH=1 (HCl), and pH=14 (NaOH) solutions for 2 hours. All derivatives were stable in acid, but only UiO-66-NO_2 was stable in base, with UiO-66-NH_2 showing complete and UiO-66 and UiO-66-Br showing partial amorphization. Conversely, a separate report showed

enhanced chemical stability and CO_2 uptake in a UiO-66 derivative using dimethyl-BDC as a ligand.[108]

3.4.1.2 UiO-66 Titanium Post-synthetic Exchange

Interestingly, UiO-66 has also been reported to be post-synthetically exchanged with Ti^{4+} without significant loss of surface area.[104,109,110] Substitution of the Zr^{4+} cation with Ti^{4+} increases the surface area and the overall pore volume as expected, because these measurements are gravimetric, and titanium is significantly lighter than zirconium. It was found that the pore dimensions actually decreased upon titanium exchange, and that the exchanges were not complete, with the highest reported exchange showing 56 wt% titanium loading with randomly exchanged sites. This partial loading still was able to drastically increase the affinity of the framework for CO_2 as shown in Figure III-9, due to the new, smaller pore size providing significantly increased adsorption enthalpy for CO_2.[110] Membranes made with partially exchanged Ti-UiO-66 also show greatly enhanced CO_2 permeability with retained selectivity when compared to Zr-UiO-66.[110] However, this field still requires more study to better understand structure property relationships.

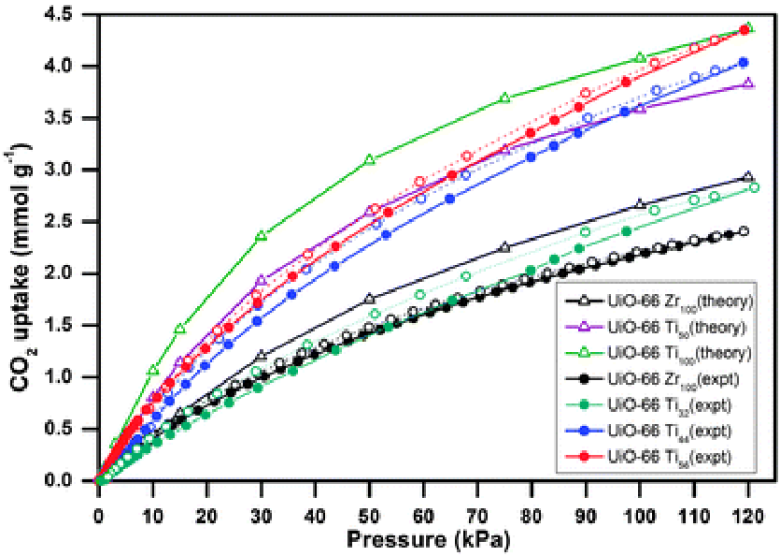

Figure III-9. The increased CO_2 uptake of UiO-66 after post-synthetic titanium exchange. Reproduced with permission from reference 110. Copyright 2013 The Royal Society of Chemistry.

3.4.1.3 The UiO-66 Series and Modulated Synthesis

An important note is that modulation of the MOF nanoparticules through the use of HCl or various carboxylic acids does not have to increase the crystal size, and can instead influence other properties like the measured surface area. This modulation has been used in many UiO-66 derivatives both to increase surface area and to create open metal sites for catalysis, as shown in Figure III-10.[111] No catalytic activity would be expected for a defect-free sample of UiO-66, as the Zr_6O_8 SBU is coordinatively completely covered with linker carboxylates and hydroxyl or water moieties. In this case, a combination of HCl and triflouroacetic acid(TFA) was used to increase the number of missing-linker defects in UiO-66, while producing crystals of the same size and shape as the non-modulated synthesis. The addition of HCl pushes the solution towards the

presence of more $ZrCl_4$ and protonated carboxylic acids. TFA, as a much stronger acid than acetic or benzoic acid, has a weaker conjugate base. Thus, it will not prevent nucleation as well as stronger competing carboxylate ligands, and will act as a weaker and more easily removed ligand, allowing its removal under harsh heating and vacuum.

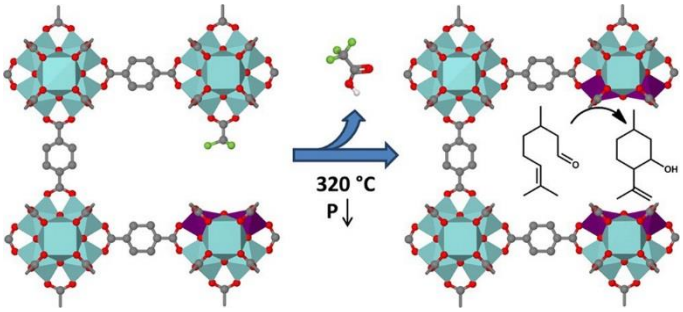

Figure III-10. UiO-66 modulated synthesis to increase surface area and catalytic activity. Reproduced with permission from reference 111. Copyright 2013 American Chemical Society.

Synthesis modulation using stronger monocarboxylic competing reagents has been shown to increase the size of the MOF crystals, even allowing the growth of single crystals suitable for X-ray diffraction, as shown in Figure III-11.[61] This work was the first example of single-crystal structures found for a zirconium MOF, and extension of the use of modulating reagents also allows the synthesis of MOFs that are not obtainable at all, even as crystalline powders, without it.[97] The amount of modulator must be carefully tuned to produce the desired size of MOF crystals, depending on the MOF system studied. It was hypothesized that the reason for large single crystals being formed of this system only after approximately 30 equivalents of benzoic or acetic acid were added was because at

these high levels of modulator, the formation of molecular zirconium benzoate complexes is favored. These complexes were then linked by BDC or BPDC linkers displacing the benzoate or acetate ligands, with more equivalents of modulator kinetically disfavoring the formation of the presumably thermodynamically favored MOF product. This results in few nucleation sites, which can then grow into large single crystals, and contrasts with the non-modulated synthesis where the zirconium is quickly ligated by linker molecules only, with many nucleation sites immedatiely forming and only the relatively weak solvent molecules as ligands to displace and allow correction of disordered or amorphous products.

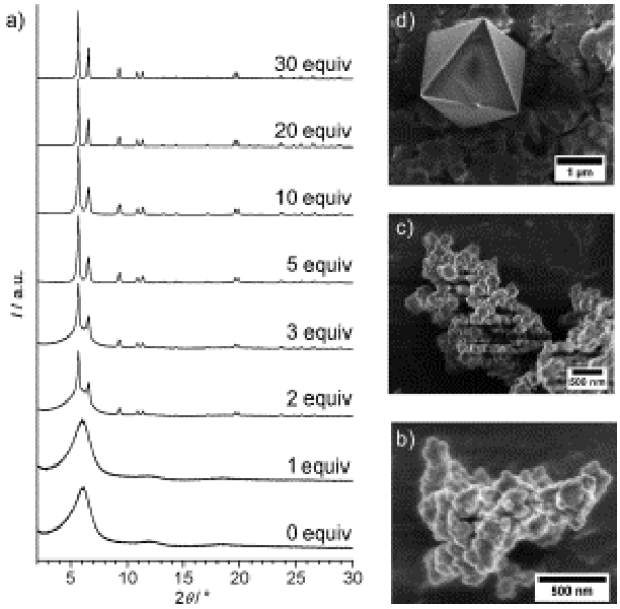

Figure III-11. UiO-67 prepared with b)no benzoic acid, c) 3 equivalents of benzoic acid, and d) 30 equivalents of benzoic acid. Reproduced with permission from reference 61. Copyright 2011 John Wiley and Sons, Inc.

However, significantly lowered thermal stability was found for UiO-66 single crystals synthesized with large quantities of competing monocarboxylate ligand. Later studies proved that this was due to the missing linker defects created by the disordered ligation of the SBUs by non-linker carboxylate ligands, as shown in Figure III-12.[84] Replacement of BDC linkers by TFA was shown to be energetically accessible at high TFA/HCl concentrations.[112] Furthermore, the number of these defects could be tuned with varying synthesis time and modulator concentration, with BET surface areas varying from 1000 m^2/g to 1600m^2/g for UiO-66 depending on the number of vacancies. However, the thermal and chemical stability of the MOF decreases as the surface area decreases, as missing linkers both lower the structural integrity of the MOF and expose the SBUs to an increased amount of interaction from non-linking species such as water that will destroy the framework upon sufficient substitution.

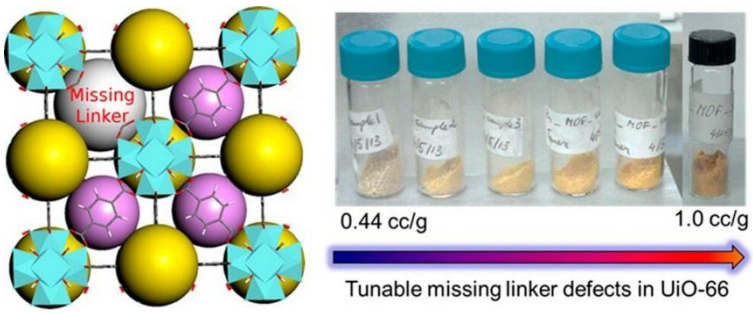

Figure III-12. The proportion of missing-linker defects in UiO-66 changes with amount of modulator used. Reproduced with permission from reference 84. Copyright 2014 American Chemical Society.

An extensive study of this behavior showed that UiO-66 synthesized at 220°C with a 2:2:1 HCl:BDC:Zr ratio produced a sample with a negligible amount of missing-linker defects.[113] This „ideal“ UiO-66 sample was far more thermally stable than samples synthesised at other temperatures and with other methods, losing crystallinity between 400° C and 450° C. The PXRD measurements used to determine this are more accurate measures of the thermal stability of a MOF than previously used methods such as the 540°C temperature reported originally reported for decomposition of UiO-66, as thermal gravimetric analysis(TGA) may not record significant weight loss at the temperature of framework breakdown and amorphization at which the crystal will lose its porosity.This report de-emphased the use of HCl, as opposed to the original report of UiO-66 which used no additional HCl or modulator, but it may have played an important role in the formation of the highly stable and crystalline „ideal“ UiO-66 samples, by aiding in the dissociation of BDC and altering the chemical equilibrium. The reproducibility of UiO-66 synthesis without HCl or other modulating reagent added has been inconsistent, and some UiO-66 derivatives are not synthetically accessible without HCl or modulator added.[114]

The use of HCl in the synthesis can affect the growth of the MOF crystals, both for reasons stated above and because HCl is produced as a biproduct of the synthesis, as what is left over when the ligands are deprotonated and the zirconium is dechlorinated.[115] An alternative synthesis using zirconium propoxide yields UiO-66 with no HCl needed or produced, but only in the presence of at least 15 equivalents of acetic acid. These conditions using acetic or benzoic acid produced a pH of between 1.3 and 4 necessary to

form UiO-66 with zirconium propoxide as a starting material. Interestingly, addition of HNO_3 until a pH of 1.5 is reached resulted in no product formed, indicating that the presence of a modulating reagent of some sort may be necessary for even microcrystalline UiO-66 formation from zirconium propoxide as opposed to $ZrCl_4$.[115]

Modulating reagents were also recently used to synthesize a MOF isoreticular to UiO-66 with a significantly *smaller* linker – a zirconium-based squarate MOF, ZrSQU, shown in Figure III-13.[116] This MOF was synthesized with the use squaric acid, $ZrCl_4$(or $HfCl_4$ to synthesize the Hf analogue), HCl and acetic or formic aicd in DMF at 110° C, and no crystalline material is able to be isolated without the presence of a high concentration of monocarboxylic modulator. When acetic acid is used as the modulator, the MOF shows a non-porous type II isotherm for nitrogen sorption, while when the smaller formic acid modulator is used, there is a type I isotherm corresponding to a surface area of 179 m^2 g^{-1}. However, both MOFs adsorb hydrogen. This indicates that while the modulating carboxylates both create missing linker defects, only the defects occupied by formic acid create windows large enough for nitrogen to pass, and shows that the pore and window sizes of the UiO-66 system can be tuned to be selective even for molecules like hydrogen and helium.

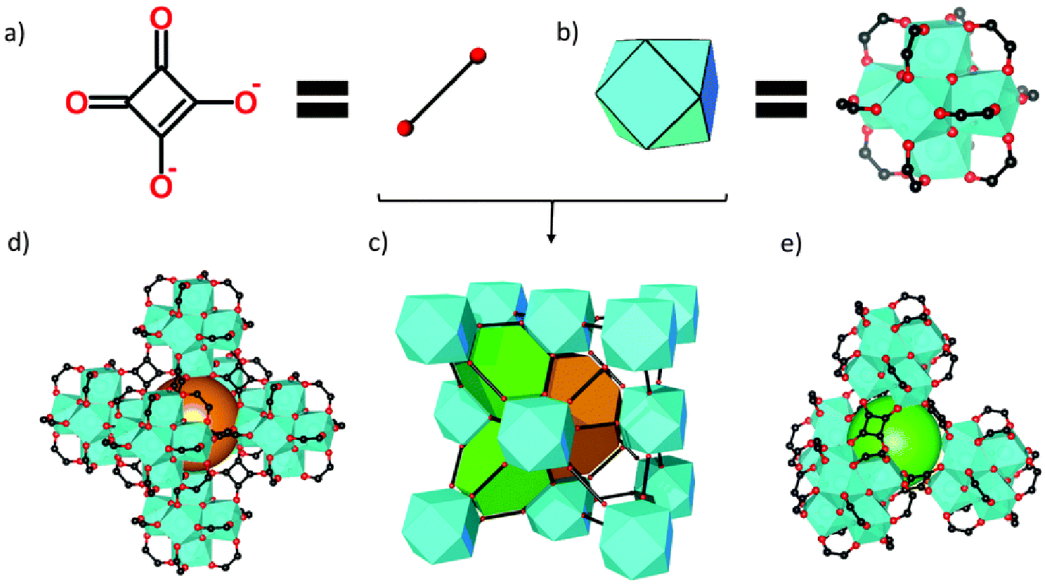

Figure III-13. Structural and topological representation of ZrSQU. SQU linkers (a) and $Zr_6O_4(OH)_4(C_2O_2)_{12}$ clusters (b) stack in an fcu-lattice (c), delineating octahedral (orange, d) and tetrahedral (green, e) cages with triangular windows. (Zr = blue; O = red; C = black). Reproduced from reference 116 with permission from The Royal Society of Chemistry.

3.4.1.4 UiO-66 Series Applications

UiO-66 and derivatives have been investigated for several applications common to MOFs. One investigated application for functionalized or titanium exchanged UiO-66 is the CO_2 uptake and permeability mentioned above for UiO-66 derivatives with smaller pores. These smaller pores result in a better size-match and heat of adsorption for CO_2 than that found in UiO-66, or larger derivatives. However, UiO-67 showed higher H_2 uptake at 77K than UiO-66, due to its higher surface area.[107] At 77K, the size match or heat of adsorption between the framework and a target sorbed molecule is less important than the raw surface area, as very little heat of adsorption is required to sorb even H_2 onto

any available surface area. However, at higher temperatures, heat of adsorption becomes more important, and UiO-67's large, open pores and open metal sites only accessible through missing linker defects that create even larger pores may not be a good match for small molecule adsorption.

Recently, several novel applications that are more specialized than the classic MOF gas sorption applications have been explored for functionalized UiO-66 derivatives. Using postsynthetic exchange, dihydro-1,2,4,5-tetrazine-3,6-dicarboxylate was partially exchanged with BDC in a sample of UiO-66. As shown in Figure III-14, this ligand undergoes a visible color change upon oxidation by the gases nitric oxide or nitrogen dioxide, making it useful as a sensor for oxidizing gases. It is reversibly reduced back to its original form by aqeous sodium dithionite, and can be reused without loss of MOF crystallinity or effectiveness.[117]

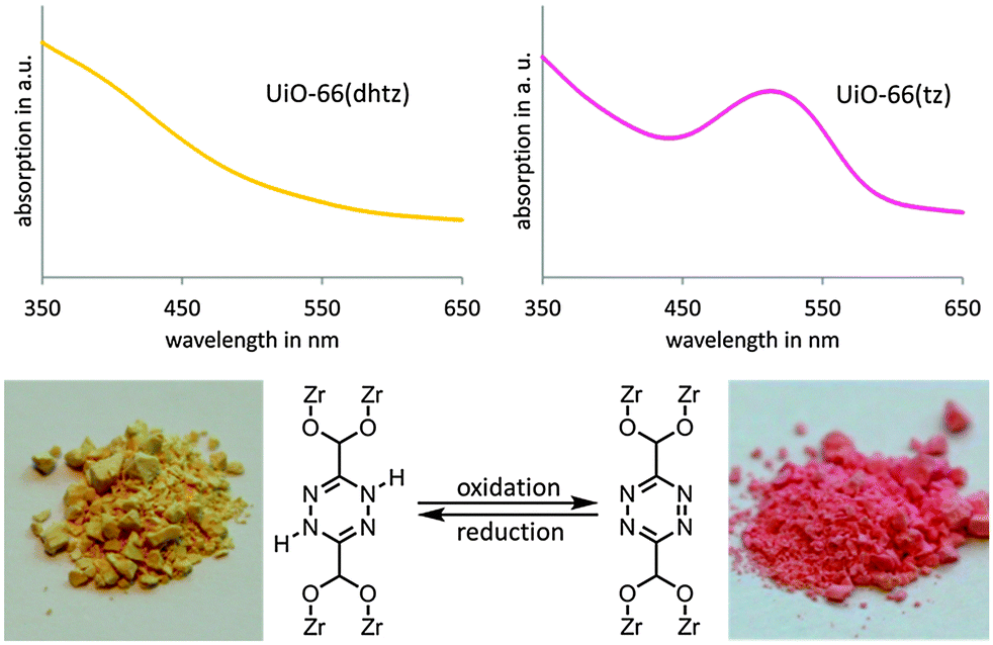

Figure III-14. Dihydro-1,2,4,5-tetrazine-3,6-dicarboxylate ligand exchange. Reprinted with permission from reference 117. Reprinted with permission from The Royal Society of Chemistry.

UiO-67 has been modified with a disordered partial loading of $PtCl_2(H_2bpydc)$ linkers to synthesize UiO-67-Pt(II/IV), as shown in Figure III-15. [118] This was achieved through 3 separate methods: one pot synthesis, premade linker synthesis, and postsynthesis functionalization, with highly crystalline products found for the products of premade linker synthesis and postsynthesis functionalization. Temperature stability was shown to be the same for each derivative, and reactivity was explored primarily by extended X-ray absorption fine structure(EXAFS) spectroscopy. $BpydcPt^0$, $bpydcPt^0(CO)_2$ dicarbonyl complexes, substitution of Pt-bound Cl- for bulky dithiol ligands, and $bpydcPt^{IV}Br_4$ products were all measured, showing the accessibility, reactivity, and stability of the bound platinum in the MOF.

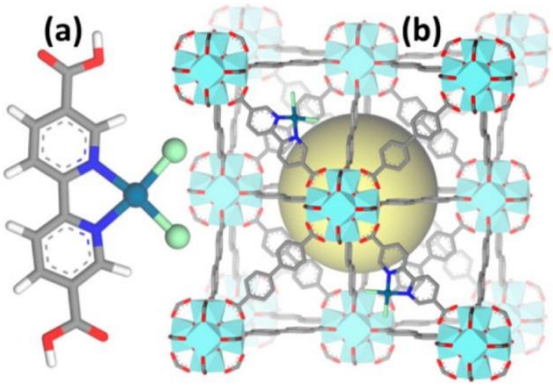

Figure III-15. UiO-67-Pt(II/IV) using $PtCl_2(H_2bpydc)$ linkers. Reprinted with permission from reference 118. Copyright 2015 American Chemical Society.

Uio-66, UiO-67, and UiO-66-NH_2 were investigated for sorption-based heating and cooling applications through measurement of their water adsorption isotherms. Materials with high H_2O stability and adsorption enthalpy will release that enthalpy as heat upon water adsorption if dry, and can take up heat energy from the environment, cooling it, to evaporate or desorb the water when wet. These effects can be exploited to create efficient heat pumping devices, especially if water adsorption takes place at low relative pressures, an effect that also requires high hydrophilicity and adsorption enthalpy.[119] High water adsorption enthalpy of around 120 kJ mol^{-1} at around 0.8 g g^{-1} loading, and water uptake occuring at low partial pressures below 0.2 p/p_0 were found for UiO-66-NH_2, but the maximum water loading fell significantly short of the total pore volume, due to hydrophobic domains in each MOF pore, but this effect is minimized in UiO-66-NH_2 due to the hydrophilicity of the amine moieties. However, though the PXRD of UiO-66-NH_2 remains crystalline after 40 adsorption-desorption cycles, the water and nitrogen adsorption capacity of the MOF steadily decreases with use, and at a faster rate

than the MIL-125-NH_2 also tested, as shown in Figure III-16. UiO-66-NH_2 is found to have a decrease in micropore volume of 42% and a decrease in total pore volume of 33% after 40 water sorption cycles. This indicates that UiO-66-NH_2, while relatively water stable, is not water stable enough for this application, especially when compared to MIL-125-NH_2, which only lost 3.6% of total pore volume over 40 sorption cycles. The increased hydrolytic stability of the Ti_8O_8-based MIL-125-NH_2over the Zr_6O_8 UiO-66-NH_2 is an interesting and important result that should inform further research into the relationship between MOF structures and their chemical stability. [119]

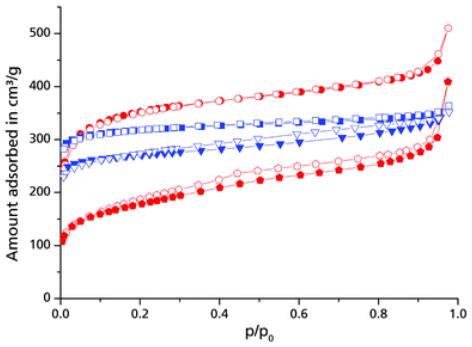

Figure III-16. N_2 ad-/desorption isotherms of H_2N-UiO-66 before (●) and after (⬟) the cycling procedure, and of H_2N-MIL-25 before (■) and after (▼) the cycling procedure. Adsorption is depicted with filled and desorption with empty symbols. Reproduced from reference 119 with permission of The Royal Society of Chemistry.

To contrast with the squarate-based MOF already described, a squaramide-incorporating MOF, UiO-67 functionalized with a squaramide-based moiety attached to the BPDC linker, was shown to act as a catalyst dramatically increasing the rate of several Friedel-Crafts reactions, as shown in Figure III-17.[120] This is an example of a recently

developed hydrogen-bond donating organocatalyst, which catalyze a wide variety of reactions which form bonds useful for organic synthesis.[121]

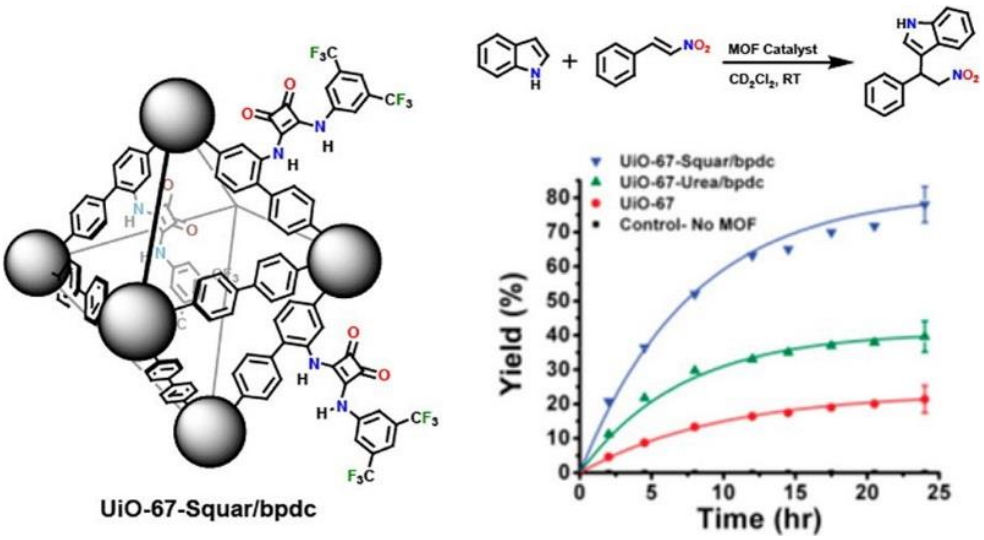

Figure III-17. (A) Reaction conditions for F-C reaction between indole and β-nitrostyrene. (B) UiO-67-Squar/bpdc (blue) shows drastically improved catalytic activity over UiO-67-Urea/bpdc (green) and UiO-67 (red). The MOF-free control shows no detectable yield (black). Reaction progress was monitored by ^{1}H NMR spectroscopy. Standard deviation at 24 h determined using multiple synthesized batches of respective MOFs. Product determined to be racemic by chiral HPLC. Reprinted with permission from Reference 120. Copyright 2015 American Chemical Society.

UiO-66 derivatives were recently tested for photocatalytic activity.[122,123]As described for titanium-based MOFs, the band gap of a MOF can be easily tuned by modification of the organic linker. Unmodified UiO-66 absorbs only in the UV region due to a LMCT, while UiO-66-NH_2 shows a strong redshift into the visible region between 300 and 450 nm, due to the nitrogen lone pair's ability to resonate through the benzene raising the energy of the ligand's HOMO and reducing the energy required for the

LMCT.[124] The photocatalytic oxidation of As^{3+} to As^{5+} in the presence of oxygen and simulated sunlight was tested, and as expected, the rate found for the oxidation was 0 in the absence of catalyst and/or oxygen. It was highest for the most electron-rich ligand, UiO-66-NH_2, and decreased linearly as the BDC-functionalizing group became more electron-withdrawing, as shown in Figure III-18.

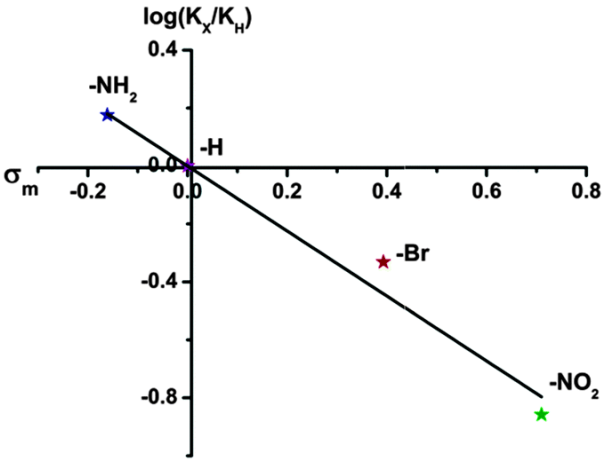

Figure III-18. Hammett plot for oxidation of aqueous As(III) with UiO-66-X (X = H, NH_2, NO_2 and Br) catalysts. Reproduced from reference 124 with permission of The Royal Society of Chemistry.

3.4.2 Zirconium Porphyrinic MOFs

We now move on to zirconium porphyrinic MOFs as an example to further explain the stability, predictability and diversity of Zr-MOFs. The tetrakis(4-carboxyphenyl)porphyrin (TCPP) ligand is a tetratopic linker with square planar symmetry. The connectivity and symmetry of Zr-clusters is highly variable. It can be a 12-connected truncated tetrahedron node, 8 connected tetragonal prism node or a 6-

connected hexagon node. A combination of the cluster node and the ligand node will result in different topologies. (Table 3.1) Some of the topology is not possible because of the limitation of bond angle and the ligand conformation. For the allowed topology, we would be able to get MOF structures (Figure III-19, Figure III-20).

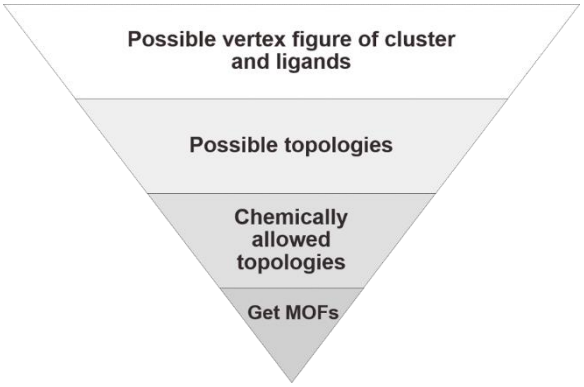

Figure III-19. Topology guided design of zirconium-porphyrin MOFs.

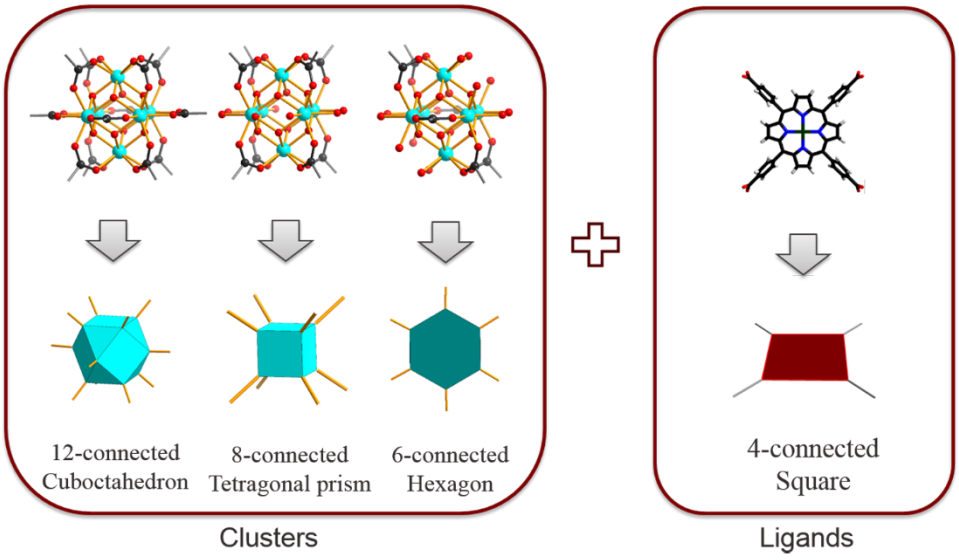

Figure III-20. Possible vertex figure of cluster and ligands.

Table III-1. Possible combinations of clusters and ligands

Node 1 (ligand)	Node 2 (clusters)	Topology	MOFs
Square	Cuboctahedron	ftw	PCN-221, PCN-228
Square	Tetragonal prism	csq	PCN-222
		scu	PCN-223
		sqc	PCN-225
Square	Hexagon	she	PCN-224

The combination of square and cuboctahedron nodes will give rise to ftw topology. (Table III-1) However, the Zr_6O_8 cluster and TCPP ligand cannot form a network of ftw topology because of the conformation of the ligand. In an ideal case, the benzene ring should be perpendicular to the porphyrin ring in TCPP ligand in order to eliminate the steric hindrance (Figure III-21a). However, in ftw topology, the benzene ring will be forced to a coplanar fashion with the porphyrin ring (Figure III-21 b). The strong steric hindrance prevents the formation of the ftw structure with Zr_6O_8 cluster and TCPP ligand. There are two possible ways to form the ftw topology. First, the connectivity of cluster could be changed. In this case, if the Zr_6O_8 cluster is replaced by Zr_8O_8, the benzene ring can be perpendicular to the porphyrin ring in TCPP ligand and the steric hindrance can be avoided. The resultant structure is nominated as PCN-221.[101] Another way is to elongate the TCPP ligand so that the benzene ring can rotate freely. We designed an elongated TCPP ligand, TCP-1, in which the carboxylate and the porphyrin ring is spaced with two

benzene rings. This design allows the peripheral benzoates to rotate freely to stay in the same plane as the porphyrin center without significantly increasing the inherent energy. The ligand can be further elongated; all of them form cubic crystals with ftw topology, namely PCN-228, PCN-229 and PCN-230 respectively[125]. A short time later, CPM-99 was reported which exhibits similar structure as PCN-228. A carbonized pyrolytic derivative of the Fe-porphyrinic version, CPM-99Fe/C, was shown to exhibit oxygen reduction reaction catalytic activity comparable to a 20% Pt/C catalyst while also demonstrating increased methanol stability and higher overall stability than the 20% Pt/C.[126]

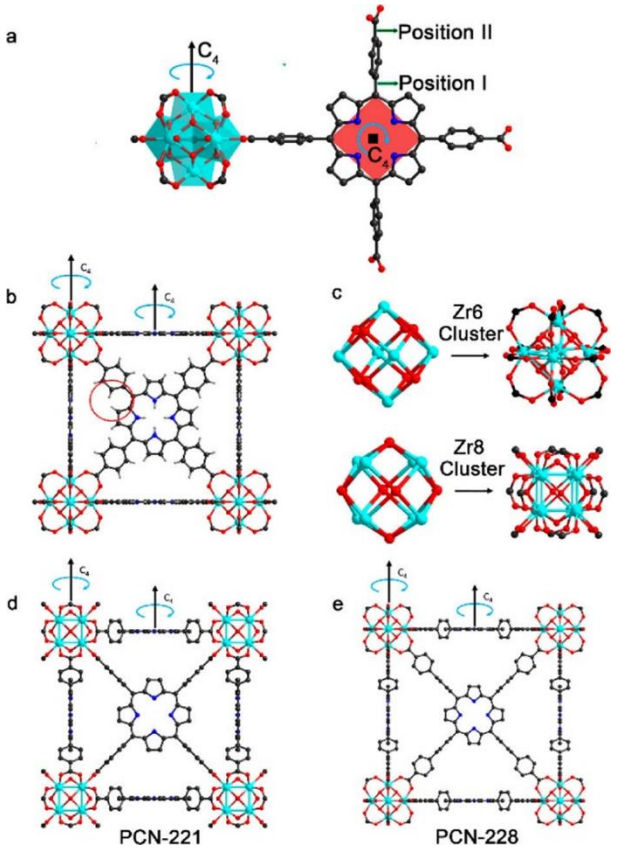

Figure III-21. (a) Representation of the connections of Zr_6O_8 and TCPP, and the sterically controlled phenyl and carboxylate angle. (b) Substitution of the Zr_6O_8 cluster and TCPP in ftw topology and the chemically forbidden conformation of ligand (highlighted with red circle). (c) Representation of the Zr_6O_8 and Zr_8O_6 cluster, and the 90° rotation of the carboxylate groups between these two clusters. (d) Structure of PCN-221 constructed with Zr_8O_6 cluster and TCPP. (e) Structure of PCN-228 constructed with Zr_6O_8 cluster and TCP-1 (ethyl groups were omitted for clarity). Reprinted with permission from reference 125. Copyright 2015 American Chemical Society.

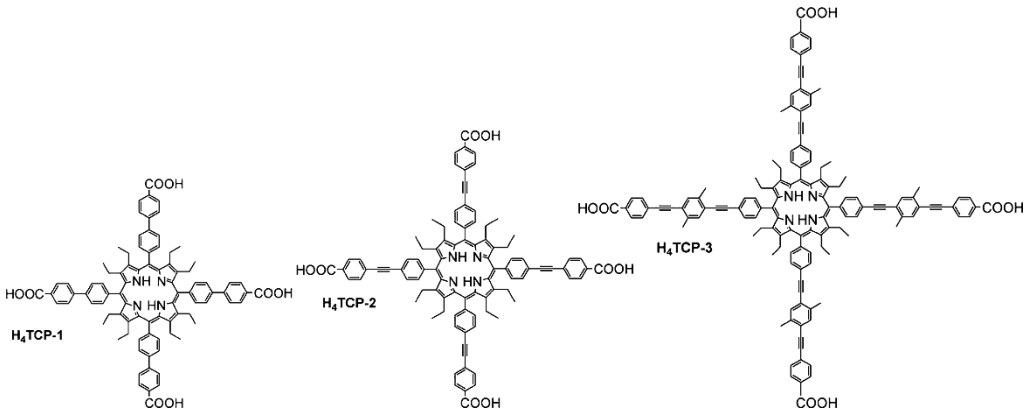

Figure III-22. Structure of elongated porphyrinic ligands. Reprinted with permission from reference 125. Copyright 2015 American Chemical Society.

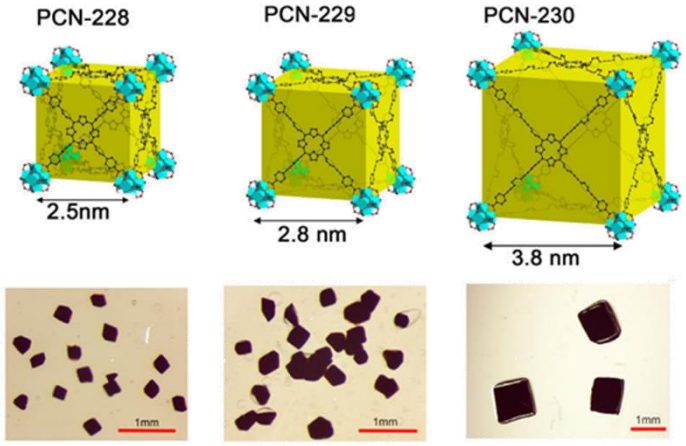

Figure III-23. Structure of MOFs with elongated porphyrinic ligands. Reprinted with permission from reference 125. Copyright 2015 American Chemical Society.

The connectivity of the Zr_6O_8 cluster can be reduced from 12 to 8. The vertex figure for 8-connected Zr_6O_8 cluster is tetragonal prism. The combination of square and tetragonal prism will give rise to csq, scu and sqc topologies, corresponding to PCN-222[14],

PCN-223[101] and PCN-225[64] respectively(Figure III-22, Figure III-23). It should be noted that the structure of PCN-223 can be viewed as a derivate from scu topology. PCN-223 is a disordered structure. The N_2 uptake indicates a small pore size which may attribute to the triangular channel. There is a way to simplify the disorder. First, the 8 connected Zr_6O_8 cluster with tetragonal prism symmetry forms a structure with scu topology. Then, the terminal OH of Zr_6O_8 clusters further react with carboxylate linker, giving rise to the installation of TCPP linkers in the rhombic channel. As a result, the overall structure has a shp-a topology with triangular channels. (Figure III-24)

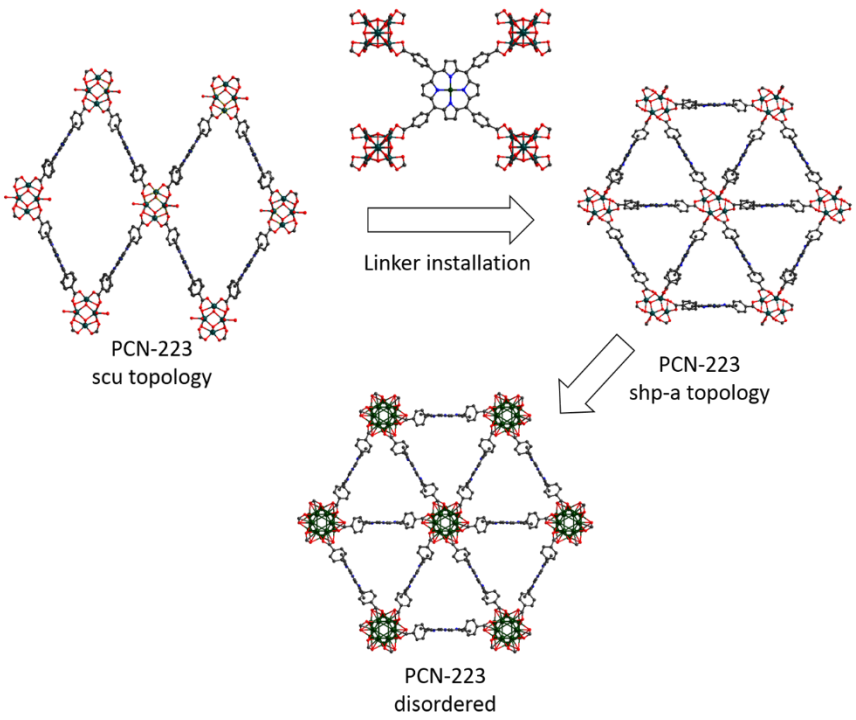

Figure III-24. The shp-a topology derived from scu topology by linker installation.

The connection number of Zr- clusters can be further reduced to 6. The vertex figure for 6 connected Zr_6O_8 cluster is a hexagon. The combination of a square and a hexagon will give rise to she topology corresponding to PCN-224.[127]

These porphyrinic Zr-MOFs obtained from variation of the synthetic conditions exhibit not only different pore sizes and shapes but also different chemical stabilities, which offer eligible candidates for different applications.

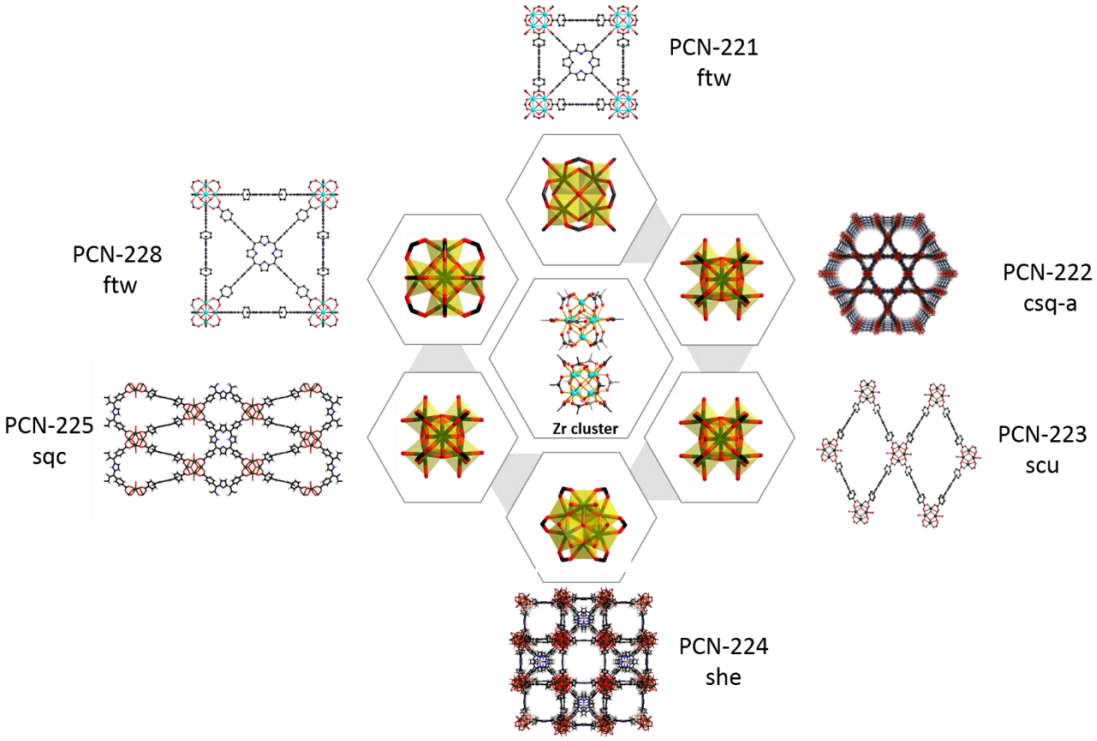

Figure III-25. Structure of zirconium porphyrinic MOFs.

PCN-221 is composed of 12 connected Zr_8O_6 clusters and TCPP linkers with a (4,12)-connected ftw topology. The Zr_8O_6 cluster features an idealized Zr_8 cube, in which each Zr atom resides on one vertex and each face of the cube is capped by one μ_4-oxygen atom. On each edge of the cube, a carboxylate from a porphyrinic ligand bridges two Zr atoms to afford a 3D MOF with a ftw topology, in which two types of polyhedral cages with diameters of ~1.1 and ~2.0 nm and a cage opening of ~0.8 nm are found. PCN-221 exhibits high surface areas and gas uptakes. With accessible active porphyrinic iron(III) centers, PCN-221 catalyzes the oxidation of cyclohexane with very high selectivity toward ketone and alcohol products.[101]

PCN-222 is composed of 8-connected Zr_6O_8 clusters and TCPP linkers with a (4, 8)-connected csq topology. (Figure III-25) A N_2 uptake of 1009 cm^3 g^{-1} (STP) and a Brunauer-Emmett-Teller (BET) surface area of 2200 m^2 g^{-1} have been observed for PCN-222(Fe). Evaluation of a density functional theory (DFT) simulation from the N_2 sorption curve indicates that there are two types of pores, with sizes of 1.3 nm and 3.2 nm, assigned to triangular microchannels and hexagonal mesochannels, respectively. The powder X-ray diffraction (XRD) patterns and N_2 uptake remain unchanged upon immersion in water, boiling water, as well as 2M, 4M, 8M, and concentrated aqueous HCl solutions for 24 h, confirming high stability. PCN-222 also exhibits biomimetic catalytic activities towards the oxidation reaction of pyrogallol. The active site of the catalyst is located on the inner wall of an open channel with a diameter of 3.7 nm and shows good activity for the oxidation of a variety of substrates. [14]

PCN-223 is a disordered structure. It contains the unprecedented D_{6h}-symmetric 12-connected Zr_6O_8 cluster, which gives rise to the shp-a network. The shp-a network can be viewed as a derivate of scu topology by installing TCPP linkers in the rhombic channels, giving rise to triangular channels. PCN-223 has uniform one-dimensional (1D) triangular channels with porphyrinic walls. With the highest connectivity among the Zr-MOFs, PCN-223 shows excellent stability in aqueous environments with pH values ranging from 0 to 10. A naked cationic iron(III) porphyrin center in PCN-223(Fe) is also generated that catalyzes the hetero-Diels-Alder (hDA) reaction between unreactive aldehydes and a diene in very high yield with excellent recyclability.[97]

PCN-224 is assembled with 6-connected Zr_6O_8 clusters and TCPP linkers with a (4, 6)-connected she topology. It not only exhibits the highest BET surface area ($2600 m^2/g$) among all the reported porphyrinic MOFs but also remains intact in pH = 0 to pH = 11 aqueous solutions. PCN-224(Co) exhibits high catalytic activity for the CO_2/propylene oxide coupling reaction and can be used as a recoverable heterogeneous catalyst.[127]

The combination between the 8-connected Zr_6O_8 cluster and TCPP linkers give rise to a MOF with two types of open channels, representing a (4,8)-connected sqc net. The MOF remains intact in both boiling water and aqueous solutions with pH ranging from 1 to 11, an extensive pH range for a MOF to remain stable. Given its exceptional stability and pH dependent fluorescent intensity, the MOF can potentially be applied in fluorescent pH sensing.[64]

3.4.3 Towards Rationally Designed Zr-MOFs

3.4.3.1 PIZOFs

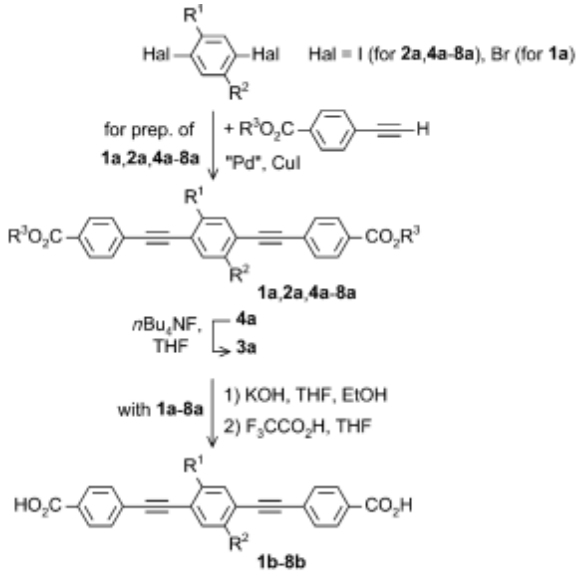

a,b	R^1	R^2	R^3	yield (%) of **a**	yield (%) of **b**
1	H	NH_2	Et	37	92
2	OMe	OMe	Et	96	92
3	OMe	OCH_2CCH	Et	75	79
4	OMe	$OCH_2CCTIPS$	Et	87	77
5	OPent	OPent	Et	78	73
6	dodec	dodec	Et	83	89
7	$O(CH_2CH_2O)_2Me$	$O(CH_2CH_2O)_2Me$	Et	80	86
8	OMe	$O(CH_2)_3$-furan	Me	96	96

Figure III-26. PIZOF ligands. Reprinted with permission from Reference 62. Copyright 2011 John Wiley and Sons, Inc.

By using the extended linkers $HO_2C[PE\text{-}P(R^1,R^2)\text{-}EP]CO_2H$, shown in Figure III-26, along with a modulated synthesis approach, the Behrens group synthesized a series of 8 porous interpenetrated zirconium organic frameworks(PIZOFs) of high chemical and thermal stability.[62] Their structure can be described as one elongated, isoreticular UiO-66

topology interpenetrated by an identical framework, with the SBUs of one framework occupying the tetrahedral holes of the other. This is similar to a sphalerite or diamond cubic structure except that the SBUs are linked to the 12 non-adjacent instead of the 4 adjacent SBUs, with the long, semi-flexible linear linkers bending to pass each other. This divides all pores into convex and concave tetrahedral shapes, seen in Figure III-27.[62] The PIZOF series possesses a BET surface areas similar to that of UiO-66, such as 1250m^2/g for PIZOF-2, while having slightly reduced thermal stability(350°C) and similar chemical stability to that of UiO-66 or UiO-67.

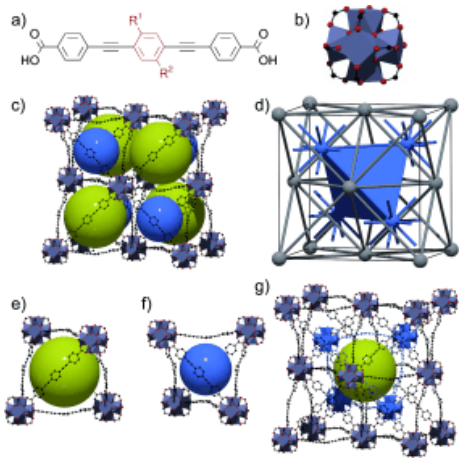

Figure III-27. The PIZOF structure, which consists of interpenetrated fcu topologies. Reprinted with permission from Reference 62. Copyright 2011 John Wiley and Sons, Inc.

3.4.3.2 Zr(IV) based metal–organic frameworks with intentionally altered topology

As the fcu topology of the UiO-66 series has tetrahedral and octahedral pores gated by windows of limited size, it is not suitable for the adsorption of large guest molecules.

For example, UiO-66 was reported to trap benzoic acid molecules used as a modulating reagent, which could not be removed after synthesis and reduced the thermal stability and the surface area of the resulting MOF.[61] To synthesize a MOF with the stability imparted by the Zr_6O_8 SBU with larger windows and thus the ability to incorporate or remove larger guests, the topology should be altered by changing the symmetry of the linker or SBU. This was accomplished in DUT-51(Zr) and (Hf), topologically and chemically identical frameworks synthesized from the reaction of the metal tetrachloride, the bent dithieno[3,2-*b*;2′,3′-*d*]thiophene-2,6-dicarboxylate (DTTDC) linker, and benzoic acid in DMF at 120°C for 72 hours. The reduction in linker symmetry, combined with the presence of non-linking benzoic acid allows the Zr_6O_8 unit to form an 8-connected SBU and a structure of reo-topology found through single-crystal XRD, shown in Figure III-28.[69]

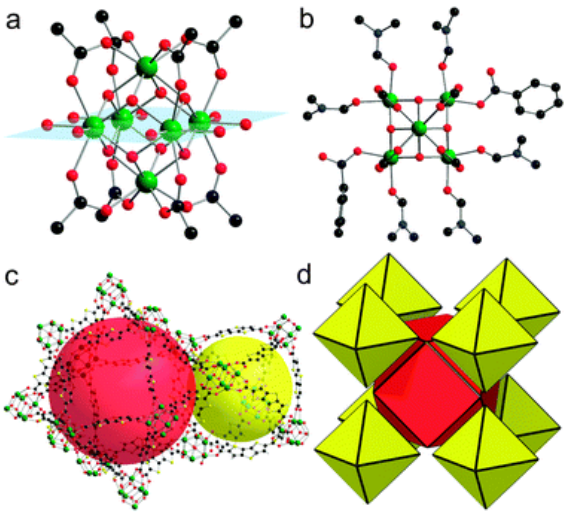

Figure III-28. DUT-51(Zr) and (Hf). Reprinted with permission from Reference 69. Copyright 2012 of The Royal Society of Chemistry.

This structure has fewer ligands per unit volume than a similar 12-connected structure would, and thus the windows leading into its large 15.6 Å octahedral and 18.8 Å cuboctahedral pores are larger, allowing the adsorption of large dye molecules such as rhodamine 6G, Nile red, and brilliant green. A BET surface area of 2335 m^2g^{-1} was calculated from nitrogen adsorption isotherm measurements, and high water stability was confirmed by checking PXRD after soaking the MOFs in water for 12 hours.

3.4.3.3 NU-1000

As in PCN-222/MOF-545 described in the porphyrin-based Zr-MOF section, the combination of a 4-connected square node with the bridging carboxylates perpendicular to the plane of the square and the adaptable Zr_6O_8 SBU will produce a framework with a tetragonal-prism 8-connected Zr_6 SBU of csq, scu, or sqc topology, depending on the tuning of the modulating reagent and other synthesis conditions. [21,128] To design a MOF suitable for gas phase metalation with aluminum, Mondloch et al. chose this system, which has mesoporous channels, is highly stable, and possess crystallographically ordered Al-functionalizable groups such as the terminal hydroxyls on the Zr_6O_8. The 1,3,6,8-tetrakis(*p*-benzoicacid)pyrene (H_4TBAPy) ligand was designed to symmetrically suitable, and when reacted with $ZrCl_4$ and benzoic acid in DEF single crystals of NU-1000 were isolated, with powder product obtained from the reaction in DMF.[129] NU-1000 has the same topology as PCN-222, replacing the porphyrin ligand center with a pyrene center, and it possesses a BET surface area of 2320 m^2 g^{-1}. After activation to replace benzoic ligands with the terminal hydroxyls needed, Atomic Layer Deposition(ALD) was used to deposit zinc or aluminum within the channels. Diffuse reflectance infrared fourier

transform spectroscopy(DRIFTS) measurements were used to confirm that the loaded metals reacted with hydroxyl groups. The MOFs containing the deposited aluminum or zinc were then used as Lewis acid catalysts for the Knoevenagel condensation to confirm their presence, activity, and lack of leaching after filtration.

The NU-1000 system, as a convenient platform for deposition of many different chemical species, has undergone extensive investigation. Solvent-assisted ligand incorporation(SALI) was explored as a method to further functionalize NU-1000. In the original synthesis of NU-1000, benzoate ligands were removed to facilitate their replacement by metal-functionalizable hydroxyl groups. After removal of the benzoate ligands, these sites can then be replaced by over 30 other carboxylic functional groups as shown in Scheme 1.[130]

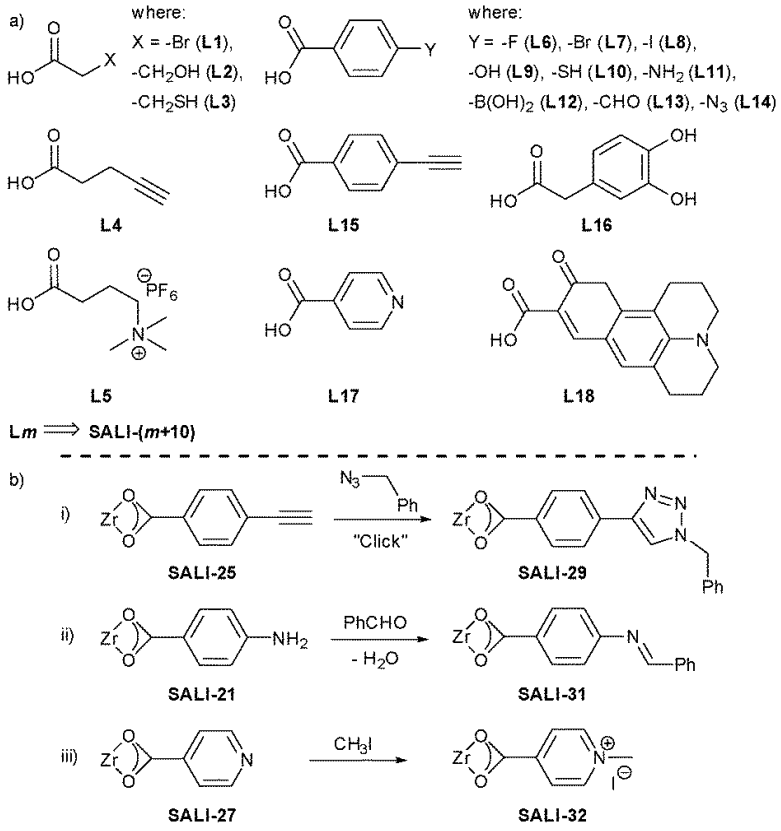

Scheme 3.1. a) Carboxylic functional groups (CFGs) incorporated through SALI into NU-1000; (b) secondary functionalization reactions: (i) "click", (ii) imine condensation and (iii) methylation, involving SALI derivatives of NU-1000. Reprinted with permission from Reference 130. Copyright 2014 of The Royal Society of Chemistry.

In this way, it has been shown that the mesoporous channels of NU-1000 can be functionalized with a vast variety of functional groups and functionalities, whether organic or metallic. It has also been functionalized with phosphonate ligands in addition to the carboxylate-based ligands shown above.[131] There is typically increased binding strength of phosphonates to zirconium compared to carboxylates.[132] This enables both increased stability for the incorporated ligands and the possibility of sequential incorporation of a phosphonate and then a carboxylate-based ligand. Interestingly, the MOF framework itself

collapses in the presence of an excess of phosphonate-based ligand, as the tridentate phosphonate ligand may begin to take the place of the framework TBAPy ligands. The phosphonate ligation mode, as compared to the carboxylate ligation, is shown in Figure III-29.

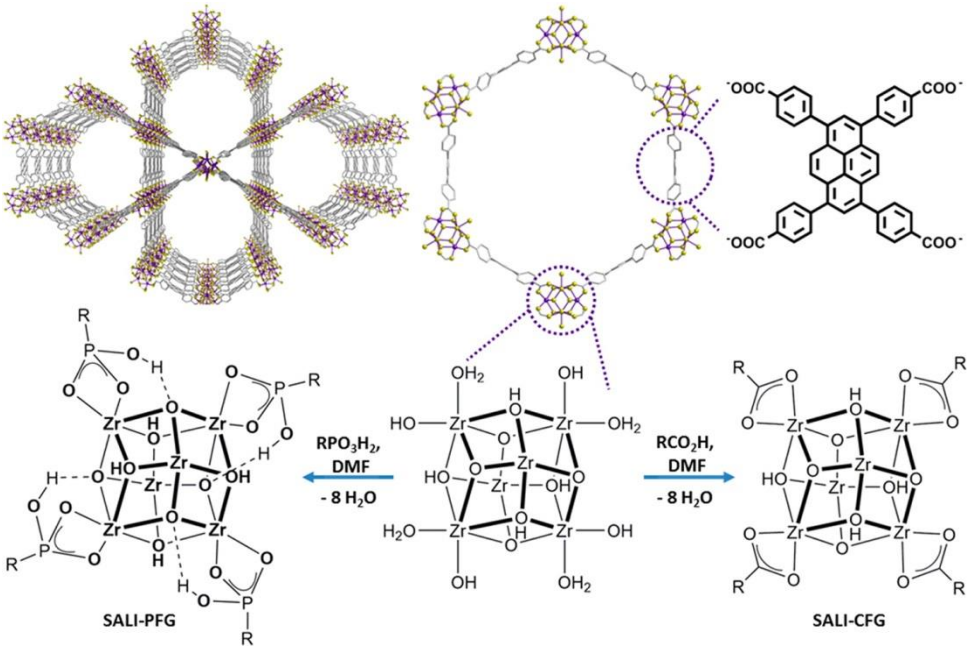

Figure III-29. Molecular Representations of NU-1000(top) and Depictions of Solvent-Assisted Ligand Incorporation (SALI) (bottom). Reprinted with permission from Reference 131. Copyright 2015 American Chemical Society.

3.5 SUMMARY AND CONCLUSIONS

Group 4 metal-based MOFs have been extensively studied in recent years due to the ease of their synthesis combined with their high thermal and chemical stability. In this chapter, we have been able to cover only a small fraction of the great number of published

relevant MOFs, but we hope we have been able to show a representative sample of the materials exhibiting the varied applications and properties common to titanium, zirconium, and halfnium-based frameworks. The few reported titanium-based MOFs are extremely promising due to their stability, which is in some circumstances measurably higher than that of similar zirconium based MOFs, and their promising photocatalytic applications. [119] Difficulties in their synthesis may soon be resolved by KTDA, modulated synthesis, or post-synthetic exchange strategies, such as was used to produce Ti-UiO-66. [104,109,110]

Meanwhile, the booming field of zirconium MOF development produces new advances on a continual basis, due to the ability of modulated synthesis to produce highly stable and crystalline zirconium MOFs with high variation in SBU shape and connectivity, in addition to the continuing development of the field of linker design and modification. Increasing knowledge of these factors, in addition to the study of how Zr-MOF structure, stability, and sorption and catalytic properties are related, has begun to produce an environment where rational choice of structural components can be made to explore desired functionality.

CHAPTER IV

POROUS CARBONS FOR HYDROGEN STORAGE[3]

4.1 OVERVIEW

Porous carbon-based materials are promising candidates as adsorbents to increase the gravimetric and volumetric uptake of hydrogen at cryogenic temperatures and moderate pressures. In most cases, this uptake increases linearly with surface area, but strategies to increase uptake beyond that predicted by this "Chahine rule", to increase surface area, and to otherwise improve these materials are discussed.

4.2 INTRODUCTION

In this chapter, we will summarize recent progress in the storage of hydrogen gas in porous carbon-based materials through physical or chemical interactions. The class of materials is diverse and consists of porous polymer networks (PPNs), porous organic polymers (POPs), graphene oxide frameworks (GOFs), activated carbons (ACs), metal-organic framework (MOF), derived carbons (MDCs) and other carbon class of nanomaterials. Recent advancements in preparation of these porous materials with ultrahigh surface areas makes them viable candidates for hydrogen storage, especially at low temperatures (T<123K; P>25 bar) where the weak intermolecular forces inherent to

[3] Reused with permission from "Porous Carbons for Hydrogen Storage. In *Nanostructured Materials for Next-Generation Energy Storage and Conversion*", Bosch, M.; Zhou, H.-C.: Springer-Verlag GmbH Germany, 2017. Copyright 2017 Springer-Verlag GmbH Germany

all physisorption phenomena, such as adsorption of hydrogen. This approach to hydrogen storage promises high gravimetric hydrogen uptake at higher temperature; distinct to cryogenic storage approach (≤ 123 K), which require cooling with nitrogen (77 K) or argon (87 K) and a resultant insulation capsule. Room temperature (≥ 123 K) interactions occur because, the adsorption forces of the hydrogen to the pockets, surfaces, and functional groups are carefully chosen to maximize intermolecular forces between the hydrogen molecules and material. Thus, it is essential to maximize the adsorption enthalpy of any porous material for hydrogen storage, because, for the use of these materials to be economical, requires cooling temperature close to room temperature to avoid additional costs in materials and weight. For this reason, special consideration will be given in this overview to attempt to increase the adsorption enthalpy of hydrogen in engineered porous materials at higher than cryogenic temperatures.

These materials are engineered to meet the current US Department of Energy (DOE) 2020 performance targets for hydrogen storage materials, namely, materials that can store 5.5 weight-percent (wt %) of hydrogen for the gravimetric target, 0.040 kg hydrogen / L for the volumetric target, and at $333/ kg stored hydrogen capacity for the cost target. It should be noted that this target is for the complete storage system "including the tank, storage media, safety system, valves, regulators, piping, mounting brackets, insulation, added cooling capacity, and any other balance-of-plant components," not just the porous material, so the material must have a significantly higher capacity. This DOE benchmark essentially excludes all organic synthesis requiring many steps or resulting in low yields, or use of anything other than low-cost bulk commodities. This is where porous

polymers may have an advantage over materials such as metal-organic frameworks (MOFs) or metal-hydride based materials, that require expensive components, and expertise, whereas with carbon-based polymers can potentially be synthesized at a much lower cost, depending on the synthesis steps chosen, with a lower skill-set once the methodology has been perfected.

4.3 ADSORPTIVE HYDROGEN STORAGE

4.3.1 The Chahine Rule

Most of these materials have a total hydrogen storage capacity that linearly scales to their surface area, based on the physisorption interactions. Experimentally, it was found that most materials with optimum pore size of 7 Å stored about 2 wt% H_2 per gram of material per 1000 m^2/g surface area at 77 K. At higher temperature, this storage dropped to 0.35 wt% per 1000 m^2/g surface area at 120 bar pressure at 298 K; which was not greatly influenced by an increase in pressure, for example almost trebling the pressure, gave a new storage value of 0.45 wt% per 1000 m^2/g surface area at 300 bar hydrogen pressure. This phenomenon is known as the "Chahine rule".[133] It should be noted that this rule is only applied to materials that have pores appropriate to the size of hydrogen in the low Ångström range (Å). Porous materials with large open pores (≥ 10 Å) and a high surface area (≥ 6000 m^2/g) as measured by nitrogen (N_2) adsorption (77 K) may not have as high H_2 uptake as calculated, as H_2 may not condense into these pores as easily as N_2. Current porosity materials areas in the range of 4000 - 7000 m^2/g surface area,[23] less than what is required to meet the 2020 DOE targets using physisorption at room temperature alone

using porous materials. Most research focuses on materials with high hydrogen gas (H_2) uptake at 77 K. As some of these materials reach hydrogen sorption saturation or near saturation at 77 K at high pressure, while none reach saturation at (293 K) room temperature. Therefore, an intermediate temperature may be suited to sorption, higher than cryogenic temperatures but lower than room temperature.

In general, hydrogen uptake at 77 K and 1 bar (100,000 Pa ≈ 750.06 Torr or mmHg) was found to be linearly related to the hydrogen uptake at 298 K and 100 bars in porous adsorbents, (Figure IV-1 for plot of adsorption versus temperature) with uptake occurring mostly in extremely small micropores, under either (77K or 298 K) set of conditions.[134] This occurred across many different types of adsorbents, as long as those adsorbents were primarily microporous in morphology. In contrast, the adsorbents with larger pores had relatively high uptakes at 77 K, but showed small uptakes, below 0.5 wt% at 298 K and 100 bars pressure. Clearly, hydrogen is able to be adsorbed into larger pores but only at low temperature. However, the porous materials with the highest overall surface area also have relatively larger pores, and are not suitable for hydrogen adsorption at higher temperatures. To improve hydrogen adsorption at higher temperatures, materials must be designed with maximum pore volume and surface area, but also, pore size optimized to hydrogen uptake at the temperature and pressure allowed. A material with optimal hydrogen uptake at 77 K and 1 bar is not likely to be the best material at 77 K at 100 bars or 298 K and 100 bars of pressure. Under the conditions in Figure IV-1, only pores below 1 nm diameter contribute significantly to hydrogen uptake, unlike at 77 K and 100 bars where hydrogen can adsorb efficiently into larger pores.[134]

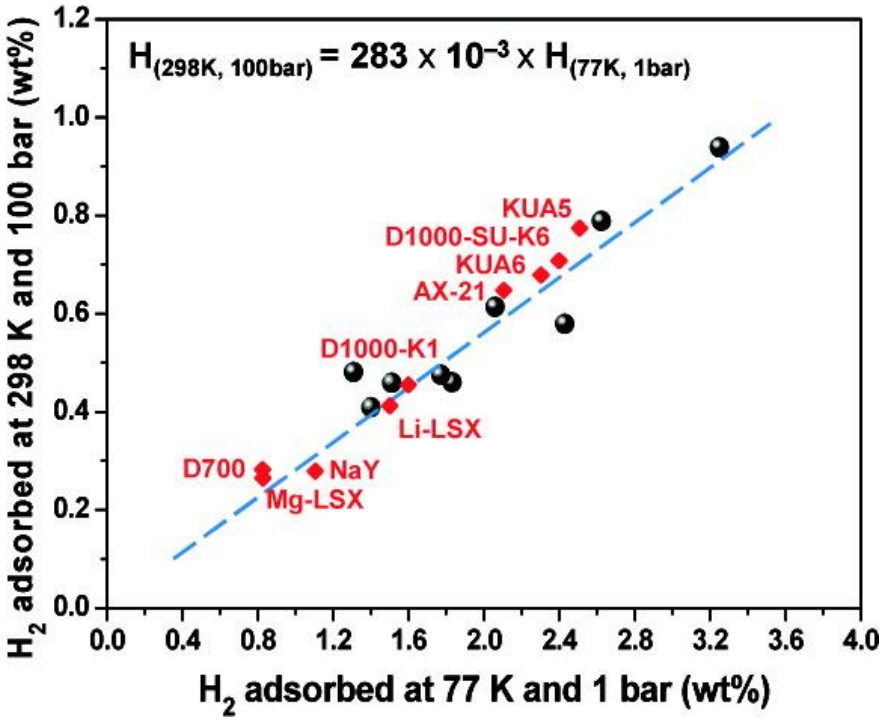

Figure IV-1. A linear relationship between hydrogen uptake at 77K, 1 bar, and 298K, 100 bar. Reprinted with permission from 134. Copyright 2012 American Chemical Society.

4.3.2 Deliverable (or Working) Capacity

Deliverable capacity is the difference in hydrogen uptake between a low and high-pressure (e.g. 1-100 bars) environment and is more important than total capacity for most hydrogen storage applications. Depending on the material used, some amount of hydrogen will remain in the material at a low pressure, and unless the material is re-activated by heat, vacuum, or some other input of energy to remove it, that amount of hydrogen cannot be used as a fuel source. In this manner, the deliverable capacity is less than total capacity, and is a more practical consideration. An analysis of isotherms at different pressure levels

can yield information on adsorption capacity but materials with high total uptake at very low pressure may not yield a practical deliverable capacity.

4.3.3 BET Surface Area

The Brunauer–Emmett–Teller (BET) method can over-estimate the surface area of highly microporous materials, due to quasi-capillary condensation occurring at a P/P_0 range of 0.1-0.3 (where P and P_0 are the equilibrium and the saturation pressure of adsorbates at the temperature of adsorption) although analysis applied below this region is expected to give valid results.[135] This is of critical importance for hydrogen sorbents, which often have very small pore sizes. At a temperature below the critical temperature, many molecular species may condense into a liquid form inside the pores. This phenomenon occurs normally in type II and Type IV of the pressure-temperature isotherms. But in materials with microporous pockets that have very high affinity for N_2, adsorption occurs at a very low pressure, lower than the isotherm calibration, giving rise to a higher standard error.

The BET calculations can further over-estimate the surface area of materials that have pores 1 nm or larger, "due to the overlap of pore-filling and formation of monolayer-consisting of these two types of pores."[136,137] The BET surface area calculations attempt to estimate the monolayer loading, where low-pressure pore-filling nitrogen adsorption is "counted" as monolayer-formation adsorption and used to determine the surface area. For example, for graphene-slit pores, a diameter of 13.2 angstroms drastically overestimates surface area due to inclusion of second-layer molecules in the monolayer regime (see Figure IV-2 for conceptual model of hydrogen adsorption) where H_2 uptakes are also

susceptible to experimental error if appropriate control and checks in the experimental setup are not properly implemented.[138]

In general, the porosity or uptake behavior of a material cannot be described adequately by one or two parameters. Complete porosity data would include multiple gas loading isotherms at a variety of temperatures and as pressures ranging from zero until saturation is reached, if possible. "BET surface areas should always be given with the range used for analysis."[139] In most cases, this is not the case, and hence BET surface areas must always be assumed to be provisional. In all cases, BET surface area results are less informative than complete H_2 (or other gas of interest) and N_2 uptake isotherms, which should be examined for isotherm type, total uptake values, and saturation.

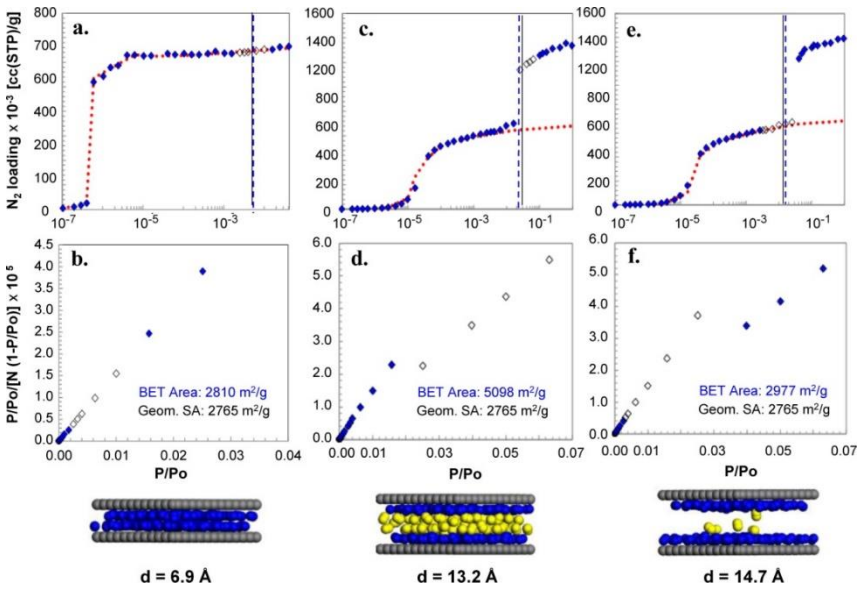

Figure IV-2. Even when all BET consistency criteria are applied, calculated surface area can differ dramatically from calculated "true" nitrogen accessible surface area in certain types of pores. Reprinted with permission from 5a. Copyright 2015 American Chemical Society.

4.4 POROUS CARBONS WITH HIGH HYDROGEN UPTAKE

4.4.1 Activated Carbons

The theoretical maximum hydrogen adsorbed per surface area in a monolayer on the pore surfaces on a porous material is 2.28 wt% per 1000 m^2/g, assuming a surface density identical to liquid hydrogen. At 77 K, various activated carbons and single-walled carbon nanotubes (SWCNTs) of various dimensions, exhibit a surface area that is quasi-proportional to surface area, as determined from the gradient. An analysis of the plot reveals an average adsorption per surface area of 1.91 mass% per 1000 m^2/g, analogous to 84% surface coverage. At room temperature, this coverage was only 0.23 mass% per 1000 m^2/g or 10%.[133] These materials did not show changes in hydrogen adsorption

between SWCNTs and conventionally produced activated carbons. (Figure IV-3) The best conventionally prepared activated carbons have surface areas lower than MOFs, leading to a further development of high surface area materials based on porous carbon.

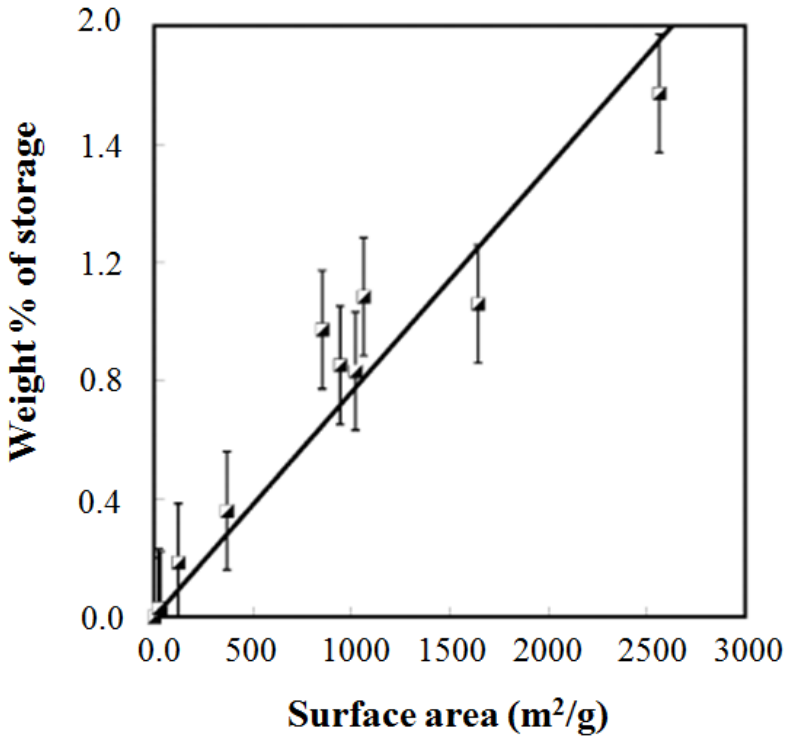

Figure IV-3. Weight % storage of activated carbons versus surface area at 77 K. The best fit line for the experimental values roughly describes the Chahine rule. Reprinted with permission from 133. Copyright 2005 Elsevier Ltd.

In general, carbon materials may be activated and made porous through "chemical activation" by reactive liquids, solids, or solvated species that can oxidize and remove some of the carbon at high temperature in an inert gas, or through "physical activation" with gasses or gas mixtures. The precise method of activation, in addition to the carbon feedstock, can influence the porosity, pore size distribution, and degree of graphitization

or oxidization of the resulting porous carbon.[140] Direct physical activation in the air tends to result in mesopore formation and surface area of only 700 m^2/g,[141] unsuitable for hydrogen storage. However, when already porous titanium carbide (TiC)-derived carbon was further activated in carbon dioxide (CO_2), a surface area of 3100 m^2/g was achieved.[142] In general, chemical activation is more expensive than physical due to the additional cost of the activating chemical, but results in higher surface area materials with greater control of porosity with narrow pore size distribution.[142-144]

A highly porous activated carbon was prepared by the further activation of commercially available activated carbon through impregnation of the carbon with potassium hydroxide (KOH), slowly heating to 750 °C under argon atmosphere, and washing with hydrochloric acid (HCl) and water consequently.[145] Oxidation of the carbon with KOH affords as one of the products potassium carbonate (K_2CO_3), which breaks down into potassium oxide (K_2O) and CO_2.[146] With a ratio of 5 grams of KOH to 1 gram of activated carbon used, a carbon with a surface area of 3190 m^2/g was produced, compared to the 1585 m^2/g of the carbon before additional activation. This material had an H_2 uptake of 7.08 wt% at 77 K and 20 bars, only slightly less than the theoretical maximum value of 7.27 wt% at that surface area (assuming an adsorbed monolayer and the density of liquid hydrogen). The authors showed some evidence that the hydrogen uptake per surface area, which is usually about 2 wt% H_2 per gram of material per 1000 m^2/g surface area at 77 K was as according to the Chahine rule, where increases in the R value of graphitic porous carbons led to an increase in hydrogen uptake. The R value is an empirical parameter relating to the ratio of the 002 Bragg peak to the background in

powder X-ray diffraction (PXRD), pattern. A large R value corresponds to more ordered, parallel single graphitic layers in most instances.

It was found that in the KOH-activated carbons, R values were close to 1 (no 002 peak present), lower than the values of other activated carbons, indicating randomly oriented graphene sheets.[145,147,148] R-value increases with edge orientation of the sheets within the pores, as sheet edges provide higher adsorption enthalpy.[149] However, these KOH activated carbons still had the highest overall wt% uptake of hydrogen, as the increased surface area and micropore volume was a more important factor at cryogenic temperatures where condensation into less-optimized larger micropores may have taken place.

Potassium hydroxide activation is a well-documented technique to attempt to achieve greater surface area and hydrogen uptake in porous carbons. This higher surface area is due to the microporous nature of the materials produced as opposed to larger pores from other activation methods.[150] For example, use of the technique on hemp stem as a carbon feedstock afforded carbon with BET surface area of 3241 m^2/g and 3.28 wt% H_2 uptake at 77 K and 1 bar pressure, at higher pressure and cryogenic temperature mesopores morphology was reported[151]. Potassium hydroxide activated carbons derived from various commercially available fungi reported a maximum BET surface area of 2526 m^2/g and hydrogen uptake of 2.4 wt% at 77 K and 1 bar pressure.[152] Chitosan-derived activated carbons (ACs) further activated with KOH achieved a BET surface area of up to 3066 m^2/g and hydrogen adsorption of 2.95 wt% at 77 K and 1 bar, and 5.61 wt% at 77 K and 4 MPa (40 bars).[153] Materials with poly(vinylidene chloride), carbonized and KOH

activated, was found to have a hydrogen uptake of 4.85 wt% at 77 K and 20 bars, with 2.43 wt% at 77 K and 1 bar.[154]

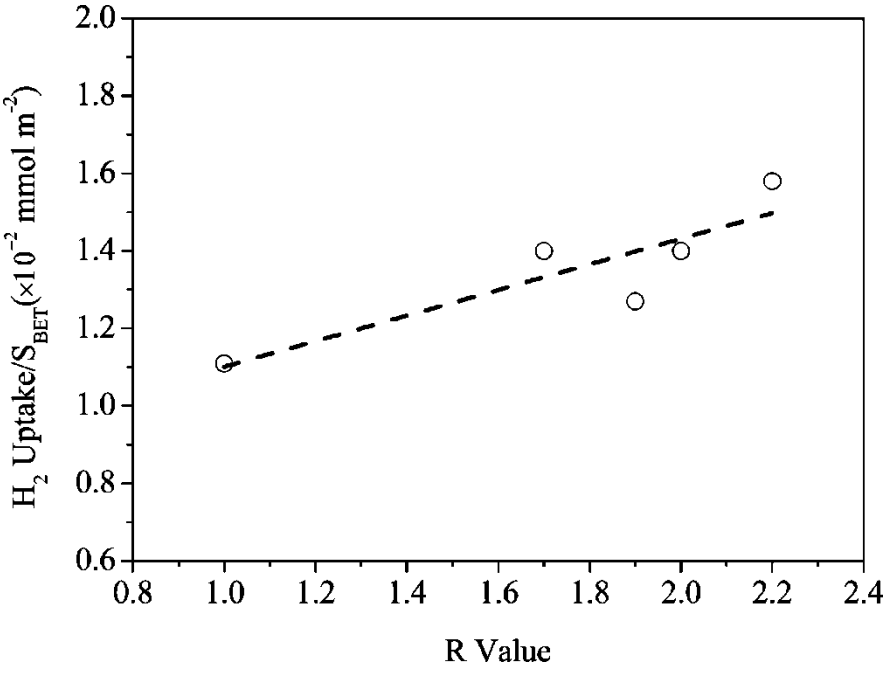

Figure IV-4. H_2 uptake/surface area vs R value. Reprinted with permission from 154. Copyright 2009 American Chemical Society.

Zinc chloride ($ZnCl_2$) or phosphoric acids (H_3PO_4) are common chemical activation reagents[150] which upon treatment produce distinct pore size distributions between 0.5-2.5 nm in activated carbons. Impregnation of feedstock with homogenously distributed amounts of $ZnCl_2$ followed by pyrolysis results in porous carbon "monoliths" that have evenly distributed and sized pores with sizes controlled by the amount of Zn added, with a total volume of micropores around the same as the volume of the salt originally added. Removal of the salt by washing physically creates the pores, and the

high temperature removes functional groups from the feedstock and bonds the surrounding carbon atoms to allow the carbon to retain the pores in its structure instead of collapsing. In contrast, H_3PO_4 activation results in a wider pore size distribution, and at high acid concentration, the volume of the porosity is higher than the volume of the acid, indicating that chemical reaction between the feedstock and the phosphoric acid takes place. Overall, as seen in Figures 4.4 and 4.5, the highest reported BET surface area among conventionally produced activated carbons was found with KOH activation process.

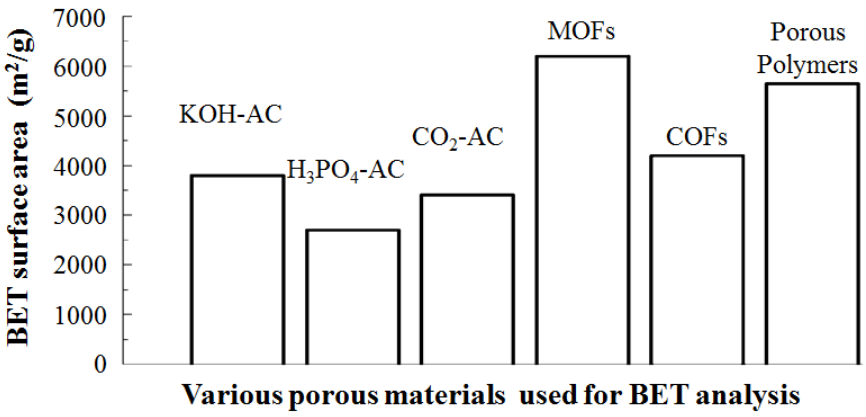

Figure IV-5. Highest reported BET surface areas for various porous materials as of 2014.

4.4.2 Porous Graphene-based Materials

Graphite oxide (GO), a form of graphite that is modified with oxide defects upon its surface, has attracted much interest both as a precursor material for graphene and other advanced materials due to its electrical and optical properties.[155] These sheets are readily

produced by oxidizing graphite, and can be suspended and processed in water.[156] The hydroxyl and other functional groups produced can then be functionalized in various ways to increase hydrogen uptake. Theoretically, high uptakes can be achieved in structures such as a graphene oxide/carbon nanotube pillared material. This may have been realized in graphene oxide / multi-walled carbon nanotube (MWCNTs) materials as shown in Figure IV-6.

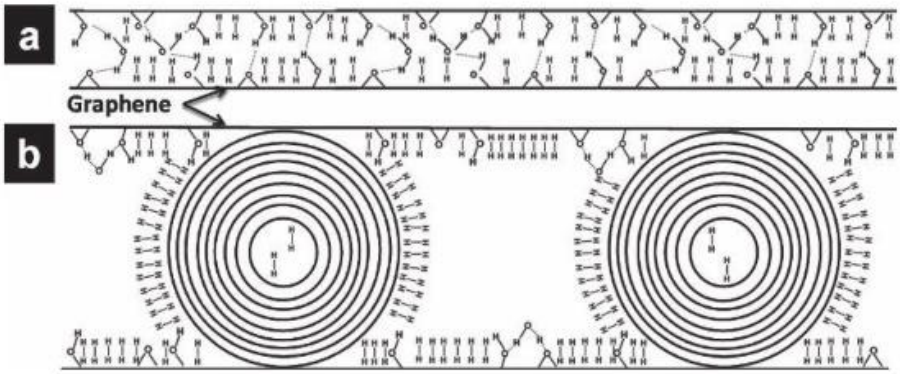

Figure IV-6. Graphene oxide / multiwalled carbon nanotube structure. Reprinted with permission from 157. Copyright 2012 Wiley Co.

This graphene oxide / MWCNT material was reported to have a hydrogen uptake of 2.6 wt% at room temperature and 50 atm (50.6 bar) pressure.[157] The researchers suggest that the liquid crystal synthesis route produces highly ordered structures with more well-defined and controllable pore size. The enhanced structure and pore size results in an increase of the uptake, just as their LC-GO dispersions were reported to have 1.4 wt% uptake at room temperature, as opposed to the 0.2 wt% reported for GO prepared by other

groups. However, this material had slow adsorption kinetics, taking 60 minutes to reach full capacity of gas uptake, with no additional information regarding the materials surface area. It seems likely that the hydrogen uptake is correlated with both the surface area and the heat of adsorption of hydrogen to the material, which is influenced by the material type, the pore size and shape.[158]

In another example, random hydroxyl groups of GO, similar to those shown below in Figure IV-7, were functionalized with benzene-1,3-diboronic acid (DBA).[155] As one GO sheet is functionalized on one side of the linker, another is functionalized on the opposite side. This functionalization process theoretically connects many layers of GO sheets into disordered graphene oxide frameworks (GOFs).

However, these materials were found to undergo swelling in polar solvents, which would not be compatible with such a rigidly linked structure. Further investigation indicated two likely outcomes either DBA molecules attached on only one side, or the GO sheets were separated by self-reacted DBA molecules (Figure IV-8a shows cross-section with DBA molecules as linkers). Optimization of synthesis conditions produced material with the specific surface area of about 1000 m^2/g. Since many of these materials follow the Chahine rule for hydrogen uptake, further development is likely to increase hydrogen storage capacities. Even materials that have high adsorption enthalpy and deviate from the Chahine rule must retain very high pore volume and overall porosity to be able to meet DOE targets.[140]

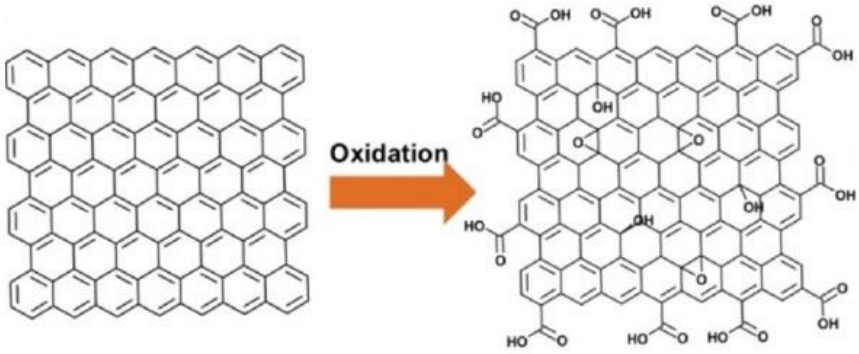

Figure IV-7. Example structures of graphitic carbon sheets and graphene oxide (GO). Reprinted with permission from 156. Copyright 2012 Elsevier *Ltd*.

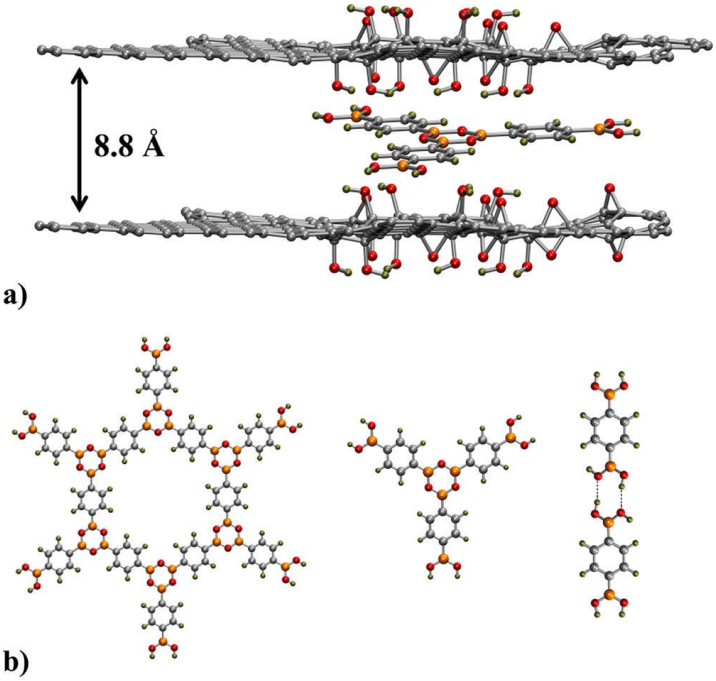

Figure IV-8. Graphene oxide sheets separated by DBA dimers, trimers, or larger polymeric units. Reprinted with permission from 155. Copyright 2015 American Chemical Society.

The DOE targets appear to be reachable by physiorption materials under cryogenic conditions due to the limited heat of adsorption of hydrogen to carbon materials. Tailored synthesis of materials with controlled pore sizes above those recommended for maximizing total hydrogen uptake in physiorption materials must be attempted in addition to chemical activation or metal doping to increase hydrogen binding energy as a means to meet the DOE target. To increase H_2 uptake at ambient conditions, including temperature and pressure, simulation studies have demonstrated that higher heat of adsorption than what is produce by small pores is required. [159] This "energy deficit" may be met if porous material are designed with pores optimized for hydrogen sorption at a higher than cryogenic temperatures, while still allowing efficient hydrogen saturation of its pores.

An example of this strategy was realized by a graphene scaffold material was made more porous through both KOH activation and hydrogen annealing, which removed oxygen moieties and broadened pores.[160] In this material, BET surface area determined to be 3400 $m^2 \cdot /g$ and the material exhibited a saturated H_2 uptake of 7.5 wt% at 77 K, while non-saturated hydrogen uptake was 1.25 wt% at 296 K. The non-saturated uptake was 4.2 wt% at 120 bar pressure at 193 K, the temperature of solid CO_2. This report also showed that hydrogen weight-percent (wt%) versus specific surface area of many porous carbons followed the Chahine Rule (summarised in Figure IV-9).

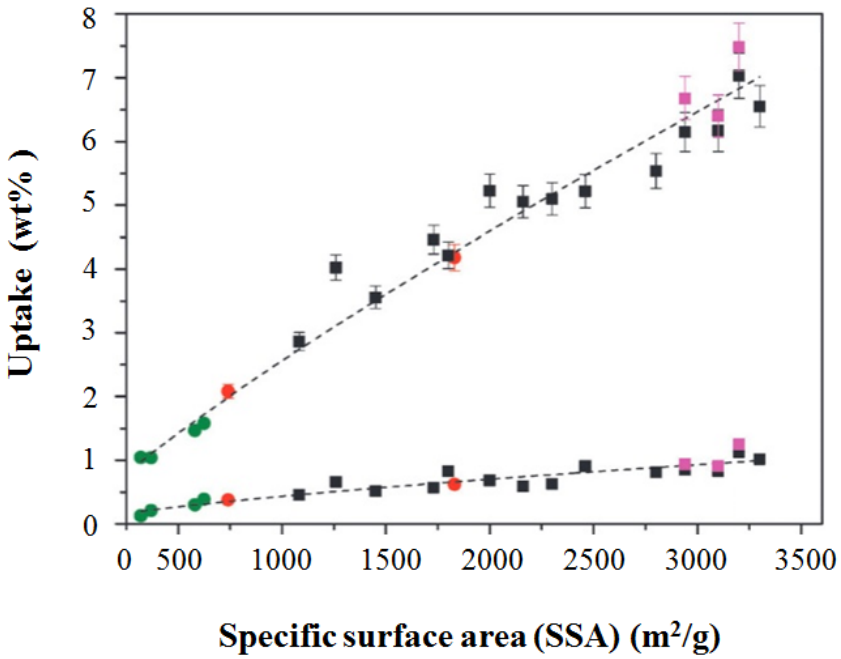

Figure IV-9. The Chahine rule illustrated for many porous carbons at different temperatures. It follows logically and has been demonstrated in a few experiments that porous carbons using physisorption should follow a Chahine line in between the two temperatures at an intermediate temperature. Reprinted with permission from 160 . Copyright 2015 Royal Society of Chemistry.

4.4.3 MOF-derived Porous Carbons

Some of the highest surface areas to be measured among porous carbons are found among MOF-derived carbons (MDCs).[161] Here, high-surface area MOFs are synthesized, sometimes with metals or functional groups specific to the application such as catalysis. Then, the MOF is calcined, or carbonized, subjected to extremely high temperatures sufficient to quickly remove the metals from the structure while somewhat preserving the pre-existing pore size and shape.[162] However, the behavior and products

of calcination of MOFs made from different metals can vary because the metals and metal oxide clusters can have very different melting points.

For example, in one study, porous carbons resulted from isoreticular metal-organic framework 1 (IRMOF-1, MOF-5, the structure has Zn_4O nodes with 1,4-benzodicarboxylic acid as struts between the nodes) had higher porosity overall than ones produced by calcination of chromium-based MOFs, as, according to the study, the Cr-based porous carbons had pores clogged with chromium oxides and carbides while the Zn oxides and carbides were removable from the crystalline structure. Carbonization of MOFs is done by slow heating under inert gas to prevent oxidization of carbon to carbides or metal to metal oxides. It was found that zinc was not present in the carbonized samples based on MOF-5 while chromium-based MOFs had residual metal still present. omwDepending on the ligand and metal used, nonporous or even porous metal oxides can be the end-product.[163] Chromium-MOF based porous carbons were observed by powder X-ray diffraction (PXRD), which contained chromium carbide and oxide at various synthesis temperatures, and were treated further with HF or HCl to remove residual chromium. This treatment was unsuccessful as confirmed by differential thermal analysis (TGA) and a drastic lowering of measured surface area, as opposed to the increase in surface area of Zn-MOF based carbon from 835 to 2393 $m^2 \cdot /g/g$ was observed. The preliminary result also indicate that MOFs based on metals with low melting and boiling points, such as zinc, may be more appropriate for development of new MDCs.

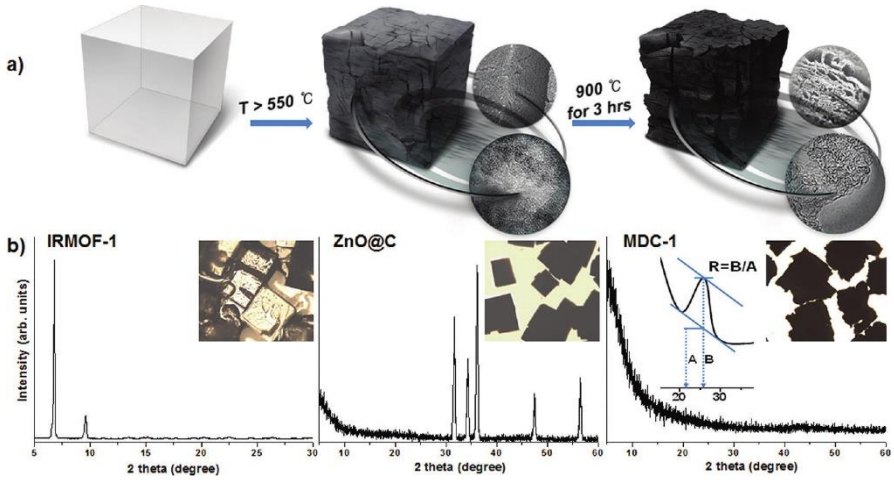

Figure IV-10. Carbonization of MOF-5(IRMOF-1) to MDC-1. Reprinted with permission from 161. Copyright 2012 American Chemical Society.

MOF-derived carbons(MDCs) in generalcan store more hydrogen per surface area than standard MOFs, when their pore sizes are smaller than the corresponding MOFs. (Figure IV-10) MDCs also usually retain overall high porosity. This is because structures containing large and open pores, such as mesopores are not as suitable for hydrogen adsorption as materials with high micropore density. It is possible that structures with hierarchically sized pores may have a higher hydrogen uptake at higher pressures. This is because ultramicropores (extremely small pores with a size similar to that of the hydrogen molecules) may become saturated at low temperature and high pressure, even though those pores are more appropriate to hydrogen sorption at higher temperature.[161] In general, both ultramicropores and extremely high total pore volume are required for high gas uptake.

An MDC derived (modified) from a Zn-BTC MOF achieved a surface area of up to 1671 m^2 /g.[164] The unmodified MOF was unsuitable for H_2 storage, due to its mesoporous nature. Carbonization of an MOF based on aluminum (Al) and 1,4-naphthalene-dicarboxlate afforded a porous carbon with a surface area of 5500m^2/g, which was confirmed by 10 repeated syntheses and measurements.[165] The carbonization was carried out at 800 °C under inert gas, followed by removal of remaining Al species with HF. This material did, however, have a wide pore size distribution of between 1 - 5 nm. Graphitization and collapse of the surface area occurred at 900 °C or above, and the material retained approximately 65% of its pore volume after compression at 10 MPa for 10 minutes. In another study, a metal-organic xerogel was prepared and carbonized, resulting in a BET surface area of 3770 m^2/g.[166]

Interestingly, a "foam-like" porous structure was observed in a carbonized Zn-MOF that was synthesized using a nitro-functionalized ligand. Rapid removal and gasification of these functional groups during carbonization result in a unique microstructure with many large macropores, which are formed by removal of the Zn products through post-carbonization washing.[167] Though this material is not suitable for hydrogen storage, it is a key example of how ligand choice can drastically affect the character of the resulting porosity in MOF carbonization.

In another study, an MDC with high surface area and pore volume, 3000 m^2/g and 5.45 cm^3/g, respectively, was synthesized through the direct carbonization of IRMOF-1 immersed in dimethylformamide (DMF). The rapid removal of the DMF molecules introduced large pores into the MDC without destroying the microporosity.

Interestingly, pyrolysis of the activated, solvent-free IRMOF-1 produced an MDC with a surface area of 3110 m^2·/g, but a total N_2 uptake of only 1720 cm^3·/g at 1 bar pressure and 77 K. The MDC derived from DMF-infused IRMOF-1 had a BET surface area of 2980 m^2/g, but a total N_2 uptake of 3526 cm^3/g. As seen in Figure IV-11, the introduction of large mesopores by this carbonization method lowered the surface area, but drastically raised the pore volume and overall porosity.[168] This is furthur example of how BET surface area is not a complete measure of the total porosity of a material, and also of how the type of porosity can be drastically altered by synthesis conditions.

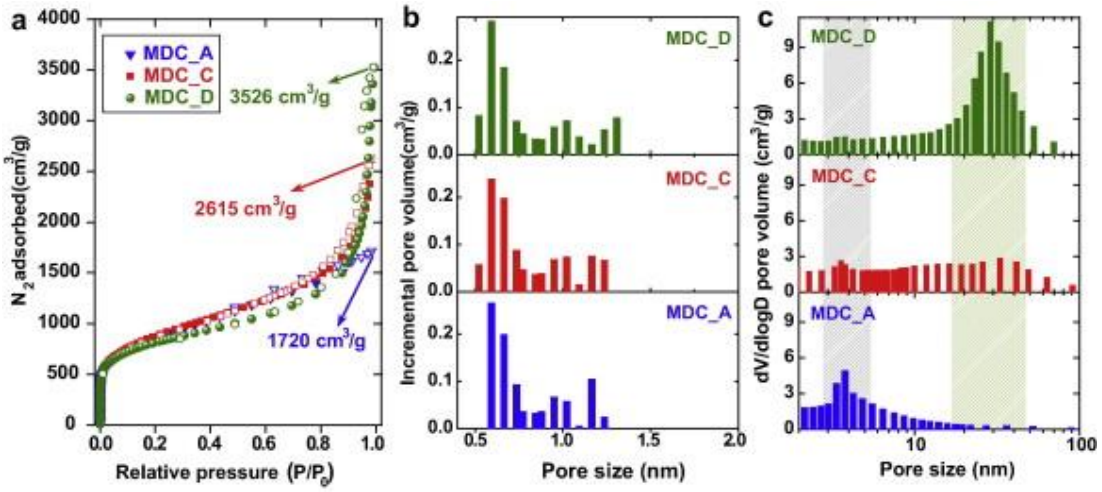

Figure IV-11. The porosity of IRMOF-1 derived MDC carbonized solvent-free (Blue) versus in chloroform(Red) or DMF(green). Reprinted with permission from 168. Copyright 2014 Elsevier *Ltd*.

In some cases, MOFs act as templating agents for other carbon sources in addition to being the carbon source themselves, similar to the use of solvents above. This can

produce templated ACs with higher surface areas than those of the original MOFs. One example of this approach is use of isoreticular metal-organic framework-3 (RMOF-3, $[Zn_4O(NH_2\text{-}BDC)_3]\cdot x$DMF, NH_2BDC = 2-amino-1,4-benzene-di-carboxylate) was used with various quantities of sucrose ($C_{12}H_{22}O_{11}$), heated to promote uptake of sucrose into the pores, and pyrolyzed in an inert atmosphere (such as Ar) at 900 °C for 6 hours.[169] The sample was washed with dilute HCl and then with a binary mixture of water / ethanol, followed by removal of remaining Zn species. A surprising observation was that the BET surface areas varied among samples based on sucrose loading, as shown in Table IV-1. The number in each sample name refers to the milligrams of sucrose used in each pyrolysis. Field-emission scanning electron microscopy (FESEM), transmission electron microscopy (TEM), PXRD, and Raman spectroscopy analyses all showed different morphology in each sample. In NPC-300, hydrogen uptake of 2.45 wt% at 77 K and 1 bar pressure was observed which was much higher than the unmodified MOF. This was attributed to the modified structure having a higher microporosity than the unmodified parent MOF. This is another example of how guest solvent or other small molecules introduced into an MOF before pyrolysis can drastically affect the properties of the final MOF-derived carbon.

Table IV-1. Textural parameters of the resultant functional nanoporous carbon (NPC) samples. Reprinted with permission from 169. Copyright 2015 Elsevier *Ltd*.

Sample	S_{BET} (m^2/g)[a]	S_{Lang} (m^2/g)[b]	S_{micro} (m^2/g)[c]	S_{meso} (m^2/g)[d]	S_{meso}/S_{micro}	V_t (cm^3/g)[e]	V_{micro} (cm^3/g)[f]	V_{meso} (cm^3/g)[g]	$V_{meso/micro}$ (cm^3/g)
Sucrose	258	391	117	141	1.2	0.17	0.08	0.09	1.125
NPC-0	392	581	299	93	0.31	0.409	0.36	0.049	0.136
NPC-150	1022	1567	898	124	0.13	0.65	0.58	0.07	0.121
NPC-300	3120	4031	2987	133	0.03	1.93	1.89	0.04	0.024
NPC-500	1761	2687	1692	69	0.04	0.74	0.58	0.16	0.103
NPC-1000	1077	1622	994	83	0.08	0.435	0.245	0.19	0.175

a) S_{BET} is the BET specific surface area.

b) S_{Lang} is the Langmuir specific surface area.

c) S_{micro} is the *t*-plot specific micropore surface area calculated from the N_2 adsorption–desorption isotherm.

d) S_{meso} is the specific mesopore surface area estimated by subtracting S_{micro} from S_{BET}.

e) V_t is the total specific pore volume determined by using the adsorption branch of the N_2 isotherm at P/P_0= 0.99.

f) V_{micro} is the specific micropore volume calculated by a non-local density functional theory (NLDFT) method.

g) V_{meso} is the specific micropore volume calculated by subtracting V_{micro} from V_t.

The morphology of the MDCs produced can be further influenced by other experimental parameters such as carbonization temperature, ligand, solvent used or temperature of reaction. For example, materials of institute Lavoisier (MIL) framework with aluminum metal [MIL(Al)] was fabricated with aluninium and oxygen (Al_3O_2) nodes with btc acid supporting struts between the nodes $Al_3O(OH)(H_2O)_2(btc)_2 \cdot nH_2O$ (btc = 1,3,5-benzenetricarboxylate), was carbonized at 800 °C under argon to produce an MDC.[170] This MDC required HF washing to remove residual aluminum oxide (Al_3O_2)

species. Upon removal of Al_3O_2, hollow octahedral carbon shells were produced, with outer morphology mimicking that of the source MOF and micro and mesoporosity in the shell. Large interconnected (50 nm) nanochannels in the center of the particles were shown by TEM (in Figure IV-12, the nanochannels are marked by vertical lines). The BET surface area of 1711 m^2/g, hydrogen uptake of 1.5 wt% at 77 K and 1 atm (1.01 bar) pressure, and pore size distribution collectively indicated that this material possessed hierarchical micro, meso, and macropores. This would make it less suitable for pure hydrogen storage, but is additional example of how metal and activating agent choice can control the nature of the pores produced.

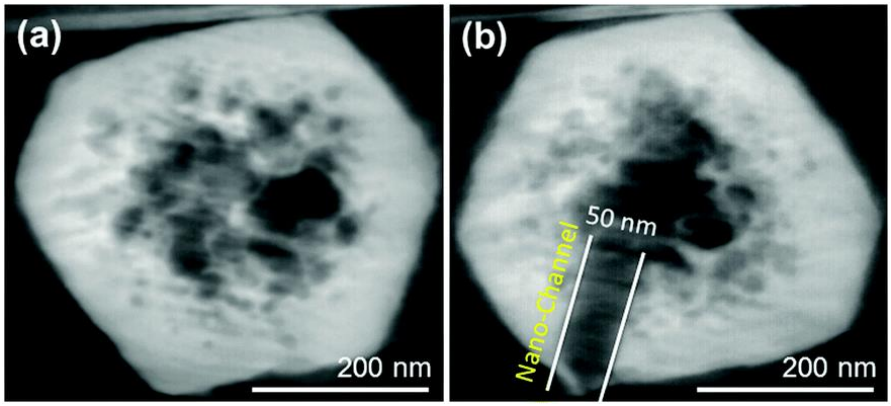

Figure IV-12. MDC cage particles with massive voids in the center of porous carbon shells. Reprinted with permission from 170. Copyright 2014 Elsevier *Ltd*.

4.4.4 Doped Porous Carbons

Lithium-atom doped graphene sheets were shown in grand canonical Monte Carlo simulation to possess a maximum hydrogen adsorption of 6.5 wt% at room

temperature and 20 bar pressure. The model is based on the assumption that if 1 atom of lithium is present per carbon and the sheets are separated by 10 angstroms, the interactions would yield between 5-7 % adsorption. However, such a structure has proved synthetically inaccessible.[159] Other simulations predicted a hydrogen uptake of up to 16 wt% in graphenes with adsorbed lithium or boron (Figure IV-13 is a graphical illustration of the various simulations.)[159] In general, high adsorption enthalpy, surface area, and pore volume that is accessible to about 2 layers of hydrogen is optimal for room temperature hydrogen storage meeting targets. However, physisorption of hydrogen onto graphitic carbon does not produce the required adsorption enthalpy, necessitating cryogenic temperatures for high uptake in most materials. One way to increase the adsorption enthalpy is to administer metal ions or particles into the pores of the carbon, due to the Kubas interaction between the hydrogen sigma bonding or antibonding orbitals with the d-orbitals of transition metals, or the polarization of the H_2 molecules by the charged metals.[171]

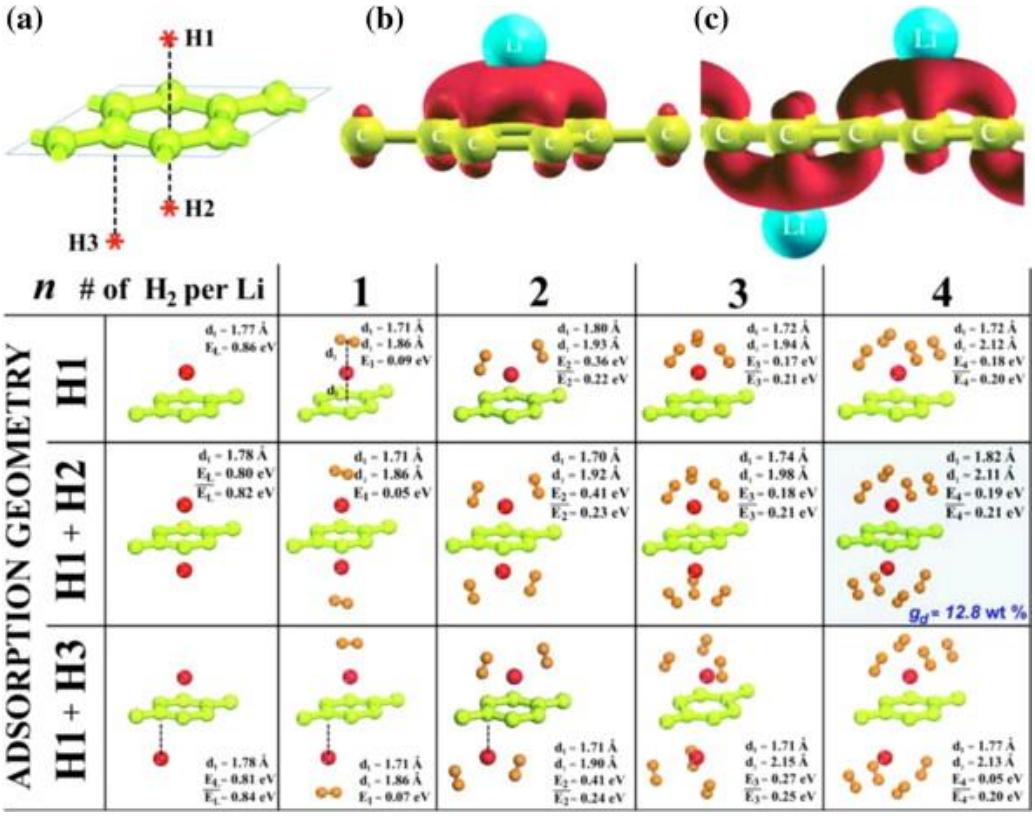

Figure IV-13. Simulation of hydrogen adsorption to Li-doped graphenes. Reprinted with permission from 159. Copyright 2015 Elsevier *Ltd*.

Metal-nanoparticles doped hierarchically porous carbon monoliths (Ni-HCPMs) were demonstrated to have hydrogen uptakes well in excess of what would be predicted by the Chahine rule, with 4.29 wt% H_2 uptake at 77 K and 5 bar pressure while possessing only 620 m^2/g surface area. [172] This is because of the hydrogen spillover effect, where chemisorption of H_2 molecules on metal nanoparticles is followed by dissociation of the hydrogen into isolated atoms bonded to the nanoparticle, which can then migrate to the graphitic activated carbon surfaces near the nanoparticles.[173] (Figure

IV-14) This drastic increase in the adsorption enthalpy would also increase uptake at higher temperatures.

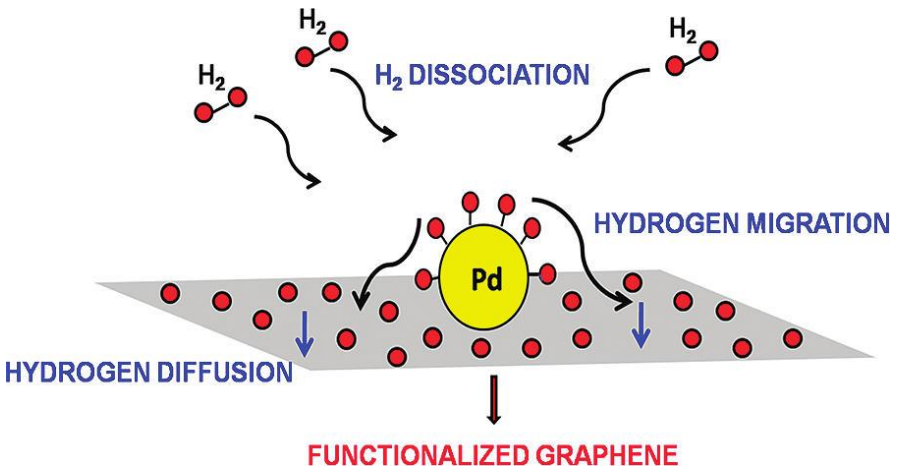

Figure IV-14. Hydrogen spillover from metal nanoparticles to graphitic porous carbons. Reprinted with permission from 173. Copyright 2011 American Chemical Society.

Carbon monoliths were prepared by suspending a nickel salt in a polymeric precursor solution of phenol, formaldehyde, NaOH, water, and pluronic P123 (E21P67E21) and F127 (E98P67E98) co-block polymers (where E is ethylene glycol monomer and P is propylene glycol). The above precursor was then heated at 100 °C for 18 hours to produce a polymeric monolith, which was then pyrolyzed and made porous under nitrogen at 600 °C with slow heating. The prepared HCPM was pyrolyzed in the same fashion except without nickel and showed a surface area of 688 $m^2 \cdot /g$, but hydrogen uptake of 1.44wt%, helping to show the efficacy of the spillover effect, which

was enhanced by using nickel nanoparticles directly within micropores. It is possible that similar materials may be fabricated starting from porous materials with the higher surface area which may have performance criteria capable of meeting the 2020 DOE targets. The previous example is an illustrtation of how pyrolysis and carbonization can make even non-porous materials into porous carbons, though templating from already porous materials tends to result in higher surface areas. Templating from nonporous Zn MOFs, for example, resulted in maximum surface area of 1278 m^2/g in one study.[174]

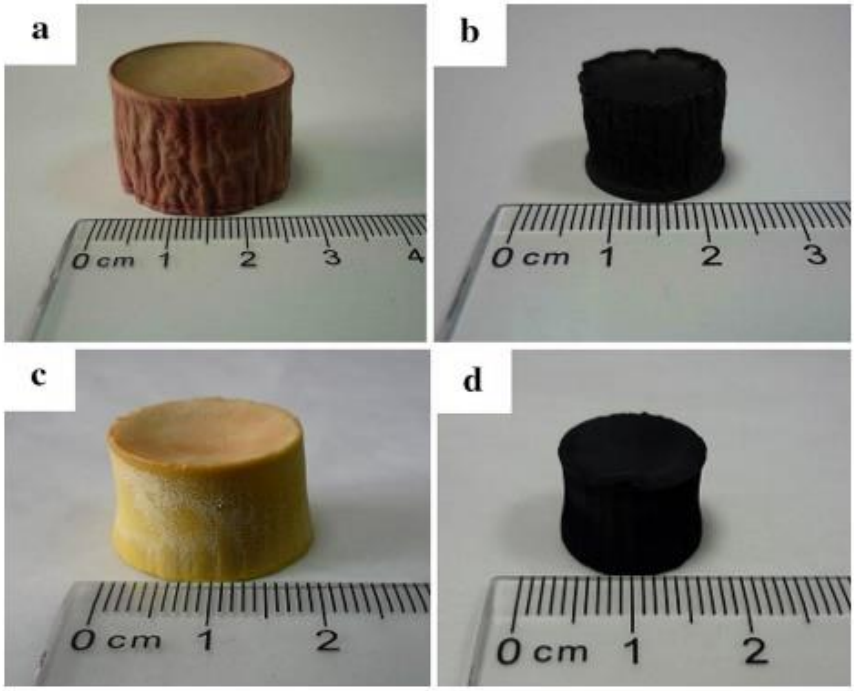

Figure IV-15. Porous carbon monoliths prepared from polymer blocks. Reprinted with permission from 172. Copyright 2015 Springer.

Nitrogen-doped (7 wt%) graphenes holding 20 wt% of Palladium (Pd) nanoparticles were shown to have hydrogen uptake of 1.9 wt% at 298 K and 20 bar pressure, even with a low surface area of 146.4 m^2/g. This was enhanced by 48.1 % by a spillover mechanism as estimated by the uptake of the nanoparticles alone under identical conditions.[175] Nitrogen doping may have increased uptake due to enhanced interaction between the nitrogen-doped graphene and the metal nanoparticles. Graphene doped with nickel boron nanoalloys through reduction showed hydrogen uptake of 2.81 wt% at 77 K and 1.06 bar pressure through spillover enhancement.[176] Another graphene with a low surface area of 272 m^2/g was doped with nickel boride (Ni-B) was shown to have 4.4 wt% hydrogen uptake at 77 K and 1.06 bar, as seen in Figure IV-16.[177] For the doping process , solutions of graphene oxide (GO) and nickel acetate ($C_4H_{14}NiO_8$) were reduced with sodium borohydride ($NaBH_4$).

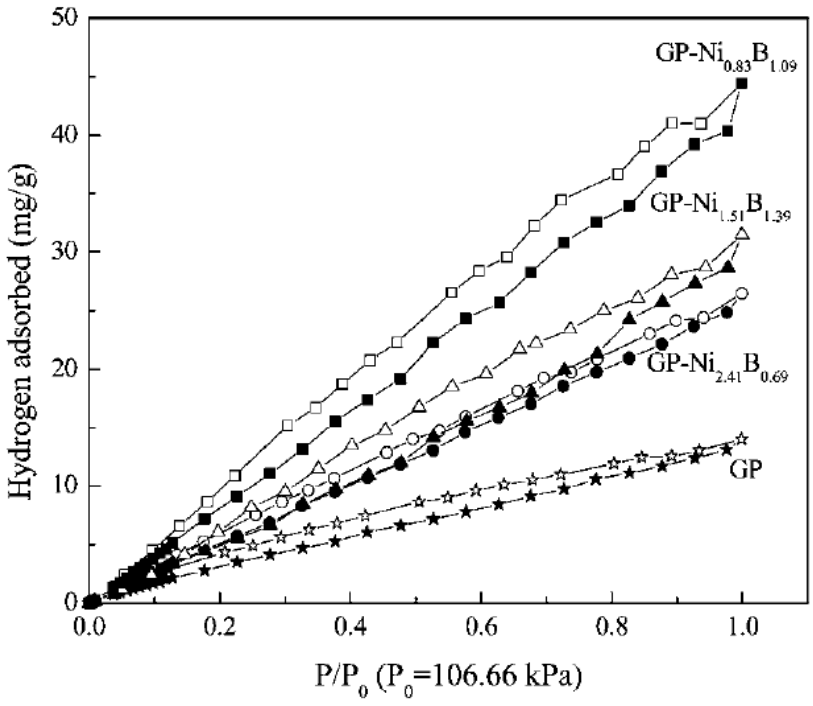

Figure IV-16. Hydrogen uptake of Ni-B doped graphenes at 77K. Closed symbols refers to adsorption, open symbol refers to desorption. Reprinted with permission from 177. Copyright 2010 Royal Society of Chemistry.

A carbon foam similar to graphene oxide was prepared, but with a higher oxide and defect concentration. The GO surface was doped with nanoparticles of an alloy of palladium (Pd) and mercury (Hg) with the formula Pd_4Hg. It was reported to have 4.6 wt% hydrogen uptake at 298 K at 20 bars.[178] However, due to the spillover mechanism of the storage, the adsorption or induction time was extremely long to achieve maximum uptake, and the uptake was not as high on other cycles. As shown in Figure IV-17, measurements were made after a 1500 minute equilibrium, with the first isothermal point being determined at a 15 min interval, subsequent points were determined at 15-40 minutes and the plots showed a very high wt% hydrogen uptake. It was hypothesized

that if all cycles had been set to 1500 minute induction time, uptake would have been identical. Attempts to reproduce the same results were successful only once, with other attempts producing materials with maximum 2 wt% uptake, with retained enhancement after doping. The isotherm also showed that a deliverable hydrogen capacity of uptake between, for example, 10 bar and 20 bars pressure, would be extremely low as a vacuum is necessary to desorb the hydrogen taken up through spillover. This mechanism will be explored further below.

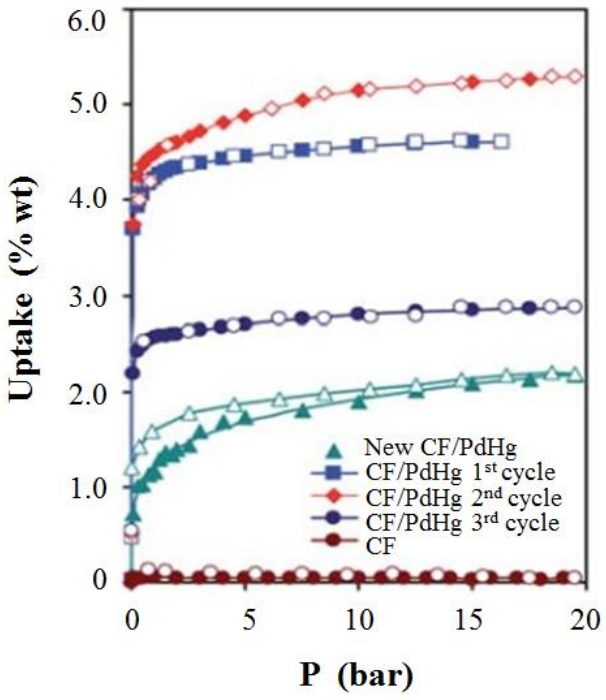

Figure IV-17. Hydrogen uptakes among Pd_4Mg-CF composite varying wildly based on cycle induction time. Reprinted with permission from 178. Copyright 2011 Royal Society of Chemistry.

4.4.5 Zeolite-templated Carbons

Zeolite-templated Carbons (ZTCs), are prepared by filling a zeolite structure with polymer feedstock such as propylene through a method such as chemical vapor deposition (CVD), heating to fill all pores with polymer, and final removal of the zeolite with HF or another etching agent.[179] Zeolite beta (for example CB850h) have demonstrated hydrogen uptake of 6.9 wt% at 77 K and 20 bars pressure. This sample was prepared from zeolite β templates and was subject to the zeolite / carbon composite obtained after the CVD step to further heat treatment under nitrogen flow for 3 h. [180] At room temperature, one ZTC preparation showed an hydrogen uptake which was proportional to their specific surface areas until 10 MPa (100 bar) pressure. However, above that pressure, having an appropriate pore size of 1.2 nm diameter seemed more important, in terms of H_2 uptake. This may be due to the condensation or multi-layer adsorption of H_2 occurring in those pores at high pressure resulting in enhanced adsorption enthalpy within the pores. Another ZTC preparation had a BET surface area of 3370m^2/g, and a hydrogen uptake of 2.2 wt% at high pressure. This reported uptake was greather than corresponding measurements using activated carbons with the similar surface area but uncontrolled pore size and shape. Hydrogen spillover was also demonstrated by an increase in capacity after Pt nanoparticle loading. This is an example of how ZTCs with the similar surface area can exhibit higher hydrogen uptake at high temperatures and low pressures. This is because their enthalpy of adsorption to hydrogen is raised after loading of metal nanoparticles. Material pore design can also raise heats of adsorption somewhat without nanoparticles, but this study also serves as

evidence that DOE targets are likely to be unontainable at room temperature through pure physisorption processes.

In another study, a physical composite of MIL-101, composed of chromium and terephthalic acid (BDC), was formed by adding ZTC to the synthesis conditions of MIL-101 metal-organic framework, resulting in crystals of MIL-101 grown in and around the ZTC particles.[181] Poly crystaline X-ray diffraction spectroscopy confirmed peaks in the composite corresponding to both structures. Slight increases in surface area and hydrogen uptake were seen from either ZTC or MIL-101 materials. The nitrogen isotherm had higher uptake in the low-pressure region due to additional micropores and hysteresis in the high-pressure region consistent with newly formed mesopores. The pore size distribution showed a new unimodal pore size as opposed to the bimodal pore size of MIL-101. The surface area of MIL-101(Cr) was 2552 m^2/g and H_2 uptake was 1.91 wt% at 77K and 1 bar pressure, ZTC was 2577 m^2/g and 2.39 wt%, and the hybrid composite was measured to have a surface area of 2957 m^2/g and 2.55 wt%. The finding of mesoporosity due to the new isotherm shape is not consistent with the narrow pore size distribution found, and the higher uptake may be primarily due to new pores formed between the ZTC and the MIL-101 grown on and around the nodes. Such pores could physically increase the porosity and uptake of the material when compared to crystals or polymer pieces that are physically separated by distances which do not enhance sorption process due to smaller pores which allow more layers of adsorbate to interact with each other (a phenomenon not accounted by BET theory).

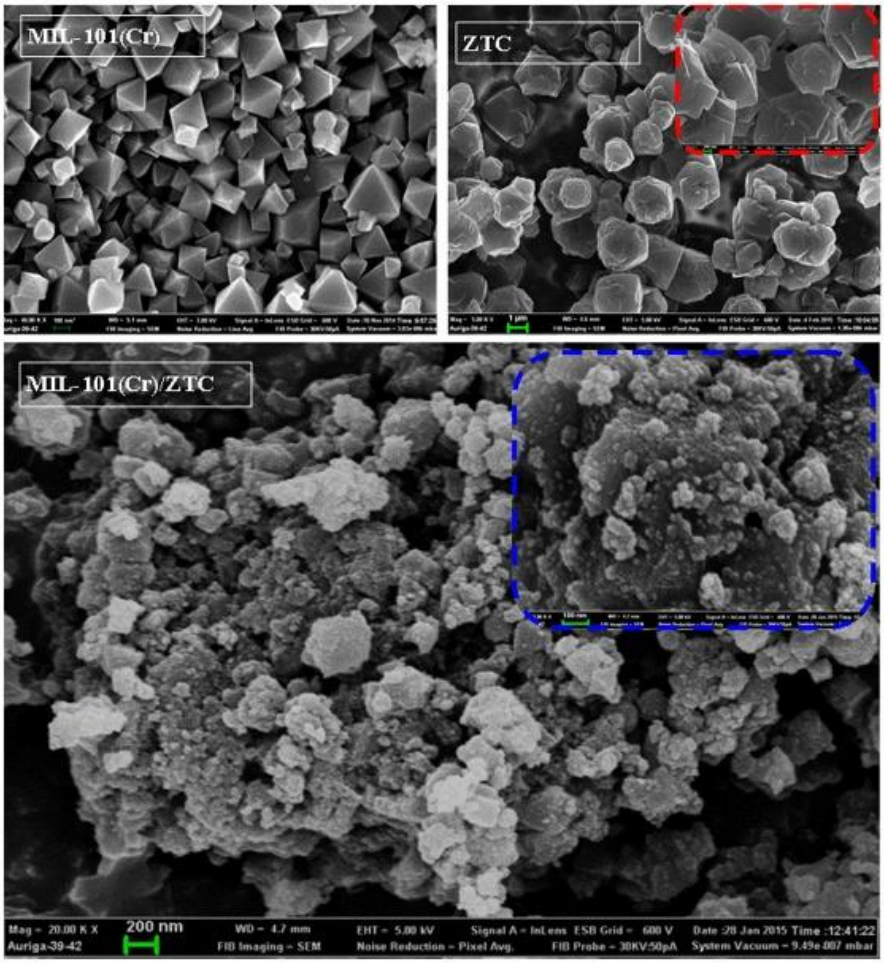

Figure IV-18. SEM Images of ZTC, MIL-101, and the composite. Reprinted with permission from 181. Copyright 2015 Springer.

Other ZTCs were hydrogen uptake as improved through post-synthetically impregnating them with 2-5 nm Pd nanoparticles. (Figure IV-18) This impregnation was accompiolished through a CO_2 supercritical mediated hydrogenation and reduction of a precursor. After Pd was added, the surface area went down from 2045 m^2/g to 1390 m^2/g, while the H_2 uptake went from 4.9 wt% at 77 K and 20 bars pressure to 4.7-5.3 wt%, indicating a higher heat of adsorption for hydrogen uptake, as the material has a

similar gravimetric uptake despite lower porosity.[182] A Pd loading of 0.4 wt% optimized for H_2 uptake is summarised in Figure IV-19, which depicts the relationship between uptake and percent metal loading. This procedure demonstrated the hydrogen spillover effect, demonstrating that a precursor of much higher intrinsic porosity would be required for optimal application. Hypothetically a material with mesopores structure could be filled with slightly smaller nanoparticles, which would then promote hydrogen spillover into now-optimal pore sizes.

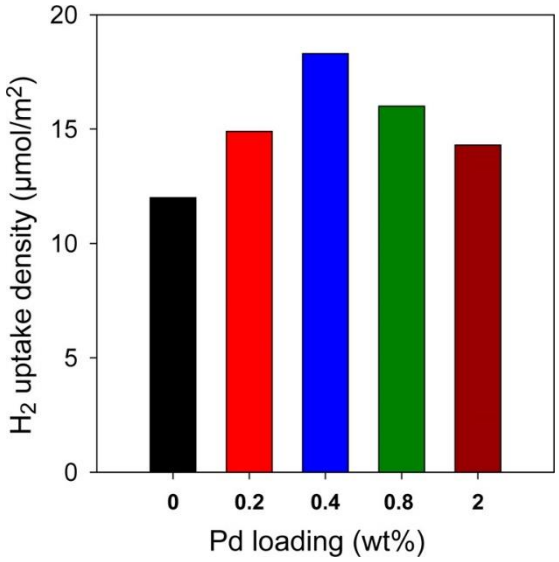

Figure IV-19. Pd loading versus H_2 uptake in Pd-doped ZTCs. Reprinted with permission from 182. Copyright 2013 American Chemical Society.

Hydrogen spillover in Pt-loaded ZTCs was studied more extensively, where they investigated both endothermic and exothermic process in addition to speciation, summarised in Figure IV-20).[183] It was found that processes increasing spillover

occurred at increased temperature and pressure, making nanoparticle loading an especially promising method for improving hydrogen uptake at higher temperatures. An appropriately prepared ZTC alone had a surface area of greater than 3000 m^2/g and pore size of 1.2 nm, resulting in hydrogen storage capacity of 2.2 wt% at 34 MPa (340 bar) pressure and room temperature. Mixing the prepared ZTC with Pt nano colloidal suspension resulted in uptake of 3.23 wt% of Pt into the carbon, without loading optimization. The BET surface area was found to decrease to 3060 m^2/g from 3220 m^2/g. The PXRD confirmed the presence of ZTC and Pt nanoparticle, as both species partly ordered and crystalline, due to the ZTC being broad template, and Pt being much smaller in size relative to the ZTC.

The study found that the dissociated hydrogen radicals, migrating throughout the ZTC surface, enabled the release of the spillover only after a degas cycle at 423 K for 6 hours to recover the chemisorbed hydrogen radicals. This spillover storage increases at higher temperature, as the diffusion of the particles onto the carbon is endothermic, which is promoted at higher temperatures. The total hydrogen uptake was not reported, although the reported hydrogen uptake for unmodified ZTC was 2.2 wt% . The lower than anticipiated uptake for the modified material may be due to the high loading of Pt nanoparticles. Collectively, this study showed that dissociative spillover would produce an increase in hydrogen uptake that is not easily reversible, making it unsuitable for hydrogen storage applications unless long adsorption and desorption times and harsh experimental conditions necessary for desorption can be remedied. The spillover based chemisorption of hydrogen radicals appears to have unfavorable desorption kinetics,

making facile recovery much more difficult.[178,184,185] This approach for hydrogen uptake is similar to chemical and other chemisorption-based hydrogen storage methods which exhibit very high uptake, but also very unfavorable desorption kinetics and thermodynamics requiring long desorption times, lower temperatures, or other harsh treatment conditions that make the overall procedure too expensive for practical DOE applications.[159]

Materials with hexagonal mesoporous silica (HMS) were also used as a template to produce a porous carbon with a BET surface area of 2644 $m^2 \cdot$/g. Here the carbon was decorated with nickel during the synthesis to increase hydrogen uptake. Resol-type resin ($HOCH_2$-ArOH, where Ar are different polyphenols) was used as the carbon source after glucose ($C_6H_{12}O_6$) and sucrose ($C_{12}H_{22}O_{11}$) sources were found to produce carbons with a BET surface area of 1100 $m^2 \cdot$/g. Nickel-decorated materials had a loss of surface area to 1326 $m^2 \cdot$/g and of mesoporosity, suggesting nickel nanoparticles filled many mesopores. Room temperature hydrogen uptake was 0.53 wt% at 20 bars pressure with no saturation shown in the isotherm for a carbon with a moderate amount of nickel, which was the highest as expected due to a balance between increased sorption and a loss of porosity due to the nickel. It was hypothesized that large Ni nanoparticle size caused a enhancement in hydrogen uptake, although this measured enhacement was less than calculated, suggesting that smaller nickel nanoparticles might be more effective in terms of improved hydrogen uptake.[186]

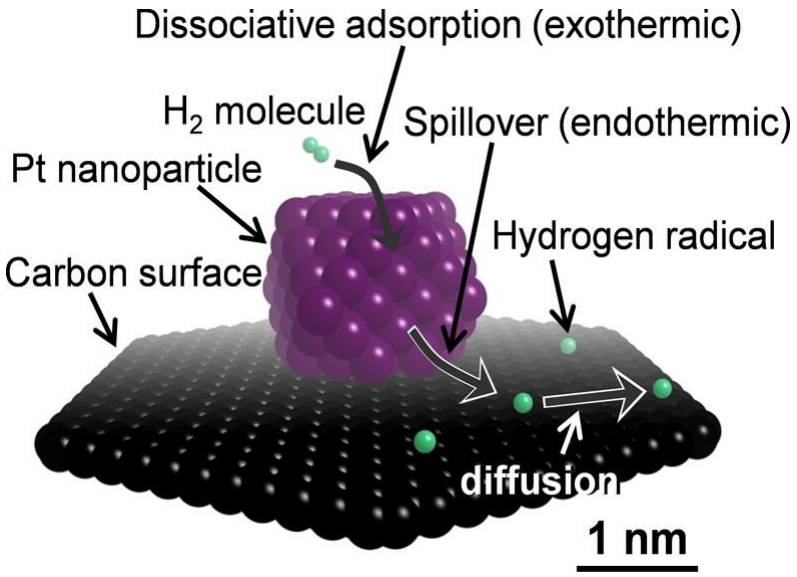

Figure IV-20. Hydrogen spillover in Pt-loaded ZTCs. Reprinted with permission from 183. Copyright 2014 American Chemical Society.

4.4.6 Carbide-derived Carbons

Carbide-derived carbons (CDCs)[187,188] usually have specific surface areas from 1000 to 2000 m^2/g and have been used for hydrogen uptake.[189] A molybdenum carbide-derived carbon was heated, exposed to chlorine gas, heated under an Ar purge, and then hydrogen annealed at 600 °C. The BET surface area of this modified CDC was 2520 m^2/g at 800 °C, with a pore size distribution between 2-4 nm, although there was pores with wider diameter, which was not suitable for hydrogen adsorption. An uptake that was 20% higher was found in the CDC material, produced at 600 °C during chlorination, that had ⅔ of the total pore volume of the more porous carbon materials; as its larger pores increased its total porosity but lowered its hydrogen uptake at 77 K and 35 bar pressure. This is an evidence that in general, large pores degrade hydrogen uptake under many

conditions, acting only as "wasted space" that does not adsorb hydrogen, unless either the heat of adsorption is increased through another mechanism, or extreme conditions such as 77 K and 100 bar pressure are adopted.[190]

Porous CDCs, which were "super activated" by chemically activating them with KOH, reached 2800 m^2/g BET surface area, with a retention of microporosity, and an increase of the hydrogen uptake from 3.8 wt% to 6.2 wt% at 77 K and 20 bar pressure.[191] This observation was found to be partially due to the porous carbons becoming more functionalized with surface oxygen moieties after oxidation by the KOH. One study demonstrated an uptake of 2.7 wt% at 77 K and 1 bar pressure, indicating higher affinity of hydrogen for this material, as shown in Figure IV-21, where the super activated materials have H_2 uptake deviated above the nominal Chahine plot.

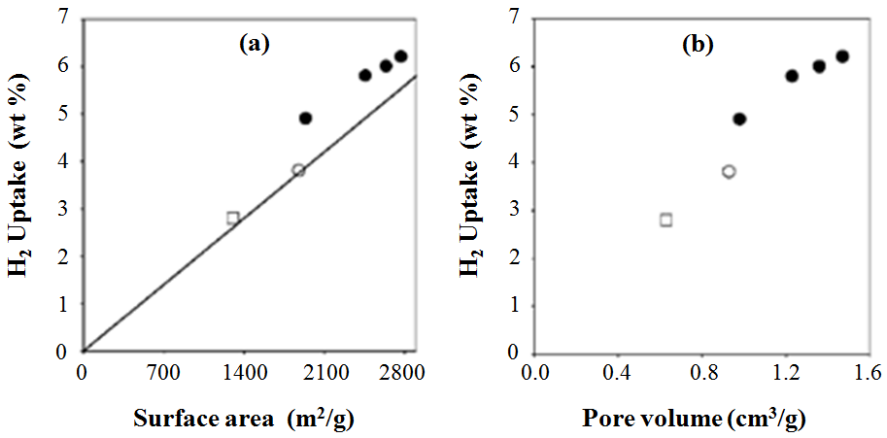

Figure IV-21. Chahine plot of H_2 uptake versus porosity of Zr-CDCs (clear symbols) and super activated CDCs (black circles). Reprinted with permission from 191. Copyright 2009 Royal Society of Chemistry.

4.4.7 Porous Polymer Networks

Porous polymer networks (PPNs) are polymers of intrinsic microporosity (PIMs), due to the geometry, symmetry, and rigidity of their monomers or other linking units.[192] The porous aromatic framework-1 (PAF-1) was synthesized from tetrakis(4-bromophenyl)methane through a Yamamoto homo-coupling.[193] The PAF-1 material exhibited a BET surface area of 5600 m^2/g and a hydrogen uptake of 10.7 wt% at 77 K and 48 bar pressure. This high hydrogen uptake may be due to the "activation" of polymer supports under relatively mild conditions that merely remove guest molecules as opposed to reacting with species within the material as chemical or physical activation does. The PAF-1 structure needed only to be placed in a vacuum at 200 °C for the uptake measurements. Highly Stable porous polymer networks-4 (PPN-4, schematically shown in Figure IV-22), was based on the approach used for the fabrication of PAF-1. The material was synthesized by an Yamamoto homo-coupling of tetrakis(4-bromophenyl)silane under reaction conditions desiogned to slow polymerization.[192] This fabricated material had a BET surface area of 6461 $m^2 \cdot/g$, which was the highest reported among all porous materials with a hydrogen uptake of 8.34 wt% at 77 K and 55 bars of pressure. Additionally, the H_2 deliverable or working capacity of PPN-4 was approximately 5.5 wt% 1.5 bar pressure at 77 K and was higher than other comparable materials at that time and currently and remains one of the highest hydrogen storage materials.

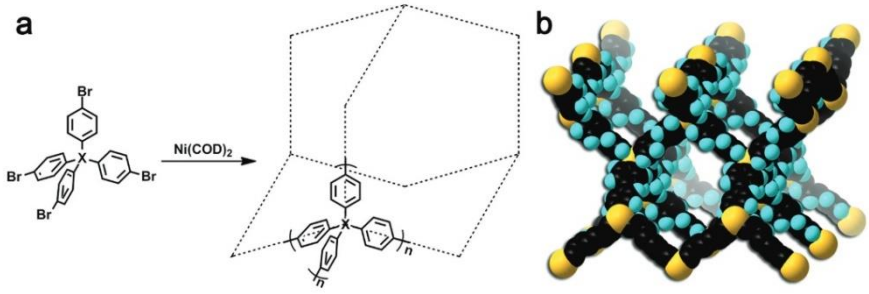

Figure IV-22. PPN-4 a) synthesis route and b) idealized structure. Reprinted with permission from 192. Copyright 2011 John Wiley and Sons.

This above example demonstrates that if the pore size can be carefully adjusted for gas capture, high uptake is feasible in meeting the DOE targets for hydrogen storage using porous materials. When the pore size is below 1 nm, hydrogen uptake (measured at 1 bar and 77 or 298 K) may also increase.[134] Therefore, to design materials with the highest uptake at these conditions, it is imperative to maximize the density of small micropores and minimize any pores above that size. However, to produce a higher deliverable capacity at a given temperature, uptake near and below 1 bar, and thus small micropores, must be minimized, while larger pores which have size and shape appropriate to saturate with hydrogen near whatever maximum pressure is allowed by a particular system must be maximized, assuming no increase of heat of adsorption due to metal doping or other techniques.

However, PAF-1 and PPN-4discussed above had a shortcoming preventing practical application , due to the expensive coupling reagent $Ni(COD)_2$ (where COD is bis(1,5-cyclooctadiene) necessary for the Yamamoto homo-coupling during the

synthesis step.[194] . The DOE target cost is $333/ kg stored hydrogen capacity, thus any porous material adopted for hydrogen storage applications will have to be synthesized in large quantities, using cheap precursors Many other porous polymers such as porous poly(triazines) have been prepared and have hydrogen uptake of 1.44 wt % at 77 K and 1 bar pressure.[195] Another triazine-based PPN, TPC-1, showed 1.02 wt % uptake at 77 K and 1 bar pressure. A wide variety of covalent organic polymers (COPs) were synthesized by the polymerization of a tetrahedral and C4-, C3-, or C2-symmetrical linking unit, producing porous polymers of up to 3624 $m^{2}\cdot/g$.[196]

The demonstrtation of the hydrogen storing capacity of PPN-4, has been adopted for gas capture of CO_2 or CH_4, catalysis, separations, or other applications, indicating this synthetic approach is flexibile and can be used towards hydrogen capture. To our knowledge no directly synthesized and vacuum-activated porous polymers have yet been reported with hydrogen uptake performance unambiguously exceeding PAF-1 or PPN-4.[197] However, PAF-1 was synthesized, carbonized under high temperature, then chemically activated with KOH.[198] This K-PAF-1-750 had improved H_2 uptake at 1 bar pressureand 77K of 3.06 wt%, but at higher pressures the hydrogen uptake was slightly reduced (though the CO_2 and CH_4 uptakes increased.) This is consistent with a decrease in mesoporosity and an increase in microporosity as confirmed by pore volume analysis, despite much lower surface area (2926 $m^{2}//g$) and total pore volume is summarised in Figure IV-23 which is a plot of pore volumes at different curation temperatures.

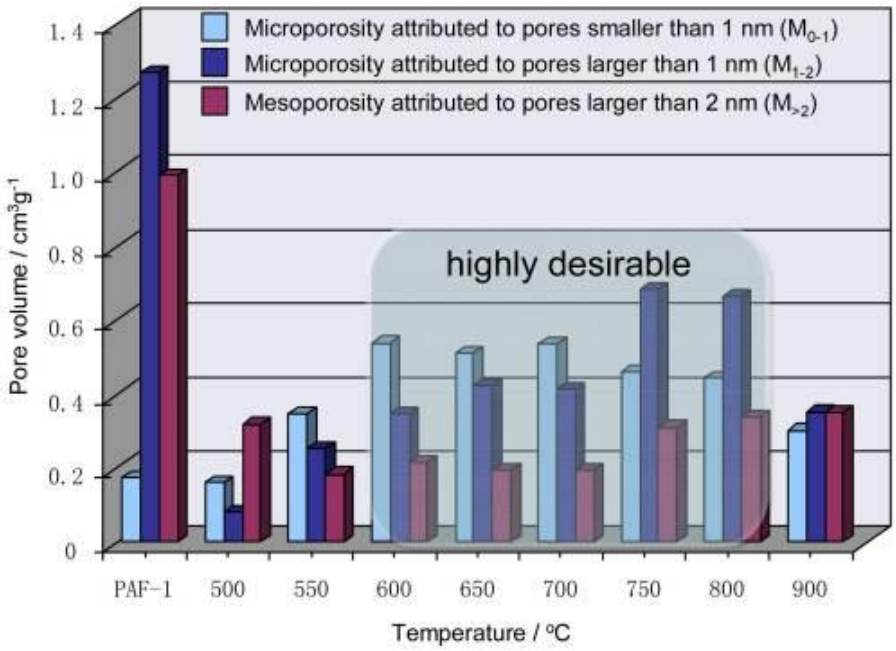

Figure IV-23. Pore volume analysis of PAF-1 versus K-PAFs KOH-activated at different temperatures. Reprinted with permission from 198. Copyright 2013 Nature Publishing Group.

4.5 SUMMARY

In the design of porous materials for hydrogen storage, carbon-based porous materials have many advantages, such as intrinsically low molecular weight, high gravimetric porosity, excellent stability, and in some cases low fabrication costs. However, advanced hydrogen sorbents have several challenges to overcome in order to meet the DOE targets, particularly at high temperatures. Because of the low heat of adsorption inherent to hydrogen physisorption, materials with very small pores, either 1 nm or less; or materials with lower pore density must be utilised at low temperatures (77 K) making them unsuitable as materials which meet the DOE target. On the other hand

materials which are engineered to increase the heat of adsorption to hydrogen promoting hydrogen spillover, have their own set of challenges which must be overcome. It is possible that DOE targets can be met with materials that have extremely high microporosity and pore volume, kept at low temperature but above 77 K and high pressures (40 bar pressure); however technical challenges remain in the engineering of sorbent materials to meet the benchmarks in terms of capacity and cost.

CHAPTER V

STEPWISE SYNTHESIS OF METAL-ORGANIC FRAMEWORKS[4]

5.1 CONSPECTUS

Metal-Organic Frameworks(MOFs) are a category of porous materials that offer unparalleled control over their surface areas (demonstrated as higher than for any other material), pore characteristics, and functionalization. This allows them to be customized for exceptional performance in a wide variety of applications, most commonly including gas storage and separation, drug delivery, luminescence, or heterogeneous catalysis. In order to optimize biomimicry, controlled separations and storage of small molecules, and detailed testing of structure-property relationships, one major goal of MOF research is "rational design" or "pore engineering", or precise control of the placement of multiple functional groups in pores of chosen sizes and shapes. MOF crystal growth can be controlled through judicious design of stepwise synthetic routes, which can also allow functionalization of MOFs in ways that were previously synthetically inaccessible. Organic chemists have developed a library of powerful techniques over the last century, allowing the total synthesis and detailed customization of complex molecules.

Our hypothesis is that total synthesis is also possible for customized porous materials, through the development of similar multi-step techniques. This will enable the

[4] Reproduced with permission from "Stepwise Synthesis of Metal–Organic Frameworks", Bosch, M.; Yuan, S.; Rutledge, W.; Zhou, H.-C. *Accounts of Chemical Research* **2017**, *50,* 857-865. Copyright 2017 American Chemical Society.

rational design of MOFs, which is a major goal of many researchers in the field. We have begun developing a library of stepwise synthetic techniques for MOFs, allowing the synthesis of ultrastable MOFs with multiple crystallographically ordered and customizable functional groups at controlled locations within the pores. In order to design MOFs with precise control over pore size and shape, stability, and the placement of multiple different functional groups within the pores at tunable distances from one another, we have concentrated on methods which allow us to circumvent the lack of control inherent to one-pot MOF crystallization.

Kinetically tuned dimensional augmentation (KTDA) is an approach using pre-formed metal clusters as starting materials and mono-topic carboxylates as equilibrium shifting agents to make single crystals of ultra-stable MOFs. Post-synthetic metathesis and oxidation(PSMO) takes advantage of the fast ligand exchange rate of a metal ion at the low oxidation state as well as the kinetic inertness of the same metal at high oxidation state to make ultrastable and highly crystalline MOFs. Multiple similar strategies have been successful for the metathesis of Fe-based MOFs to Cr^{3+}. Several highly crystalline Ti-MOFs have also been prepared. Kinetically controlled linker installation and cluster metalation methods utilize a stable MOF with inherent coordinatively unsaturated sites as matrix and post-synthetically install linkers or grow clusters on the matrix, so that a robust MOF with precisely placed functionalities is realized. This method has diverse applications especially when specific functional groups or metals having synergistic effects are desired in the proper proximity.

Exceptional porosity and stability are required for many potential applications. We have demonstrated several of these, including entrapment of nanoscaled functional moieties such as enzymes. We have developed a series of metal-organic frameworks (PCN-333) with rationally designed ultra-large mesoporous cages as single-molecule traps for enzyme encapsulation. We successfully incorporated metalloporphyrins, well-known bio-functional moieties, into robust MOFs for biomimetic catalytic applications. By rationally tuning the synthetic conditions, we obtained several different porphyrinic Zr-, Fe-, and Ti-MOFs with distinct pore size and concentrated acid or base stability, which offer eligible candidates for different applications. These and other stepwise kinetic tuning and catalyst incorporation methods are small steps towards achieving the grand challenge of detailed control of the placement of matter on an atomic and molecular level.

5.2 INTRODUCTION

One-pot Metal-Organic Framework (MOF) syntheses are often developed through trial and error. The Yaghi group has described the customization of MOF structures through the "reticular approach" of functionalizing and lengthening the linkers of known structures, and mixed-ligand MOFs are often "multivariate", or distributed randomly. This allows customization of the pore sizes of known structures, and the placement of many functional groups within them, but it can also make detailed control of the shapes of the pores and the placement of the functional groups within the pores difficult.[199,200] Many early MOFs made from divalent metals show exceptional porosity and promise for a wide variety of applications, but some proved unsuitable for many applications because of their

lack of long-term stability to ambient moisture.[2] Therefore, researchers such as Férey and Lillerud developed stable MOFs based on trivalent and tetravalent metals(M^{3+} and M^{4+}) which tend to possess much greater chemical stability due to the decreased lability of the M-O bonds.[35,201] The exceptional stability of M^{3+} and M^{4+} based MOFs have made them feasible for use in wide-scale practical applications. However, the stability of the high-valent metal-ligand bonds also causes challenges in MOF crystal growth and functionalization.

In order to produce MOFs that are chemically robust, a prerequisite for most applications, a few basic approaches have been developed over the last several years, which can be rationalized by the application of hard-soft acid-base theory. MOFs based on copper and zinc with carboxylate ligands are both easy to crystallize as large single crystals and are chemically unstable for the same reason: their metal-ligand bonds are relatively labile. Those bonds can be made less labile, increasing MOF chemical stability, by using softer, better matching ligating moieties such as those based on nitrogen heterocycles, or by using carboxylate linkers modified to protect the SBU or increase bond strength, or by using harder higher-valence metals that naturally have less labile bonds with relatively hard carboxylates.[25] The first two approaches often require complicated or expensive organic synthesis that limits the large-scale synthesis of the resulting MOFs, so our group has focused mostly on the use of high-valence metals. However, this often results either in non-crystalline, non-porous amorphous products, or MOFs that could not be grown as single crystals for characterization, with other characterization methods taking far more time and effort overall. To overcome this difficulty, we have in the last

few years developed several MOF synthesis, crystallization, and post-synthetic modification(PSM) methods, building on years of advancements in these techniques by a large number of research groups.[43,61,202]

When high-valence metal salts such as $FeCl_3$ and polycarboxylate linkers are mixed under traditional solvothermal conditions, the carboxylate linkers quickly bind to the iron to form non-crystalline, amorphous metal-ligand coordination polymers. "Modulated synthesis" using a monocarboxylic acid was developed by the Kitagawa group to alter crystal growth and morphology, and was used by the Behrens group to grow single-crystals of high-valence Zr-MOFs that had previously only been characterized using nanocrystalline powder.[43,61] This method slows nucleation both through lowering solution pH(slowing and reducing ligand deprotonation) and through competitive ligation of the metals in solution. Depending on the metal and ligand used, the exact concentration of modulating reagent can be increased over several trial reactions to allow the synthesis of amorphous products, to polycrystalline powders, typically in high yield, to large single crystals of the same MOF in lower yield, and finally to clear solutions producing no products at a high concentration of acid.[203] These methods allow the synthesis of high-valence, chemically robust MOFs with tunable crystallinity and yield. However, they still typically require the use of acidic solutions at temperatures exceeding 100°C, which limits direct one-pot incorporation of some functional groups. Our research has focused on enabling the rational design of MOFs through finding methods to overcome these and similar limitations. By using these stepwise pre- and post-synthetic modification methods, multiple functional groups can be placed at controlled positions within the structure in

order to customize materials for biomimicry, gas separation, catalysis, and other new applications.

5.3 KINETICALLY TUNED DIMENSIONAL AUGMENTATION

While the modulated synthesis method alone seemed to be sufficient for the synthesis of single-crystals of a variety of Zr-MOFs, Fe- and Ti-MOFs remained difficult to synthesize or characterize.Growing single crystals, as opposed to powders, is still difficult in these systems. This is likely because crystal nucleation is too fast and widespread, creating many microcrystalline powder particles which do not have the opportunity to continue to grow into single crystals. It may also be influenced by the lesser reversibility in the metal-ligand bond.The modulating acid concentration zone between polycrystalline powders and clear solutions was small or nonexistent. At a very high modulating reagent concentration, starting materials such as solvated metal salts may be favored, as the pH would be too low for a resulting MOF framework to be stable. Soluble metal-carboxylate clusters may also be favored when the concentration of non-linking monocarboxylates is too much higher than that of linkers. Inspired by concepts like “scale chemistry” introduced by Férey,[204] we decided not to use highly soluble metal salts as a starting material. Instead, we started from soluble metal-acetate preformed clusters, $[Fe_2M(\mu_3O)(CH_3COO)_6]$ ($M=Fe^{2+/3+}$, Co^{2+}, Ni^{2+}, Mn^{2+}, Zn^{2+}).[203]

This alters the equilibria in favor of slowing nucleation and allowing larger crystal growth in several ways. First, the less labile cluster-carboxylate bond is far slower to be displaced by an energetically very similar linking-carboxylate bond. Entropic effects, with

the displacement into solution of multiple monocarboxylates per linker, play a major role in the crystallization, and the amount of modulating acetic acid can be tuned to slow linker ligation and framework growth even further. This was validated experimentally with the synthesis and single-crystal x-ray diffraction(SCXRD) characterization of 34 different Fe-MOFs based on this cluster and 30 distinct ligands (Figure V-1).

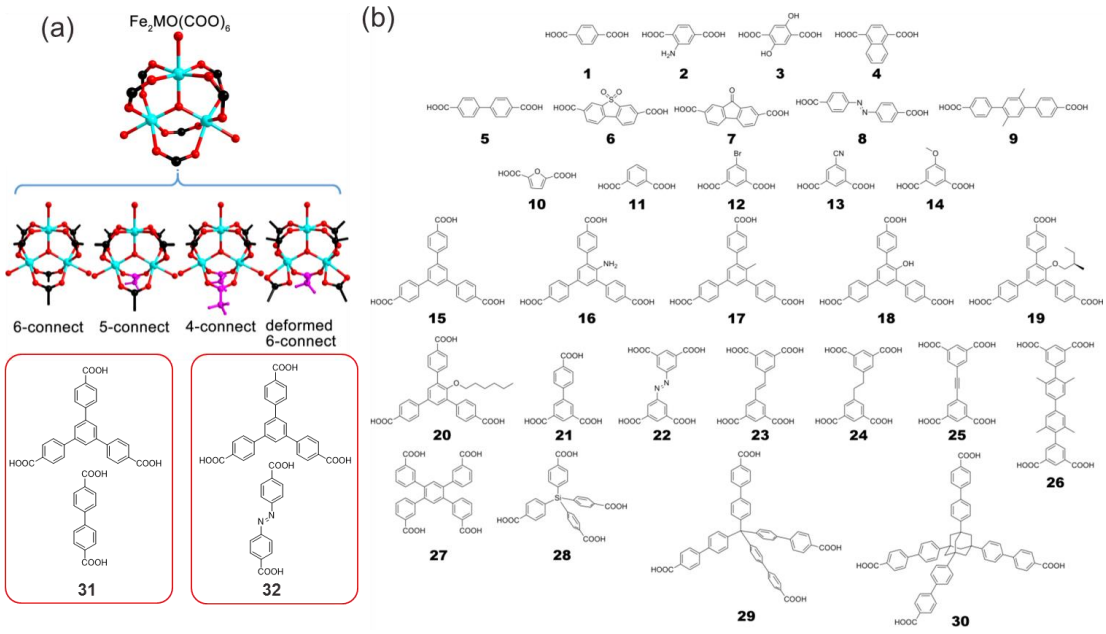

Figure V-1. (a) Four different connecting modes of the [$Fe_2M(\mu_3$-O)] cluster. Carboxylates on ligands and terminal acetates are represented by black and purple, respectively. (b) Thirty different ligands and two types of mixed ligands used in constructing Fe-MOFs.[203] Reprinted by permission from Macmillan Publishers Ltd: Nature Communications copyright 2014.

The trends observed in this work provide key insight into MOF kinetics and crystallization equilibria. We found that higher-connected ligands of similar size always

required more acetic acid to produce large single crystals, with in some cases 10 times higher concentrations of acetic acid required to get single crystals of a MOF with the same SBU, when using a tetracarboxylate linker instead of a dicarboxylate linker. This implies that the larger coordination number of the linker, displacing more acetate from the starting clusters, was a highly important factor in the MOF crystallization, though higher connectivity may increase the thermodynamic stability of the framework as well. When starting from carboxylate clusters instead of metal salts such as $FeCl_3$ less acetic acid or other nucleation-disfavoring changes were required to grow single crystals. Starting from a pre-formed cluster allows the chemist to incorporate other metals such as Co^{2+} into the (μ_3O) cluster and thus tune the SBU for other properties, and acts as a lever for crystallization control.

However, the preassembled inorganic clusters are not always preserved during the MOF formation process. The cluster should be kinetically stable under the synthetic conditions used. We aimed at using the KTDA method for the synthesis of a porphyrinic titanium MOF. A pre-formed $Ti_6O_6(O^iPr)_6(abz)_6$ (abz = 4-aminobenzoate) cluster was selected as starting material which is expected to form a she topology when combined with tetratopic porphyrinic linker (TCPP). Starting from a preformed Ti_6O_6 cluster, a single crystalline porphyrinic titanium MOF, PCN-22, was obtained. A large excess of benzoic acid was required to produce single crystals, as is typical for tetracarboxylate linkers with high-valence metals. As far as we know, this was the first report of a single-crystalline Ti-carboxylate MOF and one of very few Ti-MOFs ever reported.[205] However, the Ti_6O_6 cluster was transformed into a Ti_7O_6 cluster in PCN-22 (Figure V-2). This shows

how a robust cluster under the MOF synthetic conditions is required for the KTDA method, but as starting from a titanium salt did not produce the MOF products, it shows that even attempted KTDA can be a useful kinetic modulation method. This is similar to other examples found by our group where attempted KTDA resulted in new MOFs with different SBUs than that which were added, under conditions where the attempted original SBU was not completely stable.[206]

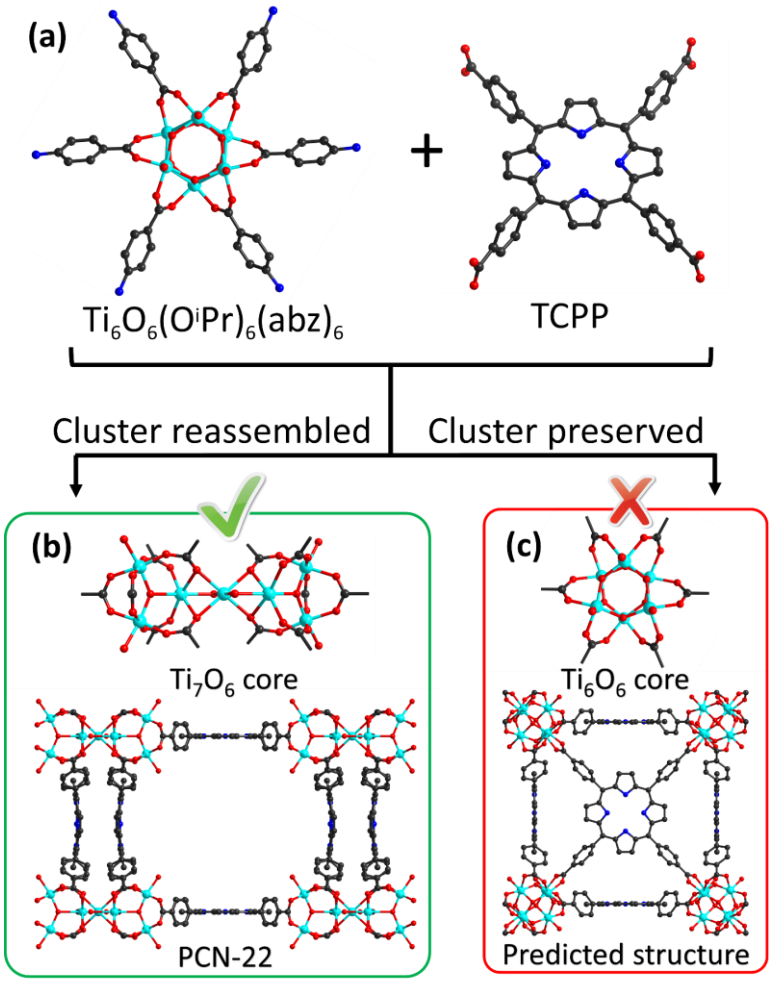

Figure V-2. (a) $Ti_6O_6(O^iPr)_6(abz)_6$ and TCPP as starting materials; (b) cluster and structure of PCN-22; (c) cluster and structure of predicted MOF with she topology.

It is worth noting that use of different amounts and types of modulating reagents can produce effects both during and after crystallization. For example, lower pKa modulators such as trifluoroacetic acid have been reported to increase the Lewis acidity, pore volume and/or surface area, and proportion of mesoporous defects in UiO-66-type Zr MOFs when compared to use of higher temperatures and higher pKa modulators, which can produce UiO-66 with few defects.[27,207] Some MOFs can even be synthesized under

basic conditions in order to influence their porosity.[208] It is possible to tune the properties of UiO-66 and many other MOFs by using different modulating reagents of different solubility and pKa. This should be tried when attempting to grow single crystals, as each solvothermal system only crystallizes in a certain range of modulator concentration. The pKa of the modulating reagent is another kinetic parameter that we can tune as part of our crystallization toolbox. However, certain systems and metals, such as Cr(III)-based MOFs which possess even less labile metal-ligand bonds than Fe(III) or Zr(IV)-based MOFs, are still difficult to crystallize directly, even with these tools. Furthermore, this method does not directly allow the rational design of new MOFs. However, KTDA is still a useful part of the synthetic toolbox, even if it does not directly provide structural control. This is because the empirical "kinetic control" methods developed as part of KTDA are used in the later structural control methods. In methods such as postsyntheic metathesis and oxidation or sequential linker installation, a MOF with a known structure is modified using the kinetic methods developed in KTDA.

5.4 POSTSYNTHETIC METATHESIS AND OXIDATION

Some extremely stable high-valence MOFs such as Ti- and Cr- based MOFs are extremely rare, due to the aforementioned difficulties in their synthesis and characterization. Building on a large variety of post-synthetic modification techniques developed by many researchers in the MOF field,[202] our group has developed a variety of approaches based on metal metathesis in order to produce MOFs based on these metals, which then demonstrate much higher chemical stability than the isoreticular parent

frameworks they are based on. Postsynthetic Metathesis and Oxidation (PSMO) refers to the synthesis of a targeted MOF based on metals such as Sc^{3+}, Zn^{2+}, or Mg^{2+}. The use of scandium^{3+} here, along with example such as Zr^{4+} MOFs, is actually a useful example of how "high-valence" and "low-valence" MOF is a shorthand that is too simplistic to be completely accurate. Sc^{3+}-based MOFs, as d^0 metals, actually tend to be less or similarly chemically stable than, for example, d^9 Cu^{2+}-based MOFs, despite their increased valence, possibly because ligand exchange is not energetically destabilized by the ligand field stabilization energy(LFSE) of the metal. Similarly, d^0 Zr^{4+} and Ti^{4+} MOFs tend to be less stable than d^3 Cr^{3+} MOFs. There are also many other factors affecting stability, such as SBU and ligand connectivity, porosity, and the functionalization and ligating moieties of the linker.

Because the original MOFs are made with labile metals, an excess of less labile metal in solution after synthesis should be entropically driven to exchange. The speed and completeness of this metal metathesis depends on both the metal concentration and the relative thermodynamic stability of each metal in the MOF SBU's coordination environment. Building on previous work by the Dinca and Cohen groups,[104,209], we reasoned that care must be taken to select MOFs with SBUs that the new metal will be stable in. Furthermore, direct exchange of low-valence to low-valence metals, while fast, did not produce an increase in MOF chemical stability, while direct exchange from low to high-valence metals was incomplete and slow. One of the solutions was to select MOFs with SBUs and coordination environments that were highly stable with the new metal, exchange for a lower-valence, unstable ion of that metal under an anoxic environment,

and then allow the air to oxidize the metal to its stable higher oxidation state. This was demonstrated in PCN-426, where Mg(μ_3-O) clusters serve as an SBU which can be easily exchanged for Fe(II) and Cr(II), which remain labile in those oxidation states. After oxidation, this process produced a MOF which was to our knowledge the first example of a Cr-MOF of sufficient crystal size and quality for characterization on a non-synchrotron single-crystal diffractometer.[31] This is an example of how even materials that cannot be directly crystallized can be synthesized and characterized through stepwise methods that change environmental conditions to "climb" over an energetic barrier into a local energy minima.

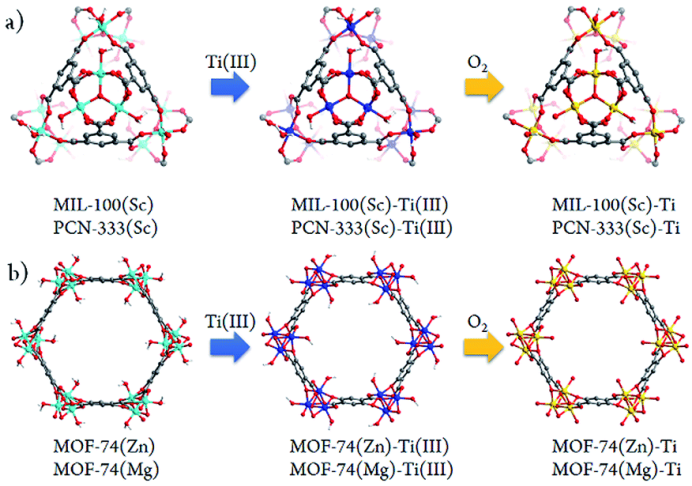

Figure V-3. The stepwise PSMO synthetic method allows high-valence metals to be used in a MOF structure that was not found through one-pot methods.[210] Published by The Royal Society of Chemistry.

PSMO was also applied to the synthesis of multiple titanium frameworks based on appropriate SBUs. MIL-100(Sc), PCN-333(Sc), MOF-74(Zn), and MOF-74(Mg) were all quickly exchanged with Ti(III), (Figure V-3) which was then oxidized in air to Ti(IV) with

varying rates of metathesis ranging from 35% in MOF-74(Mg-Ti) to 100% in MOF-74(Zn-Ti), combined with promising photocatalytic activity measurements.[210]

We soon worked to extend this process in order to stabilize and functionalize a framework, PCN-333, that was useful due to its extremely large 5.5 nm mesopores, but had relatively high chemical stability, but slightly lower than other MOFs synthesized with the same SBU, presumably due to those mesopores.[30,211] Modulated synthesis using 4,4',4''-s-triazine-2,4,6-triyl-tribenzoate (H_3TATB) with MCl_3 (M=Al, Fe, V, Sc, In) and trifluoroacetic acid produced frameworks which were isoreticular with MIL-100.[211] Due to the many-sided shapes of the larger pores in their MTN topology, isoreticular expansion produces greater pore size increases than it does in frameworks with pores that have fewer "sides" or windows. These large pores proved useful in the encapsulation and protection of several enzymes, which retained catalytic activity within the pores under conditions that unprotected enzymes were denatured under. The chemical stability of this framework, remaining intact under conditions of pH 3-9, is high for such a highly porous material, but needed to be improved for certain catalytic applications requiring more concentrated acid or basic solutions.

One metal produces MOFs which typically have higher chemical stability than that of Fe(III) – Cr(III). However, growth of PCN-333(Fe) already pushed the limits of our earlier kinetic tuning and crystallization methods, with only powder synthesized, which had to be characterized using synchrotron powder x-ray diffraction methods. Attempts to directly synthesize PCN-333(Cr) produced only amorphous, non-porous products. Furthermore, directly synthesized Cr-MOFs such as MIL-101 have proven highly difficult

to functionalize, as the high-temperature, high-pressure conditions necessary for the synthesis of even powders of these MOFs decompose many functional groups that have been used in other MOFs.[212] Both of these problems were solved simultaneously by the "dual exchange" of PCN-333(Fe) to PCN-333-N_3(Cr). Postsynthetic ligand exchange of PCN-333(Fe) allowed the functionalization of the framework with moieties that are too fragile to survive solvothermal synthesis, or that formed another framework structure when direct synthesis with a similar linker was attempted (Figure V-4).[30,213] Subsequent metal metathesis allowed such functionalities into the Cr-MOF, which was too kinetically inert for successful postsynthetic ligand exchange. Interestingly, PCN-333(Sc) showed only 64.8% exchange for Cr under conditions that produced a 99.8% exchange ratio when starting from PCN-333(Fe) at 150°C over two 30 minute incubations in $CrCl_3$ DMF solution, due to framework collapse when starting from PCN-333(Sc) – it is not stable enough to survive the exchange conditions, while PCN-333(Fe) was. Unlike in the case of PCN-426, replacing Fe(III) with Cr(III) via metathesis of Fe(II) to Cr(II) followed by oxidation was not necessary, due to the more similar ligand exchange rate constants of Fe(III) and Cr(III).

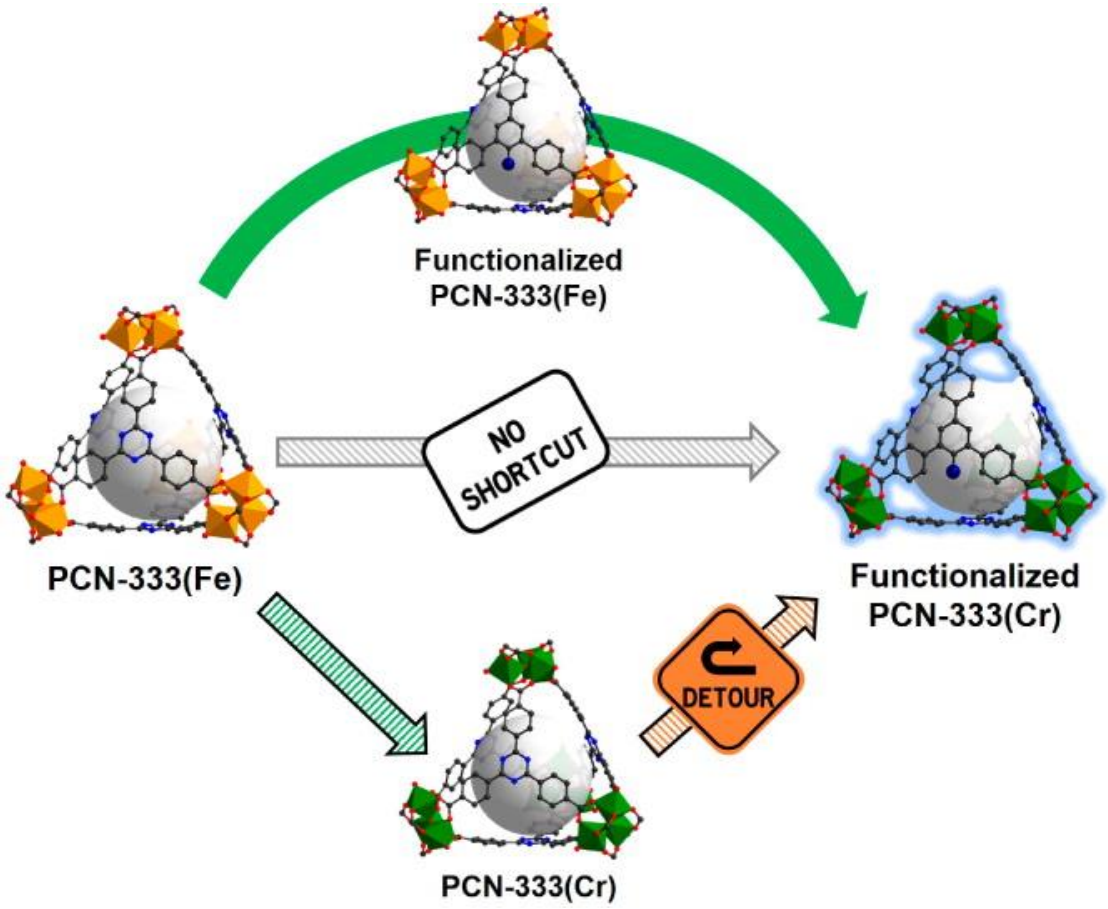

Figure V-4. Stepwise synthesis was used to functionalize PCN-333(Cr). Reprinted with permission from 30. Copyright 2015 American Chemical Society.

Another method that takes advantage of redox changes to control the metathesis reaction, "reductive labilization," was demonstrated through an alternative preparation of PCN-333(Cr). In this case, anoxic Cr(II) solutions were used for an outer-sphere reduction of Fe(III) in PCN-333(Fe) to Fe(II), which quickly exchanged with the Cr(III) that was produced by this reaction. PCN-333(Cr) was also shown to be much more chemically robust than PCN-333(Fe), showing stability over 24 hours in solutions of pH 0-11, and

surviving uptake of alkylamines, used to increase the CO_2 uptake of the material through chemisorption, while PCN-333(Fe) was degraded by the alkylamine molecules.

5.5 SEQUENTIAL LINKER INSTALLATION AND CLUSTER METALATION

MOFs have been very widely studied due to their combination of ease of crystalline synthesis, high surface area, easy functionalization, and high chemical stability. They are promising for many applications due to these properties, especially as they have been demonstrated to be functionalized simultaneously with up to 8 different moieties in controlled ratios, as in multivariate MOFs.[214] One limitation has been that placement of multiple functional groups at controlled positions, important for applications such as biomimetic catalysis, has been limited, though some post-synthetic modification approaches, such as those recently published by the Yaghi group, have been promising.[215] The synthesis of mixed-ligand MOFs offers another solution to this limitation, as each ligand can be functionalized separately, and the distance and orientation of the functional groups from each other will be known and controlled by the MOF structure. Mixed ligand MOFs are rare, have had limited chemical stability, and have mostly been confined to 2 types of linkers, with mixed phases or domains forming when more symmetrically distinct linkers are mixed in one-pot reactions.[216,217] In our experiments, one-pot solvothermal synthesis using linear linkers of different length always produced a mixture of different MOF phases, and so a kinetically controlled, stepwise approach was used to produce several new MOFs through single-crystal to single-crystal transformations.

To overcome these difficulties, we targeted the Zr_6 SBU, which possesses tunable connectivity, from 6 to 12 connections depending on the linker used in the MOF. In the UiO-66 type structure, otherwise known as the fcu topology, the carboxylates on the linear linkers must be coplanar in order for the Zr6 SBUs to form 12-connected nodes. By using a linker that twists at a 90° angle, i.e., dimethyl biphenyl dicarboxylate, instead of the unhindered, non-functionalized biphenyl dicarboxylate of UiO-67, another structure, PCN-700, is produced at lower temperatures (Figure V-5).[218] The bcu topology of PCN-700 is similar to fcu, except that 4 equatorial linkers on the SBU are missing, producing an 8-connected node. (Figure V-5).

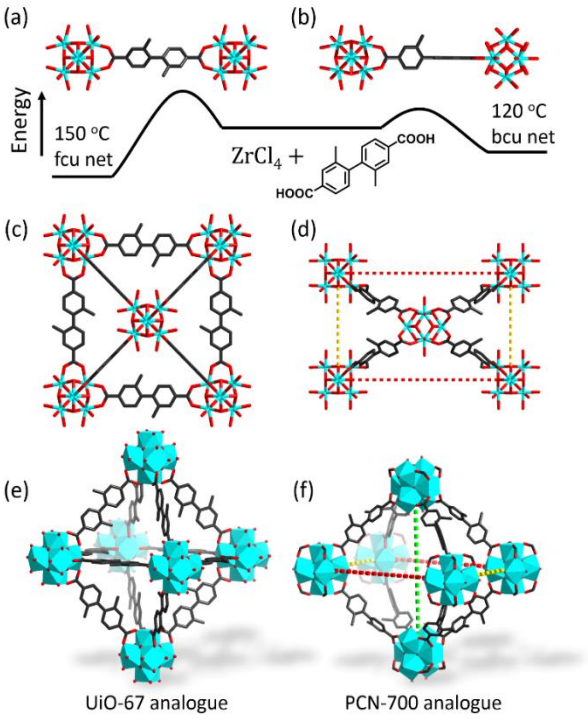

Figure V-5. Temperature control in the synthesis of PCN-700, which has unsaturated SBUs suitable for later linker installation: (a) Linker conformation in fcu nets; (b) linker conformation in bcu nets; (c) UiO-67 and (d) PCN-700 structures viewed along *a*-axis; cages of (e) UiO-67 and (f) PCN-700 structures. Reprinted with permission from 218, Copyright 2015 American Chemical Society.

The missing coordination areas on the Zr_6 SBU in PCN-700 consist of terminal oxygens that can be, in turn, displaced by a post-synthetic ligation reaction. Two of the sites have different lengths than the other two, which allows the stepwise placement of two different types of linear linkers, which can be separately functionalized (Figure V-5). Furthermore, all this takes place in a crystallographically ordered fashion, and so the precise distances of each of the 3 possible linkers and any functional groups attached to

them can be measured, which was demonstrated through the synthesis and crystallographic characterization of PCN-701, -702, -703, and -704, with different ordered linkers. PCN-700 shows a high degree of flexibility, which allows the installation of linkers with different lengths and a combination thereof.[219] Guided by geometrical analysis, eleven new MOFs were obtained by linker installation, each bearing up to three different functional groups in predefined positions (Figures 5.6 and 5.7). Systematic variation of the pore volume and decoration of the pore environment was realized by linker installation, which resulted in synergistic effects including an enhancement of H_2 adsorption capacities of up to 57%. In addition, a size-selective catalytic system for aerobic alcohol oxidation reaction was built in PCN-700 through linker installation, which shows high activity and tunable size-selectivity. Altogether, these results exemplify the capability of the linker installation method in pore environment engineering of stable MOFs with multiple functional groups, giving an unparalleled level of control.[220]

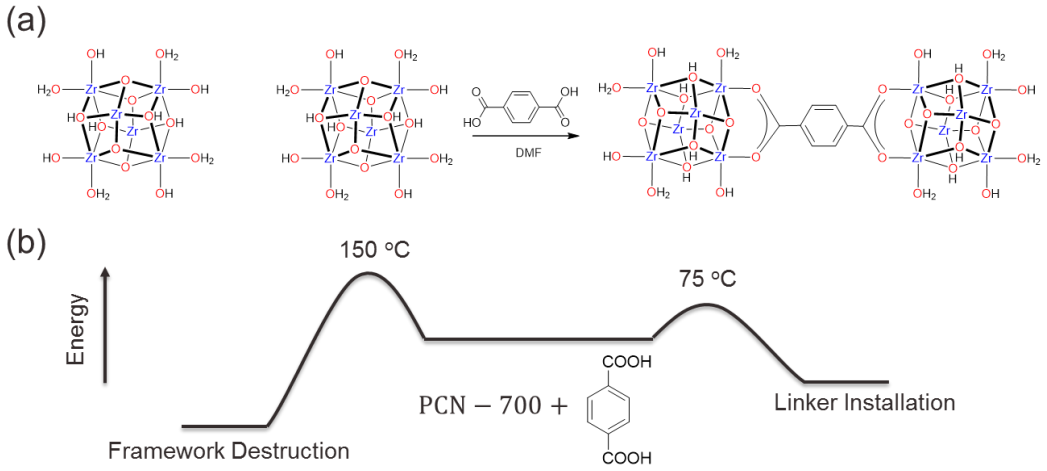

Figure V-6. (a) Chemical equation and (b) kinetic control of the stepwise linker installation process.

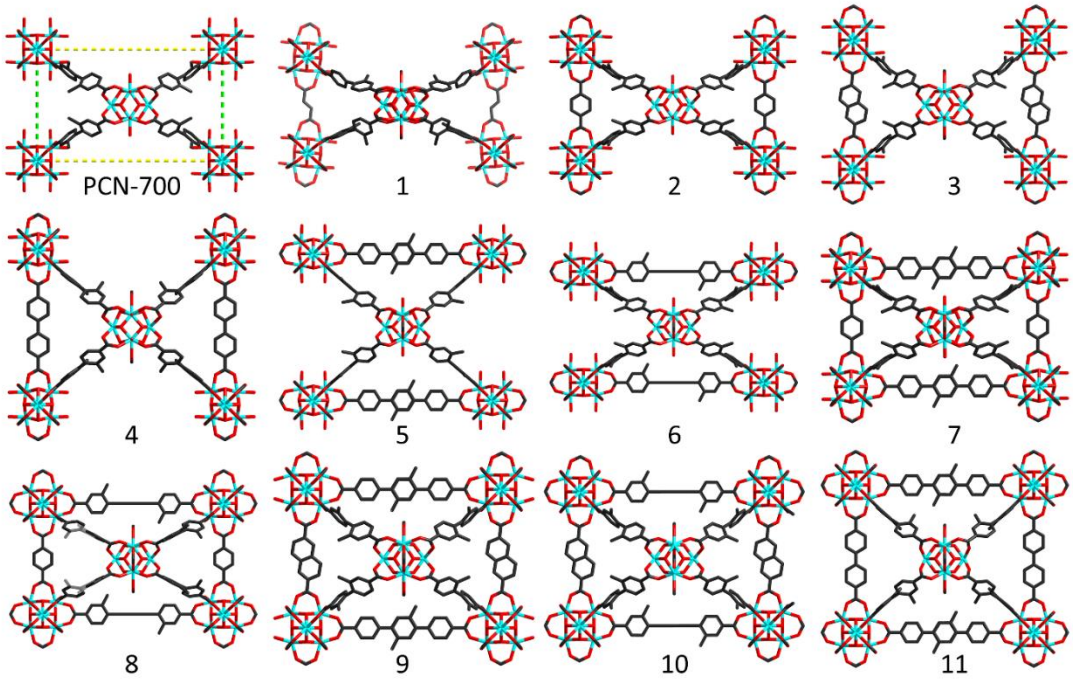

Figure V-7. Single crystal structures of eleven geometrically predicted MOFs resulted from linker installation of PCN-700. Reprinted with permissions from 220. Copyright 2016 American Chemical Society.

In addition to multifunctional mixed-linker MOFs being made synthetically accessible through the control afforded by stepwise synthesis, mixed-metal Zr MOFs have also been produced. PCN-700's terminal oxygens on its equatorial plane are postsynthetically solvothermally reactive with other metals, which over time grow onto the Zr_6 SBUs, forming decanuclear Zr_6M_4 (M=Ni, Co) clusters, which can be shown stepwise with successive SCXRD "snapshots" if the reaction is interrupted every several hours (Figure V-8).[221]

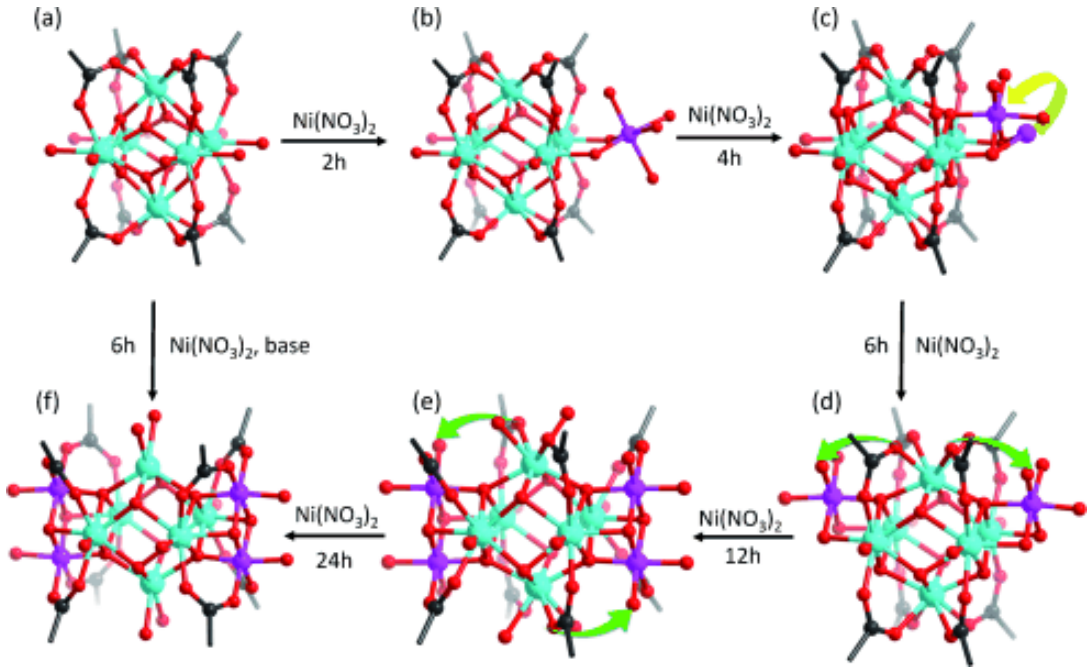

Figure V-8. Cluster transformation during the cluster metalation and ligand migration; the yellow arrows illustrate the metal migration and green arrows the ligand migrations.[221]

5.6 CONCLUSIONS

Since the late 1990s, research interest in MOFs has been growing continuously. In a recent review article, Yaghi et al. proposed that the new materials should have multiple kinds of building units, and the arrangement of these building units within crystals should have specific sequences. Advanced functionalities in MOFs require more complex structures and pore environments, accompanied by heightened challenges with their geometric design. Constructing metal−organic frameworks from multiple components is a pathway to enable sophisticated applications which require high complexity in highly ordered crystalline materials. The above-discussed research provides possible methods to increase MOF complexity while maintaining structural regularity to the maximum extent.

We have begun developing a library of stepwise synthetic techniques for MOFs, allowing the synthesis of ultrastable MOFs with multiple crystallographically ordered and customizable functional groups at controlled locations within the pores. In the long term, we expect to realize total synthesis in MOFs for customized structures and functionalities, through the development of stepwise synthetic techniques. Although currently not possible, the high designability and diverse synthetic methodologies of MOFs discovered in recent years suggest that such a feat is feasible in the future, and represents one path towards "rational design" of MOFs that is a major goal within the field.

The kinetic tuning, crystallization, and postsynthetic modification methods described here are part of a growing synthetic toolbox for MOF researchers. Each of these methods can be used to achieve the synthesis and characterization of new, targeted MOFs that would not be possible in a simple one-pot solvothermal crystallization process. Eventually, we hope to help realize the dream of rational, stepwise design of metal-organic frameworks (MOFs) with precise control over pore size and shape, stability, and the placement of multiple different functional groups within the pores at tunable distances from one another. This precise control will be necessary to produce materials optimized for energy storage, catalysis, or other applications that can benefit from the engineering of pore environments.

We have developed and demonstrated the KTDA, PSMO, sequential linker installation, structure-assisted functional anchor implantation, single-enzyme encapsulation, and other methods for this purpose. Each of these methods, more than simply allowing the synthesis of the particular MOFs published with them, can be used to

synthesize a limitless variety of MOFs customized for many different applications. The stepwise methods we have described allow researchers to overcome the harsh conditions necessary for MOF crystallization and the randomness of functional group placement that have previously limited biomimicry.

Small molecule separations are governed by selecting a separation material that has pore size, shape, and functionalization that select very preferentially between molecules that may be very similar to one another, such as racemic mixtures or different isomers of a molecule. Stepwise synthesis offers new opportunities to design MOFs for this purpose. Small molecular characterization can also be undertaken in this way, for example through the crystalline sponge or coordinative alignment methods.[222,223] Using the PSMO and sequential linker installation methods to produce materials customized for preferential interaction by multiple aligned functional groups with small molecules of interest will be a rich avenue of future investigation. The KTDA method can be used for isoreticular manipulation of the SBU of known MOFs, and modulation of their surface area and catalytic activity, as well as synthesis of MOFs not synthetically accessible through in-situ SBU assembly. Immobilization of enzymes and homogenous molecular catalysts can be used to produce robust, re-usable heterogeneous catalysts. Finally, development of new stepwise synthesis and modification techniques is vital to allow more precise pore engineering and to work towards the rational design of MOFs.

CHAPTER VI

LITHIUM INCLUSION IN INDIUM METAL-ORGANIC FRAMEWORKS SHOWING INCREASED SURFACE AREA AND HYDROGEN ADSORPTION[5]

6.1 OVERVIEW

Investigation of counterion exchange in two anionic In-MOFs showed that partial replacement of disordered ammonium cations was achieved through the pre-synthetic addition of LiOH to the reaction mixture. This resulted in a surface area increase of over 1600% in (Li [In(1,3-BDC)$_2$])$_n$ and enhancement of the H_2 uptake of approximately 275% at 80000 pascals at 77 K. This method resulted in frameworks with permanent lithium content after repeated solvent exchange as confirmed by ICP-MS. Lithium counterion replacement appears to increase porosity after activation through replacement of bulkier, softer counterions, and demonstrates tuning of pore size and properties in MOFs.

6.2 INTRODUCTION

Metal-Organic Frameworks (MOFs) are an emerging category of porous materials that consist of metal-containing units and organic linkers.[89,224] They are promising materials for the storage of fuel gases like methane and hydrogen, but so far they fall short

[5] Reproduced with permission from "Lithium inclusion in indium metal-organic frameworks showing increased surface area and hydrogen adsorption", Bosch, M.; Zhang, M. W.; Feng, D. W.; Yuan, S.; Wang, X.; Chen, Y. P.; Zhou, H. C. *Apl Materials* **2014**, *2*. Copyright 2014 by the authors.

of targets for gravimetric and volumetric capacity set to make them superior to current fuel technologies.[225,226] Recently, theoretical studies have shown that lithium doping is a viable way to increase hydrogen uptake near ambient conditions, through increased electrostatic interactions.[227] Additionally, crystalline ionic MOFs are promising materials for ion exchange and separation.[228] MOFs that are easily impregnated by lithium ions should possess several attributes.[229] First, this MOF should possess considerable stability, to retain porosity after lithium inclusion and the subsequent activation process. Second, this MOF should be negatively charged, so that Li^+ ions can be held in the framework by electrostatic forces. Many indium MOFs possess a negatively charged framework which may stabilize the presence of positively charged lithium ions in the pores.[230-232] Furthermore, it has been hypothesized that the breakdown of solvents into ionic molecules during the solvothermal reaction plays an important role in MOF synthesis, particularly in ionic MOFs which require a counterion. [233-235] In principle, it is suggested that the exchange of bulkier counterions for small lithium ions should be a facile method to increase the porosity of any MOF with an anionic framework.

In order to test the hypothesis outlined above, several synthetic methods were tried to introduce lithium into several MOFs. $In(1,3\text{-}BDC)_2^-$ (BDC=1,3-benzene dicarboxylate) and $In(NDC)_2^-$(NDC=2,6-naphthalene dicarboxylate) were synthesized according to the literature procedures.[231,232] After the crystal synthesis, exchange reactions were performed with various lithium metal sources, including lithium chloride, lithium acetate, and lithium nitrate. Unexpectedly, these efforts led to either framework collapse (possibly due to exposure to atmospheric moisture) or no increase in porosity. It is suggested that the

cations in the frameworks as reported were too bulky to be removed by a simple exchange process, and thus this approach was unsuccessful.

6.3 RESULTS & DISCUSSION

In our experimental studies, a direct synthesis method was used, which introduced LiOH directly to the solvothermal reaction mixture before sonication and heating. This was intended to bring about the immediate formation in solution of some proportion of ligand molecules that were deprotonated to form lithium carboxylates, which would then form a framework with the lithium ions close at hand for charge balancing during synthesis. This resulted in an In-BDC framework with significantly increased porosity compared to the version filled with disordered tetramethyl ammonium cations in the framework, with the greatest porosity found when a number of moles of lithium hydroxide equal to the moles of ligand present were added before solvothermal synthesis. Based on stoichiometric control, we found that addition of LiOH in ratios lower than 1:1 LiOH:ligand produced less porous MOF, while a higher proportion produced amorphous material. Attempts to produce MOF with added NaOH or KOH produced a non-crystalline, non-porous product, presumably due to the drastically increased basicity of those solutions.

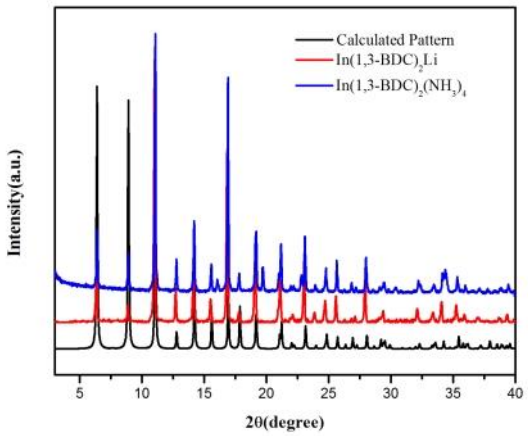

Figure VI-1. Powder XRD patterns for simulated and experimental In(1,3-BDC)$_2$ samples. The (2 $\bar{1}$ 0) reflection is at roughly 12° 2θ.

Both investigated compounds, ([N(CH$_3$)$_4$] [In(1,3-BDC)$_2$])$_n$ and (Li [In(1,3-BDC)$_2$])$_n$, possess a very similar structure to that described in the literature[231] as verified by powder X-Ray Diffraction(PXRD) (Figure VI-1), which was that of one dimensional anionic nanotubes, with each indium connected to four isophthalates, shown in Figure VI-2. Extraneous peaks were found in the PXRD measurement of ([N(CH$_3$)$_4$] [In(1,3-BDC)$_2$])$_n$ at approximately 16° , 19°, and 34.5° , likely indicating some impurity accompanied the starting materials.[231]

As shown in Figure VI-1, slight downshifting of the peaks in the PXRD for (Li [In(1,3-BDC)$_2$])$_n$ could indicate a slightly larger unit cell for the experimental pattern, while slight changes of the intensity ratios could be attributed to different occupancy, with lithium replacing tetramethyl ammonium.[236] The dimensional variation of the unit cell could be influenced by a different test temperature – the experimental PXRDs was taken

at room temperature, which should cause a slight expansion of the unit cell compared to the reported single crystal XRD taken at 100 K.[237] It could also arise from a greater degree of solvent remaining in the crystals for the PXRD pattern, as the PXRD was taken from sample directly removed from the solvent without activation. The difference in peak intensities may be caused by solvent molecules and counter ions in the channels of the structure, which could not be crystallographically localized but contribute to the experimental X-ray diffraction.[238]

For example, the highest observed intensity in the experimental pattern occurs on the (2 $\bar{1}$ 0) plane of the unit cell, which includes the line describing the center of the nanotube, shown in Figure VI-2. Therefore, a great deal of electron density is shown on this plane in the experimental pattern which is absent in the pattern simulated from the CIF. This may be because the single-crystal solution reported did not include the contents of this solvent-accessible space inside the nanotube. The large amount of electron density in the center of the nanotube shown by the experimental pattern likely consists of molecules trapped within the nanotubes, in addition to the oxygen and carbon atoms on the framework also intersected by the plane. It cannot be ruled out that some slight shift in the framework structure may have occurred as a consequence of lithium inclusion. However, the similarity of the PXRD patterns indicates that any such shift is minor.

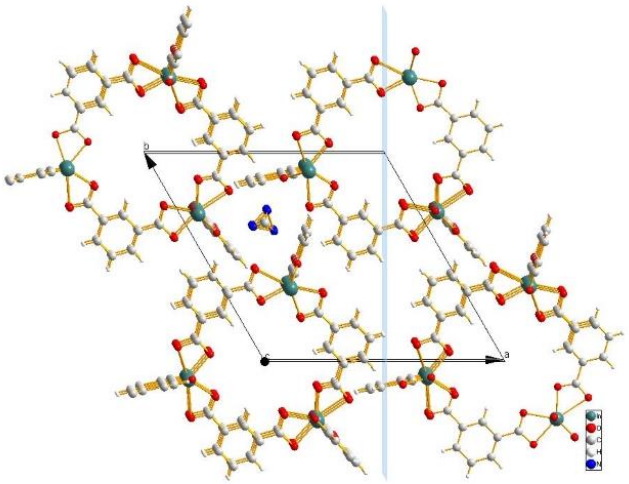

Figure VI-2. A slightly offset crystallographic view of the ab plane of ($[N(CH_3)_4]$ $[In(1,3\text{-}BDC)_2]$)$_n$, with the blue line representing the (2 $\bar{1}$ 0) plane, which continuously includes the center of the nanotube. Large white spheres correspond to carbon atoms, small white to hydrogen, red to oxygen, and green to indium. The blue corresponds to nitrogen occupying disordered positions.

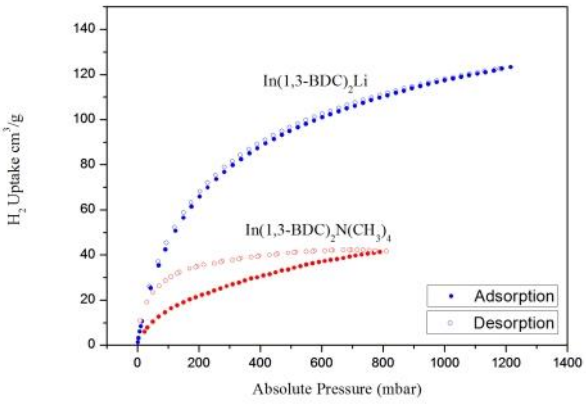

Figure VI-3. ($[N(CH_3)_4]$ $[In(1,3\text{-}BDC)_2]$)$_n$ vs (Li $[In(1,3\text{-}BDC)_2]$)$_n$ H_2 sorption measurements.

Following solvent exchange and activation, gas sorption measurements were performed on both materials. The N_2 adsorption measurements showed that BET surface area increased from approximately 26 m^2/g in $([N(CH_3)_4]\ [In(1,3\text{-}BDC)_2])_n$ to approximately 420 m^2/g in $(Li\ [In(1,3\text{-}BDC)_2])_n$. $(Li\ [In(1,3\text{-}BDC)_2])_n$ had an H_2 uptake of approximately 110cm^3/g at 800 mbar, while In-BDC-$N(CH_3)_4^+$ showed an H_2 uptake of 40cm^3/g at 800 mbar, and hysteresis in its H_2 isotherm was consistent with small pore size. (Figure VI-3) $(Li\ [In(1,3\text{-}BDC)_2])_n$ shows increased pore size as well as increased N_2 and H_2 uptake. This is consistent with a hypothesized smaller Li^+ counterion in an otherwise very similar framework.

After repeated washes of the material with dimethylformamide(DMF) and ethanol, and multiple cycles of overnight solvent exchange, ICP-MS measurements showed that $(Li\ [In(1,3\text{-}BDC)_2])_n$ possessed an indium-lithium ratio of approximately one lithium per two indium. This provides evidence that Li^+ is permanently ionically attached in the pores as a counterion, indicating significant but incomplete counterion replacement.

While the presence of lithium in the In-BDC framework can be preliminarily confirmed by the ICP results, the increased surface area, and hydrogen adsorption data, further crystallographic evidence was sought. However, single-crystal XRD characterization of $(Li\ [In(1,3\text{-}BDC)_2])_n$ was unsuccessful. Instead, synthesis of the In(2,6-NDC) series was undertaken to further explore the incorporation of Li^+ ions in anionic MOFs from the crystallographic perspective.

Single crystal XRD was taken of multiple crystals of $(Li[In(NDC)_2])_n$, all of which were solved in the *P* 4/*n* space group. The reaction mixture including LiOH contained crystals with two separate habits. Clear rods were measured which also had a framework identical to $((Et_2NH_2)[In(2,6\text{-}NDC)_2{*}2H_2O{*}DEF])_n$, while purple blocks were also isolated which had identical connectivity, but a unit cell with a short axis elongated from 8.2 Å to 8.7 Å. This corresponds to a change in the indium-indium distance,[232] and the pore length, of the same amount on that axis. However, the topology of these networks remained consistent, and significant electron density next to the indium in the clear rods found in $((Et_2NH_2)[In(2,6\text{-}NDC)_2{*}2H_2O{*}DEF])_n$ was significantly lessened in the Li^+ version, consistent with Li^+ ions replacing some proportion of $[N(CH_3)_2H_2]^+$. This is in contrast to $((Et_2NH_2)[In(2,6\text{-}NDC)_2{*}2H_2O{*}DEF])_n$ where the $(Et_2NH_2)^+$ counterion could be crystallographically located.[232] We were careful to verify this before the removal of disordered solvent electron density using the *SQUEEZE* routine of *PLATON*, which could interfere with such analysis. (Figure VI-4) ICP results also confirmed the presence of significant lithium in the pores even after washes with DMF and ethanol, though the Li-In ratio found for this sample may not be accurate due to difficulties in acquiring a sample including only one type of crystal.

Pure samples of $(Li[In(NDC)_2])_n$ crystals were not obtained in quantities necessary for gas sorption measurement, as all samples prepared with LiOH contained both types of crystals. However, this provides evidence that Li^+ can be successfully incorporated into multiple, topologically dissimilar negatively-charged indium MOFs through direct solvothermal synthesis in the presence of LiOH.

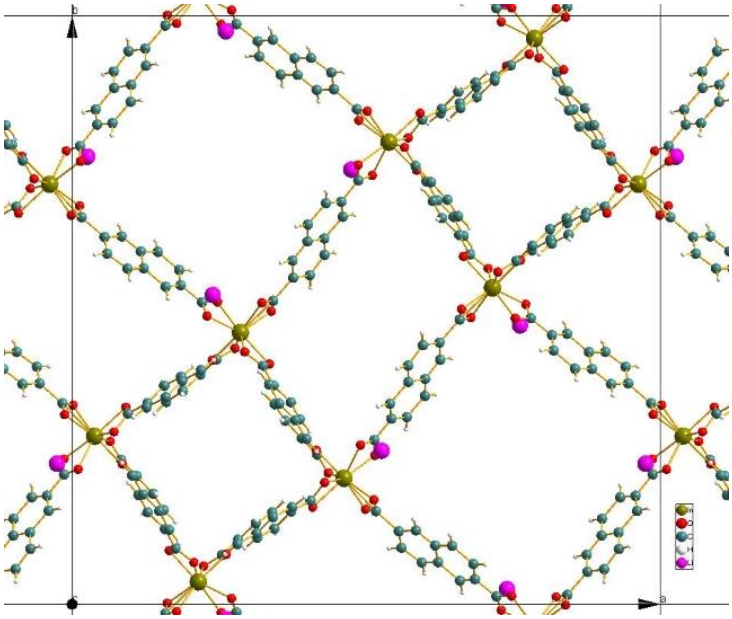

Figure VI-4. Crystallographic view of the ab plane of the framework of $(Li[In(NDC)_2])_n$, which consisted of crystals of a separate color and habit than that of $((Et_2NH_2)[In(2,6\text{-}NDC)_2{*}2H_2O{*}DEF])_n$, while possessing an identical topology.[232,239]

6.4 CONCLUSION

In conclusion, we showed that partial replacement of disordered ammonium cations with lithium ions in two anionic In-MOFs was possible through the pre-synthetic addition of LiOH to the reaction mixture. The effects of the replacement of ammonium cations in anionic In-MOFs with Li^+ were investigated, resulting in a surface area increase of over 1600% in $(Li\ [In(1,3\text{-}BDC)_2])_n$. The H_2 uptake was improved by 275% at 800 mbar. Preparation of $(Li\ [In(1,3\text{-}BDC)_2])_n$ yielded a powder product of lower crystallinity than that produced by the less basic carboxylic acid ligand. Synthesis of $(Li\ [In(NDC)_2])_n$

which was more easily crystallized provided additional evidence of lithium inclusion through ICP-MS measurements and the presence of significantly reduced counterion electron density in the lithiated version through X-ray analysis. This synthetic approach may be applicable to more MOFs possessing anionic frameworks, and replacement of bulky with small and hard counterions should be accompanied by an increase in pore volume. Furthermore, as ICP-MS indicated a molar ratio of one lithium per two indium over repeated measurements, synthetic tuning may produce a greater degree of counterion replacement and allow higher porosity than that reported here. This synthetic strategy also provides a facile method to tune the pore sizes of various anionic MOFs for example, size-selective separation of various gas molecules through counterion exchange in topologically identical frameworks.[240] Finally, this material may be promising for investigation of its Li^+ or other ion conduction properties.[241]

CHAPTER VII

MODULATED SYNTHESIS OF METAL-ORGANIC FRAMEWORKS THROUGH TUNING OF THE INITIAL OXIDATION STATE OF THE METAL[6]

7.1 OVERVIEW

Modulated solvothermal synthesis and other alterations of synthetic conditions have been used to control metal-organic framework (MOF) crystallinity, porosity, and other properties. However, so far these changes have mostly been limited to changes in solvent, pH, or modulating acid type or concentration. In this work, we introduce a new method for the tuning of MOF synthesis: modulation through alteration of the metal source's initial oxidation state. By choosing a metal source that should be reduced or oxidized at high temperature in the solvent, metal concentration can be started at zero for initially insoluble starting materials and then increased as the metal reacts with the solvent, slowing and altering crystallization compared to standard MOF solvothermal synthesis. This concept is demonstrated through the synthesis of PCN-47, PCN-48, and PCN-49, MOFs with distinct structures and porosities synthesized from the same metal and ligand with the metal initially in different oxidation states.

---

[6] Reproduced with permission from "Modulated Synthesis of Metal-Organic Frameworks through Tuning of the Initial Oxidation State of the Metal", Bosch, M.; Sun, X.; Yuan, S.; Chen, Y. P.; Wang, Q.; Wang, X.; Zhou, H. C. *European Journal of Inorganic Chemistry* **2016**, 4368-4372. Copyright 2016 Wiley-VCH Verlag GmbH & Co. KGaA.

7.2 INTRODUCTION

Metal-Organic Frameworks(MOFs) are materials generated by the linkage of rigid or semi-rigid organic polytopic ligands with metal ions or clusters to form an ordered, repeating crystalline pattern that contains potential pores, or voids.[1] These pores can often be evacuated or "activated" with vacuum and temperature, allowing the adsorption of other molecules within the material and the measurement of permanent porosity.[2] A wide variety of other molecules can interact with the framework within its pores. Furthermore, the shape, arrangement, size, and content of these pores can be manipulated through continually advancing synthetic techniques.[3,4] Because of this, MOFs can be used for gas storage or separations, catalysis, chemical sensing, drug delivery, photosensitive materials, or any of a wide variety of other applications that can take advantage of the ability to precisely influence the arrangement of atoms and functional groups in a well-defined porous material.[3-22,242]

In the last few years several new crystallization methods have been developed in order to increase the stability, porosity, and ability to tune the pore environment of MOF materials, most notably methods using acetic or other acids to perturb the coordination equilibria present in MOF solvothermal solutions, or 'modulated synthesis'.[43] It was found that a few MOFs, such as UiO-66(Zr-BDC) or MIL-101(Cr-BDC) with high hydrothermal and chemical stability could be grown as powders and were characterized by simulation and powder X-ray diffraction(PXRD), but reports of such materials were rare due to difficulties in their characterization.[35,243] In order to synthesize single crystals of MOFs

from metals that have a lack of lability which hinders crystallization, we developed the "Kinetically Tuned Dimensional Augmentation" (KTDA) method.[244]

The KTDA method combines the "dimensional augmentation" of linking pre-synthesized or known metal clusters or Secondary Building Units (SBUs) with the "kinetic tuning" of modulated synthesis, where added monocarboxylic acids lower the pH hindering ligand deprotonation, act as a surface capping agent, and compete with the linking ligand, slowing nucleation and growth. Different choices of starting metal sources can also alter the nucleation rate.[26] By tuning the amount and type of starting metal cluster or salt and modulating monocarboxylic acid, large single crystals can be grown of MOFs that were before found only as powders or not reported at all. Furthermore, this increased crystallinity as well as defect modulation introduced by tuning the temperature, amount, and strength of competing acid can alter the porosity of the MOF, for example by introducing mesoporous defects or extra open metal sites.[27,28] Other properties such as catalytic activity can be altered by similar methods.[245]

In this work, we demonstrate how modulated synthesis and kinetic tuning methods can be expanded to tune a synthesis using just one type of metal and ligand to produce MOFs of different structures and porosity. We demonstrate that very similar structures can be produced with altered connectivity, topology, unit cell, and with different gas sorption properties as well. This work demonstrates how the initial metal source, including its solubility, redox potential, and oxidation state, can serve as a kinetic parameter altering MOF synthesis similar to demonstrated parameters such as the temperature, the amount or type of solvent, or the pK_a and concentration of a modulating reagent.[246]

7.3 RESULTS & DISCUSSION

Application of the KTDA method was attempted by the synthesis of the Mn_{12}(Acetate) cluster and its use as a starting material in MOF synthesis. The Mn_{12}(Acetate) cluster has been widely studied for its unique magnetic properties.[247] We attempted to synthesize a MOF containing it as an SBU with a large variety of ligands and conditions, but the cluster was not preserved under any conditions found that produced MOF crystals, acting only as a metal source. Use of tetrakis(4-carboxyphenyl)silane(TCPS) with dimethylformamide(DMF) and acetic acid produced a variety of different MOF structures, based on variations in the manganese source. Rather than kinetic tuning producing different crystal sizes or crystallinities of the same MOF, as is usually the case, structures with different unit cells, space groups, and connectivities were produced, including a rare example of a "mixed-ligand" framework where TCPS exhibits for 4- and 3-connected modes, with an unconnected carboxylate dangling free in the pore.

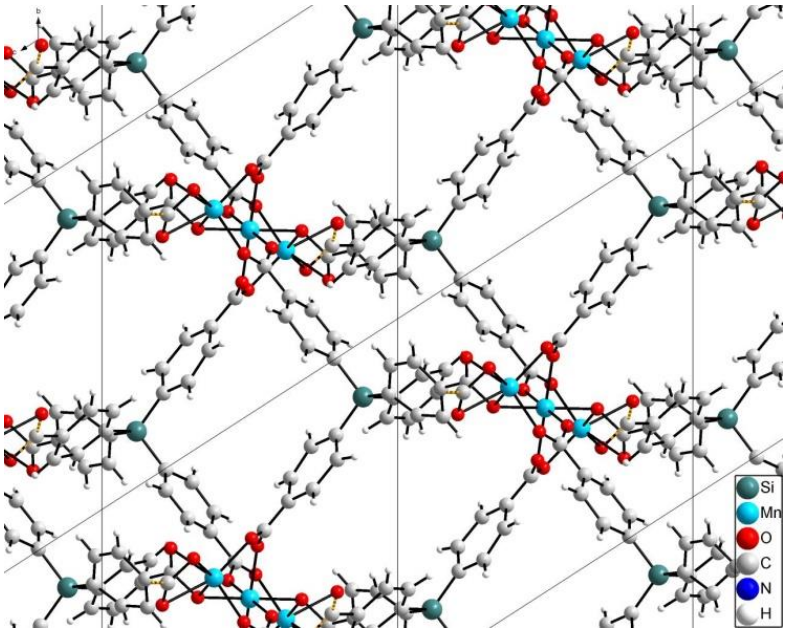

Figure VII-1. PCN-48 with the pore-filling $Mn(DMF)_6$ complex omitted for clarity.

PCN-47, consists of clusters of 3 manganese cations bridged and ligated by 8 carboxylates, where all carboxylates ligate manganese with both oxygens. The middle Mn ion has an octahedral coordination environment with significantly elongated axial ligands, while the bottom and top Mn are distorted octahedral, almost trigonal prismatic, which is controlled by ligand geometry. Its pores are filled with disordered solvent molecules.

When we attempted to synthesize this MOF starting from manganese(II) acetate tetrahydrate, a different product was obtained, PCN-48. (Figure VII-1) This MOF had a very similar SBU and connectivity of the TCPS ligand, but was solved in the P-1 space group, and no additional symmetry was found by CELL_NOW or PLATON addsym routines. This may be due to the fact that unlike PCN-47, the pores were filled with an ordered $Mn(DMF)_6$ complex, shown in Figure VII-2. No counterion was able to be located

crystallographically. This is similar to the results found by the Fujita group when using a MOF as a "crystalline sponge"; when the pore size and crystallization conditions are appropriate, small molecules or complexes can be isolated in MOF pores in a manner that is crystallographically ordered and conducive to structural determination by SCXRD.[248]

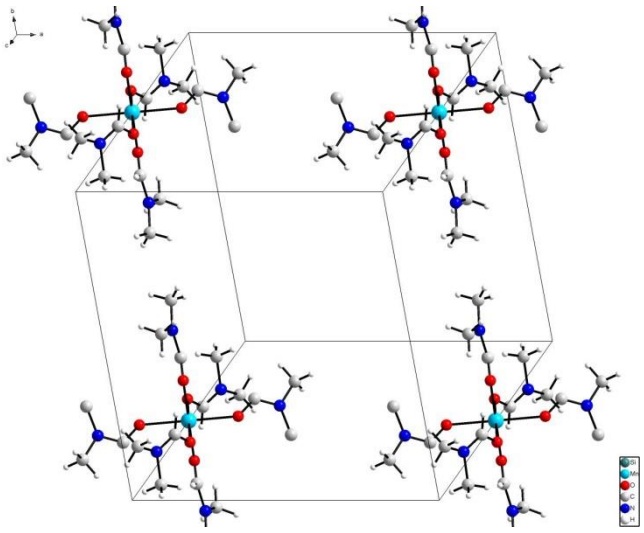

Figure VII-2. PCN-48's ordered, pore-filling $Mn(DMF)_6$ complex with the unit cell shown and the framework omitted for clarity.

Another MOF was found when the synthesis was repeated except using $KMnO_4$ as a metal source, PCN-49. $KMnO_4$ is dissolved ultrasonically as a metal source in DMF before heating in the synthesis, which is otherwise identical to that of the other two MOFs. In this MOF, which was solved in P-1, another SBU was found which has much different connectivity. It has a central octahedral Mn, but the other two manganese atoms are ligated by a DMF and water or hydroxyl molecule each. Adjacent to this ligating water or hydroxl

is the dangling carboxylate of a 3-connected TCPS ligand, which is stabilized by hydrogen bonding to another carboxylate ligating that Mn, but is not close enough to the Mn to ligate it. This is essentially a mixed-ligand MOF formed from one ligand which links in 4-connected or 3 connected modes. SEM-EDX also confirmed the presence of potassium in this framework, indicating that it may be an anionic framework with disordered potassium counterions.

In PCN-47, each Mn cluster is 8 connected to adjacent tetratopic linkers. Two crystallographically independent linkers exist in the structure. Thus, the MOF structure can be simplified into a 4,8 connected net with alb topology, the point symbol for which is $\{4^4.6^2\}_2\{4^8.6^{17}.8^3\}$. PCN-48 also contains an 8 connected cluster and 4-connected linkers. Topologically, the overall structure is simplified into a 4,8 connected flu net with a point symbol of $\{4^{12}.6^{12}.8^4\}\{4^6\}_2$. The structure of PCN-49 is more complicated compared to PCN-47 or PCN-48. Each Mn node is 7 connected. Three crystallographically independent linkers coexist in the structure, two of which are 4 connected and the other one is 3 connected leaving a carboxylate group dangling. Therefore, the structure is simplified into a 3,4,4,7-connected net containing four different nodes. It shows an unprecedented topology with point symbol of $\{3.4^3.5.6\}_2\{3^2.4^4.5^4.6^7.7^3.8\}_2\{4^2.6\}_2\{4^2.8^3.9\}$ determined by Topos 4.0.

Porosity measurements were carried out on PCN-47, PCN-48, and PCN-49, which showed significant differences in the pore characteristics of each material. BET Surface areas of 479 m^2/g, 712 m^2/g, and 582 m^2/g were found respectively for PCN-47, -48, and -49. The crystal structures indicate that micropores of approximately 1.5 nm maximum

diameter should be present in each MOF. PCN-47 and PCN-49 possesses a type 2 N_2 adsorption isotherm, indicating microporosity, while PCN-48 and shows a type 4 isotherm. This porosity cannot result from the ordered MOF structure and thus likely results from either defects in the structure or partial collapse, leaving disordered mesoporous holes in the structure. This is shown in Figure VII-3. The pore size distributions calculated by DFT from nitrogen adsorption data indicate that much of the total pore volume in PCN-48 is due to large mesopores of 5-25 nanometer width, despite the fact that it is prepared, solvent exchanged, and activated under nearly identical conditions to the microporous PCN-47 and the only slightly mesoporous\defected PCN-49.

To account for the difference in Mn concentration, we tried syntheses with equimolar amounts of manganese of each starting material, but these resulted in identical products as verified by PXRD, with lower yields. Thus, this is likely is an example of how kinetic tuning can dramatically alter the structure and likely also the stability of MOF crystals based on the oxidation state of the starting metals. The Mn_{12}(Acetate) cluster is not stable under the synthesis conditions used here once high temperature is reached, and instead acts as a source of Mn ions as the solution is heated. DMF decomposes under heat in the presence of water to form dimethylamine and formic acid.[249] This may dehydrate the solution and otherwise modulate the synthesis. Due to the high redox potential of manganese in trivalent or higher cationic state, the high-valence manganese ions in the cluster may oxidize any of these molecules and be reduced to Mn^{2+} as evidenced by the clear color of the product solutions and crystals. This was observed to occur within several hours at 120°C, while synthesis solutions remained colored and thus had a high

concentration of higher valence manganese when left to sit overnight at room temperature. The fact that higher temperature is required to allow manganese reduction in the solutions used may act to slow the nucleation or growth rates of the MOF, and changes the final crystal structure and porosity of the product. Some MOFs have reported to show a concentration-independent nucleation rate during formation, but this depends on the system and still requires a minimum metal concentration before another nucleation step becomes rate-limiting.[250] If this is the case, the rate at which the solution's temperature is increased may also be important, and future studies will examine the effects of slower heating rates combined with this method.

The disordered mesoporosity of PCN-48 could be due to large defects introduced by the high concentration of acetic acid in the synthesis conditions.[27,28] As the Mn^{2+} is highly labile, substitution of modulating acetates for linker carboxylates is highly reversible. This serves to promote ordered crystallinity over irreversible, amorphous products, and may also promote missing-linker defects that subsequently propagate into missing SBUs and large mesopores as the crystals grow. Another possible explanation is that the $Mn(DMF)_6$ clusters of PCN-48 are only present in PCN-48, and their removal during washing or activation may have partially collapsed the MOF structure. Subsequent solvent exchange may have removed the amorphous products from the collapsed regions, resulting in the variously sized mesoporous defects seen.

7.4 CONCLUSION

Our experimental observation is that PCN-47 formed from a Mn_{12}(Acetate) cluster is completely microporous, while PCN-48 formed from $Mn(CH_3COO)_2 \cdot 4H_2O$ under otherwise nearly identical conditions possesses mesoporous defects with increased surface area and pore volume, possibly due to modulated growth or lesser MOF stability. PCN-49, synthesized from a $KMnO_4$ metal source, exhibits slight mesoporosity, likely due to a smaller proportion of similar defects, and a crystal structure with an unprecedented, complicated topology. Experimental verification of the kinetics of PCN-47 and PCN-49 nucleation and growth is necessary to determine whether the *in-situ* dissolution of the Mn_{12}(Acetate) cluster at high temperature is slow enough to serve as a rate-limiting step. Oxidation of DMF by high-valence manganese from potassium permanganate in solution should proceed very rapidly at 120°C, yet PCN-49 is obtained instead of PCN-47 or PCN-48.

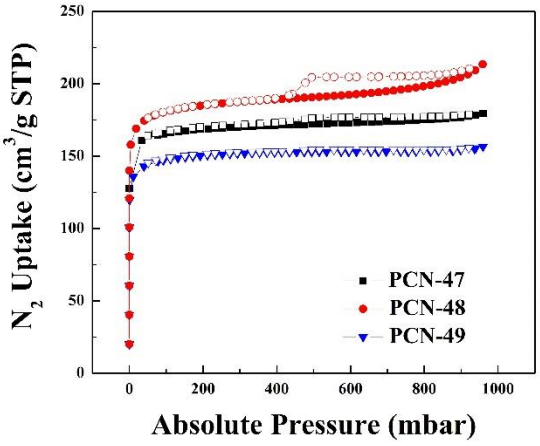

Figure VII-3. N_2 uptake isotherms for PCN-47, PCN-48, and PCN-49. Hysteresis and a type 4 isotherm is seen for PCN-48. This is likely due to partial MOF collapse during activation, and may indicate that PCN-48 is less stable than PCN-47 or PCN-49.

A thermodynamically most stable consistent MOF product is usually obtained from different metal salts. Exceptions to this have been produced through changes in pH or metal-ligand concentration ratio.[64,218,250] These parameters are held relatively constant here, and variation of pH and concentration ratios produced either no product or the same products, based on the metal source used. These MOFs may be kinetically trapped products altered by the initial state of the solution, despite the fact that the high-valence manganese should be reduced to Mn^{2+} relatively quickly at temperature and the solutions should thereafter be nearly identical. It has been demonstrated that different MOF structures can form under different pH and other initial conditions.[251] If this is the case, synthetic conditions may be possible which could achieve each structure from the same metal salt, but these conditions have not yet been found. Future detailed studies of how the initial metal source affects the kinetics of MOF growth, including the rate at which the

Mn_{12}(Acetate) cluster is dissolved, the rate of high valence manganese redox, and the nucleation and growth rates of the resulting MOF crystals, will help resolve this mystery.

We expect that the use of different metal sources as a kinetic parameter to alter the MOF products produced will be a widely used technique in the future to produce new MOFs and alter the properties of existing MOFs. PCN-47 is an example of the use of an insoluble or partially soluble metal source that slowly goes into solution and is reduced to slow nucleation of the MOF crystals and alter the final product, and while further study of this method is necessary, use of novel metal sources that are oxidized or reduced under heating should be applicable to almost any MOF as a potentially valuable synthetic technique.

7.5 EXPERIMENTAL SECTION

The Mn_{12}(Acetate) cluster was prepared according to the literature.[247] Tetrakis(4-carboxyphenyl)silane was also synthesized according to the literature.[252]

Synthesis of PCN-47: 0.15 grams of Mn_{12}(Acetate) (0.96 mmol of Mn ions) and 0.15 grams of tetrakis(4-carboxyphenyl)silane (0.293 mmol) were added to 30 mL of dimethylformamide(DMF) in a 40 mL vial. 3 mL of glacial acetic acid was then added to the solution. The vial was tightly capped, shaken by hand, and then sonicated for 15 minutes or until all ligand is solvated, as the Mn_{12}(Acetate) cluster is insoluble under these conditions and appears to be stable until high temperatures are reached. The vial was then placed into a preheated 120°C oven for 12 hours. Crystals were removed directly from the vials for characterization by SCXRD.

Synthesis of PCN-48: 0.15 grams (0.612 mmol) of $Mn(CH_3COO)_2 \cdot 4H_2O$ and 0.15 grams of tetrakis(4-carboxyphenyl)silane (0.293 mmol) were added to 30 mL of dimethylformamide in a 40 mL vial. 3 mL of glacial acetic acid was then added to the solution. The vial was tightly capped, shaken by hand, and then sonicated for 15 minutes or until all reactants were solvated. The vial was then placed into a preheated 120°C oven for 12 hours. Crystals were removed directly from the vials for characterization by SCXRD. Synthesis was repeated at a 0.95/0.293 molar ratio of Mn to ligand, with the same products produced as verified by PXRD and SCXRD.

Synthesis of PCN-49: 0.15 grams of $KMnO_4$ (0.95 mmol) and 0.15 grams of tetrakis(4-carboxyphenyl)silane (0.293 mmol) were added to 30 mL of dimethylformamide in a 40 mL vial. 3 mL of glacial acetic acid was then added to the solution. The vial was tightly capped, shaken by hand, and then sonicated for 15 minutes or until all reactants were solvated. The vial was then placed into a preheated 120°C oven for 12 hours. Crystals were removed directly from the vials for characterization by SCXRD. Synthesis was repeated at various reactant ratios and vial sizes with the same products produced as verified by PXRD and SCXRD.

After each reaction, 30 mL DMF was used to wash the product through centrifugation for 3 times to remove unreacted ligand. A solvent exchange procedure was conducted by soaking the products in anhydrous methanol with centrifugation and refreshing with new methanol. This procedure was conducted 3 times each day for 3 days. This solvent exchange procedure was repeated with anhydrous dichloromethane for

another 3 days. Before BET Surface area measurements, each sample was then dried and activated under vacuum at room temperature for 24 hours.

CHAPTER VIII

CARBAMATE TETHERING OF ALKYLAMINES TO AMINE-INCORPORATED POROUS POLYMERS ALLOWS EXCEPTIONAL CARBON CAPTURE CYCLING PERFORMANCE AND UPTAKE

8.1 OVERVIEW

Porous materials with incorporated amines or alkylamines are promising next-generation sorbents, with the potential to replace current aqueous alkylamines for the capture of acidic gases, such as carbon dioxide.[253] Recent porous materials, particularly porous polymer networks (PPNs), demonstrate improved uptakes while requiring lower regeneration energy, primarily due to their significantly lower heat capacity compared to aqueous solutions.[254,255] However, current absorbent materials rarely maintain high performance over multiple regeneration cycles, unless they are chemically tethered by covalent or ionically bonded moieties.[256] We have developed a novel PPN, named PPN-150-DETA, which possesses one of the highest initial CO_2 uptakes under flue gas conditions (up to 27.16 wt.%) and extremely low manufacturing and recycling energy costs. When PPN-150 is synthesized with cyanuric acid to act as a templating reagent, PPN-151 is formed, and PPN-151-DETA is the highest uptake adsorbent which maintains working capacity over many regeneration cycles for carbon dioxide gas capture under industrially relevant conditions. PPN-150 and 151-DETA were formed via the carbamate tethering of alkylamines to PPN-150 followed by deliberately gentle reactivation. By

controlling the temperature and regeneration time, “partial reactivation” of PPN-151-DETA after the first CO_2 uptake cycle ensures that a small portion of the initially chemisorbed CO_2 tethers the alkylamines to each other and to the polymer backbone, preventing alkylamines from volatilizing during regeneration and drastically improving cycling performance. Using this method, there is no loss of CO_2 uptake beyond initial carbamate tethering for more than fifteen regeneration cycles after the initial partial reactivation. To the best of our knowledge, PPN-150-DETA shows the highest CO_2 uptake under flue gas capture conditions among alkylamine-loaded porous materials, while PPN-151-DETA is the first low cost absorbent which combines high CO_2 uptake and high recyclability.

8.2 INTRODUCTION

Aqueous alkylamine solutions, primarily monoethanolamine (MEA) at 30-40 wt. % in water, are the most common currently used technology for the removal of acid gases, such as CO_2 from power plants.[257,258] They provide efficient capture at temperatures ranging from 20-50°C due to the chemisorption of the weakly acidic target molecules to the strongly basic amines. However, their “parasitic energy penalty” of up to 30% of the electricity produced in an average power plant, due to their high heat capacity, prevents their widespread application.[259] For this reason, solid sorbents of CO_2 with inherently lower parasitic energy penalty are an active and promising area of investigation.[260] The presence of water can double the uptake of this reaction via interaction with CO_2 to allow for single amine binding. Under dry conditions, two amine molecules are required to form

a carbamate salt due to the need for both a donor and acceptor to stabilize the carbamate.[261] However, when water is present, it can serve as the proton acceptor from the carbamic acid instead of a second amine during CO_2 capture.[257] In this case, only one amine is required per CO_2 absorbed, and other species such as bicarbonate are formed.[262] The main challenges impeding the implementation of solid sorbents in commercial CO_2 separation applications for flue gas capture are high cost and poor cycling performance. Current applications for these materials, such as acid gas removal or "gas sweetening" in petrochemical and natural gas processing plants, could also greatly benefit from an increase in performance and cost-effectiveness.[263] Amine-based chemisorption is more effective than physisorption of these gases, because the working capacity is much higher under flue gas conditions and selectivity for acid gasses is increased.[264]

Porous materials have been widely used for gas adsorption, separation and selective capturing, because they have high surface area, high dynamic uptake capacity and enable facile gas release. CO_2 physisorbents typically have acceptable uptakes only at lower temperatures (0-25°C) and are much less selective for CO_2 and other acid gases over other molecules that are usually present.[265] These competing molecules, such as water, are captured by these less selective materials from flue gas and in natural gas sweetening processes.[17,266] Porous materials can incorporate alkylamines to induce chemisorption, further enhancing the CO_2 uptake and selectivity.[267] A high-performance example reported by Gadipelli et. al. is alkylamines immobilized on MOF-derived carbon monolith (MDCM).[268] This system shows over 200 mg g-1 of CO_2 adsorption capacity using

simulated flue gas over several repeated cycles, outperforming other previously reported sorbents. However, while this adsorbent shows excellent performance for CO_2 capture, its production costs are still high because of its synthetic process requiring MOF-5 to be carbonized, and it still shows some loss of capacity over ten cycles.[269] Target gas uptake, selectivity, and overall cost effectiveness for amine gas treatment must exceed those of aqueous amines for new materials to be considered superior for gas capture. They must have at least comparable uptake of the target gas, though whether volumetric or gravimetric uptake is more important depends on the particular application. For example, in an air purifying respirator, the complete removal of dangerous agents is paramount, which requires very high acid gas/air selectivity, in addition to high volumetric uptake. For CO_2 flue capture, overall cost-effectiveness taking into account the energy cost of regeneration is paramount, as MEA solutions have been estimated to require around 30% of the electricity produced in a power plant in order to regenerate them an isolate the separated CO_2, which may be the factor most responsible for preventing widespread adoption.[270,271]

The most important factor that should be considered when developing new methodology is cost-effectiveness. Ideally, a material should have low cost of production, require lower energy cost per per kilogram of acid gas separated. It should demonstrate superior cycling performance, being able to withstand more cycles before experiencing significant degradation, requiring replacement or rejuvenation as alkylamine must be added to the solvent or polymer. Materials must also maintain high uptake at industrially

relevant temperatures, typically between 20-50°C, and completely desorb at appropriate temperatures, typically <100°C, as temperature swing adsorption cycles are often more cost effective than pressure-swing or other methods.[272]

8.3 RESULTS & DISCUSSION

We have developed materials, PPN-150-DETA and PPN-151-DETA, which succeed on all of these metrics. PPN-150 consists of a low-cost porous melamine formaldehyde resin (or mPMF), similar to that previously reported by the Ying group,[273] which has then been modified through the loading of various alkylamine species into its high pore volume, which are then tethered through an additional carbamate-forming dry CO_2 loading. PPN-151 is similar but with the addition of a small amount of cyanuric acid during synthesis to act as a templating reagent. Melamine cyanurate is a very strong hydrogen-bond network that has a melting point of 350°C while the synthesis is done at 170°C, so this produces small melamine cyanurate "sheets" that are interspersed within the polymer and change the pore size distribution, similar to sheets of graphite in graphitic activated carbons. mPMF alone has a CO_2 uptake of 14.3 wt% at 1 bar and 273 K, and an uptake of 5.5 wt % at 0.15 bar and 273 K. However, this uptake drops off rapidly at higher temperatures. This is because its amines are part of the rigid framework and are unable to facilitate carbamate formation due to the long, fixed distances between them as well as their poor Lewis basic character, meaning that its uptake is primarily via physisorption. To improve these materials for the conditions in which aqueous alkylamine solutions are currently used, they are post-synthetically modified into materials such as PPN-150-

DETA or -TEPA by loading them with alkylamines such as Diethylenetriamine(DETA) or Tetraethylenetetraamine(TEPA). These loaded amines are then tethered through dry CO_2 uptake, producing framework-amine carbamates as shown by IR spectroscopy. Other porous materials loaded with alkylamines have showed very promising performance, but their application has been hampered by excessive cost of production, lack of tethering degrading their cycling performance, or generally lower uptake.[256,262,267,268,274]

By controlling the regeneration conditions, we can leave some of these carbamates behind by incomplete removal of the CO_2 absorbed by the polymer. This prevents the loss of alkylamines and lower cycling performance exhibited by previous alkylamine-loaded porous materials, because they act as chemical tethers preventing the volatilization of the alkylamines during regeneration.[268] We have shown initial total CO_2 uptakes of up to 27.16 wt. % using CO_2 gas mixture breakthrough analysis on flue gas simulant mixtures.(Figure VIII-1)

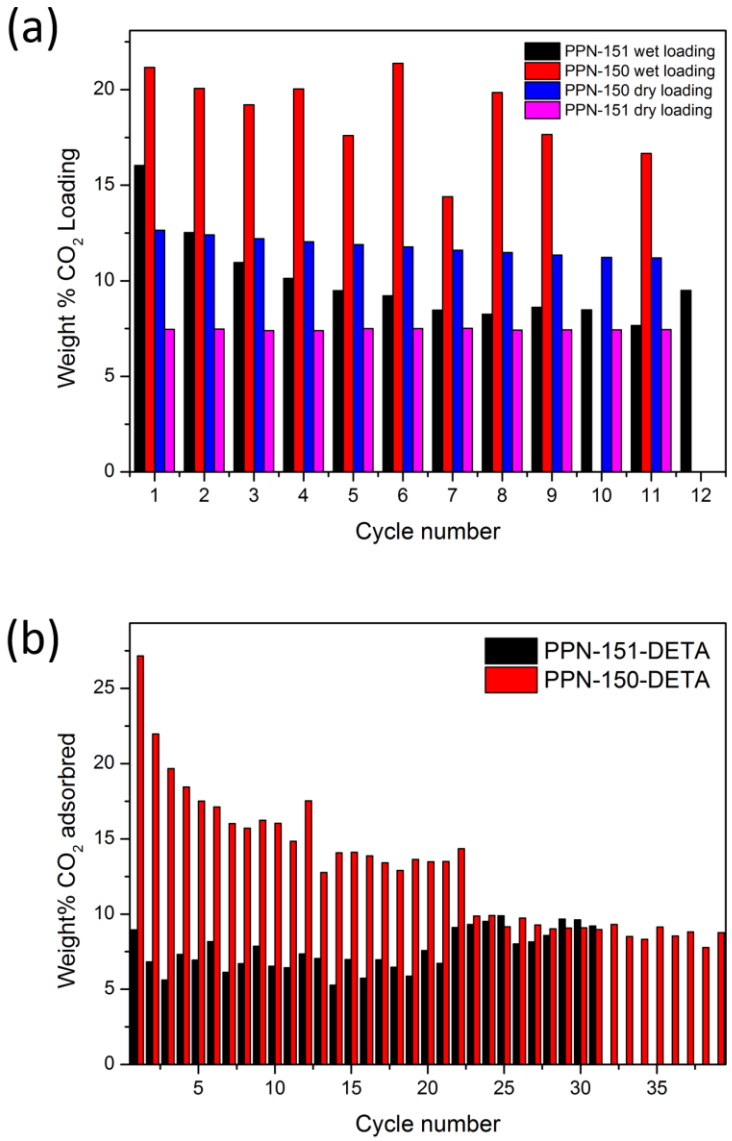

Figure VIII-1. a) CO_2 uptake measurements measured by breakthrough instrument comparing uptakes with humid "wet" flue gas conditions with 2% v/v water and 15% CO_2, balance N_2 with "dry" conditions containing 15% CO_2, balance N_2 and no added humidity. b) PPN-150 and PPN-151 wet flue gas cycles reactivated at 85°C up through cycle 22, then reactivated at 89°C. All were reactivated for 10 minutes.

Because the maximum uptake is so high, we can maximize overall cost-effectiveness and minimize the energy cost of flue gas capture by choosing less harsh reactivation conditions, to leave more carbamates behind. Figure VIII-1 illustrates how harsh or extended reactivation conditions can lower cycling performance, through the loss of alkylamines. Figure VIII-2 shows how more gentle reactivation conditions lower the working capacity on the second cycle, but allows high cycling performance and minimizes the energy required for cycling, a key parameter for CO_2 flue gas capture.[254] Through carbamate tethering in a preparative first cycle, we retain high working capacities with negligible loss of capacity for at least 15 more cycles. Even PPN-151-DETA's stable working capacity of 12.5 wt. % with carbamate tethering is to our knowledge better than that of any other material tested in flue gas simulant conditions, other than a few materials which demonstrated loss of cycling performance after 5-20 cycles, dropping the performance below that of PPN-150.[268,275,276]

According to recent results in the field of alkylamine-based carbon capture, the uptake capacity of alkylamine-loaded porous materials is directly proportional to the density of reactive amine sites.[268] Activated carbons with very high pore volumes loaded with alkylamines have been prepared with CO_2 adsorption capacity, but their cycling capacity has been relatively low due to the lack of strong interactions with the amines, resulting in the loss of alkylamines during regeneration. Meanwhile, conventionally tethered materials typically have much lower overall CO_2 uptake due to the non-amine tethering moieties using pore volume, resulting in less alkylamine density.[270]

To solve this problem, polymers with primary and secondary amine moieties as part of the backbone can be used, which can both take up CO_2 on their own and help tether alkylamines through hydrogen bonding. Due to the chemistry of alkylamine CO_2 capture, it is possible to improve the cycling performance of these materials through a new technique we have developed termed "residual carbamate tethering." When CO_2 reacts with alkylamines, one amine molecule attacks the CO_2 but loses a proton, resulting in a negative charge stabilized by a positive charge caused by the proton reacting with a basic moiety nearby, such as another amine. When reactivated, the reaction is reversed and the captured CO_2 leaves. However, when the material is only partially reactivated for a limited amount of time, some of the carbamate moieties remain, and can act as a tether. The next cycle will have slightly lower CO_2 capacity, but the ionically-tethered alkylamines will remain in the material instead of slowly leaving as the material is cycled, resulting in a higher cycling performance.

After the first exposure to dry CO_2, a small amount of uptake is lost due to the amines used for the carbamate tethering as well as some amines being lost through volatilization as they were not initially tethered. However, because of this tethering, further loss of uptake is prevented for in future cycles compared to what is seen if the material was completely reactivated, or in porous materials where the alkylamine is only physisorbed rather than tethered or retained through stronger bonding such as hydrogen bonding between the loaded and polymer backbone amines. When untethered porous materials are used, or complete, harsh reactivation is used on PPN-150, the uptake decays

from the maximum first cycle at a rate proportional to the loss of loaded amines during the removal of CO_2. When partial reactivation and carbamate tethering is used with a temperature swing adsorption(TSA) process of 40°C-85°C, there is no overall loss of uptake between the second and sixteenth cycles (Figure VIII-2)

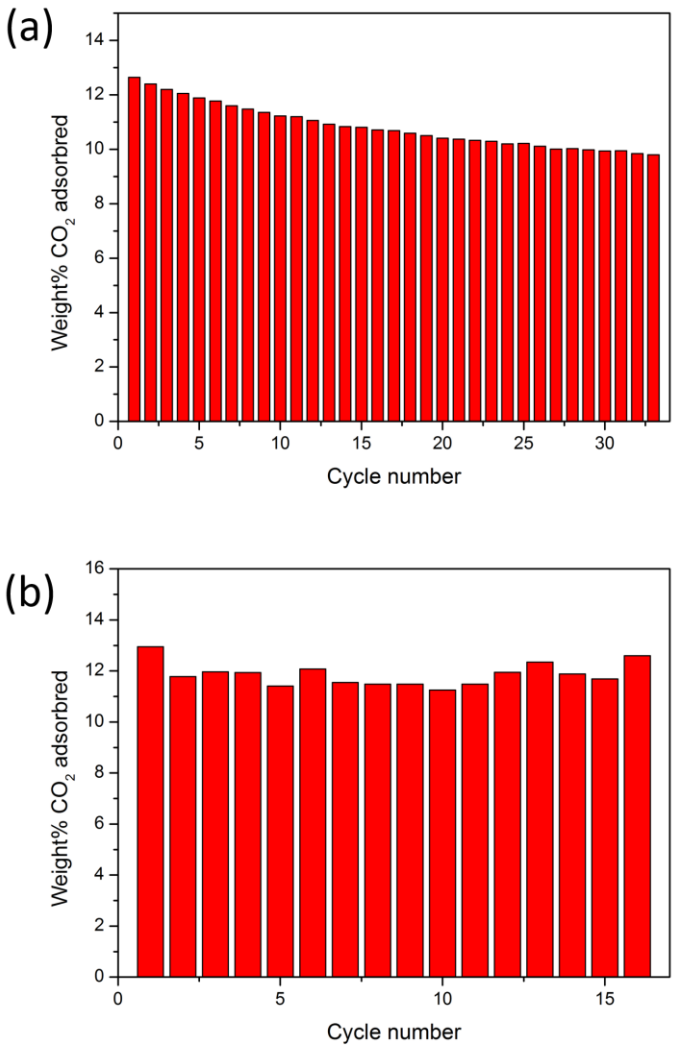

Figure VIII-2. a) Breakthrough cycling of lab-scale PPN-151-DETA (1 bar, 313K (40°C), 15% CO_2, and 85% N_2, 200mL/min) showing no loss of uptake for fifteen cycles after a preparative first cycle, due to gentle reactivation at 85°C for 2 minutes. b) TGA CO_2 cycling performance for PPN-150-DETA over 30 cycles (adsorption: 40°C and 50 ml·min^{-1} CO_2. desorption: 85°C and 50 ml·min^{-1} He) for 30 minutes. This demonstrates how longer or harsher reactivation than necessary can lower cycling performance.

This contrasts with breakthrough measurements taken on the TGA instrument through flowing CO_2 over 10mg of PPN-150-DETA (Figure VIII-2b). Longer reactivation times, and subsequent loss of DETA over many cycles, are required to achieve the same CO_2 uptake. This is because nitrogen flowing over a sample is inherently less efficient at quickly removing freed CO_2 than when it flows through a column packed with the sample. Furthermore, when packed columns are regenerated, alkylamines lost from particles within the column may be re-adsorbed by other particles further along the column, minimizing loss and maximizing cycling performance. Another example of this is TGA CO_2 uptake measurements of PPN-150-tetraethylenepentamine(TEPA) with 100°C activation for 2 hours, which started with a maximum CO_2 uptake of 15.9 wt. %. Despite the lower vapor pressure of this alkylamine, the harsh reactivation conditions remove all carbamates and some TEPA, lowering cycling performance by 2.2% after only 4 cycles. This loss per cycle is very similar to that of PPN-150-DETA measured by TGA(Figure VIII-2b). Contrast this with PPN-150-DETA measured by breakthrough, which has no loss of performance over 15 cycles despite the more volatile alkylamine.

To show that carbamate salts are left in the framework even after partial reactivation, we took a PPN-150-DETA sample that had been regenerated under conditions identical to those in Figure VIII-2, along with samples regenerated more harshly (100°C and 120°C for ‘medium’ and ‘harsh’ respectively) and ran IR

spectra.(Figure VIII-3). They show strong, broads peaks for all samples near 3300 cm^{-1} corresponding to amine and ammonium N-H bonds. We can contrast the lack of absorption near 2950 cm^{-1} in the CO_2 loaded sample to the large peak present at the same location after gentle 85°C reactivation and in the unloaded mPMF polymer.[273] This peak is much reduced after harsh reactivation. Another small peak appears in the CO_2 loaded polymer at 1188 cm^{-1}. These changes correspond to the conversion of primary and secondary amines to ammonium carbamates.[262,274] TGA measurements confirm high CO_2 uptake, cycling performance, and the loss of carbamate-forming CO_2 only under harsher regeneration conditions. A CO_2 uptake isotherm at 273K shows almost complete hysteresis, i.e., almost no desorption of adsorbed CO_2 even at low pressures, because the chemisorbed carbamates do not desorb under such a low temperature.

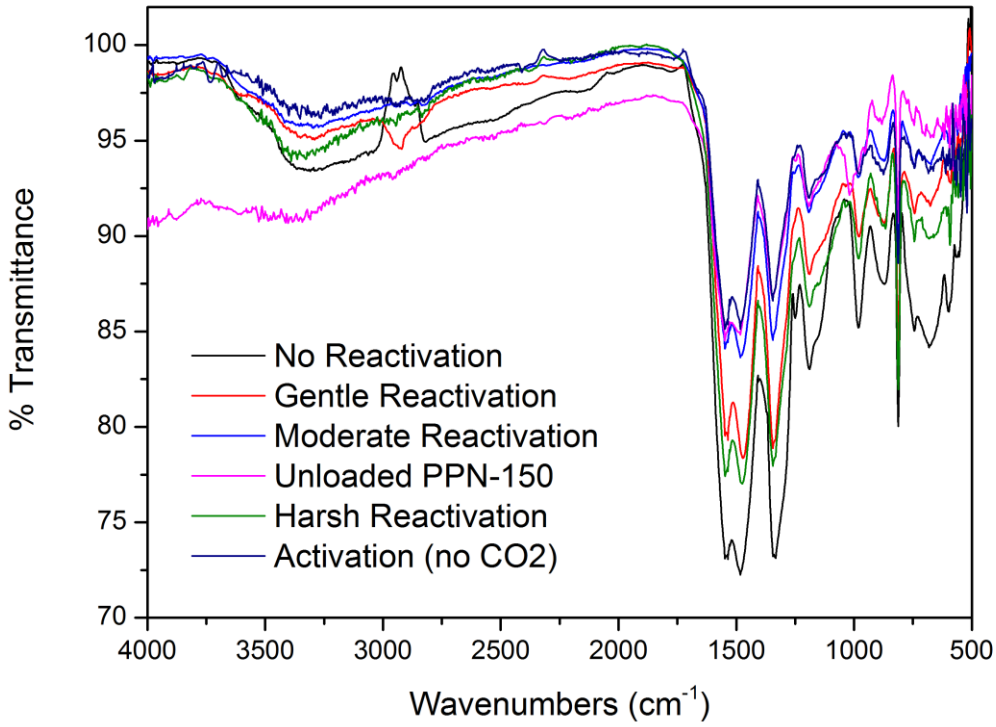

Figure VIII-3. FTIR spectra showing CO_2-saturated PPN-150 losing intensity at 2950 cm-1 and gaining a peak at 1188 cm-1.

Nitrogen isotherms were taken at 77K of the unloaded PPN-150 before loading and modification into PPN-150-DETA and PPN-151-DETA (Figure VIII-4) PPN-150 samples show BET surface areas slightly higher than and pore volumes slightly lower than those previously reported for mPMF, around 1171 $m^2\ g^{-1}$ and 1.75 $cm^3\ g^{-1}$ for the samples used here.[273] As the Guo group showed, by achieving higher pore volumes in these materials, we could likely increase the CO_2 uptake even further through increased alkylamine loading.[268] mPMF materials have been previously reported with pore volumes

of up to 3.0 cm^3 g^{-1},[273] which theoretically may allow for gravimetric uptakes nearly double those we are reporting. However, the relatively high remaining pore volume in PPN-150-DETA indicates that some pores may be too large for optimal DETA tethering, and that either polymer synthesis producing smaller mesopore diameters or loading with larger alkylamines should be tried to further optimize these materials. Preliminary results with PPN-150-Tetraethylenepentamine(TEPA) are promising.

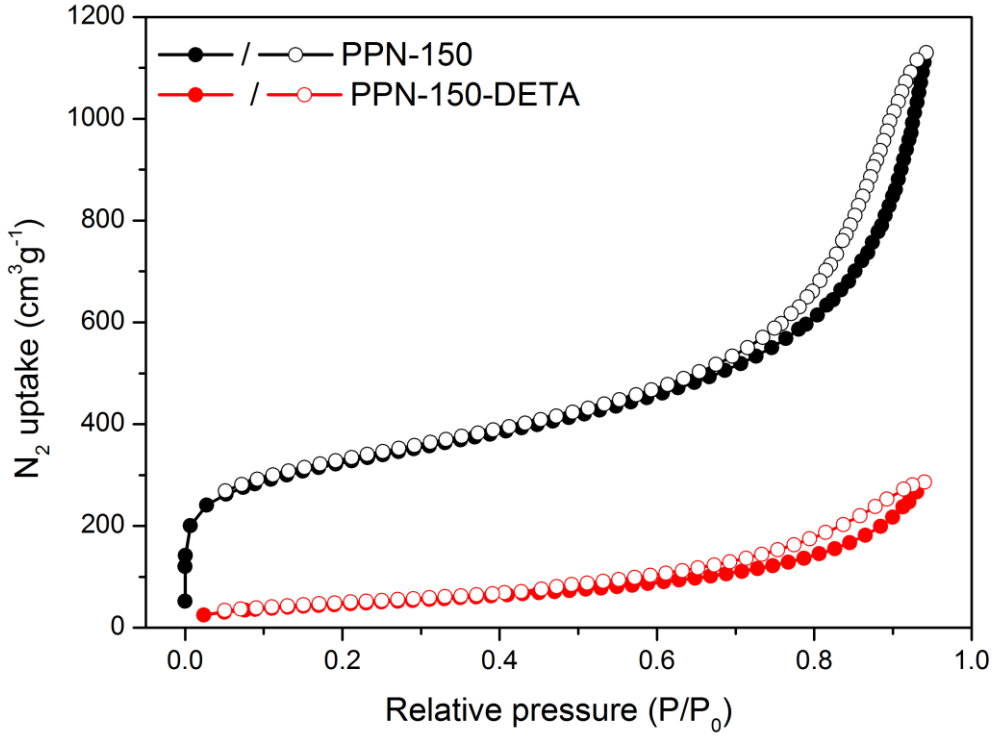

Figure VIII-4. N_2 isotherms taken at 77K on a Micromeritics ASAP 2020 gas sorption analyzer for PPN-150 before and after DETA loading. PPN-150 has a BET surface area of 1171 m^2g^{-1} and a pore volume of 1.75 cm^3g^{-1}, while PPN-150-DETA after alkylamine loading has a BET surface area of 168 m^2g^{-1} and a pore volume of 0.44 cm^3g^{-1} as calculated by Micromeritics MicroActive 4.02.

8.4 CONCLUSION

We synthesized organic porous materials, PPN-150 and PPN-151, as CO_2 sorbents which were loaded with various alkylamines. After tethering of alkylamines by carbamate formation, forms adapted for flue gas capture conditions called PPN-150-DETA and PPN-151-DETA were generated. PPN-150-DETA and PPN-151-DETA have extremely high CO_2 uptakes, initially exceeding those of Mg-MOF-74-en or TEPA@MDCM under flue gas conditions, but has extremely low cost and much higher recyclability than those materials. Scale-up has also been successful, as PPN-150-DETA has been produced on a 150-gram scale at a 92% yield. Alkylamine-tethered porous materials typically have very similar parasitic energy costs, or energy efficiencies, approximately 2-3 times better than those of aqueous amines.[259,264,270] The regeneration energy costs of PPN-150-DETA are much less than those of aqueous amine solutions, because its heat capacity is far lower than that of aqueous solutions. They should also be significantly lower than that of similar tethered porous materials, because its optimal regeneration temperature is lower than that of similar materials (85°C compared to 100-120°C). Studies of the energy efficiency of these materials, in addition to optimization of porosity and alkylamine loading, are ongoing.

8.5 EXPERIMENTAL SECTION

PPN-150 was produced similarly to mPMF in the literature, though changes in the reactor type appear to drastically change the properties of the final material.[273] What follows is the synthesis of the samples we used for loading. These samples were intended to mimic mPMF-3 from Reference 21, but we were unable to achieve the same pore volume as was reported, but found greater BET surface area (Figure VIII-4). It is also important to note that any leaks whatsoever in the synthesis vessels, or inability to hold pressure, typically resulted in nonporous or much less porous products.

Synthesis of PPN-150: A solution of melamine (0.3777 g), paraformaldehyde (0.1621 g), and DMSO (3.36 mL) was added to a Teflon lined autoclave and heated in an oven at 120° C for 1 hr. The solution was then sonicated to make a homogeneous solution and heated in an oven at 170° C for 48 hr. After the solution cooled to room temperature, the solid product was quickly washed with 200mL DMSO and 200mL acetone, partially dried in air, crushed with a mortar and pestle, and washed with methanol in a Sohxlet extractor for 48 hr. The white solid was then dried under vacuum, and BET measurements were performed after activation under vacuum at 185° C for 12 hr.

Synthesis of PPN-151: The experiment was then altered to include melamine (0.7591 g), paraformaldehyde (0.4131 g), cyanuric acid (0.0589 g), and DMSO (7.8 mL). The solution was added to a glass vial and heated in an oven at 120° C for 1 hr, sonicated to make a homogeneous solution, and heated in an oven at 170° C for 48 hr. After the solution cooled to room temperature, the solid product was quickly washed with 200mL

DMSO and 200mL acetone, partially dried in air, crushed with a mortar and pestle and washed repeatedly with methanol in a Sohxlet extractor for 48 hr. The white solid was then dried under vacuum, and BET measurements were performed after activation under vacuum at 185° C for 12 hr.

Alkylamine loading: A sample of PPN-150, which had previously been ground via mortar and pestle, was placed into a 250ml media bottle. To the sample was added cyclohexane (100ml) followed by diethylenetriamine (DETA, 40ml). The media bottle was then sonicated at 55°C for 6 hours, upon which the media bottle was allowed to sit at room temperature overnight. The mixture was then filtered using a fritted glass funnel and a water aspirator and then washed with methanol (200ml total). Once dried, the loaded sample was placed onto a vacuum line at room temperature using a round bottom flask equipped with a fritted glass vacuum adaptor. The excess DETA was trapped using a dual liquid nitrogen trap system. After 9 hours on the liquid nitrogen trap system, the extracted excess DETA was collected and combined with the filtrate from the MeOH washes. The combined solvent was removed under reduced pressure to separate DETA from the lower boiling cyclohexane and methanol. A total of 20.5 ml of DETA was collected in this fashion indicating that 19.5 ml, or 1.15g DETA per gram of sorbent, had been loaded. The DETA loaded sample was allowed to remain on the vacuum line overnight at room temperature. The final mass of the loaded sample was taken, giving a change in mass of 19.5690g. From the density of DETA it was determined that 19.6ml DETA, or 1.16g DETA per gram sorbent, had been loaded into the sample.

CHAPTER IX

ADDING HEAVY ALKANES TO ADSORBENTS MAXIMIZES NATURAL GAS STORAGE CAPACITY

9.1 OVERVIEW

Natural gas adsorbents such as Metal-Organic Frameworks are a highly promising technology for applications such as methane-powered vehicles, economical flare gas capture, and natural gas separation and purification. In order to further improve them, we show that the addition of a precisely controlled portion of heavier alkanes to the adsorbent can increase the overall uptake both gravimetrically and volumetrically. Depending on the adsorbent and conditions, it is also possible to cleanly separate alkanes based on molecular weight during desorption. This allows the reuse of a MOF/heavy alkane mixture to combine adsorption and absorption and maximize methane uptake in a given volume. We also show that unprocessed natural gas does not need to be separated before transport when using an ultra-stable MOF adsorbent. The MOF is robust to impurities and the methane and overall uptakes of the heavier natural gas mixture are both much higher than that of pure methane.

9.2 INTRODUCTION

The substantial increase in the production of natural gas since 2008 has led to a sustained reduction in cost of energy derived from this commodity relative to liquid oil, effectively enabling new domestic sources for American fossil fuels production and needs.[277] It has long been known that a switching from coal and liquid hydrocarbons could reduce US carbon dioxide emissions.[278] New research factoring alternative sources of natural gas verified this even when accounting for logistical inefficiencies, as shale gas life cycle greenhouse gas (GHG) emissions are 6% lower than conventional natural gas, 23% lower than gasoline and 33% lower than coal.[279] Unfortunately, a large amount of this benefit is lost due the lack of containment infrastructure as vast amounts of fuel gases are taken from oil fields in regions far removed from consumption.

Natural gas, whose principle ingredient is methane, can be contained in pipeline infrastructure for transport or fixed tank units for transport and storage.[280] In the last 5 years, pipeline fixed costs, regulation, land access and gas conditioning safety issues have overcome the huge demand increase in natural gas causing little expansion in US pipeline infrastructure. Given that natural gas is a gaseous state at atmospheric conditions and that the relatively low 0.04 MJ/L (at 25°C, 1 bar) volumetric energy density of natural gas compared to other contained fossil fuels such as gasoline (34.80 MJ/L), many energy-intensive solutions have been proposed to capture, store and transport natural gas into the US energy infrastructure.[281] Where massive economies of scale can be established, natural gas is compressed at 250 bar (3,600 psi), commonly referred to as compressed natural gas

(CNG), or liquefied at -160°C, commonly referred to as liquefied natural gas (LNG). These century-old technologies can respectively improve the ideal energy density of natural gas to 9.2 MJ/L (CNG) or 22.2 MJ/L (LNG), which can be downgraded by ~30% volumetrically due to their real cylindrical containment requirements.[282] Unfortunately, the intensity of the energy needs of both applications create critical cost issues, which have failed to deliver on logistical support to the diverse demographic of America's natural gas boom.

The result of incumbent technology issues was the intentional venting or flaring of 288,743 million cubic feet (MMSCFD) of natural gas lost in the US in 2014.[283] At an average of $4.00 price per British Thermal Unit (BTU), this was a loss in value of $1,178,071,440 from the energy sector and a substantial anthropogenic addition in GHGs and other pollutants to the environment.[284] Some estimates go further and suggest that the monthly loss in just the North Dakota Bakken Shale amounts to $100 million per month.[285] Clearly a new approach to natural gas densification is needed to solve this problem.

The present approach leverages contemporary adsorption technology and addresses the problems posed by CNG and LNG by significantly extending efficient densification of natural gas with an adsorbent. Ideally, we would dissolve some ratio of natural gas in a higher alkane solvent and store its methane base gas at higher energy density under adsorbed natural gas (ANG). ANG is driven by physisorptive materials, which interact with methane through weak van der Waals forces.[286,287] Candidate materials are wide ranging, but due to the known requirements for high surface areas, controlled

pore diameters and moderate binding energy (heat of adsorption), most of the research has been focused on zeolites, activated carbons, and metal-organic frameworks (MOFs), sometimes called coordination polymers. Traditional materials such as zeolites and activated carbons could only inconsistently reach total reported methane storage capacities of 150v(STP)/v and 195v(STP)/v respectively.[288] Unfortunately, systematically both materials have bulk macroporosity and each have negative individual characteristics such as the ionic nature of zeolites and the pore volume/distribution of activated carbons.

The use of MOFs for storing natural gas as a main component was first reported in 1997.[289] In the 2000s, theoretical works suggested a conceptual MOF, IRMOF-993, could have a volumetric methane storage capacity well above activated carbon. PCN-14 was synthesized in 2008, and with a reported total methane uptake of 230v(STP)/v; this encouraging result suggested that MOF physisorption of methane could substitute CNG tanks.[290] Other paddlewheel Cu^{+2} based MOFs (HKUST-1, UTSA-76, NU-111 and PCN-66) have been shown to have total methane uptake values similar to that of PCN-14, but due to the low chemical stability of MOFs based on divalent cations, these MOFs are not stable to exposure to trace natural gas pollutants like hydrogen sulfide or even humidity.[291,292]

An iron-cobalt cluster-based MOF PCN-250, was a radical departure from previously reported ANG MOFs in its forecasted $10/Kg manufacturability (DOE targets based on raw materials at the ton level). More importantly, the material exhibited total reported methane storage capacity of 210v(STP)/v (Figure IX-1) (A), a flat heat of

adsorption curve (B), superior thermal stability up to 400° C (C) and stability in boiling water and under full range of pH conditions where the crystal structure (D) and surface area (E) maintained integrity.[97]

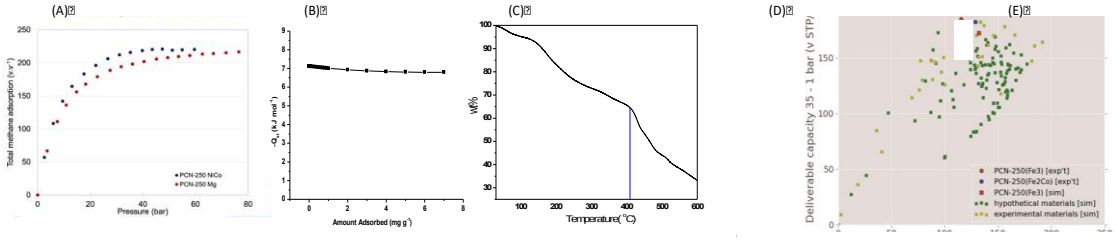

Figure IX-1. Performance and chemical stability testing of PCN-250.

More recent high-performance methane sorbent MOFs, such as MOF-519 or Al-soc-MOF-1, are limited because of their large ligands requiring multiple organic synthesis steps, which are expensive to produce at scale.[293,294] They may also suffer from chemical stability issues, as similarly to how Zr-MOFs with larger pores and lower-connectivity SBUs have been reported to have limited chemical stability compared to ones with smaller pores and higher SBU and ligand connectivity, some Al-MOFs typically collapse upon extended exposure to humid conditions.[295] To achieve high methane uptake performance at a low cost with high stability and cyclability, we developed a new approach.

The need to elevate volumetric ANG performance at a low cost requires that we look beyond porous adsorbent design. Taking a page out of historical solutions for natural gas bulk transport, whereby investigators sought to reduce compression and/or

refrigeration for natural gas storage, we applied the concept, dating back to at least the 1950s, of doping the methane system with a C_2-C_{10} hydrocarbon to the adsorbent vessel.[296,297] The combination of absorbing methane in higher alkanes at high pressures, while simultaneously adsorbing it on the surface of a porous material is called HAANG, or High Alkane Adsorbed Natural Gas. The doped system allows a higher volume of methane (or natural gas) to be stored than with the adsorbent alone at a given pressure. Methane is highly soluble in hydrocarbon mixtures.[298] Most of the higher alkane is also retained in and on the adsorbent through many working cycles of adsorption and desorption. This two-phase condition, liquid and vapor, is achievable at suitable pressures (30-65 bar) and temperatures (260-323°K) for ANG technology.

9.3 RESULTS & DISCUSSION

In many cases, gas uptake capacity is directly related to the internal specific surface area for a given porous material. For example, in hydrogen adsorption, it is found that each incremental increase in 500 m^2/g of specific surface area can roughly adsorb an additional 1 wt% H_2; which is known as Chahine's Rule (CR).[299] Though the Chahine's Rule is widely used in hydrogen adsorption prediction, researchers have found that the gravimetric capacity of methane uptake is reasonably well correlated with the gravimetric surface area for MOFs.[300] MOFs with large pores and ultrahigh BET surface areas, gravimetrically, uptake is 0.05-0.07 cm^3 methane per square meter BET surface area at 35 bar.[301] However, we found that PCN-250, which has a BET surface area of 1395 m^2/g and a methane uptake of 209 cm^3/g at 35 bar, corresponds to 0.15 cm^3 methane per square

meter, likely due to its high density of open metal sites, and pore sizes appropriate to stabilizing multilayer adsorption.

To increase this capacity without the expense that, for example, isoreticular ligand expansion would entail, we tested a high molecular weight alkane-doping concept. This activity included doping the methane system with a C_2-C_{10} hydrocarbon to the adsorbent vessel. Several tests were conducted with four MOF varieties and seven alkanes, reaching an increase in total volumetric methane uptake of up to 27%. While an absorbent-assisted approach in CNG has been proposed before, the composition must be constantly adjusted to regulate the mixture, meaning the tank must be separately piped for solvent addition and possibly extraction to maintain the two-phase state.[302] The porous adsorbent framework improves this process, as it was found to retain the doped hydrocarbon (C_{10}) during desorption from the framework.

After close examination of the factors that would impact the methane uptake of MOFs, including PCN-250 and other iron MOFs, we identified that the structure of PCN-250 is very suitable for methane uptake and the purity and pore sizes are crucial. There are several reasons why methane molecules cannot fully occupy the void in PCN-250. First of all, in lower-cost (Fe_3)PCN-250, the axial ligands on the Fe_3 cluster were not completely removed. Secondly, the leftover space is not enough for one methane molecule to enter in one cage, which means that the PCN-250 has not been fully optimized for CH_4 adsorption. Keeping this in mind, we tried different activation methods in order to produce missing linker defects which should maximize methane uptake, as long as larger

mesopores are avoided. Metal-ligand fragment coassembly or 300°C activation under nitrogen can each be used to increase the mesoporosity and pore volume of PCN-250 at the expense of surface area. Chevreau et al. developed a high-temperature activation process and showed that it reduces one of the Fe(III) atoms in the Fe_3O cluster to Fe(II), allowing it to release its bound hydroxyl ion and creating an extra open metal site in the resulting MOF.[303]

We prepared mesoporous PCN-250, as indicated by its type 4 nitrogen adsorption isotherm and subsequent pore size distribution calculations, with extended 7-day Sohxlet extraction in methanol. Certain conditions may lead to the formation of defects, or areas within the crystals where linkers or metal nodes are not present. When the defects get as large as mesopores (relative to its near perfect form) the gas uptake of the adsorbent usually decreases. This is mainly due to the availability of less overall surface area in a volume of mesopores compared to the same volume filled with micropores.

Normally, mesoporosity is antithetical to optimizing methane uptake.[287] However, by combining adsorption of methane in the MOF with the absorption of methane by higher alkanes contained in the mesopores and inter-particle macropores, we were able to increase the methane uptake, especially at high ANG pressures (40-100 bar). We found that heavier natural gas mixtures adsorbed more gas the heavier the mixture was, as expected.(Figure IX-2).

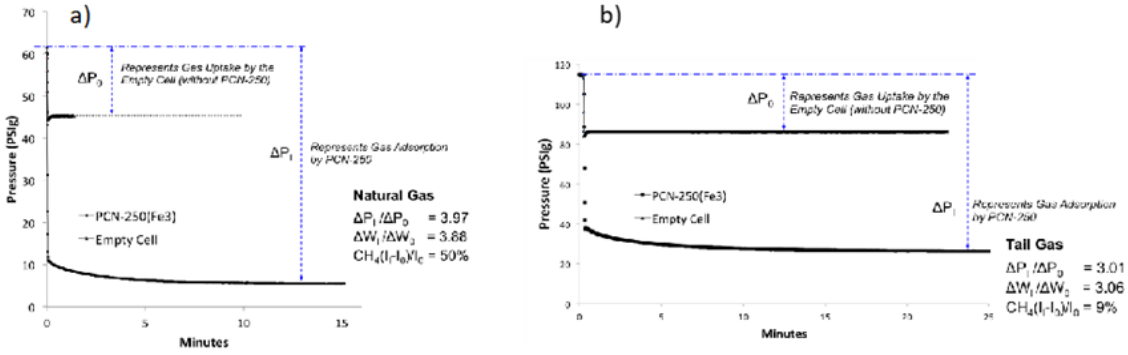

Figure IX-2. a) Real-time, unprocessed natural gas adsorption evaluation of the test cell with and without PCN-250(Fe_3), b) Real-time tail gas adsorption evaluation of the test cell with and without PCN-250(Fe_3); pressure drop measured by the transducer indicates gas adsorbed by the MOF vs. the gas stored in the empty test cell.

To optimize this behavior for the highest total methane uptake, the ratio of mesopores to micropores and mesopores to heavy alkane must be carefully tuned. The initial test results showed that in purely microporous MOFs, addition of too high of a volume of heavy alkanes could actually decrease the gravimetric methane uptake, presumably because the heavy alkanes adsorb in the micropores, and may block windows and pores deeper within the interior of the MOF crystals. However, in MOFs that have been treated by modulated synthesis, metal-ligand-fragment coassembly, or extended Soxhlet extraction to become partially mesoporous, addition of carefully controlled amounts of heavier alkanes can increase the total and excess methane uptakes to be higher than that found at the same pressures in the purely microporous version of the same MOF. Extended Soxhlet extraction is a method that was found to be able to modify microporous PCN-250 to become mesoporous in a controlled fashion.

For obtaining mesoporous PCN-250, seven days of Soxhlet solvent extraction with methanol was applied to the as-synthesized microporous PCN-250 to fully remove the high boiling point solvents (*e.g.* DMF) or unreacted components. At the same time, mesopores have been created during the process. The mesoporous PCN-250 sample had 10 nm mesopores. The mesoporous PCN-250 was also fully activated and used for gas uptake, with smaller pores and winders shown in Figure IX-3.

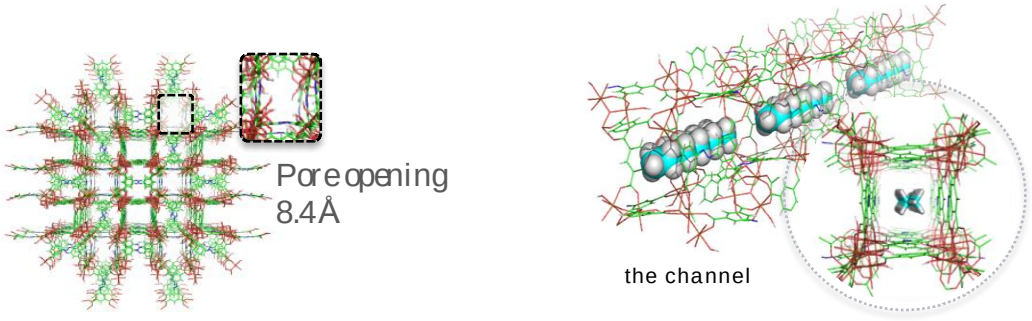

Figure IX-3. Theoretical decane space-filling in the pores of PCN-250. This is an illustration of the relative size of the pore to the alkane, in actual adsorption decane would be likely to adsorb against one wall or corner.

The two samples showed color differences in solid form (Figure IX-4a and Figure IX-4b). Note that these experiments were done with PCN-250(Fe_3) activated at 180°C, which exhibited lower performance than the PCN-250(Fe_2Co) and PCN-250($Fe(III)_2Fe(II)$).

The N_2 isotherms (Figure IX-4c and Figure IX-4d) at 77 K clearly indicated structural differences between the two PCN-250 adsorbents. As expected, nitrogen uptake was lower in the mesoporous PCN-250 compared to the microporous PCN-250. The

inserted figures in Figure 2c and Figure 2d show that mesoporous PCN-250 had 10 nm mesopores, whereas the microporous PCN-250 shows very little mesoporosity.

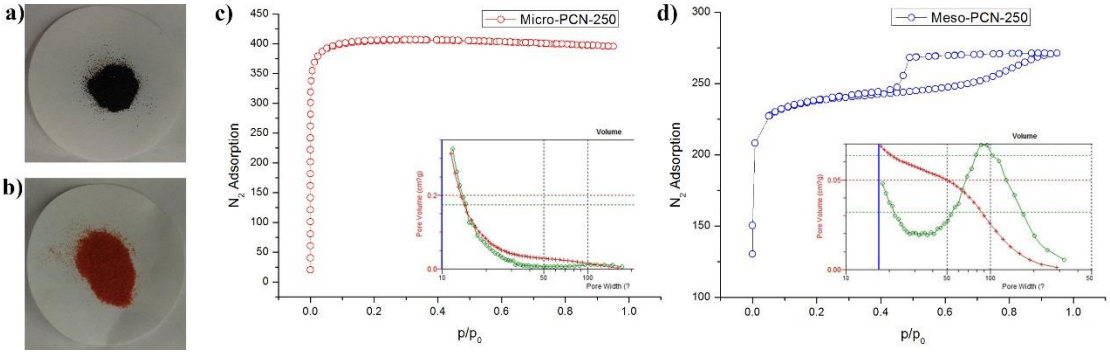

Figure IX-4. Crystal form of a) microporous-PCN-250 and b) post-synthetically treated mesoporous-PCN-250, N_2 isotherms and pore size of c) microporous-PCN-250 and d) mesoporous-PCN-250.

High-pressure methane uptake for each adsorbent was measured by HPVA-II at 298 K. For the microporous PCN-250 adsorbent (Figure IX-4a), total methane uptake at 65 bar was measured as 180 v/v (cm^3/cm^3), lower than expected and indicative of insufficient washing or solvent exchange. By injecting decane (33 microliters or 24 milligrams of decane per gram of MOF) into pre-activated PCN-250 adsorbent under an inert atmosphere (in glove box) after activation (180 ^oC for 12 h), the HPVA data show considerably decreased methane uptake (117 cm^3/cm^3 at 65 bar), possibly due to the presence of decane molecules blocking uptake by being adsorbed preferentially into surface micropores, with transport deeper into the crystals disfavored in the microporous sample, but not in the mesoporous sample filled with missing-linker and missing cluster

defects . It is unlikely that appreciable decane was removed the by gas sorption analyzer prior to adsorption measurement, because its vapor pressure is 3 times lower than the maximum vacuum of the instrument, and it is additionally adsorbed by the MOF. It is possible that a lower amount of decane or different adsorption conditions could produce a different effect even in microporous materials. The weight percentage of decane used is very low, and when more decane is used, performance decreases which are much higher than the weight percentage were seen. This suggests a process more complicated than simple higher alkane pore filling.

If the decane could travel freely throughout all the pores of PCN-250, it is unlikely we would see an uptake decrease of 35% after the addition of 0.24 wt% of decane. It is possible that decane primarily coats PCN-250 particles due to PCN-250's small pore and window sizes, and partially coating the surfaces of particles with decane allows us to take advantage of increased confinement effects.[304] One hypothesis is that when large mesopores are available, it fills them preferentially and absorbs some methane. Absorption alone, however, seems unlikely to account for such a disproportionately (by weight) large increase in uptake. We see an increase in 40 cm^3 methane g^{-1} uptake, or approximately 27 mg or 1.663 mmol of methane, from 24 mg or 0.1693 mmol of decane added(both per gram of MOF). This corresponds to a mole percentage of almost 10 mmol methane/mmol decane, almost 20 times higher than the methane/decane solubilities reported at similar temperatures and pressures.[305] Thus, simple absorption, or the lack of adsorption, cannot explain the effects shown here. The mesoporous sample may allow transport of the decane

within the pores, while the microporous sample remained coated, with some pores completely blocked.

When the amount of decane is sufficient to completely cover MOF crystallites, this may prevent them from being accessible to methane at all.[306] If this is the case, the increased performance of the mesoporous sample may be more due to its smaller particle size. Smaller particles would mean much higher particle-surface area as opposed to internal surface area, meaning that comparatively more decane would be optimal for smaller crystals, and less decane for larger crystals. It could also be that the decane remains in liquid form at certain pressures in the smaller macropores between the smaller crystals, able to absorb methane, while in the sample which retains higher crystallinity and larger crystals, the decane coats the crystals, goes into surface pores, or otherwise blocks adsorption. Further experiments involving samples of different crystal sizes of the same MOF should be able to help investigate these hypotheses.

In contrast, total methane uptake at 65 bar for mesoporous PCN-250 without decane was 171 cm^3/cm^3 at 65 bar (Figure IX-5b). The slightly decreased uptake should share the same reason as decreased N_2 adsorption for mesoporous absorbent, due to decreased surface area. However, when decane was added, the total methane uptake was dramatically increased. Especially at high pressures, the total uptake for mesoporous PCN-250 with decane was 210 cm^3/cm^3, which was a 22.8% increase from mesoporous PCN-250 and 16.7% increase from microporous PCN-250.

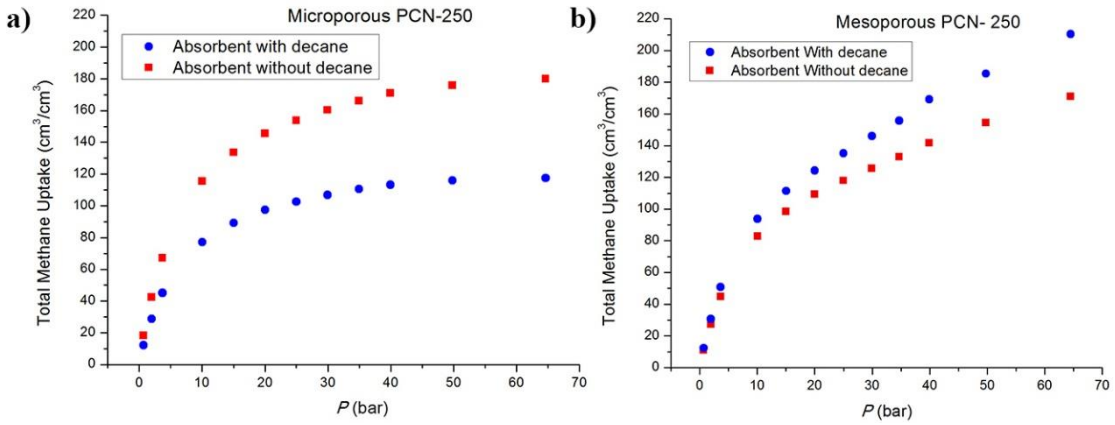

Figure IX-5. High-pressure volumetric methane uptake of a) microporous-PCN-250 and b) meso-PCN-250, with and without adding decane as doping reagent.

These results showed that at high pressures, adding small amounts of the doping reagent (decane) into the mesoporous PCN-250 improved the total volumetric methane uptake compared to the microporous PCN-250, despite the mesoporous MOF's lower surface area. The use of this method should provide a straightforward way to increase overall methane uptake and working capacity in any MOF-based adsorbent, because it increases uptake at high pressure while lowering it at low pressures (1-5 bar,) which is critical to working cycles where uptake at low pressure is counterproductive.

It is likely that the decrease of methane uptake when adding a relatively higher amount of decane to microporous PCN-250 may ascribe to the doping reagent blocking the entrance window of the micropores of the absorbent. If less quantity is used or another doping reagent with smaller size is tried, the HAANG method may also work for microporous adsorbents as well. There will be differing volumes of interparticle or

interpellet macropores in different systems after pelletization or compaction of the MOF powder (which typically has a real density far less than that of the crystal density calculated for the volumetric uptakes,) and addition of higher alkanes could better make use of the available volumes in these systems as well. Volumetric uptakes calculated from gravimetric isotherm data typically give values that are much better than those that could actually be realized because of unused interparticle macropores. To better illustrate the difference that HAANG could make in a real world natural gas storage system, we constructed an apparatus for direct volumetric measurement of methane uptake, shown in Figure IX-6a. This would also be valuable in comparison to results from a commercial high-pressure adsorbent system based on pressure dosing measurements, shown in Figure IX-6b.

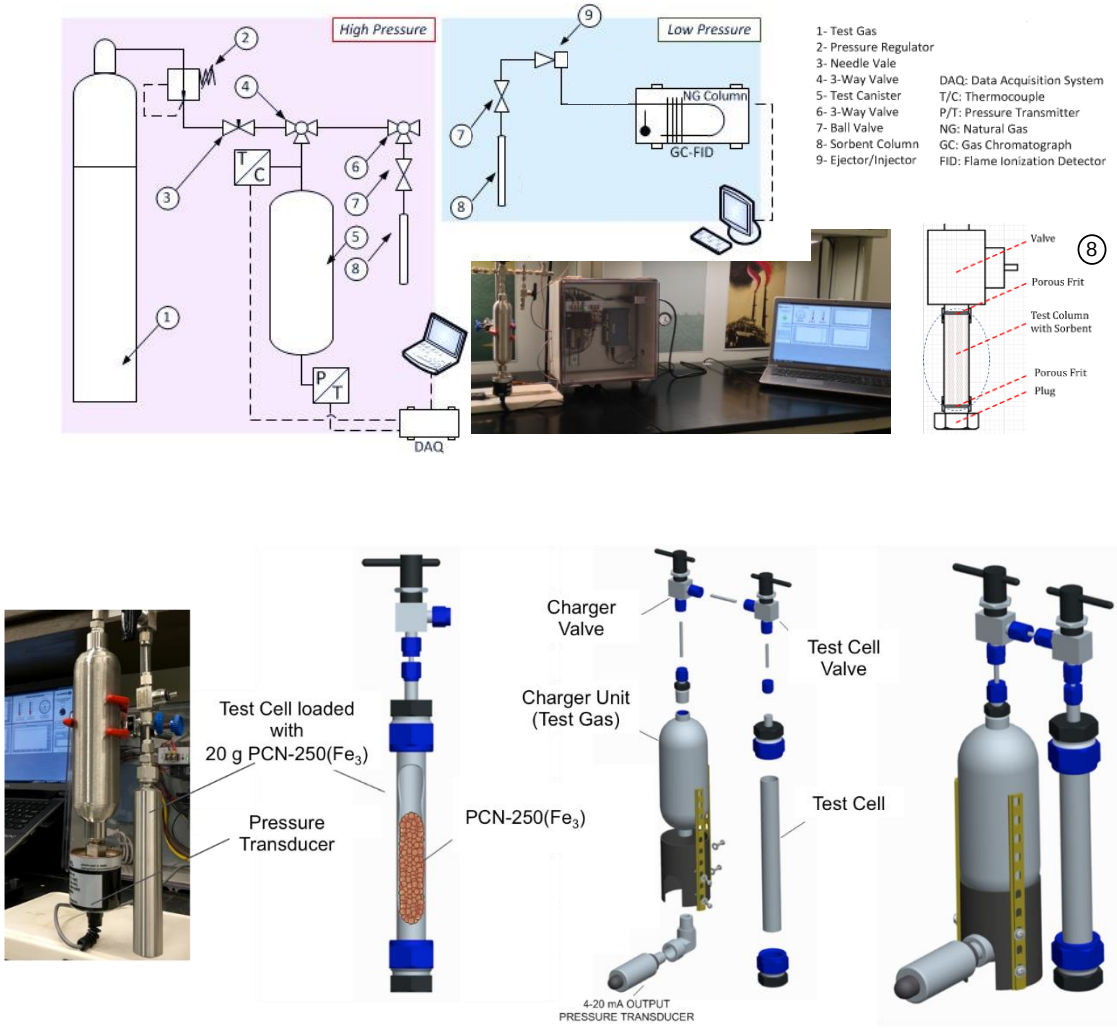

Figure IX-6. Design of the alkane adsorption test cell used for measurement by high-pressure adsorption followed by desorption into a GC.

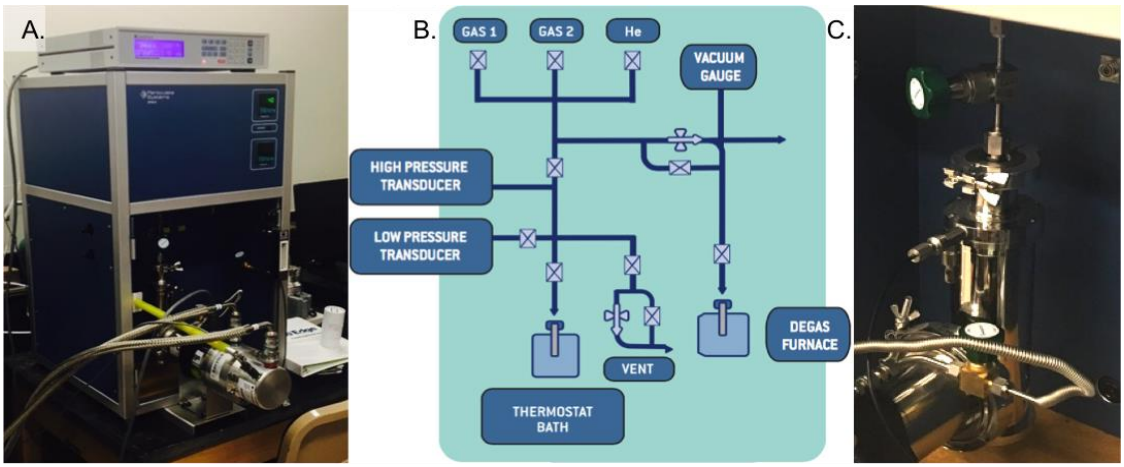

Figure IX-7. (A) High-pressure volumetric analyzer(HPVA) (B) Unit's system schematic showing the transducers used to precisely measure the system pressure (C) Test cell where MOFs are tested under methane gas.

The porous adsorbent framework was found to retain higher molecular weight hydrocarbon during desorption from the framework using a gas chromatograph after desorption (Figure IX-6). For example, when using a mixture of methane and propane, the methane is desorbed first before the propane is desorbed. In fact, it has been discovered that it is possible to desorb completely the methane gas from the porous adsorbent framework before the propane begins to desorb. The use of higher molecular weight hydrocarbons (such as n-butane) leads to a greater difference in elution times (compared to propane). This difference in elution times is most likely based on the relative size, polarity, and polarizability of the mixture of components. We used higher molecular weight alkanes as a solvent (HAANG), as the resulting alkane mixture should have a much higher critical point than pure methane, and when combined with methane adsorption showed higher methane uptake than either method alone. The adsorption of the higher

alkanes to the MOF also prevents separation and higher alkane recovery issues that have stymied attempts to increase the density of methane using alkane mixtures in the past.

It is possible to release methane from a porous adsorbent framework without releasing the hydrocarbon. Ideally to achieve this the porous adsorbent framework should comprise pores that are larger enough to encapsulate the solvent hydrocarbon molecules but small enough to provide sufficient Van der Waals interactions to retain the solvent hydrocarbon molecules at suitable discharge pressures (2-5 bar).[287]

Generally, it has been believed that the optimum pore diameter of the porous adsorbent framework is at least 1.5 times the kinetic diameter of methane, or other guest gas molecule, and preferably the pore diameter of the porous adsorbent framework is from about 1.5 times to about 2.5 times the kinetic diameter of methane or other guest gas molecule, favoring 2 times the kinetic diameter of methane, or other guest gas molecule. For testing purposes, we selected the stable MOFs UiO-66 and UiO-67.

In the first specific combination was methane and propane. Methane has a kinetic diameter of approximately 3.8 Angstroms while propane has a kinetic diameter of approximately 4.3 Angstrom. A porous adsorbent framework comprising pores having a pore diameter ranging from about 8 to about 11 Angstroms and having a pore opening of about 6.0 Angstroms provides the required pore size such that the pores are large enough to encapsulate propane and also small enough to retain propane after the methane is released. The pores are not however so small that they prevent methane from releasing at suitable discharge pressures. A suitable porous adsorbent framework having the required

pore size for this specific combination, a diameter ranging from 8 to 11 angstroms and a pore opening of 6.0 angstroms, is UiO-66.[35]

Here, propane was fed to the 50-mL pressure storage vessel with the porous adsorbent UiO-66 at room temperature at 60 PSI. Figure IX-8 is a set of GC chromatograms showing desorbed methane from UiO-66 in the presence and absence of propane. The results were an increase in total volumetric methane uptake of 18.03% and the full desorption of methane before propane over time.

The second combination was methane and n-butane. Methane has a kinetic diameter of approximately 3.8 Angstroms while N-butane has a kinetic diameter of approximately 4.3 Angstroms. A porous adsorbent framework comprising pores having a pore diameter ranging from about 11.5 to about 23 Angstroms and having a pore opening of 8.0 Angstroms provides the required pore size such that the pores are large enough to encapsulate n-butane and also small enough to retain n-butane after the methane is released. The pores are not however so small that they prevent methane from releasing at suitable discharge pressures. A suitable porous adsorbent framework having the required pore size for this specific combination, a diameter ranging from 8 to 11 angstroms and a pore opening of 6.0 angstroms, is UiO-67.[35]

Here, n-butane was fed to the storage vessel with the porous adsorbent UiO-67 at room temperature. Figure IX-8 is a set of GC chromatograms showing desorbed methane from UiO-67 in the presence and absence of n-butane. The results were an increase in

total volumetric methane uptake of 7.11% and the full desorption of methane before n-butane over time.

The next combination was methane and n-decane with adsorbent PCN-250. 60 μL n-decane (43.8 mg) (in liquid phase) was fed to the storage vessel with the 250 mg porous adsorbent at room temperature. Following, methane gas was introduced at 65 bar. Figure IX-8 is a GC-FID chromatogram comparing desorbed methane from PCN-250 at atmospheric pressure in the presence and absence of n-decane. The results were an increase in total volumetric methane desorption of 18.00% and the full desorption of methane, with the n-decane remaining adsorbed in the system. This result is inconsistent with the loss of uptake after a lower amount of decane was added to the microporous adsorbent in a glove box. One possible explanation is decreased particle size in the compacted, microporous PCN-250 sample used for this measurement, compared to the loosely packed large single crystals used in the HPVA-II analyzer. Increased particle surface area and smaller inter-particle macropores could increase the optimal decane loading before surface coverage and pore blocking occurs. Another explanation is that since we are directly measuring only the methane desorbed at 1 bar, this could be an increase in working capacity, not uptake. In this case, preferential adsorption of the heavy alkane at one bar drastically lowers methane uptake, while not lowering the uptake much at higher pressure.

This is roughly consistent with the increase in uptake seen with the HPVA high pressure methane isotherms for the mesoporous PCN-250 sample, where approximately

as many grams of methane uptake increase was measured (through pressure changes) as grams of decane were added. As the HPVA works through measuring methane added to the system to produce a given pressure, while the GC measures methane desorption from the material at atmospheric pressure with a flame ionization detector after the material is desorbed from the material into the GC, then passes through a chromatographic column, this represents confirmation of the concept through a completely different principle. However, the PCN-250 sample that showed an increase in uptake through this method was microporous, similar to the sample that showed a major decrease in uptake using the HPVA.

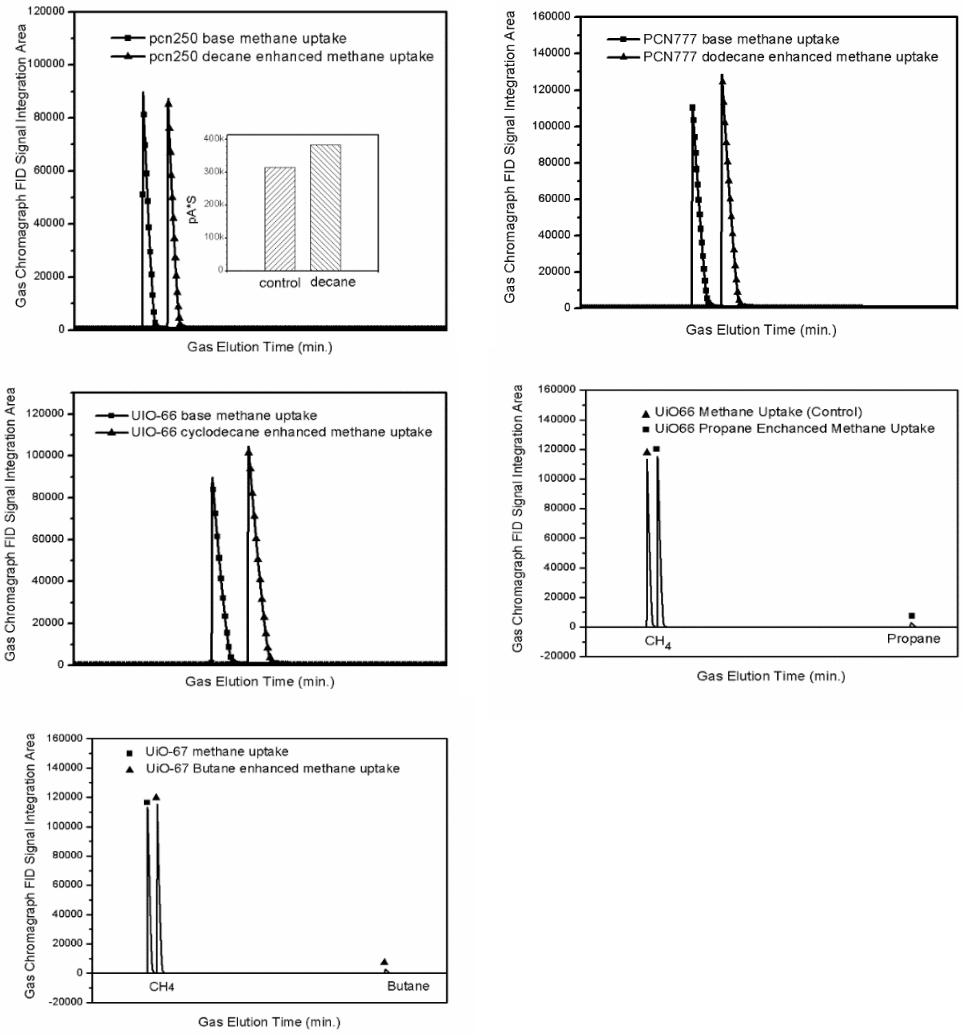

Figure IX-8. GC Chromatograms comparing desorbed methane from MOFs versus desorbed methane from MOFs dosed with small amounts of heavier alkanes. Propane and butane were eventually desorbed from the MOFs, while decane, cyclodecane, and dodecane were retained.

Several tests were conducted with MOFs UIO-66, UIO-67, PCN-250 and PCN-777 and alkanes including propane, n-butane, hexane, octane, n-decane, cyclodecane and dodecane. The highest uptake achieved was with the mesoporous MOF PCN-777 with dodecane, a result of an increase in total volumetric methane uptake of 27%. (Figure IX-8) Interestingly, that after only a small amount of loading, the improvements trended towards decreasing results, suggesting far more analytical study is needed to understand this system and demonstrate the system as a proof of concept. (Figure IX-9)

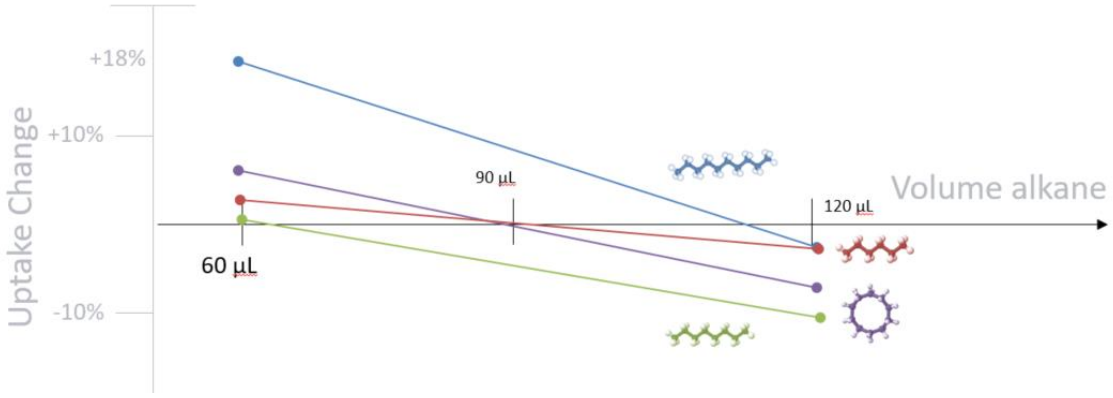

Figure IX-9. In PCN-250, too much alkane lowered methane uptake instead of increasing it.

9.4 CONCLUSION

In our attempts to combine adsorption on a solid with absorption in a liquid to maximize methane uptake in a given volume, we found surprising behavior that merits

further investigation. Extremely small volumes of heavier alkane can, depending on the porous material, increase methane uptake beyond the solubility of methane in the heavier alkane at the temperature and pressure used. Higher doses of heavy alkanes appear to decrease methane uptake in the porous material far more than preferential pore filling would account for. We confirmed these results through multiple separate gas uptake measurement methods. Further study of this phenomenon is required to investigate the mechanistic factors responsible for the effects seen, and to determine what crystal properties, such are pore size or particle size, most effect the amount of a given alkane that decreases versus increases methane uptake.

CHAPTER X

CONCLUSIONS

This dissertation has described methods for the alteration of advanced porous materials in order to tune their uptakes and selectivities for various gases relevant to clean energy technologies. Novel synthetic methods were developed in order to discover new MOF structures as well as to produce gas adsorbents with optimized performance by tuning the size and contents of MOF pores to be appropriate for hydrogen, methane, or CO_2 sorption in temperature and pressure ranges needed for practical application. This was accomplished both by changing the pore size and contents of existing MOFs, and through synthesis of new materials that still retain high porosity and appropriate pore size. Development of advanced MOF synthesis and pore engineering methods will guide other researchers, especially the concept that has recently shown the most promising results: combination of gases and liquids in order to simultaneously take advantage of adsorption and absorption.

We began in parts 2 through 5 with a comprehensive review of recent progress in the development of advanced porous materials for methane, hydrogen, and carbon dioxide uptake. Increasing the stability of Metal-Organic Frameworks, primarily through the development of synthetic methods for the crystallization of MOFs based on high-valence metals such as Zr^{4+}, Fe^{3+}, and Cr^{3+}, has allowed us to grow and characterize materials that are robust to extremely harsh chemical conditions while still retaining their high tunability and precise functionalization. It is important not to forget,

however, that “high-valence MOFs are stable” is an oversimplification, as we explained when we covered group 4 metals as secondary building units. Ti-MOFs tend to be significantly less chemically stable that Fe or Cr-MOFs, due to Ti’s d^0 nature allowing them no ligand field stabilization energy to disfavor substitution from connecting ligands to basic molecules like water or amines, which can quickly collapse Ti-MOF frameworks.

Zr-MOFs have the same lack of LFSE, but tend to be robust as long as their linkers are short and their connectivity remains high, as in the 12-connected UiO-66. Unlike the small, hard Ti ions, their larger ionic diameter is a better match for bonding with carboxylates. Zr-MOFs also form stable, large Zr_6 and Zr_8 oxo clusters which can bond to up to 12 carboxylates, and this high connectivity stabilizes their frameworks as well. Zr-MOFs built from 6 and 8-connected clusters, longer linkers, or with too many missing cluster or missing linker defects quickly lose chemical stability. We also covered catalytic porphyrin Zr-MOFs and explored the burgeoning field of the rational design of MOFs, which is being led by Zr-MOFs due to their unique combination of facile crystallization, tunability, and stability.

We also studied porous carbons and their applications in hydrogen storage. Though porous carbons and polymers lack the precise pore size control and tunability of MOFs, they can still achieve extremely high surface areas which are useful for adsorption. There are a great many synthetic methods for porous carbons and polymers, including chemical and temperature-based activation, graphene oxide production, MOF-

derived porous carbons, which are typically produced from the calcination of Zn-based and other MOFs with low-boiling metals, various templating methods, and polymerization of rigid polytopic monomers to produce PPNs. These can have performances that sometimes rival those of MOFs for applications such as gas uptake, separations, or catalysis. Finally, we cover methods our group has developed for the rational design of MOFs using stepwise synthesis methods. Our dream is the "total synthesis" of customized pore space in a MOF using multi-step post-synthetic modification techniques, similarly to how organic chemists achieve the "total synthesis" of complicated molecules after many steps.

We have developed several techniques to work towards this goal. We started with Kinetically Tuned Dimensional Augmentation, which allows us to pre-synthetically choose and alter the metal SBU with more control that using metal salts for solvothermal MOF synthesis. We also developed Postsynthetic Metathesis and Oxidation, which we use to grow ultra-stable MOFs such as functionalized Cr-MOFs that would otherwise be synthetically inaccessible. This is accomplished by growing a MOF of a more labile metal, such as Mg or even Fe, then postsynthetically exchanging ligands and/or metals from saturated solutions into the MOF. We found that exchanging more labile Cr^{2+} in solution, then exposing the MOF to air to oxidize to Cr^{3+}, accomplished complete or near-complete metal exchange, unlike the direct metal metathesis that had been tried earlier. We showed that even highly mesoporous MOFs like PCN-333 with its 5.5nm pores become incredibly robust when exchanged with Cr^{3+}.

We built on both of these techniques to develop Sequential Linker Installation and Sequential Cluster Metalation, stepwise synthesis techniques that use the unique advantages of Zr-MOFs to take a major step towards the dream of rational design of MOFs: the postsynthetic installation of multiple distinct functional groups and/or metals at crystallographically ordered locations within the pores of a robust MOF. We start with a MOF, PCN-700, which is similar to UiO-66 except for the multiple sites on its SBU that are hydroxyl-functionalized instead of hosting a carboxylate, and we post-synthetically install, metals, monocarboxylates, or 2 different sites for new linkers between them of various length ranges that can also be used to tune the pore size and shape of the MOF.

We then moved on to covering the replacement of ammonium with lithium cations in a pair of anionic MOFs, which show drastically increased porosity and hydrogen uptake afterwards. We found that pre-synthetic synthesis modulation was the most efficient way to accomplish that. We also found that just as the crystallization of MOFs can be modulated through changing pH or the addition of various competing monotopic ligands, using metals in unstable oxidation states can also change the crystallization conditions enough to alter the MOF product. PCN-47, -48, and -49, Mn^{2+} MOFs grown from Mn^{2+}, $Mn^{3+/4+}$, and Mn^{7+} sources, show distinct crystal structures, porosities, and pore size distributions despite all being composed of Mn^{2+} SBUs only.

Flue gas CO_2 capture is most efficient through the reaction of amines and CO_2 to form carbamate salts. The first reason for this is the temperature range needed –

adsorption must be around 40°C, a temperature that is too high for good uptake with most CO_2 physisorbents. The second is the presence of water and possible presence of SO_2 or other molecules that could quickly collapse chemically fragile MOFs. Water actually assists amine-CO_2 capture, as it can act as a proton acceptor after amine attacks the CO_2, eventually resulting in bicarbonate formation that requires only one amine per CO_2 molecule captured instead of two. The most relevant parameters for amine-based CO_2 sorbents are the density of accessible amine moieties, the cost, the cyclability, and the energy cost for regeneration. For these reasons, amine-loaded porous polymers are an avenue we have investigated at length. We found an alkylamine-polymer composite that has extremely high uptake, low cost, and most importantly, unprecedented cycling performance, due to its framework-incorporated amines allowing carbamate formation directly with the loaded alkylamines to tether them.

Another avenue where liquid-solid composites were able to show interesting results was in the alkane loading of PCN-250. We found that when tiny, optimized amounts of heavier alkanes were loaded into MOF crystals such as UiO-66, PCN-250, and PCN-777, the volumetric uptake of methane significantly increased. Because the pore sizes of these MOFs are slightly too large for highly efficient methane packing, a certain amount of heavier liquid filling pore space can make multilayer adsorption more favored at accessible temperatures and pressures. It is possible that a methane and decane binary mixture has a high enough critical point to more easily undergo capillary condensation or other densification, as we saw the best methane uptake performance

increases in mesoporous PCN-777 and in PCN-250 that had been modified to become mesoporous. Another possible mechanism is “capping” of methane into the interior at higher partial pressures when heavy surface alkanes partially block the exits, a mechanism shown with other heavy alkanes in porous material composites. Larger amounts of heavy alkanes drastically lowered methane uptake to a level disproportionately lower than the amount of alkane added, indicating a possible surface covering or pore blocking mechanism. Further investigation will be necessary to differentiate between these possible explanations.

Future work will concentrate on exploiting the combination of absorbents and adsorbents in solid-liquid composite systems for applications such as acid gas separations, natural gas storage, and even yet underexplored applications like homogenous-heterogenous tandem catalysis. We have shown that partially loading porous materials with liquids, more efficient use of pore space can be achieved. For example, the methane uptake of MOFs normally less suitable for uptake can be improved by partial liquid filling of their pores. By carefully controlling regeneration conditions, smaller molecules can be desorbed while the larger liquid molecules can be retained indefinitely, whether they are alkylamines, alkanes, or yet unforeseen parts of novel solid-liquid composites. The development of novel advanced porous materials is currently very promising, whether they are modified pre-synthetically, post-synthetically in a stepwise fashion, or made into composites.

REFERENCES

(1) Batten, S. R.; Champness, N. R.; Chen, X. M.; Garcia-Martinez, J.; Kitagawa, S.; Ohrstrom, L.; O'Keeffe, M.; Suh, M. P.; Reedijk, J. Terminology of Metal-Organic Frameworks and Coordination Polymers (Iupac Recommendations 2013). *Pure and Applied Chemistry* **2013**, *85*, 1715-1724.

(2) Zhou, H. C.; Long, J. R.; Yaghi, O. M. Introduction to Metal-Organic Frameworks. *Chemical Reviews* **2012**, *112*, 673-674.

(3) Stock, N.; Biswas, S. Synthesis of Metal-Organic Frameworks (Mofs): Routes to Various Mof Topologies, Morphologies, and Composites. *Chemical Reviews* **2012**, *112*, 933-969.

(4) Cohen, S. M. Postsynthetic Methods for the Functionalization of Metal–Organic Frameworks. *Chemical Reviews* **2012**, *112*, 970-1000.

(5) Suh, M. P.; Park, H. J.; Prasad, T. K.; Lim, D. W. Hydrogen Storage in Metal-Organic Frameworks. *Chemical Reviews* **2012**, *112*, 782-835.

(6) Ma, S. Q.; Sun, D. F.; Yuan, D. Q.; Wang, X. S.; Zhou, H. C. Preparation and Gas Adsorption Studies of Three Mesh-Adjustable Molecular Sieves with a Common Structure. *Journal of the American Chemical Society* **2009**, *131*, 6445-6451.

(7) Sumida, K.; Rogow, D. L.; Mason, J. A.; McDonald, T. M.; Bloch, E. D.; Herm, Z. R.; Bae, T. H.; Long, J. R. Carbon Dioxide Capture in Metal-Organic Frameworks. *Chemical Reviews* **2012**, *112*, 724-781.

(8) Bétard, A.; Fischer, R. A. Metal–Organic Framework Thin Films: From Fundamentals to Applications. *Chemical Reviews* **2012**, *112*, 1055-1083.

(9) Cui, Y.; Yue, Y.; Qian, G.; Chen, B. Luminescent Functional Metal–Organic Frameworks. *Chemical Reviews* **2012**, *112*, 1126-1162.

(10) Gagnon, K. J.; Perry, H. P.; Clearfield, A. Conventional and Unconventional Metal–Organic Frameworks Based on Phosphonate Ligands: Mofs and Umofs. *Chemical Reviews* **2012**, *112*, 1034-1054.

(11) Getman, R. B.; Bae, Y.-S.; Wilmer, C. E.; Snurr, R. Q. Review and Analysis of Molecular Simulations of Methane, Hydrogen, and Acetylene Storage in Metal–Organic Frameworks. *Chemical Reviews* **2012**, *112*, 703-723.

(12) Horcajada, P.; Gref, R.; Baati, T.; Allan, P. K.; Maurin, G.; Couvreur, P.; Férey, G.; Morris, R. E.; Serre, C. Metal–Organic Frameworks in Biomedicine. *Chemical Reviews* **2012**, *112*, 1232-1268.

(13) Kreno, L. E.; Leong, K.; Farha, O. K.; Allendorf, M.; Van Duyne, R. P.; Hupp, J. T. Metal–Organic Framework Materials as Chemical Sensors. *Chemical Reviews* **2012**, *112*, 1105-1125.

(14) Feng, D.; Gu, Z. Y.; Li, J. R.; Jiang, H. L.; Wei, Z.; Zhou, H. C. Zirconium-Metalloporphyrin Pcn-222: Mesoporous Metal-Organic Frameworks with Ultrahigh Stability as Biomimetic Catalysts. *Angew Chem Int Ed Engl* **2012**, *51*, 10307-10310.

(15) O'Keeffe, M.; Yaghi, O. M. Deconstructing the Crystal Structures of Metal–Organic Frameworks and Related Materials into Their Underlying Nets. *Chemical Reviews* **2012**, *112*, 675-702.

(16) Suh, M. P.; Park, H. J.; Prasad, T. K.; Lim, D.-W. Hydrogen Storage in Metal–Organic Frameworks. *Chemical Reviews* **2012**, *112*, 782-835.

(17) Sumida, K.; Rogow, D. L.; Mason, J. A.; McDonald, T. M.; Bloch, E. D.; Herm, Z. R.; Bae, T.-H.; Long, J. R. Carbon Dioxide Capture in Metal–Organic Frameworks. *Chemical Reviews* **2012**, *112*, 724-781.

(18) Wang, C.; Zhang, T.; Lin, W. Rational Synthesis of Noncentrosymmetric Metal–Organic Frameworks for Second-Order Nonlinear Optics. *Chemical Reviews* **2012**, *112*, 1084-1104.

(19) Wu, H.; Gong, Q.; Olson, D. H.; Li, J. Commensurate Adsorption of Hydrocarbons and Alcohols in Microporous Metal Organic Frameworks. *Chemical Reviews* **2012**, *112*, 836-868.

(20) Yoon, M.; Srirambalaji, R.; Kim, K. Homochiral Metal–Organic Frameworks for Asymmetric Heterogeneous Catalysis. *Chemical Reviews* **2012**, *112*, 1196-1231.

(21) Feng, D.; Gu, Z.-Y.; Li, J.-R.; Jiang, H.-L.; Wei, Z.; Zhou, H.-C. Zirconium-Metalloporphyrin Pcn-222: Mesoporous Metal–Organic Frameworks with Ultrahigh Stability as Biomimetic Catalysts. *Angewandte Chemie International Edition* **2012**, *51*, 10307-10310.

(22) Zhang, W.; Xiong, R.-G. Ferroelectric Metal–Organic Frameworks. *Chemical Reviews* **2012**, *112*, 1163-1195.

(23) Farha, O. K.; Eryazici, I.; Jeong, N. C.; Hauser, B. G.; Wilmer, C. E.; Sarjeant, A. A.; Snurr, R. Q.; Nguyen, S. T.; Yazaydın, A. Ö.; Hupp, J. T. Metal–Organic Framework Materials with Ultrahigh Surface Areas: Is the Sky the Limit? *Journal of the American Chemical Society* **2012**, *134*, 15016-15021.

(24) Brunauer, S.; Emmett, P. H.; Teller, E. Adsorption of Gases in Multimolecular Layers. *Journal of the American Chemical Society* **1938**, *60*, 309-319.

(25) Bosch, M.; Zhang, M.; Zhou, H.-C. Increasing the Stability of Metal-Organic Frameworks. *Advances in Chemistry* **2014**, *2014*, 8.

(26) McGuire, C. V.; Forgan, R. S. The Surface Chemistry of Metal-Organic Frameworks. *Chemical Communications* **2015**, *51*, 5199-5217.

(27) Shearer, G. C.; Chavan, S.; Ethiraj, J.; Vitillo, J. G.; Svelle, S.; Olsbye, U.; Lamberti, C.; Bordiga, S.; Lillerud, K. P. Tuned to Perfection: Ironing out the Defects in Metal-Organic Framework Uio-66. *Chemistry of Materials* **2014**, *26*, 4068-4071.

(28) Sholl, D. S.; Lively, R. P. Defects in Metal–Organic Frameworks: Challenge or Opportunity? *The Journal of Physical Chemistry Letters* **2015**, *6*, 3437-3444.

(29) Lian, X. Z.; Feng, D. W.; Chen, Y. P.; Liu, T. F.; Wang, X.; Zhou, H. C. The Preparation of an Ultrastable Mesoporous Cr(Iii)-Mof Via Reductive Labilization. *Chemical Science* **2015**, *6*, 7044-7048.

(30) Park, J. Y.; Feng, D. W.; Zhou, H. C. Dual Exchange in Pcn-333: A Facile Strategy to Chemically Robust Mesoporous Chromium Metal-Organic Framework with Functional Groups. *Journal of the American Chemical Society* **2015**, *137*, 11801-11809.

(31) Liu, T. F.; Zou, L. F.; Feng, D. W.; Chen, Y. P.; Fordham, S.; Wang, X.; Liu, Y. Y.; Zhou, H. C. Stepwise Synthesis of Robust Metal-Organic Frameworks Via Postsynthetic Metathesis and Oxidation of Metal Nodes in a Single-Crystal to Single-Crystal Transformation. *Journal of the American Chemical Society* **2014**, *136*, 7813-7816.

(32) Purewal, J. J.; Liu, D.; Yang, J.; Sudik, A.; Siegel, D. J.; Maurer, S.; Muller, U. Increased Volumetric Hydrogen Uptake of Mof-5 by Powder Densification. *International Journal of Hydrogen Energy* **2012**, *37*, 2723-2727.

(33) Yang, J.-M.; Liu, Q.; Sun, W.-Y. Shape and Size Control and Gas Adsorption of Ni(Ii)-Doped Mof-5 Nano/Microcrystals. *Microporous and Mesoporous Materials* **2014**, *190*, 26-31.

(34) Li, H.; Eddaoudi, M.; O'Keeffe, M.; Yaghi, O. M. Design and Synthesis of an Exceptionally Stable and Highly Porous Metal-Organic Framework. *Nature* **1999**, *402*, 276-279.

(35) Cavka, J. H.; Jakobsen, S.; Olsbye, U.; Guillou, N.; Lamberti, C.; Bordiga, S.; Lillerud, K. P. A New Zirconium Inorganic Building Brick Forming Metal Organic Frameworks with Exceptional Stability. *Journal of the American Chemical Society* **2008**, *130*, 13850-13851.

(36) Ferey, G.; Mellot-Draznieks, C.; Serre, C.; Millange, F.; Dutour, J.; Surble, S.; Margiolaki, I. A Chromium Terephthalate-Based Solid with Unusually Large Pore Volumes and Surface Area. *Science* **2005**, *309*, 2040-2042.

(37) Chui, S. S.-Y.; Lo, S. M.-F.; Charmant, J. P. H.; Orpen, A. G.; Williams, I. D. A Chemically Functionalizable Nanoporous Material [Cu3(Tma)2(H2o)3]N. *Science* **1999**, *283*, 1148-1150.

(38) Ma, S.; Simmons, J. M.; Sun, D.; Yuan, D.; Zhou, H.-C. Porous Metal-Organic Frameworks Based on an Anthracene Derivative: Syntheses, Structure Analysis, and Hydrogen Sorption Studies. *Inorganic Chemistry* **2009**, *48*, 5263-5268.

(39) Li, H.; Eddaoudi, M.; Groy, T. L.; Yaghi, O. M. Establishing Microporosity in Open Metal-Organic Frameworks: Gas Sorption Isotherms for Zn(Bdc) (Bdc = 1,4-Benzenedicarboxylate). *Journal of the American Chemical Society* **1998**, *120*, 8571-8572.

(40) Dolomanov, O. V.; Bourhis, L. J.; Gildea, R. J.; Howard, J. A. K.; Puschmann, H. Olex2: A Complete Structure Solution, Refinement and Analysis Program. *Journal of Applied Crystallography* **2009**, *42*, 339-341.

(41) Li, H.; Shi, W.; Zhao, K.; Li, H.; Bing, Y.; Cheng, P. Enhanced Hydrostability in Ni-Doped Mof-5. *Inorganic Chemistry* **2012**, *51*, 9200-9207.

(42) Hupp, J. T.; Poeppelmeier, K. R. Better Living through Nanopore Chemistry. *Science* **2005**, *309*, 2008-2009.

(43) Tsuruoka, T.; Furukawa, S.; Takashima, Y.; Yoshida, K.; Isoda, S.; Kitagawa, S. Nanoporous Nanorods Fabricated by Coordination Modulation and Oriented Attachment Growth. *Angewandte Chemie International Edition* **2009**, *48*, 4739-4743.

(44) Rosi, N. L.; Eddaoudi, M.; Kim, J.; O'Keeffe, M.; Yaghi, O. M. Infinite Secondary Building Units and Forbidden Catenation in Metal-Organic Frameworks. *Angewandte Chemie International Edition* **2002**, *41*, 284-287.

(45) Mustafa, D.; Breynaert, E.; Bajpe, S. R.; Martens, J. A.; Kirschhock, C. E. A. Stability Improvement of Cu-3(Btc)(2) Metal-Organic Frameworks under Steaming Conditions by Encapsulation of a Keggin Polyoxometalate. *Chemical Communications* **2011**, *47*, 8037-8039.

(46) Tan, K.; Nijem, N.; Canepa, P.; Gong, Q.; Li, J.; Thonhauser, T.; Chabal, Y. J. Stability and Hydrolyzation of Metal Organic Frameworks with Paddle-Wheel Sbus Upon Hydration. *Chemistry of Materials* **2012**, *24*, 3153-3167.

(47) Kusgens, P.; Rose, M.; Senkovska, I.; Frode, H.; Henschel, A.; Siegle, S.; Kaskel, S. Characterization of Metal-Organic Frameworks by Water Adsorption. *Microporous and Mesoporous Materials* **2009**, *120*, 325-330.

(48) Yuan, D. Q.; Zhao, D.; Sun, D. F.; Zhou, H. C. An Isoreticular Series of Metal-Organic Frameworks with Dendritic Hexacarboxylate Ligands and Exceptionally High Gas-Uptake Capacity. *Angewandte Chemie-International Edition* **2010**, *49*, 5357-5361.

(49) Zhao, D.; Yuan, D.; Sun, D.; Zhou, H.-C. Stabilization of Metal−Organic Frameworks with High Surface Areas by the Incorporation of Mesocavities with Microwindows. *Journal of the American Chemical Society* **2009**, *131*, 9186-9188.

(50) Li, M.; Li, D.; O'Keeffe, M.; Yaghi, O. M. Topological Analysis of Metal–Organic Frameworks with Polytopic Linkers and/or Multiple Building Units and the Minimal Transitivity Principle. *Chemical Reviews* **2013**, *114*, 1343-1370.

(51) Zhang, M.; Chen, Y.-P.; Zhou, H.-C. Structural Design of Porous Coordination Networks from Tetrahedral Building Units. *CrystEngComm* **2013**, *15*, 9544-9552.

(52) Wei, Z. W.; Lu, W. G.; Jiang, H. L.; Zhou, H. C. A Route to Metal-Organic Frameworks through Framework Templating. *Inorganic Chemistry* **2013**, *52*, 1164-1166.

(53) Veidis, M. V.; Schreiber, G. H.; Gough, T. E.; Palenik, G. J. Jahn-Teller Distortions in Octahedral Copper(Ii) Complexes. *Journal of the American Chemical Society* **1969**, *91*, 1859-1860.

(54) Bhunia, M. K.; Hughes, J. T.; Fettinger, J. C.; Navrotsky, A. Thermochemistry of Paddle Wheel Mofs: Cu-Hkust-1 and Zn-Hkust-1. *Langmuir* **2013**, *29*, 8140-8145.

(55) Kim, Y.; Das, S.; Bhattacharya, S.; Hong, S.; Kim, M. G.; Yoon, M.; Natarajan, S.; Kim, K. Metal-Ion Metathesis in Metal-Organic Frameworks: A Synthetic Route to New Metal-Organic Frameworks. *Chemistry-a European Journal* **2012**, *18*, 16642-16648.

(56) Chevreau, H.; Devic, T.; Salles, F.; Maurin, G.; Stock, N.; Serre, C. Mixed-Linker Hybrid Superpolyhedra for the Production of a Series of Large-Pore Iron(Iii) Carboxylate Metal–Organic Frameworks. *Angewandte Chemie International Edition* **2013**, *52*, 5056-5060.

(57) Zhang, M.; Chen, Y.-P.; Bosch, M.; Gentle, T.; Wang, K.; Feng, D.; Wang, Z. U.; Zhou, H.-C. Symmetry-Guided Synthesis of Highly Porous Metal–Organic Frameworks with Fluorite Topology. *Angewandte Chemie International Edition* **2014**, *53*, 815-818.

(58) Valenzano, L.; Civalleri, B.; Chavan, S.; Bordiga, S.; Nilsen, M. H.; Jakobsen, S.; Lillerud, K. P.; Lamberti, C. Disclosing the Complex Structure of Uio-66 Metal Organic Framework: A Synergic Combination of Experiment and Theory. *Chemistry of Materials* **2011**, *23*, 1700-1718.

(59) DeCoste, J. B.; Peterson, G. W.; Jasuja, H.; Glover, T. G.; Huang, Y. G.; Walton, K. S. Stability and Degradation Mechanisms of Metal-Organic Frameworks Containing the Zr6o4(Oh)(4) Secondary Building Unit. *Journal of Materials Chemistry A* **2013**, *1*, 5642-5650.

(60) Guillerm, V.; Ragon, F.; Dan-Hardi, M.; Devic, T.; Vishnuvarthan, M.; Campo, B.; Vimont, A.; Clet, G.; Yang, Q.; Maurin, G.; Ferey, G.; Vittadini, A.; Gross, S.; Serre, C. A Series of Isoreticular, Highly Stable, Porous Zirconium Oxide Based Metal-Organic Frameworks. *Angewandte Chemie-International Edition* **2012**, *51*, 9267-9271.

(61) Schaate, A.; Roy, P.; Godt, A.; Lippke, J.; Waltz, F.; Wiebcke, M.; Behrens, P. Modulated Synthesis of Zr-Based Metal–Organic Frameworks: From Nano to Single Crystals. *Chemistry – A European Journal* **2011**, *17*, 6643-6651.

(62) Schaate, A.; Roy, P.; Preuße, T.; Lohmeier, S. J.; Godt, A.; Behrens, P. Porous Interpenetrated Zirconium–Organic Frameworks (Pizofs): A Chemically Versatile Family of Metal–Organic Frameworks. *Chemistry – A European Journal* **2011**, *17*, 9320-9325.

(63) Feng, D. W.; Gu, Z. Y.; Li, J. R.; Jiang, H. L.; Wei, Z. W.; Zhou, H. C. Zirconium-Metalloporphyrin Pcn-222: Mesoporous Metal-Organic Frameworks with Ultrahigh Stability as Biomimetic Catalysts. *Angewandte Chemie-International Edition* **2012**, *51*, 10307-10310.

(64) Feng, D. W.; Chung, W. C.; Wei, Z. W.; Gu, Z. Y.; Jiang, H. L.; Chen, Y. P.; Darensbourg, D. J.; Zhou, H. C. Construction of Ultrastable Porphyrin Zr Metal-Organic Frameworks through Linker Elimination. *Journal of the American Chemical Society* **2013**, *135*, 17105-17110.

(65) Jiang, H. L.; Feng, D. W.; Wang, K. C.; Gu, Z. Y.; Wei, Z. W.; Chen, Y. P.; Zhou, H. C. An Exceptionally Stable, Porphyrinic Zr Metal-Organic Framework Exhibiting Ph-Dependent Fluorescence. *Journal of the American Chemical Society* **2013**, *135*, 13934-13938.

(66) Yoon, M.; Srirambalaji, R.; Kim, K. Homochiral Metal–Organic Frameworks for Asymmetric Heterogeneous Catalysis. *Chemical Reviews* **2011**, *112*, 1196-1231.

(67) Zhang, M.; Bosch, M.; Gentle, T.; Zhou, H.-C. *CrystEngComm* **2014**, *16*, ASAP, 10.1039/C1034CE00321G.

(68) Kandiah, M.; Nilsen, M. H.; Usseglio, S.; Jakobsen, S.; Olsbye, U.; Tilset, M.; Larabi, C.; Quadrelli, E. A.; Bonino, F.; Lillerud, K. P. Synthesis and Stability of Tagged Uio-66 Zr-Mofs. *Chemistry of Materials* **2010**, *22*, 6632-6640.

(69) Bon, V.; Senkovskyy, V.; Senkovska, I.; Kaskel, S. Zr(Iv) and Hf(Iv) Based Metal-Organic Frameworks with Reo-Topology. *Chem. Commun.* **2012**, *48*, 8407-8409.

(70) Dinca, M.; Dailly, A.; Liu, Y.; Brown, C. M.; Neumann, D. A.; Long, J. R. Hydrogen Storage in a Microporous Metal-Organic Framework with Exposed Mn2+ Coordination Sites. *Journal of the American Chemical Society* **2006**, *128*, 16876-16883.

(71) Banerjee, R.; Phan, A.; Wang, B.; Knobler, C.; Furukawa, H.; O'Keeffe, M.; Yaghi, O. M. High-Throughput Synthesis of Zeolitic Imidazolate Frameworks and Application to Co2 Capture. *Science* **2008**, *319*, 939-943.

(72) Huang, X.-C.; Lin, Y.-Y.; Zhang, J.-P.; Chen, X.-M. Ligand-Directed Strategy for Zeolite-Type Metal–Organic Frameworks: Zinc(Ii) Imidazolates with Unusual Zeolitic Topologies. *Angewandte Chemie International Edition* **2006**, *45*, 1557-1559.

(73) Liu, Y.; Kravtsov, V. C.; Larsen, R.; Eddaoudi, M. Molecular Building Blocks Approach to the Assembly of Zeolite-Like Metal-Organic Frameworks (Zmofs) with Extra-Large Cavities. *Chemical Communications* **2006**, 1488-1490.

(74) An, J.; Geib, S. J.; Rosi, N. L. Cation-Triggered Drug Release from a Porous Zinc−Adeninate Metal−Organic Framework. *Journal of the American Chemical Society* **2009**, *131*, 8376-8377.

(75) Zhang, M.; Lu, W.; Li, J.-R.; Bosch, M.; Chen, Y.-P.; Liu, T.-F.; Liu, Y.; Zhou, H.-C. Design and Synthesis of Nucleobase-Incorporated Metal-Organic Materials. *Inorganic Chemistry Frontiers* **2014**, *1*, 159-162.

(76) Colombo, V.; Galli, S.; Choi, H. J.; Han, G. D.; Maspero, A.; Palmisano, G.; Masciocchi, N.; Long, J. R. High Thermal and Chemical Stability in Pyrazolate-Bridged Metal-Organic Frameworks with Exposed Metal Sites. *Chemical Science* **2011**, *2*, 1311-1319.

(77) Herm, Z. R.; Wiers, B. M.; Mason, J. A.; van Baten, J. M.; Hudson, M. R.; Zajdel, P.; Brown, C. M.; Masciocchi, N.; Krishna, R.; Long, J. R. Separation of Hexane Isomers in a Metal-Organic Framework with Triangular Channels. *Science* **2013**, *340*, 960-964.

(78) Makal, T. A.; Wang, X.; Zhou, H. C. Tuning the Moisture and Thermal Stability of Metal-Organic Frameworks through Incorporation of Pendant Hydrophobic Groups. *Crystal Growth & Design* **2013**, *13*, 4760-4768.

(79) Yang, C.; Kaipa, U.; Mather, Q. Z.; Wang, X.; Nesterov, V.; Venero, A. F.; Omary, M. A. Fluorous Metal–Organic Frameworks with Superior Adsorption and Hydrophobic Properties toward Oil Spill Cleanup and Hydrocarbon Storage. *Journal of the American Chemical Society* **2011**, *133*, 18094-18097.

(80) Horcajada, P.; Salles, F.; Wuttke, S.; Devic, T.; Heurtaux, D.; Maurin, G.; Vimont, A.; Daturi, M.; David, O.; Magnier, E.; Stock, N.; Filinchuk, Y.; Popov, D.; Riekel, C.; Férey, G.; Serre, C. How Linker's Modification Controls Swelling Properties of Highly Flexible Iron(Iii) Dicarboxylates Mil-88. *Journal of the American Chemical Society* **2011**, *133*, 17839-17847.

(81) Padial, N. M.; Quartapelle Procopio, E.; Montoro, C.; López, E.; Oltra, J. E.; Colombo, V.; Maspero, A.; Masciocchi, N.; Galli, S.; Senkovska, I.; Kaskel, S.; Barea, E.; Navarro, J. A. R. Highly Hydrophobic Isoreticular Porous Metal–Organic Frameworks for the Capture of Harmful Volatile Organic Compounds. *Angewandte Chemie International Edition* **2013**, *52*, 8290-8294.

(82) Zhang, Y. B.; Su, J.; Furukawa, H.; Yun, Y. F.; Gandara, F.; Duong, A.; Zou, X. D.; Yaghi, O. M. Single-Crystal Structure of a Covalent Organic Framework. *Journal of the American Chemical Society* **2013**, *135*, 16336-16339.

(83) Kong, X. Q.; Deng, H. X.; Yan, F. Y.; Kim, J.; Swisher, J. A.; Smit, B.; Yaghi, O. M.; Reimer, J. A. Mapping of Functional Groups in Metal-Organic Frameworks. *Science* **2013**, *341*, 882-885.

(84) Wu, H.; Chua, Y. S.; Krungleviciute, V.; Tyagi, M.; Chen, P.; Yildirim, T.; Zhou, W. Unusual and Highly Tunable Missing-Linker Defects in Zirconium Metal–Organic Framework Uio-66 and Their Important Effects on Gas Adsorption. *Journal of the American Chemical Society* **2013**, *135*, 10525-10532.

(85) Vermoortele, F.; Bueken, B.; Le Bars, G.; Van de Voorde, B.; Vandichel, M.; Houthoofd, K.; Vimont, A.; Daturi, M.; Waroquier, M.; Van Speybroeck, V.; Kirschhock, C.; De Vos, D. E. Synthesis Modulation as a Tool to Increase the Catalytic Activity of Metal-Organic Frameworks: The Unique Case of Uio-66(Zr). *Journal of the American Chemical Society* **2013**, *135*, 11465-11468.

(86) Horcajada, P.; Gref, R.; Baati, T.; Allan, P. K.; Maurin, G.; Couvreur, P.; Férey, G.; Morris, R. E.; Serre, C. Metal–Organic Frameworks in Biomedicine. *Chemical Reviews* **2011**, *112*, 1232-1268.

(87) Zhou, H. C.; Kitagawa, S. Metal-Organic Frameworks (Mofs). *Chemical Society Reviews* **2014**, *43*, 5415-5418.

(88) Evans, J. D.; Sumby, C. J.; Doonan, C. J. Post-Synthetic Metalation of Metal-Organic Frameworks. *Chemical Society Reviews* **2014**, *43*, 5933-5951.

(89) Zhou, H.-C.; Long, J. R.; Yaghi, O. M. Introduction to Metal–Organic Frameworks. *Chemical Reviews* **2012**, *112*, 673-674.

(90) Stock, N.; Biswas, S. Synthesis of Metal-Organic Frameworks (Mofs): Routes to Various Mof Topologies, Morphologies, and Composites. *Chemical Reviews* **2011**, *112*, 933-969.

(91) Lu, W.; Wei, Z.; Gu, Z.-Y.; Liu, T.-F.; Park, J.; Park, J.; Tian, J.; Zhang, M.; Zhang, Q.; Gentle Iii, T.; Bosch, M.; Zhou, H.-C. Tuning the Structure and Function of Metal-Organic Frameworks Via Linker Design. *Chemical Society Reviews* **2014**, *43*, 5561-5593.

(92) Dan-Hardi, M.; Serre, C.; Frot, T.; Rozes, L.; Maurin, G.; Sanchez, C.; Férey, G. A New Photoactive Crystalline Highly Porous Titanium(Iv) Dicarboxylate. *Journal of the American Chemical Society* **2009**, *131*, 10857-10859.

(93) Hendon, C. H.; Tiana, D.; Fontecave, M.; Sanchez, C.; D'Arras, L.; Sassoye, C.; Rozes, L.; Mellot-Draznieks, C.; Walsh, A. Engineering the Optical Response of the Titanium-Mil-125 Metal-Organic Framework through Ligand Functionalization. *J Am Chem Soc* **2013**, *135*, 10942-10945.

(94) Horiuchi, Y.; Toyao, T.; Saito, M.; Mochizuki, K.; Iwata, M.; Higashimura, H.; Anpo, M.; Matsuoka, M. Visible-Light-Promoted Photocatalytic Hydrogen Production by Using an Amino-Functionalized Ti(Iv) Metal–Organic Framework. *The Journal of Physical Chemistry C* **2012**, *116*, 20848-20853.

(95) Fu, Y.; Sun, D.; Chen, Y.; Huang, R.; Ding, Z.; Fu, X.; Li, Z. An Amine-Functionalized Titanium Metal-Organic Framework Photocatalyst with Visible-Light-Induced Activity for Co2 Reduction. *Angew Chem Int Ed Engl* **2012**, *51*, 3364-3367.

(96) Rozes, L.; Sanchez, C. Titanium Oxo-Clusters: Precursors for a Lego-Like Construction of Nanostructured Hybrid Materials. *Chemical Society Reviews* **2011**, *40*, 1006-1030.

(97) Feng, D.; Wang, K.; Wei, Z.; Chen, Y.-P.; Simon, C. M.; Arvapally, R. K.; Martin, R. L.; Bosch, M.; Liu, T.-F.; Fordham, S.; Yuan, D.; Omary, M. A.; Haranczyk, M.; Smit, B.; Zhou, H.-C. Kinetically Tuned Dimensional Augmentation as a Versatile Synthetic Route Towards Robust Metal–Organic Frameworks. *Nat Commun* **2014**, *5*.

(98) Ivanchikova, I. D.; Lee, J. S.; Maksimchuk, N. V.; Shmakov, A. N.; Chesalov, Y. A.; Ayupov, A. B.; Hwang, Y. K.; Jun, C.-H.; Chang, J.-S.; Kholdeeva, O. A. Highly Selective H2o2-Based Oxidation of Alkylphenols to P-Benzoquinones over Mil-125 Metal–Organic Frameworks. *European Journal of Inorganic Chemistry* **2014**, *2014*, 132-139.

(99) Nasalevich, M. A.; Goesten, M. G.; Savenije, T. J.; Kapteijn, F.; Gascon, J. Enhancing Optical Absorption of Metal-Organic Frameworks for Improved Visible Light Photocatalysis. *Chem Commun (Camb)* **2013**, *49*, 10575-10577.

(100) Toyao, T.; Saito, M.; Horiuchi, Y.; Mochizuki, K.; Iwata, M.; Higashimura, H.; Matsuoka, M. Efficient Hydrogen Production and Photocatalytic Reduction of Nitrobenzene over a Visible-Light-Responsive Metal–Organic Framework Photocatalyst. *Catalysis Science & Technology* **2013**, *3*, 2092.

(101) Feng, D.; Jiang, H. L.; Chen, Y. P.; Gu, Z. Y.; Wei, Z.; Zhou, H. C. Metal-Organic Frameworks Based on Previously Unknown Zr8/Hf8 Cubic Clusters. *Inorg Chem* **2013**, *52*, 12661-12667.

(102) Gao, J.; Miao, J.; Li, P. Z.; Teng, W. Y.; Yang, L.; Zhao, Y.; Liu, B.; Zhang, Q. A P-Type Ti(Iv)-Based Metal-Organic Framework with Visible-Light Photo-Response. *Chem Commun (Camb)* **2014**, *50*, 3786-3788.

(103) DeCoste, J. B.; Peterson, G. W.; Jasuja, H.; Glover, T. G.; Huang, Y.-g.; Walton, K. S. Stability and Degradation Mechanisms of Metal-Organic Frameworks Containing the Zr6o4(Oh)4 Secondary Building Unit. *Journal of Materials Chemistry A* **2013**, *1*, 5642-5650.

(104) Kim, M.; Cahill, J. F.; Fei, H.; Prather, K. A.; Cohen, S. M. Postsynthetic Ligand and Cation Exchange in Robust Metal–Organic Frameworks. *Journal of the American Chemical Society* **2012**, *134*, 18082-18088.

(105) Taube, H. Rates and Mechanisms of Substitution in Inorganic Complexes in Solution. *Chemical Reviews* **1952**, *50*, 69-126.

(106) Kandiah, M.; Usseglio, S.; Svelle, S.; Olsbye, U.; Lillerud, K. P.; Tilset, M. Post-Synthetic Modification of the Metal-Organic Framework Compound Uio-66. *Journal of Materials Chemistry* **2010**, *20*, 9848-9851.

(107) Chavan, S.; Vitillo, J. G.; Gianolio, D.; Zavorotynska, O.; Civalleri, B.; Jakobsen, S.; Nilsen, M. H.; Valenzano, L.; Lamberti, C.; Lillerud, K. P.; Bordiga, S. H2storage in Isostructural Uio-67 and Uio-66 Mofs. *Physical Chemistry Chemical Physics* **2012**, *14*, 1614-1626.

(108) Huang, Y.; Qin, W.; Li, Z.; Li, Y. Enhanced Stability and Co2 Affinity of a Uio-66 Type Metal-Organic Framework Decorated with Dimethyl Groups. *Dalton Transactions* **2012**, *41*, 9283-9285.

(109) Hon Lau, C.; Babarao, R.; Hill, M. R. A Route to Drastic Increase of Co2 Uptake in Zr Metal Organic Framework Uio-66. *Chemical Communications* **2013**, *49*, 3634-3636.

(110) Smith, S. J. D.; Ladewig, B. P.; Hill, A. J.; Lau, C. H.; Hill, M. R. Post-Synthetic Ti Exchanged Uio-66 Metal-Organic Frameworks That Deliver Exceptional Gas Permeability in Mixed Matrix Membranes. *Sci. Rep.* **2015**, *5*.

(111) Vermoortele, F.; Bueken, B.; Le Bars, G.; Van de Voorde, B.; Vandichel, M.; Houthoofd, K.; Vimont, A.; Daturi, M.; Waroquier, M.; Van Speybroeck, V.; Kirschhock, C.; De Vos, D. E. Synthesis Modulation as a Tool to Increase the Catalytic Activity of Metal–Organic Frameworks: The Unique Case of Uio-66(Zr). *Journal of the American Chemical Society* **2013**, *135*, 11465-11468.

(112) Vandichel, M.; Hajek, J.; Vermoortele, F.; Waroquier, M.; De Vos, D. E.; Van Speybroeck, V. Active Site Engineering in Uio-66 Type Metal-Organic

Frameworks by Intentional Creation of Defects: A Theoretical Rationalization. *CrystEngComm* **2015**, *17*, 395-406.

(113) Shearer, G. C.; Chavan, S.; Ethiraj, J.; Vitillo, J. G.; Svelle, S.; Olsbye, U.; Lamberti, C.; Bordiga, S.; Lillerud, K. P. Tuned to Perfection: Ironing out the Defects in Metal–Organic Framework Uio-66. *Chemistry of Materials* **2014**, *26*, 4068-4071.

(114) Katz, M. J.; Brown, Z. J.; Colon, Y. J.; Siu, P. W.; Scheidt, K. A.; Snurr, R. Q.; Hupp, J. T.; Farha, O. K. A Facile Synthesis of Uio-66, Uio-67 and Their Derivatives. *Chemical Communications* **2013**, *49*, 9449-9451.

(115) Tulig, K.; Walton, K. S. An Alternative Uio-66 Synthesis for Hcl-Sensitive Nanoparticle Encapsulation. *RSC Advances* **2014**, *4*, 51080-51083.

(116) Bueken, B.; Reinsch, H.; Reimer, N.; Stassen, I.; Vermoortele, F.; Ameloot, R.; Stock, N.; Kirschhock, C. E. A.; De Vos, D. A Zirconium Squarate Metal-Organic Framework with Modulator-Dependent Molecular Sieving Properties. *Chemical Communications* **2014**, *50*, 10055-10058.

(117) Nickerl, G.; Senkovska, I.; Kaskel, S. Tetrazine Functionalized Zirconium Mof as an Optical Sensor for Oxidizing Gases. *Chemical Communications* **2015**, *51*, 2280-2282.

(118) Øien, S.; Agostini, G.; Svelle, S.; Borfecchia, E.; Lomachenko, K. A.; Mino, L.; Gallo, E.; Bordiga, S.; Olsbye, U.; Lillerud, K. P.; Lamberti, C. Probing Reactive Platinum Sites in Uio-67 Zirconium Metal–Organic Frameworks. *Chemistry of Materials* **2015**, *27*, 1042-1056.

(119) Jeremias, F.; Lozan, V.; Henninger, S. K.; Janiak, C. Programming Mofs for Water Sorption: Amino-Functionalized Mil-125 and Uio-66 for Heat Transformation and Heat Storage Applications. *Dalton Transactions* **2013**, *42*, 15967-15973.

(120) McGuirk, C. M.; Katz, M. J.; Stern, C. L.; Sarjeant, A. A.; Hupp, J. T.; Farha, O. K.; Mirkin, C. A. Turning on Catalysis: Incorporation of a Hydrogen-Bond-Donating Squaramide Moiety into a Zr Metal–Organic Framework. *Journal of the American Chemical Society* **2015**, *137*, 919-925.

(121) Malerich, J. P.; Hagihara, K.; Rawal, V. H. Chiral Squaramide Derivatives Are Excellent Hydrogen Bond Donor Catalysts. *Journal of the American Chemical Society* **2008**, *130*, 14416-14417.

(122) Nasalevich, M. A.; Goesten, M. G.; Savenije, T. J.; Kapteijn, F.; Gascon, J. Enhancing Optical Absorption of Metal-Organic Frameworks for Improved Visible Light Photocatalysis. *Chemical Communications* **2013**, *49*, 10575-10577.

(123) Yuan, S.; Lu, W.; Chen, Y.-P.; Zhang, Q.; Liu, T.-F.; Feng, D.; Wang, X.; Qin, J.; Zhou, H.-C. Sequential Linker Installation: Precise Placement of Functional

Groups in Multivariate Metal–Organic Frameworks. *Journal of the American Chemical Society* **2015**, *137*, 3177-3180.

(124) Nasalevich, M. A.; van der Veen, M.; Kapteijn, F.; Gascon, J. Metal-Organic Frameworks as Heterogeneous Photocatalysts: Advantages and Challenges. *CrystEngComm* **2014**, *16*, 4919-4926.

(125) Liu, T.-F.; Feng, D.; Chen, Y.-P.; Zou, L.; Bosch, M.; Yuan, S.; Wei, Z.; Fordham, S.; Wang, K.; Zhou, H.-C. Topology-Guided Design and Syntheses of Highly Stable Mesoporous Porphyrinic Zirconium Metal–Organic Frameworks with High Surface Area. *Journal of the American Chemical Society* **2015**, *137*, 413-419.

(126) Lin, Q.; Bu, X.; Kong, A.; Mao, C.; Zhao, X.; Bu, F.; Feng, P. New Heterometallic Zirconium Metalloporphyrin Frameworks and Their Heteroatom-Activated High-Surface-Area Carbon Derivatives. *Journal of the American Chemical Society* **2015**.

(127) Feng, D.; Chung, W. C.; Wei, Z.; Gu, Z. Y.; Jiang, H. L.; Chen, Y. P.; Darensbourg, D. J.; Zhou, H. C. Construction of Ultrastable Porphyrin Zr Metal-Organic Frameworks through Linker Elimination. *J Am Chem Soc* **2013**, *135*, 17105-17110.

(128) Morris, W.; Volosskiy, B.; Demir, S.; Gándara, F.; McGrier, P. L.; Furukawa, H.; Cascio, D.; Stoddart, J. F.; Yaghi, O. M. Synthesis, Structure, and Metalation of Two New Highly Porous Zirconium Metal–Organic Frameworks. *Inorganic Chemistry* **2012**, *51*, 6443-6445.

(129) Mondloch, J. E.; Bury, W.; Fairen-Jimenez, D.; Kwon, S.; DeMarco, E. J.; Weston, M. H.; Sarjeant, A. A.; Nguyen, S. T.; Stair, P. C.; Snurr, R. Q.; Farha, O. K.; Hupp, J. T. Vapor-Phase Metalation by Atomic Layer Deposition in a Metal–Organic Framework. *Journal of the American Chemical Society* **2013**, *135*, 10294-10297.

(130) Deria, P.; Bury, W.; Hupp, J. T.; Farha, O. K. Versatile Functionalization of the Nu-1000 Platform by Solvent-Assisted Ligand Incorporation. *Chemical Communications* **2014**, *50*, 1965-1968.

(131) Deria, P.; Bury, W.; Hod, I.; Kung, C.-W.; Karagiaridi, O.; Hupp, J. T.; Farha, O. K. Mof Functionalization Via Solvent-Assisted Ligand Incorporation: Phosphonates Vs Carboxylates. *Inorganic Chemistry* **2015**.

(132) Gagnon, K. J.; Perry, H. P.; Clearfield, A. Conventional and Unconventional Metal–Organic Frameworks Based on Phosphonate Ligands: Mofs and Umofs. *Chemical Reviews* **2011**, *112*, 1034-1054.

(133) Panella, B.; Hirscher, M.; Roth, S. Hydrogen Adsorption in Different Carbon Nanostructures. *Carbon* **2005**, *43*, 2209-2214.

(134) Yang, S. J.; Im, J. H.; Nishihara, H.; Jung, H.; Lee, K.; Kyotani, T.; Park, C. R. General Relationship between Hydrogen Adsorption Capacities at 77 and 298 K

and Pore Characteristics of the Porous Adsorbents. *The Journal of Physical Chemistry C* **2012**, *116*, 10529-10540.

(135) Kaneko, K.; Ishii, C.; Ruike, M.; Kuwabara, H. Origin of Superhigh Surface-Area and Microcrystalline Graphitic Structures of Activated Carbons. *Carbon* **1992**, *30*, 1075-1088.

(136) Gómez-Gualdrón, D. A.; Moghadam, P. Z.; Hupp, J. T.; Farha, O. K.; Snurr, R. Q. Application of Consistency Criteria to Calculate Bet Areas of Micro- and Mesoporous Metal–Organic Frameworks. *Journal of the American Chemical Society* **2015**.

(137) Wang, T. C.; Bury, W.; Gómez-Gualdrón, D. A.; Vermeulen, N. A.; Mondloch, J. E.; Deria, P.; Zhang, K.; Moghadam, P. Z.; Sarjeant, A. A.; Snurr, R. Q.; Stoddart, J. F.; Hupp, J. T.; Farha, O. K. Ultrahigh Surface Area Zirconium Mofs and Insights into the Applicability of the Bet Theory. *Journal of the American Chemical Society* **2015**, *137*, 3585-3591.

(138) Demirocak, D. E.; Srinivasan, S. S.; Ram, M. K.; Goswami, D. Y.; Stefanakos, E. K. Volumetric Hydrogen Sorption Measurements - Uncertainty Error Analysis and the Importance of Thermal Equilibration Time. *International Journal of Hydrogen Energy* **2013**, *38*, 1469-1477.

(139) Duren, T.; Millange, F.; Ferey, G.; Walton, K. S.; Snurr, R. Q. Calculating Geometric Surface Areas as a Characterization Tool for Metal-Organic Frameworks. *Journal of Physical Chemistry C* **2007**, *111*, 15350-15356.

(140) Sevilla, M.; Mokaya, R. Energy Storage Applications of Activated Carbons: Supercapacitors and Hydrogen Storage. *Energy and Environmental Science* **2014**, *7*, 1250-1280.

(141) Feng, B.; Bhatia, S. K. Variation of the Pore Structure of Coal Chars During Gasification. *Carbon* **2003**, *41*, 507-523.

(142) Osswald, S.; Portet, C.; Gogotsi, Y.; Laudisio, G.; Singer, J. P.; Fischer, J. E.; Sokolov, V. V.; Kukushkina, J. A.; Kravchik, A. E. Porosity Control in Nanoporous Carbide-Derived Carbon by Oxidation in Air and Carbon Dioxide. *Journal of Solid State Chemistry* **2009**, *182*, 1733-1741.

(143) Cabria, I.; Lopez, M. J.; Alonso, J. A. The Optimum Average Nanopore Size for Hydrogen Storage in Carbon Nanoporous Materials. *Carbon* **2007**, *45*, 2649-2658.

(144) Sevilla, M.; Valle-Vigon, P.; Fuertes, A. B. N-Doped Polypyrrole-Based Porous Carbons for Co2 Capture. *Advanced Functional Materials* **2011**, *21*, 2781-2787.

(145) Wang, H. L.; Gao, Q. M.; Hu, J. High Hydrogen Storage Capacity of Porous Carbons Prepared by Using Activated Carbon. *Journal of the American Chemical Society* **2009**, *131*, 7016-7022.

(146) Yang, S. J.; Jung, H.; Kim, T.; Park, C. R. Recent Advances in Hydrogen Storage Technologies Based on Nanoporous Carbon Materials. *Progress in Natural Science: Materials International* **2012**, *22*, 631-638.

(147) Liu, Y.; Xue, J. S.; Zheng, T.; Dahn, J. R. Mechanism of Lithium Insertion in Hard Carbons Prepared by Pyrolysis of Epoxy Resins. *Carbon* **1996**, *34*, 193-200.

(148) Subramanian, V.; Luo, C.; Stephan, A. M.; Nahm, K. S.; Thomas, S.; Wei, B. Supercapacitors from Activated Carbon Derived from Banana Fibers. *The Journal of Physical Chemistry C* **2007**, *111*, 7527-7531.

(149) Qu, D. Investigation of Hydrogen Physisorption Active Sites on the Surface of Porous Carbonaceous Materials. *Chemistry – A European Journal* **2008**, *14*, 1040-1046.

(150) Molina-Sabio, M.; Rodriguez-Reinoso, F. Role of Chemical Activation in the Development of Carbon Porosity. *Colloids and Surfaces a-Physicochemical and Engineering Aspects* **2004**, *241*, 15-25.

(151) Yang, R.; Liu, G.; Li, M.; Zhang, J.; Hao, X. Preparation and N 2, Co 2 and H 2 Adsorption of Super Activated Carbon Derived from Biomass Source Hemp (Cannabis Sativa L.) Stem. *Microporous and Mesoporous Materials* **2012**, *158*, 108-116.

(152) Wang, J.; Senkovska, I.; Kaskel, S.; Liu, Q. Chemically Activated Fungi-Based Porous Carbons for Hydrogen Storage. *Carbon* **2014**, *75*, 372-380.

(153) Wróbel-Iwaniec, I.; Díez, N.; Gryglewicz, G. Chitosan-Based Highly Activated Carbons For hydrogen Storage. *International Journal of Hydrogen Energy* **2015**, *40*, 5788-5796.

(154) Cai, J.; Qi, J.; Yang, C.; Zhao, X. Poly(Vinylidene Chloride)-Based Carbon with Ultrahigh Microporosity and Outstanding Performance for Ch4 and H2 Storage and Co2 Capture. *ACS Applied Materials & Interfaces* **2014**, *6*, 3703-3711.

(155) Mercier, G.; Klechikov, A.; Hedenström, M.; Johnels, D.; Baburin, I. A.; Seifert, G.; Mysyk, R.; Talyzin, A. V. Porous Graphene Oxide/Diboronic Acid Materials: Structure and Hydrogen Sorption. *The Journal of Physical Chemistry C* **2015**.

(156) Krishnan, D.; Kim, F.; Luo, J.; Cruz-Silva, R.; Cote, L. J.; Jang, H. D.; Huang, J. Energetic Graphene Oxide: Challenges and Opportunities. *Nano Today* **2012**, *7*, 137-152.

(157) Aboutalebi, S. H.; Aminorroaya-Yamini, S.; Nevirkovets, I.; Konstantinov, K.; Liu, H. K. Enhanced Hydrogen Storage in Graphene Oxide-Mwcnts Composite at Room Temperature. *Advanced Energy Materials* **2012**, *2*, 1439-1446.

(158) Srinivas, G.; Zhu, Y. W.; Piner, R.; Skipper, N.; Ellerby, M.; Ruoff, R. Synthesis of Graphene-Like Nanosheets and Their Hydrogen Adsorption Capacity. *Carbon* **2010**, *48*, 630-635.

(159) Gadipelli, S.; Guo, Z. X. Graphene-Based Materials: Synthesis and Gas Sorption, Storage and Separation. *Progress in Materials Science* **2015**, *69*, 1-60.

(160) Klechikov, A.; Mercier, G.; Sharifi, T.; Baburin, I. A.; Seifert, G.; Talyzin, A. V. Hydrogen Storage in High Surface Area Graphene Scaffolds. *Chemical Communications* **2015**, *51*, 15280-15283.

(161) Yang, S. J.; Kim, T.; Im, J. H.; Kim, Y. S.; Lee, K.; Jung, H.; Park, C. R. Mof-Derived Hierarchically Porous Carbon with Exceptional Porosity and Hydrogen Storage Capacity. *Chemistry of Materials* **2012**, *24*, 464-470.

(162) Segakweng, T.; Musyoka, N.; Ren, J.; Crouse, P.; Langmi, H. Comparison of Mof-5- and Cr-Mof-Derived Carbons for Hydrogen Storage Application. *Research on Chemical Intermediates* **2015**, 1-11.

(163) Kim, T. K.; Lee, K. J.; Cheon, J. Y.; Lee, J. H.; Joo, S. H.; Moon, H. R. Nanoporous Metal Oxides with Tunable and Nanocrystalline Frameworks Via Conversion of Metal–Organic Frameworks. *Journal of the American Chemical Society* **2013**, *135*, 8940-8946.

(164) Wang, W. Q.; Yuan, D. Q. Mesoporous Carbon Originated from Non-Permanent Porous Mofs for Gas Storage and Co2/Ch4 Separation. *Scientific Reports* **2014**, *4*.

(165) Hu, M.; Reboul, J.; Furukawa, S.; Torad, N. L.; Ji, Q.; Srinivasu, P.; Ariga, K.; Kitagawa, S.; Yamauchi, Y. Direct Carbonization of Al-Based Porous Coordination Polymer for Synthesis of Nanoporous Carbon. *Journal of the American Chemical Society* **2012**, *134*, 2864-2867.

(166) Xia, W.; Qiu, B.; Xia, D.; Zou, R. Facile Preparation of Hierarchically Porous Carbons from Metal-Organic Gels and Their Application in Energy Storage. *Scientific Reports* **2013**, *3*, 1935.

(167) Kongpatpanich, K.; Horike, S.; Fujiwara, Y.; Ogiwara, N.; Nishihara, H.; Kitagawa, S. Formation of Foam-Like Microstructural Carbon Material by Carbonization of Porous Coordination Polymers through a Ligand-Assisted Foaming Process. *Chemistry-a European Journal* **2015**, *21*, 13278-13283.

(168) Yang, S. J.; Kim, T.; Lee, K.; Kim, Y. S.; Yoon, J.; Park, C. R. Solvent Evaporation Mediated Preparation of Hierarchically Porous Metal Organic Framework-Derived Carbon with Controllable and Accessible Large-Scale Porosity. *Carbon* **2014**, *71*, 294-302.

(169) Jayaramulu, K.; Datta, K. K. R.; Shiva, K.; Bhattacharyya, A. J.; Eswaramoorthy, M.; Maji, T. K. Controlled Synthesis of Tunable Nanoporous Carbons

for Gas Storage and Supercapacitor Application. *Microporous and Mesoporous Materials* **2015**, *206*, 127-135.

(170) Aijaz, A.; Sun, J.-K.; Pachfule, P.; Uchida, T.; Xu, Q. From a Metal-Organic Framework to Hierarchical High Surface-Area Hollow Octahedral Carbon Cages. *Chemical Communications* **2015**, *51*, 13945-13948.

(171) Kubas, G. J. Metal-Dihydrogen and Sigma-Bond Coordination: The Consummate Extension of the Dewar-Chatt-Duncanson Model for Metal-Olefin Bonding. *Journal of Organometallic Chemistry* **2001**, *635*, 37-68.

(172) Liu, Y. R.; Li, D.; Lin, B. P.; Sun, Y.; Zhang, X. Q.; Yang, H. Hydrothermal Synthesis of Ni-Doped Hierarchically Porous Carbon Monoliths for Hydrogen Storage. *Journal of Porous Materials* **2015**, *22*, 1417-1422.

(173) Parambhath, V. B.; Nagar, R.; Sethupathi, K.; Ramaprabhu, S. Investigation of Spillover Mechanism in Palladium Decorated Hydrogen Exfoliated Functionalized Graphene. *Journal of Physical Chemistry C* **2011**, *115*, 15679-15685.

(174) Aiyappa, H. B.; Pachfule, P.; Banerjee, R.; Kurungot, S. Porous Carbons from Nonporous Mofs: Influence of Ligand Characteristics on Intrinsic Properties of End Carbon. *Crystal Growth & Design* **2013**, *13*, 4195-4199.

(175) Vinayan, B. P.; Sethupathi, K.; Ramaprabhu, S. Facile Synthesis of Triangular Shaped Palladium Nanoparticles Decorated Nitrogen Doped Graphene and Their Catalytic Study for Renewable Energy Applications. *International Journal of Hydrogen Energy* **2013**, *38*, 2240-2250.

(176) Wang, Y.; Liu, J.; Wang, K.; Chen, T.; Tan, X.; Li, C. M. Hydrogen Storage in Ni–B Nanoalloy-Doped 2d Graphene. *International Journal of Hydrogen Energy* **2011**, *36*, 12950-12954.

(177) Wang, Y.; Guo, C. X.; Wang, X.; Guan, C.; Yang, H.; Wang, K.; Li, C. M. Hydrogen Storage in a Ni-B Nanoalloy-Doped Three-Dimensional Graphene Material. *Energy & Environmental Science* **2011**, *4*, 195-200.

(178) Psofogiannakis, G. M.; Steriotis, T. A.; Bourlinos, A. B.; Kouvelos, E. P.; Charalambopoulou, G. C.; Stubos, A. K.; Froudakis, G. E. Enhanced Hydrogen Storage by Spillover on Metal-Doped Carbon Foam: An Experimental and Computational Study. *Nanoscale* **2011**, *3*, 933-936.

(179) Nishihara, H.; Hou, P.-X.; Li, L.-X.; Ito, M.; Uchiyama, M.; Kaburagi, T.; Ikura, A.; Katamura, J.; Kawarada, T.; Mizuuchi, K.; Kyotani, T. High-Pressure Hydrogen Storage in Zeolite-Templated Carbon. *The Journal of Physical Chemistry C* **2009**, *113*, 3189-3196.

(180) Yang, Z. X.; Xia, Y. D.; Mokaya, R. Enhanced Hydrogen Storage Capacity of High Surface Area Zeolite-Like Carbon Materials. *Journal of the American Chemical Society* **2007**, *129*, 1673-1679.

(181) Musyoka, N.; Ren, J.; Annamalai, P.; Langmi, H.; North, B.; Mathe, M.; Bessarabov, D. Synthesis of a Hybrid Mil-101(Cr)/Ztc Composite for Hydrogen Storage Applications. *Research on Chemical Intermediates* **2015**, 1-9.

(182) Masika, E.; Bourne, R. A.; Chamberlain, T. W.; Mokaya, R. Supercritical Co2 Mediated Incorporation of Pd onto Templated Carbons: A Route to Optimizing the Pd Particle Size and Hydrogen Uptake Density. *ACS Applied Materials & Interfaces* **2013**, *5*, 5639-5647.

(183) Nishihara, H.; Ittisanronnachai, S.; Itoi, H.; Li, L.-X.; Suzuki, K.; Nagashima, U.; Ogawa, H.; Kyotani, T.; Ito, M. Experimental and Theoretical Studies of Hydrogen/Deuterium Spillover on Pt-Loaded Zeolite-Templated Carbon. *The Journal of Physical Chemistry C* **2014**, *118*, 9551-9559.

(184) Zhou, Q.; Wang, C.; Fu, Z.; Yuan, L.; Yang, X.; Tang, Y.; Zhang, H. Hydrogen Adsorption on Palladium Anchored Defected Graphene with B-Doping: A Theoretical Study. *International Journal of Hydrogen Energy* **2015**, *40*, 2473-2483.

(185) Wang, L.; Lachawiec, J. A. J.; Yang, R. T. Nanostructured Adsorbents for Hydrogen Storage at Ambient Temperature: High-Pressure Measurements and Factors Influencing Hydrogen Spillover. *RSC Advances* **2013**, *3*, 23935-23952.

(186) Shi, J.; Li, W.; Li, D. Synthesis, Nickel Decoration, and Hydrogen Adsorption of Silica-Templated Mesoporous Carbon Material with High Surface Area. *The Journal of Physical Chemistry C* **2015**, *119*, 23430-23435.

(187) Yushin, G.; Dash, R.; Jagiello, J.; Fischer, J. E.; Gogotsi, Y. Carbide-Derived Carbons: Effect of Pore Size on Hydrogen Uptake and Heat of Adsorption. *Advanced Functional Materials* **2006**, *16*, 2288-2293.

(188) Gogotsi, Y.; Dash, R. K.; Yushin, G.; Yildirim, T.; Laudisio, G.; Fischer, J. E. Tailoring of Nanoscale Porosity in Carbide-Derived Carbons for Hydrogen Storage. *Journal of the American Chemical Society* **2005**, *127*, 16006-16007.

(189) Kim, H. S.; Singer, J. P.; Gogotsi, Y.; Fischer, J. E. Molybdenum Carbide-Derived Carbon for Hydrogen Storage. *Microporous and Mesoporous Materials* **2009**, *120*, 267-271.

(190) Yeon, S.-H.; Knoke, I.; Gogotsi, Y.; Fischer, J. E. Enhanced Volumetric Hydrogen and Methane Storage Capacity of Monolithic Carbide-Derived Carbon. *Microporous and Mesoporous Materials* **2010**, *131*, 423-428.

(191) Sevilla, M.; Foulston, R.; Mokaya, R. Superactivated Carbide-Derived Carbons with High Hydrogen Storage Capacity. *Energy & Environmental Science* **2010**, *3*, 223-227.

(192) Yuan, D.; Lu, W.; Zhao, D.; Zhou, H.-C. Highly Stable Porous Polymer Networks with Exceptionally High Gas-Uptake Capacities. *Advanced Materials* **2011**, *23*, 3723-3725.

(193) Ben, T.; Ren, H.; Ma, S.; Cao, D.; Lan, J.; Jing, X.; Wang, W.; Xu, J.; Deng, F.; Simmons, J. M.; Qiu, S.; Zhu, G. Targeted Synthesis of a Porous Aromatic Framework with High Stability and Exceptionally High Surface Area. *Angewandte Chemie International Edition* **2009**, *48*, 9457-9460.

(194) Sun, L. B.; Li, A. G.; Liu, X. D.; Liu, X. Q.; Feng, D. W.; Lu, W. G.; Yuan, D. Q.; Zhou, H. C. Facile Fabrication of Cost-Effective Porous Polymer Networks for Highly Selective Co2 Capture. *Journal of Materials Chemistry A* **2015**, *3*, 3252-3256.

(195) Wu, S.; Liu, Y.; Yu, G.; Guan, J.; Pan, C.; Du, Y.; Xiong, X.; Wang, Z. Facile Preparation of Dibenzoheterocycle-Functional Nanoporous Polymeric Networks with High Gas Uptake Capacities. *Macromolecules* **2014**, *47*, 2875-2882.

(196) Xiang, Z.; Mercado, R.; Huck, J. M.; Wang, H.; Guo, Z.; Wang, W.; Cao, D.; Haranczyk, M.; Smit, B. Systematic Tuning and Multifunctionalization of Covalent Organic Polymers for Enhanced Carbon Capture. *Journal of the American Chemical Society* **2015**, *137*, 13301-13307.

(197) Lu, W. G.; Wei, Z. W.; Yuan, D. Q.; Tian, J.; Fordham, S.; Zhou, H. C. Rational Design and Synthesis of Porous Polymer Networks: Toward High Surface Area. *Chemistry of Materials* **2014**, *26*, 4589-4597.

(198) Li, Y.; Ben, T.; Zhang, B.; Fu, Y.; Qiu, S. Ultrahigh Gas Storage Both at Low and High Pressures in Koh-Activated Carbonized Porous Aromatic Frameworks. *Scientific Reports* **2013**, *3*, 2420.

(199) Eddaoudi, M.; Kim, J.; Rosi, N.; Vodak, D.; Wachter, J.; O'Keeffe, M.; Yaghi, O. Systematic Design of Pore Size and Functionality in Isoreticular Mofs and Their Application in Methane Storage. *Science* **2002**, *295*, 469-472.

(200) Furukawa, H.; Cordova, K. E.; O'Keeffe, M.; Yaghi, O. M. The Chemistry and Applications of Metal-Organic Frameworks. *Science* **2013**, *341*.

(201) Serre, C.; Millange, F.; Surblé, S.; Férey, G. A Route to the Synthesis of Trivalent Transition-Metal Porous Carboxylates with Trimeric Secondary Building Units. *Angewandte Chemie International Edition* **2004**, *43*, 6285-6289.

(202) Tanabe, K. K.; Cohen, S. M. Postsynthetic Modification of Metal-Organic Frameworks-a Progress Report. *Chemical Society Reviews* **2011**, *40*, 498-519.

(203) Feng, D. W.; Wang, K. C.; Wei, Z. W.; Chen, Y. P.; Simon, C. M.; Arvapally, R. K.; Martin, R. L.; Bosch, M.; Liu, T. F.; Fordham, S.; Yuan, D. Q.; Omary, M. A.; Haranczyk, M.; Smit, B.; Zhou, H. C. Kinetically Tuned Dimensional Augmentation as a Versatile Synthetic Route Towards Robust Metal-Organic Frameworks. *Nature Communications* **2014**, *5*, 5723.

(204) Férey, G. Building Units Design and Scale Chemistry. *Journal of Solid State Chemistry* **2000**, *152*, 37-48.

(205) Yuan, S.; Liu, T.; Feng, D.; Tian, J.; Wang, K.; Qin, J.; Zhang, Q.; Chen, Y.; Bosch, M.; Zou, L.; Teat, S.; Dalgarno, S.; Zhou, H. A Single Crystalline Porphyrinic Titanium Metal-Organic Framework. *Chemical Science* **2015**, *6*, 3926-3930.

(206) Bosch, M.; Sun, X.; Yuan, S.; Chen, Y.-P.; Wang, Q.; Wang, X.; Zhou, H.-C. Modulated Synthesis of Metal-Organic Frameworks through Tuning of the Initial Oxidation State of the Metal. *European Journal of Inorganic Chemistry* **2016**, 4368–4372.

(207) Shearer, G. C.; Chavan, S.; Bordiga, S.; Svelle, S.; Olsbye, U.; Lillerud, K. P. Defect Engineering: Tuning the Porosity and Composition of the Metal–Organic Framework Uio-66 Via Modulated Synthesis. *Chemistry of Materials* **2016**, *28*, 3749-3761.

(208) Bosch, M.; Zhang, M.; Feng, D.; Yuan, S.; Wang, X.; Chen, Y.-P.; Zhou, H.-C. Lithium Inclusion in Indium Metal-Organic Frameworks Showing Increased Surface Area and Hydrogen Adsorption. *APL Mater.* **2014**, *2*, 124103.

(209) Brozek, C. K.; Dinca, M. Ti3+-, V2+/3+-, Cr2+/3+-, Mn2+-, and Fe2+-Substituted Mof-5 and Redox Reactivity in Cr- and Fe-Mof-5. *Journal of the American Chemical Society* **2013**, *135*, 12886-12891.

(210) Zou, L.; Feng, D.; Liu, T.-F.; Chen, Y.-P.; Yuan, S.; Wang, K.; Wang, X.; Fordham, S.; Zhou, H.-C. A Versatile Synthetic Route for the Preparation of Titanium Metal-Organic Frameworks. *Chemical Science* **2016**, *7*, 1063-1069.

(211) Feng, D. W.; Liu, T. F.; Su, J.; Bosch, M.; Wei, Z. W.; Wan, W.; Yuan, D. Q.; Chen, Y. P.; Wang, X.; Wang, K. C.; Lian, X. Z.; Gu, Z. Y.; Park, J.; Zou, X. D.; Zhou, H. C. Stable Metal-Organic Frameworks Containing Single-Molecule Traps for Enzyme Encapsulation. *Nature Communications* **2015**, *6*, 5979.

(212) Lammert, M.; Bernt, S.; Vermoortele, F.; De Vos, D. E.; Stock, N. Single- and Mixed-Linker Cr-Mil-101 Derivatives: A High-Throughput Investigation. *Inorganic Chemistry* **2013**, *52*, 8521-8528.

(213) Park, J.; Feng, D.; Zhou, H.-C. Structure-Assisted Functional Anchor Implantation in Robust Metal–Organic Frameworks with Ultralarge Pores. *Journal of the American Chemical Society* **2015**, *137*, 1663-1672.

(214) Deng, H. X.; Doonan, C. J.; Furukawa, H.; Ferreira, R. B.; Towne, J.; Knobler, C. B.; Wang, B.; Yaghi, O. M. Multiple Functional Groups of Varying Ratios in Metal-Organic Frameworks. *Science* **2010**, *327*, 846-850.

(215) Fracaroli, A. M.; Siman, P.; Nagib, D. A.; Suzuki, M.; Furukawa, H.; Toste, F. D.; Yaghi, O. M. Seven Post-Synthetic Covalent Reactions in Tandem Leading to Enzyme-Like Complexity within Metal-Organic Framework Crystals. *Journal of the American Chemical Society* **2016**, *138*, 8352-8355.

(216) Lalonde, M. B.; Mondloch, J. E.; Deria, P.; Sarjeant, A. A.; Al-Juaid, S. S.; Osman, O. I.; Farha, O. K.; Hupp, J. T. Selective Solvent-Assisted Linker Exchange (Sale) in a Series of Zeolitic Imidazolate Frameworks. *Inorganic Chemistry* **2015**, *54*, 7142-7144.

(217) Deria, P.; Mondloch, J. E.; Karagiaridi, O.; Bury, W.; Hupp, J. T.; Farha, O. K. Beyond Post-Synthesis Modification: Evolution of Metal-Organic Frameworks Via Building Block Replacement. *Chemical Society Reviews* **2014**, *43*, 5896-5912.

(218) Yuan, S.; Lu, W. G.; Chen, Y. P.; Zhang, Q.; Liu, T. F.; Feng, D. W.; Wang, X.; Qin, J. S.; Zhou, H. C. Sequential Linker Installation: Precise Placement of Functional Groups in Multivariate Metal-Organic Frameworks. *Journal of the American Chemical Society* **2015**, *137*, 3177-3180.

(219) Yuan, S.; Zou, L.; Li, H.; Chen, Y.-P.; Qin, J.; Zhang, Q.; Lu, W.; Hall, M. B.; Zhou, H.-C. Flexible Zirconium Metal-Organic Frameworks as Bioinspired Switchable Catalysts. *Angewandte Chemie* **2016**, *128*, 10934-10938.

(220) Yuan, S.; Chen, Y.-P.; Qin, J.-S.; Lu, W.; Zou, L.; Zhang, Q.; Wang, X.; Sun, X.; Zhou, H.-C. Linker Installation: Engineering Pore Environment with Precisely Placed Functionalities in Zirconium Mofs. *Journal of the American Chemical Society* **2016**, 8912.

(221) Yuan, S.; Chen, Y. P.; Qin, J. S.; Lu, W. G.; Wang, X.; Zhang, Q.; Bosch, M.; Liu, T. F.; Lian, X. Z.; Zhou, H. C. Cooperative Cluster Metalation and Ligand Migration in Zirconium Metal-Organic Frameworks. *Angewandte Chemie-International Edition* **2015**, *54*, 14696-14700.

(222) Lee, S.; Kapustin, E. A.; Yaghi, O. M. Coordinative Alignment of Molecules in Chiral Metal-Organic Frameworks. *Science* **2016**, *353*, 808-811.

(223) Inokuma, Y.; Yoshioka, S.; Ariyoshi, J.; Arai, T.; Hitora, Y.; Takada, K.; Matsunaga, S.; Rissanen, K.; Fujita, M. X-Ray Analysis on the Nanogram to Microgram Scale Using Porous Complexes. *Nature* **2013**, *495*, 461-466.

(224) Long, J. R.; Yaghi, O. M. The Pervasive Chemistry of Metal-Organic Frameworks. *Chemical Society Reviews* **2009**, *38*, 1213-1214.

(225) Zhang, M. W.; Chen, Y. P.; Bosch, M.; Gentle, T.; Wang, K. C.; Feng, D. W.; Wang, Z. Y. U.; Zhou, H. C. Symmetry-Guided Synthesis of Highly Porous Metal-Organic Frameworks with Fluorite Topology. *Angewandte Chemie-International Edition* **2014**, *53*, 815-818.

(226) Peng, Y.; Krungleviciute, V.; Eryazici, I.; Hupp, J. T.; Farha, O. K.; Yildirim, T. Methane Storage in Metal–Organic Frameworks: Current Records, Surprise Findings, and Challenges. *Journal of the American Chemical Society* **2013**, *135*, 11887-11894.

(227) Rao, D. W.; Lu, R. F.; Xiao, C. Y.; Kan, E. J.; Deng, K. M. Lithium-Doped Mof Impregnated with Lithium-Coated Fullerenes: A Hydrogen Storage Route for High Gravimetric and Volumetric Uptakes at Ambient Temperatures. *Chemical Communications* **2011**, *47*, 7698-7700.

(228) Zhao, X.; Bu, X.; Wu, T.; Zheng, S.-T.; Wang, L.; Feng, P. Selective Anion Exchange with Nanogated Isoreticular Positive Metal-Organic Frameworks. *Nat Commun* **2013**, *4*.

(229) Xu, Q.; Liu, D. H.; Yang, Q. Y.; Zhong, C. L.; Mi, J. G. Li-Modified Metal-Organic Frameworks for Co2/Ch4 Separation: A Route to Achieving High Adsorption Selectivity. *Journal of Materials Chemistry* **2010**, *20*, 706-714.

(230) Huang, Y.; Lin, Z.; Fu, H.; Wang, F.; Shen, M.; Wang, X.; Cao, R. Porous Anionic Indium–Organic Framework with Enhanced Gas and Vapor Adsorption and Separation Ability. *ChemSusChem* **2014**, n/a-n/a.

(231) Bu, F.; Xiao, S. J. A 4-Connected Anionic Metal-Organic Nanotube Constructed from Indium Isophthalate. *Crystengcomm* **2010**, *12*, 3385-3387.

(232) Huh, S.; Kwon, T. H.; Park, N.; Kim, S. J.; Kim, Y. Nanoporous in-Mof with Multiple One-Dimensional Pores. *Chemical Communications* **2009**, 4953-4955.

(233) Kahrovic, E.; Orioli, P.; Bruni, B.; Di Vaira, M.; Messori, L. Crystallographic Evidence for Decomposition of Dimethylformamide in the Presence of Ruthenium(Iii) Chloride. *Inorganica Chimica Acta* **2003**, *355*, 420-423.

(234) An, J. Y.; Geib, S. J.; Rosi, N. L. Cation-Triggered Drug Release from a Porous Zinc-Adeninate Metal-Organic Framework. *Journal of the American Chemical Society* **2009**, *131*, 8376-+.

(235) Zhang, M. W.; Chen, Y. P.; Zhou, H. C. Structural Design of Porous Coordination Networks from Tetrahedral Building Units. *Crystengcomm* **2013**, *15*, 9544-9552.

(236) Cullity, B. D.: *Elements of X-Ray Diffraction*; 2d ed.; Addison-Wesley Pub. Co.: Reading, Mass., 1978.

(237) Nijem, N.; Veyan, J.-F.; Kong, L.; Li, K.; Pramanik, S.; Zhao, Y.; Li, J.; Langreth, D.; Chabal, Y. J. Interaction of Molecular Hydrogen with Microporous Metal Organic Framework Materials at Room Temperature. *Journal of the American Chemical Society* **2010**, *132*, 1654-1664.

(238) Ladd, M. F. C.; Palmer, R. A.: *Structure Determination by X-Ray Crystallography*; 4th ed.; Kluwer Academic/Plenum Publishers: New York, 2003.

(239) Dolomanov, O. V.; Bourhis, L. J.; Gildea, R. J.; Howard, J. A. K.; Puschmann, H. Olex2: A Complete Structure Solution, Refinement and Analysis Program. *Journal of Applied Crystallography* **2009**, *42*, 339-341.

(240) Li, J.-R.; Kuppler, R. J.; Zhou, H.-C. Selective Gas Adsorption and Separation in Metal-Organic Frameworks. *Chemical Society Reviews* **2009**, *38*, 1477-1504.

(241) Panda, T.; Kundu, T.; Banerjee, R. Structural Isomerism Leading to Variable Proton Conductivity in Indium(Iii) Isophthalic Acid Based Frameworks. *Chemical Communications* **2013**, *49*, 6197-6199.

(242) Serre, C.; Kitagawa, S.; Dietzel, P. D. Introduction to Special Issue: Metal Organic Frameworks. *Microporous and Mesoporous Materials* **2012**, *157*, 1-2.

(243) Llewellyn, P. L.; Bourrelly, S.; Serre, C.; Vimont, A.; Daturi, M.; Hamon, L.; De Weireld, G.; Chang, J.-S.; Hong, D.-Y.; Kyu Hwang, Y.; Hwa Jhung, S.; Férey, G. High Uptakes of Co2 and Ch4 in Mesoporous Metal—Organic Frameworks Mil-100 and Mil-101. *Langmuir* **2008**, *24*, 7245-7250.

(244) Feng, D. W.; Wang, K. C.; Wei, Z. W.; Chen, Y. P.; Simon, C. M.; Arvapally, R. K.; Martin, R. L.; Bosch, M.; Liu, T. F.; Fordham, S.; Yuan, D. Q.; Omary, M. A.; Haranczyk, M.; Smit, B.; Zhou, H. C. Kinetically Tuned Dimensional Augmentation as a Versatile Synthetic Route Towards Robust Metal-Organic Frameworks. *Nature Communications* **2014**, *5*.

(245) Kiyonaga, T.; Higuchi, M.; Kajiwara, T.; Takashima, Y.; Duan, J.; Nagashima, K.; Kitagawa, S. Dependence of Crystal Size on the Catalytic Performance of a Porous Coordination Polymer. *Chemical Communications* **2015**, *51*, 2728-2730.

(246) Guasch, J.; Dietzel, P. D. C.; Collier, P.; Acerbi, N. The Effect of Solvent and Temperature in the Synthesis of Cpo-27-Ni by Reflux. *Microporous and Mesoporous Materials* **2015**, *203*, 238-244.

(247) Thomas, L.; Lionti, F.; Ballou, R.; Gatteschi, D.; Sessoli, R.; Barbara, B. Macroscopic Quantum Tunnelling of Magnetization in a Single Crystal of Nanomagnets. *Nature* **1996**, *383*, 145-147.

(248) Inokuma, Y.; Arai, T.; Fujita, M. Networked Molecular Cages as Crystalline Sponges for Fullerenes and Other Guests. *Nat Chem* **2010**, *2*, 780-783.

(249) Ren, J.; Langmi, H. W.; North, B. C.; Mathe, M.; Bessarabov, D. Modulated Synthesis of Zirconium-Metal Organic Framework (Zr-Mof) for Hydrogen Storage Applications. *International Journal of Hydrogen Energy* **2014**, *39*, 890-895.

(250) Stavitski, E.; Goesten, M.; Juan-Alcañiz, J.; Martinez-Joaristi, A.; Serra-Crespo, P.; Petukhov, A. V.; Gascon, J.; Kapteijn, F. Kinetic Control of Metal–Organic Framework Crystallization Investigated by Time-Resolved in Situ X-Ray Scattering. *Angewandte Chemie International Edition* **2011**, *50*, 9624-9628.

(251) Dietzel, P. D. C.; Blom, R.; Fjellvåg, H. Base-Induced Formation of Two Magnesium Metal-Organic Framework Compounds with a Bifunctional Tetratopic Ligand. *European Journal of Inorganic Chemistry* **2008**, *2008*, 3624-3632.

(252) Zhang, B.; Wang, Z. Microporous Thermosetting Film Constructed from Hyperbranched Polyarylate Precursors Containing Rigid Tetrahedral Core: Synthesis, Characterization, and Properties. *Chemistry of Materials* **2010**, *22*, 2780-2789.

(253) Sanz-Pérez, E. S.; Murdock, C. R.; Didas, S. A.; Jones, C. W. Direct Capture of Co2 from Ambient Air. *Chemical Reviews* **2016**, *116*, 11840-11876.

(254) Sculley, J. P.; Verdegaal, W. M.; Lu, W.; Wriedt, M.; Zhou, H.-C. High-Throughput Analytical Model to Evaluate Materials for Temperature Swing Adsorption Processes. *Advanced Materials* **2013**, *25*, 3957-3961.

(255) Potter, M. E.; Pang, S. H.; Jones, C. W. Adsorption Microcalorimetry of Co2 in Confined Aminopolymers. *Langmuir* **2017**, *33*, 117-124.

(256) Li, H.; Wang, K. C.; Feng, D. W.; Chen, Y. P.; Verdegaal, W.; Zhou, H. C. Incorporation of Alkylamine into Metal-Organic Frameworks through a Bronsted Acid-Base Reaction for Co2 Capture. *Chemsuschem* **2016**, *9*, 2832-2840.

(257) Xie, H. B.; Zhou, Y. Z.; Zhang, Y. K.; Johnson, J. K. Reaction Mechanism of Monoethanolamine with Co2 in Aqueous Solution from Molecular Modeling. *Journal of Physical Chemistry A* **2010**, *114*, 11844-11852.

(258) Lv, B. H.; Guo, B. S.; Zhou, Z. M.; Jing, G. H. Mechanisms of Co2 Capture into Monoethanolamine Solution with Different Co2 Loading During the Absorption/Desorption Processes. *Environmental Science & Technology* **2015**, *49*, 10728-10735.

(259) Yu, J.; Xie, L.-H.; Li, J.-R.; Ma, Y.; Seminario, J. M.; Balbuena, P. B. Co2 Capture and Separations Using Mofs: Computational and Experimental Studies. *Chemical Reviews* **2017**.

(260) Xu, C.; Hedin, N. Microporous Adsorbents for Co2 Capture – a Case for Microporous Polymers? *Materials Today* **2014**, *17*, 397-403.

(261) Kim, Y. K.; Hyun, S. M.; Lee, J. H.; Kim, T. K.; Moon, D.; Moon, H. R. Crystal-Size Effects on Carbon Dioxide Capture of a Covalently Alkylamine-Tethered Metal-Organic Framework Constructed by a One-Step Self-Assembly. *Scientific Reports* **2016**, *6*.

(262) Patel, H. A.; Yavuz, C. T. Highly Optimized Co2 Capture by Inexpensive Nanoporous Covalent Organic Polymers and Their Amine Composites. *Faraday Discussions* **2015**, *183*, 401-412.

(263) Gutierrez, J. P.; Ruiz, E. L. A.; Erdmann, E. Energy Requirements, Ghg Emissions and Investment Costs in Natural Gas Sweetening Processes. *Journal of Natural Gas Science and Engineering* **2017**, *38*, 187-194.

(264) Huck, J. M.; Lin, L. C.; Berger, A. H.; Shahrak, M. N.; Martin, R. L.; Bhown, A. S.; Haranczyk, M.; Reuter, K.; Smit, B. Evaluating Different Classes of

Porous Materials for Carbon Capture. *Energy & Environmental Science* **2014**, *7*, 4132-4146.

(265) Yang, D.-A.; Cho, H.-Y.; Kim, J.; Yang, S.-T.; Ahn, W.-S. Co2 Capture and Conversion Using Mg-Mof-74 Prepared by a Sonochemical Method. *Energy & Environmental Science* **2012**, *5*, 6465-6473.

(266) Yu, J.; Balbuena, P. B. Water Effects on Postcombustion Co2 Capture in Mg-Mof-74. *The Journal of Physical Chemistry C* **2013**, *117*, 3383-3388.

(267) Choi, S.; Watanabe, T.; Bae, T.-H.; Sholl, D. S.; Jones, C. W. Modification of the Mg/Dobdc Mof with Amines to Enhance Co2 Adsorption from Ultradilute Gases. *The Journal of Physical Chemistry Letters* **2012**, *3*, 1136-1141.

(268) Gadipelli, S.; Patel, H. A.; Guo, Z. An Ultrahigh Pore Volume Drives up the Amine Stability and Cyclic Co2 Capacity of a Solid-Amine@Carbon Sorbent. *Advanced Materials* **2015**, *27*, 4903-4909.

(269) DeSantis, D.; Mason, J. A.; James, B. D.; Houchins, C.; Long, J. R.; Veenstra, M. Techno-Economic Analysis of Metal-Organic Frameworks for Hydrogen and Natural Gas Storage. *Energy & Fuels* **2017**, *31*, 2024-2032.

(270) Lu, W.; Bosch, M.; Yuan, D.; Zhou, H.-C. Cost-Effective Synthesis of Amine-Tethered Porous Materials for Carbon Capture. *ChemSusChem* **2015**, *8*, 433-438.

(271) Dawson, R.; Cooper, A. I.; Adams, D. J. Chemical Functionalization Strategies for Carbon Dioxide Capture in Microporous Organic Polymers. *Polymer International* **2013**, *62*, 345-352.

(272) Marx, D.; Joss, L.; Hefti, M.; Mazzotti, M. Temperature Swing Adsorption for Postcombustion Co2 Capture: Single- and Multicolumn Experiments and Simulations. *Industrial & Engineering Chemistry Research* **2016**, *55*, 1401-1412.

(273) Tan, M. X.; Zhang, Y.; Ying, J. Y. Mesoporous Poly(Melamine–Formaldehyde) Solid Sorbent for Carbon Dioxide Capture. *ChemSusChem* **2013**, *6*, 1186-1190.

(274) Kim, Y. K.; Hyun, S.-m.; Lee, J. H.; Kim, T. K.; Moon, D.; Moon, H. R. Crystal-Size Effects on Carbon Dioxide Capture of a Covalently Alkylamine-Tethered Metal-Organic Framework Constructed by a One-Step Self-Assembly. *Scientific Reports* **2016**, *6*, 19337.

(275) Liu, F. J.; Huang, K.; Yoo, C. J.; Okonkwo, C.; Tao, D. J.; Jones, C. W.; Dai, S. Facilely Synthesized Meso-Macroporous Polymer as Support of Poly (Ethyleneimine) for Highly Efficient and Selective Capture of Co2. *Chemical Engineering Journal* **2017**, *314*, 466-476.

(276) Xie, W.; Ji, X.; Fan, T.; Feng, X.; Lu, X. Co2 Uptake Behavior of Supported Tetraethylenepentamine Sorbents. *Energy & Fuels* **2016**, *30*, 5083-5091.

(277) Tullo, A. The Shale Gale Revitalizes Us Chemical Production. Chemical & Engineering News. *91*2013.

(278) Deluchi, M. A. Greenhouse-Gas Emissions from the Use of New Fuels for Transportation and Electricity. *Transportation Research Part a-Policy and Practice* **1993**, *27*, 187-191.

(279) Burnham, A.; Han, J.; Clark, C. E.; Wang, M.; Dunn, J. B.; Palou-Rivera, I. Life-Cycle Greenhouse Gas Emissions of Shale Gas, Natural Gas, Coal, and Petroleum. *Environmental Science & Technology* **2012**, *46*, 619-627.

(280) Brandt, A. R.; Heath, G. A.; Kort, E. A.; O'Sullivan, F.; Petron, G.; Jordaan, S. M.; Tans, P.; Wilcox, J.; Gopstein, A. M.; Arent, D.; Wofsy, S.; Brown, N. J.; Bradley, R.; Stucky, G. D.; Eardley, D.; Harriss, R. Methane Leaks from North American Natural Gas Systems. *Science* **2014**, *343*, 733-735.

(281) Menon, V. C.; Komarneni, S. Porous Adsorbents for Vehicular Natural Gas Storage: A Review. *Journal of Porous Materials* **1998**, *5*, 43-58.

(282) Makal, T. A.; Li, J. R.; Lu, W. G.; Zhou, H. C. Methane Storage in Advanced Porous Materials. *Chemical Society Reviews* **2012**, *41*, 7761-7779.

(283) Natural Gas Gross Withdraws and Production. https://www.eia.gov/dnav/ng/ng_prod_sum_a_EPG0_VGV_mmcf_a.htm.

(284) Diaz-Mendez, S. E.; Hernandez-Guerrero, A.; Sciubba, E.; Chavez, R. H. Extended Exergy Accounting Applied to the Flaring Practice in Oil Fields. *International Journal of Exergy* **2012**, *10*, 442-453.

(285) Exclusive: Bakken Flaring Burns More Than $100 Million a Month http://uk.reuters.com/article/us-bakken-flaring-idUKBRE96S05320130729.

(286) Kondo, M.; Yoshitomi, T.; Seki, K.; Matsuzaka, H.; Kitagawa, S. Three-Dimensional Framework with Channeling Cavities for Small Molecules: {[M-2(4,4 '-Bpy)(3)(No3)(4)]Center Dot Xh(2)O}(N) (M = Co, Ni, Zn). *Angewandte Chemie-International Edition* **1997**, *36*, 1725-1727.

(287) Fu, J.; Tian, Y.; Wu, J. Z. Seeking Metal-Organic Frameworks for Methane Storage in Natural Gas Vehicles. *Adsorption-Journal of the International Adsorption Society* **2015**, *21*, 499-507.

(288) Celzard, A.; Fierro, V. Preparing a Suitable Material Designed for Methane Storage: A Comprehensive Report. *Energy & Fuels* **2005**, *19*, 573-583.

(289) Duren, T.; Sarkisov, L.; Yaghi, O. M.; Snurr, R. Q. Design of New Materials for Methane Storage. *Langmuir* **2004**, *20*, 2683-2689.

(290) Ma, S. Q.; Sun, D. F.; Simmons, J. M.; Collier, C. D.; Yuan, D. Q.; Zhou, H. C. Metal-Organic Framework from an Anthracene Derivative Containing Nanoscopic

Cages Exhibiting High Methane Uptake. *Journal of the American Chemical Society* **2008**, *130*, 1012-1016.

(291) Peng, Y.; Krungleviciute, V.; Eryazici, I.; Hupp, J. T.; Farha, O. K.; Yildirim, T. Methane Storage in Metal-Organic Frameworks: Current Records, Surprise Findings, and Challenges. *Journal of the American Chemical Society* **2013**, *135*, 11887-11894.

(292) Low, J. J.; Benin, A. I.; Jakubczak, P.; Abrahamian, J. F.; Faheem, S. A.; Willis, R. R. Virtual High Throughput Screening Confirmed Experimentally: Porous Coordination Polymer Hydration. *Journal of the American Chemical Society* **2009**, *131*, 15834-15842.

(293) Gandara, F.; Furukawa, H.; Lee, S.; Yaghi, O. M. High Methane Storage Capacity in Aluminum Metal-Organic Frameworks. *Journal of the American Chemical Society* **2014**, *136*, 5271-5274.

(294) Alezi, D.; Belmabkhout, Y.; Suyetin, M.; Bhatt, P. M.; Weselinski, L. J.; Solovyeva, V.; Adil, K.; Spanopoulos, I.; Trikalitis, P. N.; Emwas, A. H.; Eddaoudi, M. Mof Crystal Chemistry Paving the Way to Gas Storage Needs: Aluminum-Based Soc-Mof for Ch4, O-2, and Co2 Storage. *Journal of the American Chemical Society* **2015**, *137*, 13308-13318.

(295) Burtch, N. C.; Jasuja, H.; Walton, K. S. Water Stability and Adsorption in Metal–Organic Frameworks. *Chemical Reviews* **2014**, *114*, 10575-10612.

(296) Engshuber, M. Non-Conventional Methods of Storing Natural-Gas. *Energietechnik* **1980**, *30*, 353-358.

(297) Arthur, M. H., Jr Henry M. Nelly, and Young, Alexander Russell. Method of Storing Natural Gas 2,535,148.

(298) Xia, S. Q.; Ma, P. S.; Guo, Y. G.; Hua, C. Determination and Study of the Solubility of Methane in Mixtures of Methanol Plus Various Hydrocarbons at High Pressures. *Journal of Chemical and Engineering Data* **2006**, *51*, 1035-1038.

(299) Poirier, E.; Chahine, R.; Bose, T. K. Hydrogen Adsorption in Carbon Nanostructures. *International Journal of Hydrogen Energy* **2001**, *26*, 831-835.

(300) Wilmer, C. E.; Farha, O. K.; Yildirim, T.; Eryazici, I.; Krungleviciute, V.; Sarjeant, A. A.; Snurr, R. Q.; Hupp, J. T. Gram-Scale, High-Yield Synthesis of a Robust Metal-Organic Framework for Storing Methane and Other Gases. *Energy & Environmental Science* **2013**, *6*, 1158-1163.

(301) Mason, J. A.; Veenstra, M.; Long, J. R. Evaluating Metal-Organic Frameworks for Natural Gas Storage. *Chemical Science* **2014**, *5*, 32-51.

(302) Hibino, K., et al. . System for Storing Dissolved Methane-Base Gas 6,584,780.

(303) Chevreau, H.; Permyakova, A.; Nouar, F.; Fabry, P.; Livage, C.; Ragon, F.; Garcia-Marquez, A.; Devic, T.; Steunou, N.; Serre, C.; Horcajada, P. Synthesis of the Biocompatible and Highly Stable Mil-127(Fe): From Large Scale Synthesis to Particle Size Control. *Crystengcomm* **2016**, *18*, 4094-4101.

(304) Luo, S.; Nasrabadi, H.; Lutkenhaus, J. L. Effect of Confinement on the Bubble Points of Hydrocarbons in Nanoporous Media. *Aiche Journal* **2016**, *62*, 1772-1780.

(305) Srivastan, S.; Darwish, N. A.; Gasem, K. A. M.; Robinson, R. L. Solubility of Methane in Hexane, Decane, and Dodecane at Temperatures from 311-K to 423-K and Pressures to 10.4-Mpa. *Journal of Chemical and Engineering Data* **1992**, *37*, 516-520.

(306) S'ong, Z. N.; Nambo, A.; Tate, K. L.; Bao, A. N.; Zhu, M. Q.; Jasinsk, J. B.; Zhou, S. J. J.; Meyer, H. S.; Carreon, M. A.; Li, S. G.; Yu, M. Nanovalved Adsorbents for Ch4 Storage. *Nano Letters* **2016**, *16*, 3309-3313.